DEVELOPMENT AND CHARACTERIZATION OF BIODEGRADABLE ELASTOMERS FOR LOCALIZED ANGIOGENIC GROWTH FACTOR DELIVERY

By

RAFI CHAPANIAN

A thesis submitted to the Department of Chemical Engineering

in conformity with the requirements for

the degree of Doctor of Philosophy

Queen's University

Kingston, Ontario, Canada

September 2009

ABSTRACT

Therapeutic angiogenesis is a promising technique to treat ischemia by creating new blood vessels. The aim of this thesis was to develop and characterize biodegradable elastomers for localized delivery of growth factors and to investigate the ability of released growth factors to induce angiogenesis. An osmotic delivery mechanism using photo-cross-linked elastomers based on trimethylene carbonate (TMC) was used to deliver vascular endothelial growth factor ($VEGF_{165}$) and hepatocyte growth factor (HGF) alone or in combination at two different doses. It was hypothesized that elastomers made of TMC can provide an effective osmotic release using trehalose as a main osmotigen and that the use of TMC would eliminate the microenvironmental pH drop implicated in denaturing acid sensitive growth factors. To obtain an insight into the degrading zone in which growth factors will be released, the *in vivo* degradation mechanism and tissue response were investigated. The *in vivo* degradation of D,L-lactide/ε-caprolactone (DLLACL) elastomers that degrade by hydrolysis was investigated for comparison. Cross-link-density played a significant role in the degradation pattern of DLLACL elastomers. TMC and TMCCL elastomers degraded by surface erosion and oxidation played a significant role in their *in vivo* degradation. To obtain an efficient release, the mechanical properties of TMC elastomers were tailored by copolymerizing TMC with CL and DLLA and/or by controlling the cross-link density. The delivery device was able to provide a sustained release of growth factors for longer than two weeks with no initial burst. Cell based bioactivity assays indicated that released growth factors were highly bioactive over the entire release period. Microenvironmental pH studies using FITC-BSA indicated no significant drop in pH in TMC elastomers that contained small amounts of DLLA. Using ^{125}I-$VEGF_{165}$, it was found that the osmotic delivery can provide a direct *in vivo-in vitro* release correlation. Released growth factors were able to induce

angiogenesis in rats when tested by subcutaneous implantation. Angiogenesis was dose dependent for both $VEGF_{165}$ and HGF. Combined release of VEGF and HGF achieved the best results. The formed blood vessels were stable during the active release period, and they were normal looking and connected to the surrounding vasculature.

ACKNOWLEDGEMENTS

I would like to thank Dr. Brian Amsden for his exceptional supervision, encouragement, and financial support. I deeply appreciate Dr. Amsden's devotion to his students, and especially his input to the fields of biomaterials and osmotic release.

I would very much like to thank my wife, Meghrig Sulahian, for her patience and encouragement during my studies. I would also like to thank my daughter, Aya who enlightened my life with her smile, and I would like to thank my parents for their support.

I very much appreciate the financial support provided by Ontario Graduate Scholarship (OGS) and Ontario Graduate Scholarship for Science and Technology (OGSST) programs that helped me to realize one of my dreams.

I would like to thank Drs. Yat Tse and Stephen Pang from the Department of Anatomy and Cell Biology for their invaluable input in the animal studies and histology.

My sincere appreciation and thanks to Dr. Herbert F. Shurvell from the Art Conservation Department for his invaluable guidance on ATR-FTIR experiments, and to Dr. Francoise Sauriol from the Chemistry Department for her guidance on NMR experiments.

I would like to thank Mr. Charles B. Cooney and Mr. Jeff Mewburn for their assistance with the scanning electron and confocal microscopies.

Finally, I would like to thank the visiting postdoctoral fellows, Dr. Laurianne Timbart and Dr. Bo Qi, and my labmates, Abby Sukarto, James Hayami, Denver Surrao, Oladunni Babasola and Laura Cornacchione for their support and friendship.

Contents

List of Figures

List of tables

Nomenclature

A	the capsule surface area
d	the diameter of solid particles
E	the modulus
h	the capsule wall thickness
$\bar{h}$	the thickness of an elastomer layer in the particle layer
k_w	the hydraulic permeability of the polymer
L	the length of a cube matrix, which has an equivalent volume to a cylindrical device
$\bar{L}_{LA}$	the average lactyl sequence length
m_t	the mass of an agent released during the osmotic phase
m_T	the weight of initially loaded agent
n	the number of solid particles in any one dimensional direction within a cube
P	the resisting pressure of the polymer
$P_{L\rightarrow T}$	the probability of a lactyl unit being beside a carbonyl unit from left to right direction.
R	the radius of cylinder
t_b	the time required for a capsule to rapture
V	the amount of water imbibed
w_0	the initial weight of the elastomer
w_w	the wet weight of the elastomer
w_d	the dry weight of the elastomer
w_e	the weight of the elastomer after sol extraction
x	the thickness of a particle layer

Greek letters

λ	the ratio of the swollen capsule radius to the original radius
ϕ	the particle volumetric loading in the device
Π	the osmotic pressure of solid particle solution in the caps

1. CHAPTER ONE

1.1. INTRODUCTION

Ischemic tissue is a tissue that is deprived of O_2 and nutrients because of a compromised coronary flow. The lack of O_2 and nutrients decrease the energy available to the cells, leading to their injury and death [1]. Current therapies for ischemic heart disease include balloon angioplasty, arterial stents, coronary bypass surgery, and the use of thrombolytic agents [1]. Current therapies, however, are associated with reperfusion injury [1, 2] since myocytes are forced to refunction under increased intracellular calcium, increased osmotic activity and low pH conditions that leads to their hypercontraction and lethal injury [2]. Therapeutic angiogenesis is a new therapy that aims at increasing the blood flow in an ischemic tissue by inducing the formation of new blood vessels using angiogenic growth factors. Using therapeutic angiogenesis prior to the coronary bypass surgery can minimize the reperfusion injury by returning myocardial cells to normal or near normal conditions [1]. Therapeutic angiogenesis could also be used for patients who cannot undergo surgery because of a chronic disease or an advanced age.

Angiogenesis is a complicated process where numerous cell types, proteolytic enzymes, cytokines and growth factors participate in the process [3]. Vascular endothelial growth factor (VEGF) is produced in ischemic tissue as a result of hypoxia [3]. VEGF induces the autocrine production of angiopoietin-2 (Ang-2) that leads to pericyte detachment, associated with the walls of blood vessels. Perivascular myofibrblasts produce VEGF, placental derived growth factor (PLGF), and storma derived factor-1 (SDF-1) to recruit bone marrow derived mononuclear cells [3]. Recruited cells, along with macrophages secrete additional angiogenic growth factors such as VEGF-B, VEGF-C and VEGF-D to initiate the sprouting of endothelial cells into new

channels [3, 4].

Systemic delivery of therapeutic proteins using intra-venous, intra-peritoneal, and subcutaneous injections cannot maximize the efficacy/dose relationship when intended for the delivery of growth factors due to issues related to systemic stability and adverse side effects [5]. For example, subcutaneously injected vascular endothelial growth factor with an amino acid sequence of 165 ($VEGF_{165}$) was cleared in four hours, and 70% of it was located in the blood, liver, spleen, lung, and kidneys [6]. Furthermore, the injected $VEGF_{165}$ is implicated in renal and hematopoietic end-organ damage [7]. To overcome difficulties associated with systemic delivery of growth factors, polymer based sustained delivery systems are being investigated [8-15].

A successful polymer-based sustained delivery system could provide a maximum efficacy/dose relationship by overcoming the obstacles pertinent to systemic and bolus injections [5]. A successful polymer-based delivery system will be a reservoir that protects the therapeutic protein from systemic degenerative factors and presents the protein to the target tissue in a sustained and controlled fashion. Unlike for peptides, a successful delivery system for therapeutic proteins has not been realized yet [5]. A simultaneous solution of protein denaturing problems, both during the device synthesis and during the delivery process, is required in order to produce a clinically viable polymer based protein delivery device [5]. Irreversible protein inactivation during the device synthesis occurs when a protein is exposed to physical, mechanical and chemical stresses, which are specific to the preparation technique [5, 16]. Potential sources of irreversible protein inactivation during delivery include adsorption to hydrophobic and charged surfaces, highly acidic micro-environmental pH, and elevated levels of moisture [16].

Other issues are the initial burst release and the incomplete release of embedded proteins. For example, the initial burst of $VEGF_{165}$ could lead to the formation of abnormal short-lived blood vessels, full of glomeruloid [17, 18], and the incomplete release (trapped proteins) could cause immunogenicity once released in a denatured form [8].

The aim of this thesis is to develop and characterize biodegradable elastomers for localized angiogenic growth factor delivery. Trimethylene carbonate (TMC), known to degrade without producing acid degradation products [19] was chosen as a base material for the delivery vehicle to eliminate acid degradation products implicated in denaturing $VEGF_{165}$ [6, 10]. Osmotic release was used because of its ability to provide a zero order release without an initial burst [8], and since osmotic release is based on fracture formation and propagation [20], the delivery vehicle was made of cross-linked networks. Two model growth factors, $VEGF_{165}$ and hepatocyte growth factor (HGF) were chosen in this thesis, because of previous difficulties associated with their sustained release in a bioactive form, and because of issues related to their ability to induce the formation of stable blood vessels when administered alone [6, 10, 12, 14, 21, 22]. The structural properties and biological activities of both $VEGF_{165}$ and HGF are provided below.

1.2. Vascular endothelial growth factor (VEGF)

VEGF is a highly specific mitogen that promotes the formation of blood vessels both in embryogenesis and wound healing processes [23, 24]. The physiological activity of VEGF is initiated by binding to cellular receptors KDR and Flt-1. VEGF exists in different amino acid sequences (121, 165, 189, and 206 AAs). $VEGF_{165}$ is the most dominant form, and VEGF with

an amino acid length of 165 and longer binds to the extracellular matrix (ECM) through its C-terminal domain interaction with heparin. The binding of VEGF to ECM is cleaved by plasmin for the initiation of the physiological function of VEGF [23, 24]. $VEGF_{165}$ exists in a dimer form, where two monomers are covalently linked by two symmetrical disulfide bonds between Cys 51 and Cys 60, and each monomer is stabilized with a cysteine knot made of three disulfide bonds (Figure 1-1).

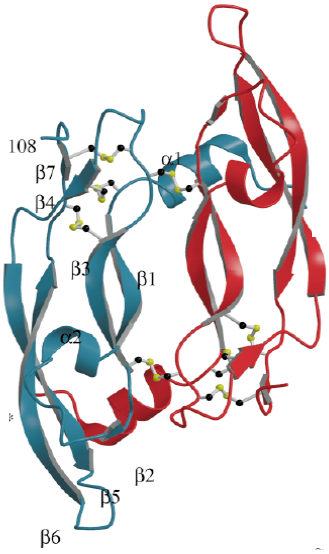

Figure 1- 1. The structure of receptor binding domain of VEGF165 [2]. One monomer of the dimer is presented in red and the second in blue. Disulfide bonds are presented in white and sulfur atoms in yellow.

The residues responsible for KDR binding are Phe17, Ile46, Glu64, Gln79 and Ile83. Those residues span the dimer interface with short three-stranded antiparallel β sheets (β2, β5 and β6) from one subunit along with the N-terminal α helix from the other subunit. The binding of $VEGF_{165}$ to the Flt-1 receptor is mediated by the loop that extends from β3 to β4 [24]. The *in vivo* half-life of $VEGF_{165}$ is around 30 min [25], and it undergoes accelerated degradation at low pH values. The N-terminal residues of recombinant human VEGF (rh-VEGF) that participate in receptor binding are prone to deamidation (Asn 10), oxidation (Met-3), and diketopiperazine reactions (Ala1-Pro2-Met3) [21] that occur at 7.4, 2.5, and 5.2 times faster, respectively, at pH 5

compared to pH 8 [21]. Hereafter, $VEGF_{165}$ will be referred to as VEGF for simplicity.

1.3. Hepatocyte growth factor (HGF)

HGF is a potent mitogen, motogen, and morphogen that is responsible for the growth, movement and differentiation of epithelial and endothelial cells in different tissues and organs [26, 27]. The physiological activity of HGF is initiated by binding to the c-Met receptor [26]. Heparin binding is important for the biological activity of HGF. The binding induces oligomerization of HGF and facilitates the c-Met mediated mitogenesis [28]. Mature HGF is composed of a 69 kDa α chain and a 34 kDa β chain, separated by four kringle domains [27]. The α chain contains the N-terminal domain and the β chain resembles a serine protease in the sequence, but without having any enzymatic activity [27]. The hairpin loop region in the N-domain plays a significant role in cell receptor and heparin binding (Figure 1-2). It is composed of one α helix and two β strands. The structure of the hairpin loop region is stabilized by two disulfide bonds; the first bond located between Cys 70 and Cys 96 connects the middle of the helix to the middle of the β strand, and the second located between Cys 74 and Cys 84 connects the C terminus of the α helix and the N terminus of the second β strand (Figure 1-2).

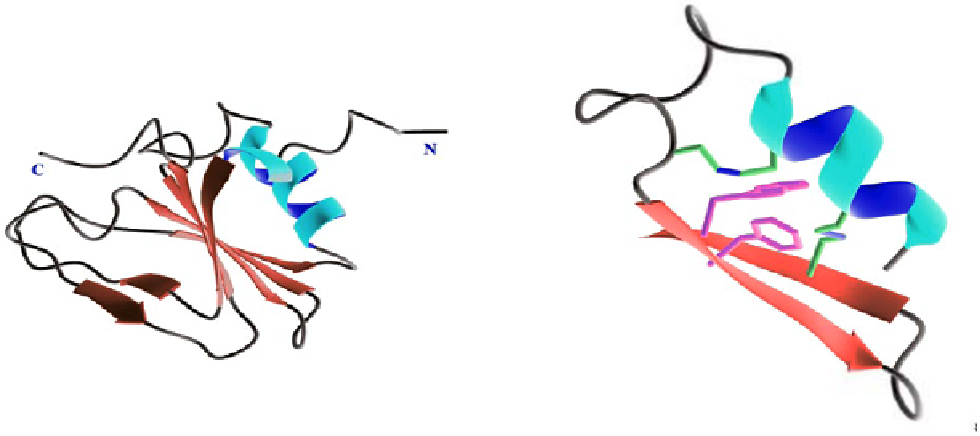

Figure 1- 2. The structure of the N domain of HGF (left) [23]. The structure of the hairpin loop region in the N domain of HGF (right) [23].

HGF has a half-life of 3.8 minutes in the circulatory system of rats. After 15 min of intravascular injection (IV) injection, 29.5 ± 0.5 % of injected ^{125}I-HGF was present in the liver and 6.2 ± 0.2 % was present in the kidneys [29]. HGF might undergo degradation at acidic pHs; HGF interacted with acidic gelatin (pI=5) was found to be less bioactive, despite its ability to induce *in vivo* angiogenesis [12].

1.4. Previous attempts in polymer-based sustained delivery of growth factors

The growth factor delivery vehicles investigated in the literature include injectable vehicles such as hydrogels [12, 14, 22, 30], microspheres [6, 31, 32] and liposomes [11, 33, 34], and implantable vehicles such as osmotic pumps [7, 17], degradable and non-degradable solid polymers such cylinders [10, 35], and scaffolds such as sponges and porous structures [15, 36, 37]. Despite advances in the design of polymer based growth factor delivery systems, there still are numerous pitfalls to overcome. Vehicles for growth factor delivery are made either from natural materials or synthetic materials. Natural materials are based on alginate, collagen, gelatin, heparin-agarose, hyaluronic acid, chitosan and fibrin [22]. Synthetic materials are based mainly on poly(lactide-co-glycolide) (PLGA), poly(ethylene glycol) (PEG) [22], and other emerging polyesters and polycarbonates [35, 38, 39].

1.4.1. Biomaterials

Polymeric degradable biomaterials are degraded either by bulk degradation or by surface erosion or by the combination of both. Bulk degrading biomaterials include poly(glycolide) [40], poly(L,lactide) [41, 42], poly(D,L-lactide) [43], and poly(ε-caprolactone) [43]. Surface eroding biomaterials include poly(ethylene carbonate) [38, 44], poly(trimethylene carbonate) [19],

poly(urethane carbonate) [45], poly(glycerol sebacate) [46], poly(polyol sebacate) [47] poly(ortho esters) [48], and poly(anhydrides) [49]. Naturally occurring biomaterials are often degraded by surface erosion [22].

Biomaterials, prone to bulk degradation, degrade by hydrolysis. The hydrolytic degradation is a result of several processes occurring concurrently, which include water absorption, ester hydrolysis, the diffusion of degradation products to the surface, and a local internal decrease in pH as a result of the production of acidic degradation products that are temporarily retained within the polymer bulk. This pH decrease catalyzes the hydrolysis. The degradation exhibits two phases: the first phase is characterized by a linear decrease in mechanical strength after an induction period, with no, or very little, loss of mass, while the second phase is characterized by the onset of mass loss, an increase in water uptake, loss of mechanical strength, and the release of low molecular weight degradation products [50-54].

Biomaterials prone to surface erosion degrade by oxidation and/or enzymatic action that occur primarily on the surface [19, 38, 55]. The hydrolytic degradation in some elastomers, especially thermosets, occurs primarily on the surface as well [46]. During the degradation, the bulk of the material remains inaccessible to the degrading species; as a result the material maintains its mechanical strength. In surface eroding materials, the mass loss starts from time zero. Other properties such as mechanical properties, sol content and water uptake do not change during the degradation [55, 56].

Therapeutic proteins are released from polymeric devices either by diffusion, matrix

erosion, combined diffusion/matrix erosion or osmotic release mechanism [8]. These delivery systems and their release mechanisms are reviewed below.

1.4.2. Injectable growth factor delivery devices

Injectable hydrogels can be delivered easily to the site of treatment using a syringe and needle. Silva *et al.* used a VEGF loaded injectable hydrogel system to treat an ischemic limb in mice. The device was made of a degradable, partially oxidized, binary alginate system. 2400 ng of VEGF was delivered to the ischemic limb of mice in 32 days according to the following sequence: 1260 ng was delivered as a burst in the first day, followed by 140 ng/day for 6 days in curvilinear fashion. The release after 7 days occurred slowly in a linear fashion, and at a rate of 12 ng/day for 25 days. The release in this system was based both on diffusion and matrix degradation, and the matrix degraded in 40 days in phosphate buffered saline (PBS) buffer [14]. According to the authors, bioactive VEGF was available in the ischemic tissue for a period of 7 to 15 days. Limb necrosis was rescued and reserved but full recovery was not achieved [14]. When the system was used for dual growth factor delivery of VEGF and beta polypeptide platelet derived growth factor (PDGF-BB), PDGF-BB was released at a slower rate due to its larger size and its stronger affinity to the alginate matrix [30].

Fibrin glue is another material investigated widely in VEGF hydrogel delivery experiments. It is available commercially as a separate mixture of fibrinogen and thrombin [22]. In a recent clinical trial, a 66-year-old man was injected intramuscularly with 100 μg of VEGF mixed in 10 ml fibrin glue for ischemic limb treatment [57]. Four months after the treatment, substantial growth of new blood vessels was observed, consequently significant reduction in pain

occurred [57]. Release from fibrin glue is characterized by a significant initial burst [22], and it was found that the glue itself has the ability to stimulate angiogenesis [58]. To reduce the initial burst and to provide long lasting release, the transglutaminase activity of Factor XIIIa was used to bind VEGF directly to the glue or to bind VEGF electrostatically to a heparin binding peptide, initially bound to the glue [59-61]. Bound VEGF was released by cell-associated enzymatic degradation of the fibrin, and it produced normal looking vessels [22]. Although fibrin is an interesting material for growth factor delivery, its use has the potential risks of infectious pathogens and immunogenicity [22].

Beside injectable hydrogels, growth factor delivery using microspheres has attracted the interest of a great number of researchers. King and Patrick prepared VEGF microspheres made of PLGA/PEG and investigated the *in vitro* release and bioactivity. To avoid dissolving VEGF in aqueous media during the preparation, King and Patrick used a solid encapsulation/single emulsion/solvent extraction technique. 60% of loaded VEGF was released as a burst during the initial 4 days, followed by a sustained release for over 28 days [32]. The release was governed by diffusion and matrix erosion. Although growth factor delivery using microspheres is attractive in terms of its delivery, it still suffers from problems such as low levels of loading and the initial burst [31, 32].

Interestingly, when Burgess and Kim investigated the *in vitro* and *in vivo* release pharmacokinetics of VEGF from PLGA microspheres, they did not observe an initial burst. 50 mg of PLGA microspheres loaded with 400 ng of VEGF was injected subcutaneously in rats. The *in vitro* release and degradation was significantly faster than the *in vivo* release and

degradation. 60 % of the embedded VEGF was released after 30 days *in vitro* compared to 48 days *in vivo*. The authors ascribed this phenomenon to a different *in vivo* sink condition. The released VEGF lost 25% of its bioactivity, and it was reasoned that the decrease in bioactivity was due to acidic products formed during polymer degradation [6]. Besides PLGA, alginate has been used to prepare VEGF microspheres and nanospheres [25]. Despite the ability of VEGF-alginate microspheres to induce extensive *in vivo* angiogenesis [62], they are characterized by possessing a high initial burst, incomplete release, and very slow and non-controllable *in vivo* degradation [25, 62].

Liposomes have also attracted the interest of many people because of their size and structural resemblance to cells. Liposomes are tiny bubbles surrounded by a phospholipid like layer. The inner gap could be filled with growth factors [63], and they could be delivered easily by injection. Issues remaining with liposomes include encapsulation efficiency, particle stability, the initial burst, and incomplete release of encapsulated proteins [34]. To overcome some of these problems, Haidar *et al.* produced cationic nano-sized phospholipid vesicles using solvent free thin-film hydration technique. The stability of produced liposomes and its encapsulation efficiency was improved significantly by covering particles with several layers of anionic alginate and cationic chitosan. The layer-by-layer covering technique, however, resulted in an incomplete release of the encapsulated protein [11].

1.4.3. Implantable growth factor delivery devices

Beside injectable growth factor delivery devices, there are numerous studies on implantable growth factor delivery devices. Implantable devices are larger in size and they

require a surgery for implantation. The advantage of implantable growth factor delivery devices, however, is the possibility of having a multifunctional task. For example, besides being a vehicle for a growth factor delivery, implantable devices could function as a scaffold for tissue engineering or they could be part of a biomedical device.

In a recent study, where the implanted device was a scaffold for tissue engineering, Elcin and Elcin impregnated highly porous sponges made of PLGA with a small amount of VEGF solution, and investigated the ability of the device to induce angiogenesis in rats [36]. The release from the PLGA sponge occurred in two phases: 60 –70 % of VEGF was released as a burst in the initial 3 days followed by a sustained slow release for more than 2 weeks. Two concentrations of VEGF, 2.5 and 5 μg, were used. The loading efficiency was greater than 80 %. In the initial 3 days, 1.66 μg of VEGF from the low dose and 2.66 μg from the high dose was released, followed by 100-200 ng/day for 12 days. VEGF with a higher dose exhibited greater amount of capillary formation. Newly formed capillaries from both VEGF doses were stable after six weeks. Sustained release in this case occurred as a result of the osmotic activity of remaining NaCl used initially as a porogen [36].

In a different study with PLGA sponges, Smith *et al.* used a combination of rapid reduction of CO_2 pressure and leaching of NaCl porogen to create a porous sponge. The loading efficiency in this case was 36 ± 1 %, and 25 % of VEGF (900 ng) was released within the first 3 days followed by 1 % (36 ng/day) release per day. The authors reported an increased number of blood vessels at 7 and 14 days [37].

In studies using chemically cross-linked collagen [15] and gelatin [12] matrices, both Tabata *et al.* and Oseki *et al.* reported the formation of new blood vessels using angiogenic growth factors such as VEGF [15] and HGF [12]. Tabata *et al.* implanted cross-linked collagen sponges impregnated with 2, 10 and 50 μg of VEGF in mice. The portion of VEGF that did not interact with the polymer matrix made up 70 – 85% of the total VEGF and it was released as a burst in the first day. The remaining VEGF was released as the matrix degraded. Tissue hemoglobin formation, which was used to assess the blood vessel formation, was at maximum with 10 μg dose when quantified after 7 days. Blood vessel formation with a 50 μg dose was slightly lower than blood vessel formation with a 10 μg dose. The authors concluded that despite its interaction with the polymer matrix, VEGF remained active *in vivo* after 28 days [15]. Oseki *et al*. implanted cross-linked gelatin matrices impregnated with 1, 5, and 10 μg of HGF in the back of mice [12]. Release of HGF was based on network degradation, and it occurred in a hyperbolic fashion. The release rate occurred at an approximate rate of 100, 500, and 1000 ng/day. The dose of 1 μg was unable to produce new capillaries, and doses of 5 and 10 μg produced the same number of capillaries. The authors of this study found that HGF complexed with acidic gelatin (pI = 5) is less bioactive *in vitro* [12], but, despite being complexed with the gel network, the released HGF was able to induce angiogenesis [12].

In a different study, where a synthetic solid elastomer was used for growth factor delivery, Gu *et al.* investigated VEGF delivery from photo-cross-linked elastomers made of tri-acrylate end-capped star-poly(D,L-lactide-co-ε-caprolatone). VEGF was lyophilized with BSA and trehalose. The lyophilized mixture was ground and sieved, the particles were suspended in a polymer solution, and the mixture was photo cross-linked at ambient temperature using UV light

[10, 35, 64]. The VEGF was released based on an osmotic release mechanism, provided by trehalose. The device was able to provide a constant release for 5 to 20 days, depending on the device geometry, solid particle composition, and elastomer cross-link density [10, 35, 64]. The acrylate functional groups protected VEGF/BSA and other proteins from free radicals generated during the photo-cross-linking process [65, 66]. The authors found that a drop in the micro-environmental pH to less than 5 occurred in as short a time as 7 days during the matrix degradation. The authors concluded that this pH drop decreased the bioactivity of released VEGF after 7 days and denatured the unreleased VEGF [10].

In a recent interesting study, Davies *et al.* investigated the effect of VEGF dose on producing stable blood vessels. VEGF was delivered into a porous scaffold of polyurethane using an osmotic pump [17]. The authors found that the dose and duration of released VEGF play a critical role in producing stable long living blood vessels. Delivery of 15 ng/day of VEGF *in vivo* was insufficient in inducing angiogenesis after 10 days. Delivery of 150 ng/day of VEGF for 42 days produced normal looking blood vessels, which were stable for 80 days after termination of the release. Blood vessels produced by a dose of 1500 ng/day were larger initially, and they regressed after 20 days. According to the authors, the minimum period of VEGF delivery required to obtain stable and long living blood vessels still needs to be elucidated [17]. Although the osmotic pump used in this study can provide VEGF for elongated periods of time, and at preprogrammed doses, it needs to be explanted from the body after releasing its content of VEGF.

In Table 1-1 below the dose, duration and main results of recent animal and pre-clinical

trials, where VEGF and HGF were used for angiogenic therapy, are summarized.

Table 1- 1. Dose and duration of delivery of VEGF and HGF in recent animal and clinical studies.

-Ref -animal -growth factor -device	Total amount in the device (μg)	Total amount released as a burst (ng)	Total amount released at second order (ng)	Daily amount released at zero order ng/day	Remarks
[17], (rat), VEGF, Osmotic pump	(1) 0.63 (2) 6.3 (3) 63	- - -	- - -	15 (42days) 150 (42days) 1500 (42days)	(1) No significant angiogenesis (2) 46±11% above average after 120 days (3) Regressed after 20 days
[14], (mice), VEGF, alginate hydrogel	3	1260 (1 day)	840 (6 days)	12 (25 days)	Rescued and reserved limb necrosis, normal tissue perfusion was not achieved
[57], (man), VEGF, Fibrin hydrogel	100	-	-	-	Significant reduction in pain and significant growth in blood vessels in ischemic limb 4 month after the treatment
[36], (rats), VEGF, PLGA sponge	(1) 2.3 (2) 4.2	1110 (12 hrs) 1720 (12 hrs)	550(2.5days) 940(2.5days)	100–200 (12 days) 100-200 (12 days)	(1and 2) capillaries stable after 6 weeks (2) exhibited greater number of capillaries
[37], (rats), VEGF, PLGA microsphere matrices	3.6	650(1day)	250(2.5days)	~ 36 (29days)	Number of blood vessels greater than control at 1 and 2 weeks
[15], (mice), VEGF, Collagen hydrogel	(1) 2 (2) 10 (3) 50	1400(1day) 7000(1day) 35000(1day)	350 (6days) 1750(6days) 8750 (6days)	14 (21 days) 71 (21 days) 357 (21 days)	(2) blood vessel formation was at maximum at 7 days (3) vessels slightly less than (2) at 7 days
[12], (mice), HGF, Gelatin hydrogel	(1) 1 (2) 5 (3) 10	- - -	750 (7days) 3750 (7days) 7500 (7days)	35 (14 days) 175 (14 days) 350 (14 days)	(1) unable to produce blood vessels at 7 days. (2) and (3) produced similar number of vessels at 7 days. Matrix interacted HGF was less bioactive

1.5. Requirements of an ideal polymer-based growth factor delivery system

Although, most of polymer-based sustained delivery devices can provide growth factor release for a period of 2 to 3 weeks, the minimum time of VEGF delivery to induce the

formation of stable long living blood vessels remains to be elucidated [17]. Regarding the therapeutic window of VEGF, low doses such as 15 ng/day are unable to induce blood vessel formation and high doses such as 1500 ng/day induce large, abnormal and short living blood vessels [12, 15, 17, 18]. In addition to the dose and duration of the growth factor release, special attention should be given to the initial burst, microenvironmental pH, growth factor–matrix interaction, incomplete release, and the rate of matrix degradation. As mentioned earlier, the initial burst could lead to the formation of abnormal short-lived blood vessels, full of glomeruloid [17, 18]. Growth factor/matrix interaction [12, 15] and drop in microenvironmental pH decreases the bioactivity of released growth factors [6, 22, 35]. Incomplete release (trapped proteins) could cause immunogenicity once released in a denatured form upon the polymer degradation [8]. Finally, it is important to determine the duration of the foreign body response, generated as a result of the administered delivery device. Previous attempts to overcome the above-mentioned issues are presented below.

1.5.1 Initial burst

To reduce the initial burst several strategies have been applied. Those include adding surfactants such as PEG 400 [67] and plasticizers such as poly(ethylene oxide monooleate)-block-poly(D,L-lactide) [68], coating microspheres with a thin layer of a polymer [69], introducing ionic interaction with proteins [70], and embedding microspheres in polymeric gel systems such as reverse thermal gelling systems [71], PVA [72], and fibrin [33]. Blending PEG or adding it to the structure provided better dispersion of the protein, and less presence at the device surface [73]. Adding plasticizer to PLGA microspheres produced particles with smooth surfaces, reducing the surface area available for the initial burst release [68]. Ionic interaction of

positively charged heparin binding domains in VEGF with free acid chain termini of PLGA reduced the initial burst [70].

1.5.2. Microenvironmental pH

To obtain maximum bioactivity, special attention should be given to the microenvironmental pH drop in a polymer based growth delivery system. Using techniques such as nuclear magnetic resonance (NMR), electron paramagnetic resonance (EPR), potentiometry, and confocal fluorescence microscope imaging [74, 75], average microenvironmental pH values ranging from 2 [76] to 6.4 [77] were detected in PLGA microspheres. The variation in pH values was due to differences in the structure and release conditions [75]. Recently, Ding and Schwendeman reported a microenvironmental pH value of 3, after only one day of locating PLGA microspheres in PBS buffer. The initial drop in pH was followed with a rise in the pH and a subsequent drop to 3 [74]. Wong-Moon *et al.* reported a pH drop below 4 in as short a time as 2 days, in PLGA microspheres located in fetal calf serum [78]. In other polymer systems that degrade by hydrolysis such as photo-cross-linked poly(DLLA-ε-CL) elastomers, a pH decrease occurred starting from day 12. However, when the elastomer was loaded with trehalose/BSA particles the pH dropped below 5 in as short as 7 days [10].

To overcome the pH drop problem, which is considered to be a significant issue in rendering the commercialization of PLGA microspheres as a delivery vehicle for therapeutic proteins [69], Zhu *et al.* and others used basic salts such as $Mg(OH)_2$ and $MgCO_3$ [16]. Others blended PEG with PLGA [74]. It was found that incorporating 3 % $Mg(OH)_2$ within the solid excipient increased the total BSA fraction released from 20 % to 80 %. BSA maintained its

structural integrity and did not aggregate for over one month [16]. Others reported that adding PEG improved the stability of BSA and ovalbumin in PLGA/PEG microspheres [79, 80]. These strategies, however, provide a limited assistance to overcome the pH drop problem, since adding basic salts or PEG only postpone and/or reduce the pH drop. For example the pH was found to be less than six in as short a time as four days in half of the pores, when PLGA was loaded with 3% $MgCO_3$. Blending PEG with PLGA, on the other hand, prevented the pH drop below five during the four weeks of incubation [74]. Considering a minimum required delivery of two weeks, and considering the accelerated degradation of VEGF at pH 5 [21], one can conclude that these strategies can only reduce the damage.

1.5.3. Incomplete release

To overcome the incomplete release of solid particles from polymer based drug delivery systems, Ashkenasy and Kost applied low intensity ultrasound to generate cracks in the polymeric membrane of swollen capsules, and consequently to release trapped particles [81]. Although the ultrasound technique was successful in releasing the trapped NaCl and salicylic acid from poly(ethylene-co-vinyl acetate) elastomer with a vinyl content of 40% (EVA 40) matrices, the efficacy of this technique is not investigated yet for growth factor delivery systems, where localized heat and pressure generated during the exposure could harm embedded growth factors [8].

1.5.4. Growth factor-matrix interaction:

To protect growth factors from being denatured in organic solvents, the solid encapsulation technique was used. In this technique growth factors are protected by formulating them with

bulking agents such as albumin and trehalose [31, 32]. This technique can also be used to minimize the growth factor/matrix interaction and adsorption of growth factors to hydrophobic or charged surfaces during the release [82].

1.6. The importance of the mechanism of degradation and foreign body response on polymer based growth factor delivery systems

In polymer based growth factor delivery systems, the significance of the mechanism of matrix degradation stems from the necessity of identifying the conditions in which a therapeutic protein will reside and function. The released growth factor would diffuse thorough a zone, where enzymes and oxidative species are present to degrade the implant. In an interesting study, Stoll *et al.* found that human interleukin-3 (hIL-3) released from poly(ethylene carbonate) that degrades by oxidation, was able to diffuse through the bio-eroding layer and to bind specific monoclonal antibodies [38], located outside the hostile zone.

1.6.1. Tissue response to biomaterials

The host reaction to biomaterial implantation is characterized by the following sequence of events: injury, blood-material interaction, provisional matrix formation, acute inflammation, chronic inflammation, granulation tissue generation, foreign body reaction, and fibrous capsule development [83]. The initial host response is activated by an injury to a vascularized connective tissue. As a result, fluid, proteins, and blood cells migrate from the vascular system into the injured site. Neutrophils predominate the site of injury for the first several days and they are replaced by monocytes, which differentiate into long living macrophages. As a result of the injury and presence of a foreign body, different cellular cascades such as the complement are

activated, and a provisional matrix is formed. The provisional matrix is made primarily of fibrin and contains different growth factors and cytokines that control the subsequent wound healing process [83]. The inflammation and subsequent events, on the other hand, aim at replacing the injured tissue and the formation of a fibroblastic scar tissue around the implant. Complement activation releases opsonins and anaphylatoxins [84]. Opsonins bind to the implant and activate neutrophils and macrophages to produce enzymes that will degrade the implant [83]. Anaphylatoxins, on the other hand, bind to specific cell receptors on neutrophils, monocytes, macrophages, mast cells, and smooth muscle cells to induce chemotaxis, vasolidation, cell activation, and adhesion [84]. Macrophages play a significant role in the chronic inflammation stage. They secrete neutral proteases, chemotactic factors, arachidonic acid and reactive oxygen metabolites, complement components, coagulation and growth factors, and cytokines [83]. Secreted growth factors assist the growth of fibroblasts, blood vessels, and epithelial cells, leading to the formation of the granulation tissue [83]. Fibroblasts synthesize collagen and proteoglycans, which are the non-cellular components of the granulation tissue. When macrophages are unable to phagocytose the implant, they fuse into multinucleated giant cells leading to the foreign body reaction [83]. Generally, implants are isolated from the surrounding tissue by a fibrous capsule [85], and the foreign body reaction occurs within and in the vicinity of the capsule. The surface chemistry and topography of the implant play a major role in the protein adsorption and its conformation, which in turn provides signals to subsequent cellular responses on the surface of the implant [86].

The morphology and kinetics of the capsule formation could impact the kinetics of released growth factors, since capsules develop within days [85], and growth factors need to

diffuse through the dense collagenous layer to initiate a biological function nearby the device.

As mentioned earlier, therapeutic proteins are released either by diffusion, matrix erosion, combined diffusion/matrix erosion or osmotic release mechanism. In this thesis the osmotic release mechanism was chosen because of its many advantages over other techniques. Osmotic release can provide a near zero order release for more than 2 weeks with low initial burst. More importantly, proteins with different physical properties can be released at similar and controlled rates [35, 87, 88]. The mechanism of osmotic release is explained below.

1.7. Osmotic release

In the osmotic pressure drug release mechanism, water vapor diffuses through the polymer matrix until it encounters a polymer-surrounded drug particle (Figure 1-3). At the particle/polymer interface, the water phase dissolves a portion of the particle, forming an activity gradient between the capsule and the surrounding medium. The activity gradient draws water into the capsule generating an osmotic pressure equal to the osmotic pressure of a saturated solution [8]. Generated pressure in the capsule is resisted by the viscoelastic nature of the polymer [8]. The outcome of this resistance is one of the following: 1) when the polymer is unable to resist the pressure, polymer bonds are broken, and cracks are formed, which connect the contents of the capsule to the pore network, pushing the content toward the surface as a result of the pressure gradient between the capsule and the exterior, 2) when the generated pressure is unable to initiate bond breakage in the polymer, a thermodynamic equilibrium is established [8, 20]. The osmotic release mechanism dominates when the total volumetric loading of the active agent in the polymer matrix is below the percolation threshold, determined to be 31.15 % for a

simple cubic lattice [89, 90]. Below the percolation threshold, particles are separated with an osmotically active polymeric membrane [89, 90].

To provide experimental evidence about the osmotic nature of the release, Gale *et al.* investigated the release of pilocarpine from monolithic systems made of EVA by using NaCl or glycerin to vary the osmotic pressure of the release medium. NaCl and glycerin were used so that the concentration gradient between the polymer matrix and the release medium does not change. When the osmotic pressure of the release medium was increased to be equal to or greater than the osmotic pressure of the pilocarpine (37 atm), the drug stopped from being released [91]. In another study, Aschkenasy and Kost found that a swollen matrix of EVA loaded with NaCl and salicylic acid shrunk when it was immersed in a saturated solution of NaCl or salicylic acid. This observation indicates that particles are separated with osmotically active polymeric membranes [81].

Once the osmotic release is established, three distinct layers in the cross-section of a cylindrical device have been observed [8, 20, 92]. An outer transparent layer, where entrapped particles were released, an intermediate layer, where swollen pockets are detected, and an inner layer composed of dry particles [8, 20, 92]. Figure 1-3 provides a representation of the three regions established during the osmotic release, taken from Amsden and used with permission [8].

Factors that control osmotically driven release rates are polymer properties, drug properties, and device geometry. Polymer properties include water permeability, tear resistance, and modulus. Drug properties include osmotic activity, solubility, particle size, particle size

distribution, loading, and homogeneity of dispersion. Increasing polymer hydrophobicity, modulus or tear resistance decreases the release rate by decreasing the burst time. On the other hand, using drug particles that have greater osmotic activity, greater solubility, larger particle size, and higher percentage loading enhances the osmotic release [8, 20, 89, 91, 93, 94].

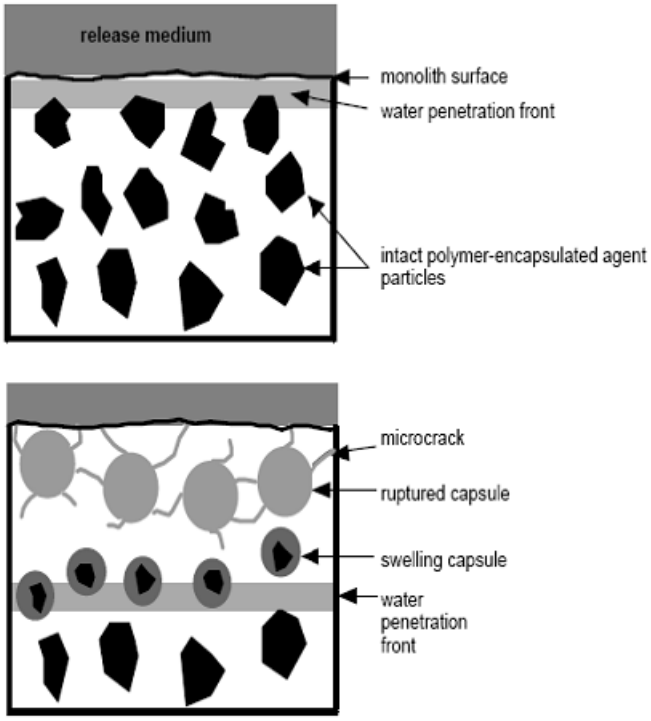

Figure 1- 3. Osmotic release mechanism. Top panel) Water vapor partitions and diffuses into the polymer matrix. Lower panel) Illustration of three zones established during the osmotic release [14].

For a capsule to rupture, the osmotic pressure of its content should be greater than the resisting pressure of the surrounding polymeric membrane. The water imbibition into a capsule is described by the following equation [93, 95]

$$\frac{dV}{dt} = \frac{k_w A(\Pi - p)}{h} \qquad (1\text{-}1)$$

where V is the amount of water imbibed, h is the capsule wall thickness, k_w is the hydraulic permeability of the polymer, A is the capsule surface area, Π is the osmotic pressure of solid

particle solution in the capsule, and p is the resisting pressure of the polymer. Elastomers with greater resisting pressure require higher osmotic pressure in the capsule to rupture, because the crack formation occurs only when Π is larger than p.

Gent and Lindley found that crack formation in rubbers depend linearly on the modulus, and it is independent of the rubber strength and extendibility [96]. The following equation formulated by Gent and Lindley describes the resisting pressure of an elastomer,

$$p = \frac{E}{6}(5 - \frac{4}{\lambda} - \frac{1}{\lambda^4}) \qquad (1\text{-}2)$$

where E is the modulus and λ is the ratio of the swollen capsule radius to the original radius. Gent and Lindley's model considers that the crack formation is due simply to a consequence of an elastic instability of pre-existing small cavities. As a result, the model depends only on the Young's modulus and not on the tensile strength. Others found that the resisting pressure of the polymer and the critical extension ratio λ_c are dependent on the fracture toughness as well [20].

Several mathematical models describing osmotic release have been formulated in the literature. One such model, created by Amsden for the osmotic release of electrolytes from non-degradable cylindrical matrices, is given by the following equation:

$$\frac{m_t}{m_T} = \frac{1}{1 + R/x}\left[(2 + \frac{x}{R})(\frac{t}{t_b}) - \frac{x}{R}(\frac{t}{t_b})^2\right] \qquad (1\text{-}3)$$

Where, m_t is the mass of an agent released during the osmotic phase, m_T is the weight of initially loaded agent, t_b is the time required for a capsule to rapture, R is the radius of cylinder, and x is the thickness of a particle layer [93]. This model was fitted to our experimental data to calculate the time required for a capsule layer to rupture [97]. Amsden's model was chosen because of its

simplicity and because the degradation of developed elastomers proceeded very slowly during the release.

Several studies have investigated the osmotic release of proteins from both non-degradable and degradable elastomers. Amsden and Cheng demonstrated the possibility of releasing proteins of different sizes and physiochemical properties such as bovine serum albumin (BSA), lysozyme, and epidermal growth factor (EGF) from elastomers made of ethylene vinyl acetate (EVA). Proteins were released at a zero order and at a similar rate. The release rate of proteins was similar to the release rate of NaCl when the concentration of the protein was below the precipitation threshold [87].

In a different study, Carelli *et al.* and Kajihara *et al.* obtained a zero order release of proteins such as interferon and serum albumin using a silicone rubber. Proteins were formulated with NaCl, glycine, and sodium glutamate to provide a sufficient osmotic pressure. In these studies the effect of loading, particle size and osmotic pressure on the release were investigated [88, 92, 98]. A zero order release was obtained for a period of as long as 30 days [98].

In contrast to non-degradable elastomers used by the two previous groups, Gu *et al.* investigated the possibility of using degradable elastomers made of poly(DLLA-co-ε-CL) [35, 64, 99] for the osmotic release of proteins. Proteins of different properties such as VEGF, interleukin (IL-2), and interferon- γ (IFN-γ) were formulated with BSA/trehalose, and they were released at a zero order and a similar rate for a period of up to 20 days. Elastomers made of poly(DLLA-co-ε-CL) degrade by hydrolysis, and it was found that matrix degradation is

implicated in denaturing VEGF, *in vitro*, after 7-10 days [10, 35].

1.8. Proposal: *in vivo* efficacy of osmotically driven growth factor release from biodegradable photo-cross-linkable elastomers

A successful polymer based sustained release delivery system for therapeutic angiogenic proteins would maximize the efficacy/dose relationship, providing an efficient treatment for diseases such as myocardial infarction, and limb ischemia [5, 14, 85]. To overcome the microenvironmental pH problem considered to be the main obstacle in the commercialization of polymer based growth factor delivery systems [69], we proposed the osmotic delivery mechanism using photo-cross-linked elastomers made of trimethylene carbonate (TMC) as a delivery system. This proposal is based on the following facts: 1) linear high molecular weight TMC polymers degrade *in vivo* rapidly and without producing acid degradation products [19], 2) the osmotic release mechanism can provide zero order release with no initial burst for a minimum period of two weeks [10, 88, 92], 3) acrylate groups can protect embedded proteins from radicals generated during the photo-polymerization process [65, 66].

The first objective of this thesis was to investigate the *in vivo* degradation mechanism and tissue response of blank photo-cross-linked elastomers. The aim of the first objective was to obtain an insight about the degrading zone in which growth factors will be released to initiate a biological function, and also to determine the total degradation time. Two groups of elastomers were implanted subcutaneously in rats. The first group were made of elastomers of poly(TMC) and poly(TMC-co-ε-CL), expected to degrade by surface erosion, and the second group were made of elastomers of poly(DLLA-co-ε-CL) known to degrade by bulk degradation. Elastomers

known to degrade by bulk degradation were used as a comparison in this study. Techniques used to investigate the *in vivo* degradation included attenuated total reflectance Fourier transform infra-red (ATR-FTIR), scanning electron microscopy (SEM), mechanical and thermal properties, mass loss, sol content, and water uptake.

Having investigated the rate and mechanism of degradation and the structure and kinetics of capsule formation, the second objective was to investigate the potential of an elastomer made of poly(TMC) as a matrix for the osmotic pressure driven release of proteins. For that purpose, bovine serum albumin (BSA) was used as a model protein and it was lyophilized with trehalose and NaCl to provide an osmotic pressure to embedded proteins. The results indicated that elastomers made of poly(TMC) were not suitable for osmotically driven release of therapeutic proteins when trehalose was intended to be the only osmotigen [97]. To overcome this problem, the mechanical properties of poly(TMC) elastomers were tailored using two techniques: copolymerizing TMC with other monomers such as ε-CL and DLLA and/or increasing the crosslink density of the elastomer, using prepolymers of lower molecular weights. The proposed prepolymer had a molecular weight of 4 kDa and consisted of 50 (mole%) TMC, 25 (mole%) ε-CL and 25 (mole%) DLLA. Adding small amounts of DLLA accelerated the rate of the *in vitro* degradation without reducing the microenvironmental pH significantly over the release period. Solid particles were formulated to contain 10% BSA, 85% trehalose, and 5% NaCl. The device provided sustained release for a period of 50 days, during which 77 ± 4 % of the BSA was released.

Having formulated the elastomer and solid particles, the third objective was to investigate

the release and bioactivity of two model growth factors, VEGF and HGF. Quantification of growth factors was performed using ELISA technique and the bioactivity was assessed based on cell proliferation assays. Growth factors were released in a sustained manner for more than 2 weeks with no initial burst, and the released growth factors were highly bioactive.

Since the *in vivo* sink condition is different from the *in vitro* sink condition, *i.e*. presence of a capsule *in vivo* and a lower content of water, the fourth objective was to investigate the rate of *in vivo* release and to compare it to the rate of *in vitro* release. To achieve this objective ^{125}I-VEGF loaded elastomer rods were implanted subcutaneously in rats, and the radioactivity of explanted rods was measured and compared to the radioactivity of rods located in an infinite sink of PBS buffer.

Having investigated the release kinetics of VEGF *in vivo*, the fifth and final objective was to investigate the *in vivo* efficacy of osmotically released VEGF and HGF in inducing angiogenesis in rats by subcutaneous implantation. Considering previous *in vivo* experiments in the literature, two doses of VEGF and HGF delivery were used, an average of 150 ng/day and an average 15 ng/day. Initial results indicated the formation of blood vessels in the vicinity of implanted rods.

2. CHAPTER TWO

Long Term *In Vivo* Degradation, and Tissue Response to, Photo-Cross-Linked Elastomers Prepared from Star Shaped Prepolymers of Poly(ε-Caprolactone-co-D,L-Lactide)

Manuscript published online in the Journal of Biomedical Materials Research Part A. March 11, 2009

Authors: Chapanian R[1], Tse MY[2], Pang SC[2], and Amsden BG[1*]

[1]Department of Chemical Engineering and [2]Department of Anatomy and Cell Biology
Queen's University, Kingston, Ontario, Canada, K7L 3N6

* To whom correspondence should be addressed

ABSTRACT

Long term *in vivo* degradation, and tissue response to, cylindrical elastomers made of photo-cross-linked *star*-poly(ε-caprolactone-*co*-D,L-lactide) triacrylate were investigated through subcutaneous implantation in rats. The elastomers were prepared via UV initiated crosslinking of prepolymers of equimolar amounts of monomers; a high crosslink density elastomer (ELAST 1250) was prepared from a prepolymer of 1250 Da and a low crosslink density elastomer (ELAST 7800) was prepared from a prepolymer of 7800 Da. The elastomers were characterized using cross-polarization magic angle spinning (CP-MAS) solid state ^{13}C NMR and attenuated total reflectance infrared (ATR-FTIR) spectroscopy. The progress of the *in vivo* degradation process was followed by employing SEM, uniaxial tensile, mass loss, water uptake, and sol content measurements. The rate of *in vivo* degradation was faster than the rate of *in vitro* degradation for both ELAST 1250 and ELAST 7800. Long term *in vivo* degradation studies indicated that both elastomers undergo bulk hydrolysis along with surface erosion occurring due to the physiological environment. In the case of low cross-link density elastomers, the onset of mass loss was accompanied with an increase in both water uptake and sol content, whereas, in the case of high crosslink density elastomers, only the water uptake increased. This degradation pattern was due to crazing of the high crosslink density elastomers. ELAST 7800 cylinders were totally degraded, and ELAST 1250 cylinders had lost 80 % of their mass, within 30 weeks. A minor host reaction with minimal vascularity and inflammation was invoked, with a milder tissue response observed with more highly crosslinked cylinders.

Key words: biodegradable elastomer, *in vivo* degradation, degradation mechanism, tissue response, crosslink density.

2.1. INTRODUCTION

Biodegradable elastomers based on aliphatic polyesters such as poly(glycolic acid) (PGA), poly(lactic acid) (PLA) and poly(ε-caprolactone) (PCL) are resorbable and can be synthesized to possess mechanical properties close to those of native tissues [39]. Biomedical applications of degradable elastomers include tissue engineering [39, 50, 100] and drug delivery [13, 101]. There are, however, relatively few reports on the *in vivo* degradation of cured, biodegradable elastomers [102-104]. For further development of these biomaterials, it is important to ascertain factors influencing their *in vivo* degradation rate.

Elastomers can be prepared as either thermoplastic or crosslinked materials [105]. The degradation of aliphatic polyester thermoplastics occurs *in vivo* primarily by bulk hydrolysis, at a rate similar to the *in vitro* degradation rate [41-43, 106]. The hydrolytic degradation is a result of several processes occurring concurrently, which include: water absorption, ester hydrolysis, the diffusion of degradation products to the surface, and a local internal decrease in pH as a result of the production of acidic degradation products that are temporarily retained within the polymer bulk. This pH decrease catalyses the hydrolysis. The degradation exhibits two phases: the first phase is characterized by a linear decrease in mechanical strength after an induction period, with no, or very little, loss of mass, while the second phase is characterized by the onset of mass loss, an increase in water uptake, loss of mechanical strength, and the release of low molecular weight degradation products.[50-54] Enzymatic action has also been implicated in the degradation of aliphatic polyesters. For example, Jeong *et al*. found that porous scaffolds

made of poly(L-lactide-co-ε-caprolactone) lost 18.7 % of their mass *in vivo* after 15 weeks compared to only 5.7 % *in vitro*. They attributed this difference to a possible role of enzymes, *in vivo* [107]. Moreover, Pitt *et al*. found significant surface erosion of implanted, crosslinked poly(ε-caprolactone), and consequently reported that both enzymatic surface erosion and hydrolytic degradation contributed to the degradation of this crosslinked polymer [103].

In the tissue engineering of scaffolds, it is desirable to have a gradual transfer of load to newly formed tissues. Crosslinked elastomers could offer this requirement since they experience a linear decrease in strength with respect to mass loss during degradation [54, 102-104]. Furthermore, the rate of degradation and swelling [50], important factors in the design of scaffolds, can be tailored easily by controlling the crosslink density [39]. Our group recently reported on the *in vivo* degradation of photocrosslinked *star*-poly(ε-caprolactone-co-D,L-lactide) elastomers in male Wistar rats, wherein cylinders of two different crosslink densities with a diameter of 1.8-2.0 mm and length of 1 cm were implanted subcutaneously for a period of 12 weeks [102]. That study demonstrated that the degradation of the elastomers is dependent on the crosslink density. Highly crosslinked networks degraded in a manner consistent with a surface erosion mechanism, while networks of low crosslink density degraded in a manner consistent with a bulk degradation mechanism. The elastomers were well tolerated in the rats for 12 weeks reaching a mass loss of only approximately 30% [102]. The aims of this study were to investigate longer term *in vivo* degradation of photo-cross-linked *star*-poly(ε-caprolactone-co-D,L-lactide) elastomers, and to more fully elucidate the degradation

mechanism of, and tissue response to, these elastomers.

2.2. MATERIALS AND METHODS

D,L-Lactide (99+%) was obtained from Purac, the Netherlands, and purified by recrystallization from dried toluene. ε-Caprolactone was obtained from Lancaster, Canada, dried over calcium hydride, distilled under high vacuum and stored over activated 4 μm molecular sieves. Toluene and dichloromethane were dried over calcium hydride and distilled under argon. Other chemicals were used without further purification. Chemicals used in polymer synthesis include stannous 2-ethylhexanoate (96%) obtained from Aldrich, Canada and glycerol obtained from BDH, USA. Chemicals used in the acrylation process include acryloyl chloride (96%), triethylamine (99.5%), and 4-dimethylaminopyridine (99%), all obtained from Aldrich, Canada. 2,2-dimethoxy-2-phenylacetophenone used as photoinitiator was obtained from Aldrich, Canada. Solvents used for purification of the synthesized polymers include ethyl acetate (99.9%), methanol (99.8%), and tetrahydrofuran, and were obtained from Fisher, Canada.

2.2.1. Preparation of Elastomer Cylinders

7800 and 1250 Da acrylated *star*-poly(D,L-lactide-*co*-ε-caprolactone) prepolymer of equimolar monomer ratio (Figure 2-1A) was prepared as described previously [102]. Briefly, heated star-copolymer was poured into a dried round-bottomed flask, the flask sealed with a rubber septum, then purged with dry argon. The following procedures were conducted in a glove box. Dried dichloromethane (DCM) was added to the flask at a ratio of polymer to solvent of 2:1 (w:v) to dissolve the polymer. Triethylamine was added at a

molar ratio of 1 mole per mole of star-copolymer (SCP) hydroxyl group, while the 4-dimethylaminopyridine catalyst was added at a molar ratio of 2×10^{-3} mole per mole of SCP terminal hydroxyl group. Finally, acryloyl chloride was diluted in dried DCM at a ratio of 1:1 (v:v) and added slowly in a drop-wise fashion at a ratio of 1.2 moles per mole of SCP hydroxyl group. The degree of acrylation of the acrylated star copolymers (ASCP) was greater than 95 %, as confirmed by end-group analysis of acrylate group peaks at δ = 5.98-6.07 ppm and the disappearance of hydroxyl peaks of terminal caproyl groups at δ = 5.42 ppm and terminal lactyl groups at 5.29 ppm in the ^{1}HNMR spectra. The DLLA content in the star-copolymers was 49% for ASCP of 1250 and 49.9% for ASCP of 7800.

To prepare elastomeric rods, ASCP prepolymer of a given molecular weight was dissolved in ethyl acetate at a ratio of 1:1 (w:w) and 1.5 w/w(polymer) % of 2,2-dimethoxy-2-phenylacetophenone was added as a photo-initiator. A previous optimization study indicated that this initiator concentration is sufficient to produce elastomers with low sol contents [105]. The mixture was poured into glass tubes, flame sealed at one end and closed with a rubber septum at the other end. Five tubes were placed horizontally on a Petri dish and exposed for 10 minutes to long-wave UV light of an intensity of 10 mW/cm^2 using a Long Wave Black-Ray 100 YP UV lamp. The septa were removed, the tubes were placed in a fume hood overnight and then in a vacuum desiccator. After evaporation of ethyl acetate, the elastomer rods were gently removed from the glass tubes and left in a vacuum oven at 45 ºC for 2 days. After sol extraction using DCM, the weights and dimensions of the rods were measured. The rods had an

average diameter of 0.67 mm, length of around 15 mm and weighed between 6-7 mg. The rods were stored at –20ºC until implantation.

2.2.2. Degradation Studies

Before subcutaneous implantation, the cylinders were sterilized by soaking in 70 % ethanol for 1 hour then left overnight to dry in a laminar flowhood. Adult male Wistar rats (Charles River Laboratories, P.Q. Canada) weighing 250 g were used. Four elastomeric rods were implanted in each rat, and the implantation procedures were followed as described previously [102]. At 1, 4, 8, 14, 20, 26, and 30 weeks following implantation, rats were terminated by direct injection of a hypotonic solution into the heart. Consequently, the rats were shaved and the cylinders excised with the surrounding skin. The fibrous tissue capsules surrounding the implants were cut from the side and the cylinders were pulled out gently with tweezers. At later time points, the capsules were cut in the middle and the pasty polymer or small remaining solid particles pushed out by pressing. One cylinder at each study point was excised with the surrounding tissue and fixed in 4% paraformaldehyde in phosphate-buffered saline, processed for paraffin embedding, and stained with Masson's trichrome for histological examination. These studies were done under the guidelines of the Queen's University Animal Care Committee code of ethics governing animal experimentation (protocol # Amsden 2007-043-R1).

An *in vitro* degradation study was performed in pH 7.4 phosphate buffered saline. The pH of the buffer was maintained by replacing the buffer twice a week.

2.2.3. Physical measurements of explanted cylinders

For each time point up to week 14, 4 rats were sacrificed, and for each remaining time point 2 rats were sacrificed. From the 8 recovered cylinders up to week 14, three were used for tensile measurements, two were examined via SEM, and two were recovered along with the surrounding tissue for histology. Samples remaining from the tensile measurements were used to determine the sol content. Starting from week 20, the explanted samples were not suitable for tensile studies. Therefore, three of the four recovered samples were used for SEM and the sol content. The fourth sample along with surrounding tissue was used for histological examination. Immediately after explantation, the wet weights of the samples were measured. Dry weights were obtained by leaving the samples in a vacuum oven at 45ºC for 6 days. In order to determine sol content, dried samples were immersed in 3 ml dichloromethane per cylinder. The dichloromethane was replaced three times at 2 hr intervals, after which the samples were dried at 45ºC under vacuum for 6 days. Water uptake, mass loss, and sol content were determined from triplicate samples unless otherwise mentioned.

The mechanical properties of the freshly explanted elastomers were measured in uniaxial tension using an Instron uniaxial tensile tester model 4443. The crosshead speed was set at 500 mm/min according to ASTM D412. All specimens were tested at room temperature. Data analysis was carried out using a Merlin 4.11 Series IX software package.

SEM images were recorded with a JSM-840 scanning microscope using a 10 kV

electric field and a tungsten filament. For bulk images, samples were freeze-fractured in liquid nitrogen and glued into holes made in a solid polyester mold. For surface images, double-sided adhesive tape was used to anchor the samples to the specimen holder. The samples were gold coated under vacuum using a VI-A pulse-sputter coating system from Anatech Ltd.

^{13}C NMR spectra of non-cross linked ASCP were acquired on a 500 MHz Bruker-Avance spectrometer at a polymer concentration of 10% using $CDCL_3$ as solvent. The solid state, ^{13}C NMR was acquired using cross-polarization magic angle spinning (CP-MAS) spectrometry. The samples were run on a 600 MHz Bruker-Avance spectrometer at a spinning rate of 14 050 Hz, contact time of 2 ms, and a relaxation delay of 2 s. Attenuated total reflectance Fourier transform infrared (ATR-FTIR) analyses were performed using a Nicolet Avatar 320 FTIR with a golden gate, a single pass diamond attenuated total reflectance attachment was employed, operating with 32 scans and at a resolution of 4 cm^{-1}. Data was analyzed using GRAMS/32 AI(32) (6) software.

2.2.4. Statistics

All data are presented as the mean ± the standard deviation about the mean.

2.3. RESULTS AND DISCUSSION

2.3.1. Characterization of Elastomers

The chemical structure of the prepolymers were investigated using ^{13}C NMR and that of the elastomers using solid state ^{13}C NMR. As an example, the NMR spectra of

both acrylated prepolymer of 1250 Da and its corresponding elastomer, ELAST 1250, are provided in Figure 2-1B. A high degree of acrylation was obtained as indicated by the absence of peaks corresponding to carbons next to terminal groups (C_4 at 67.1 ppm and C_5 at 20.7 ppm). Upon photocrosslinking, peaks corresponding to C_{12}, C_{13} and C_{14} of the terminal acrylate group disappeared and new peaks, C_{15}, C_{16}, and C_{17}, appeared. These peak assignments, corresponding to the acrylate carbons, are in agreement with those of Bertmer *et al.*, for methacrylate carbons in UV cured oligo(L-lactide-*ran*-glycolide)dimethacrylates [108].

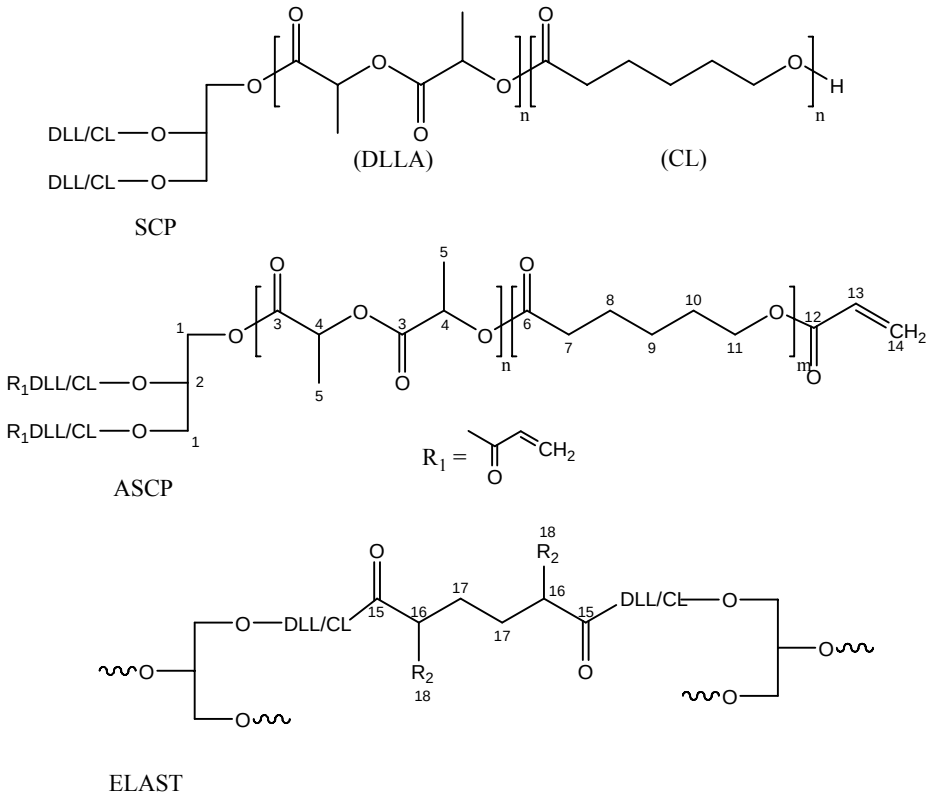

Figure 2-1A

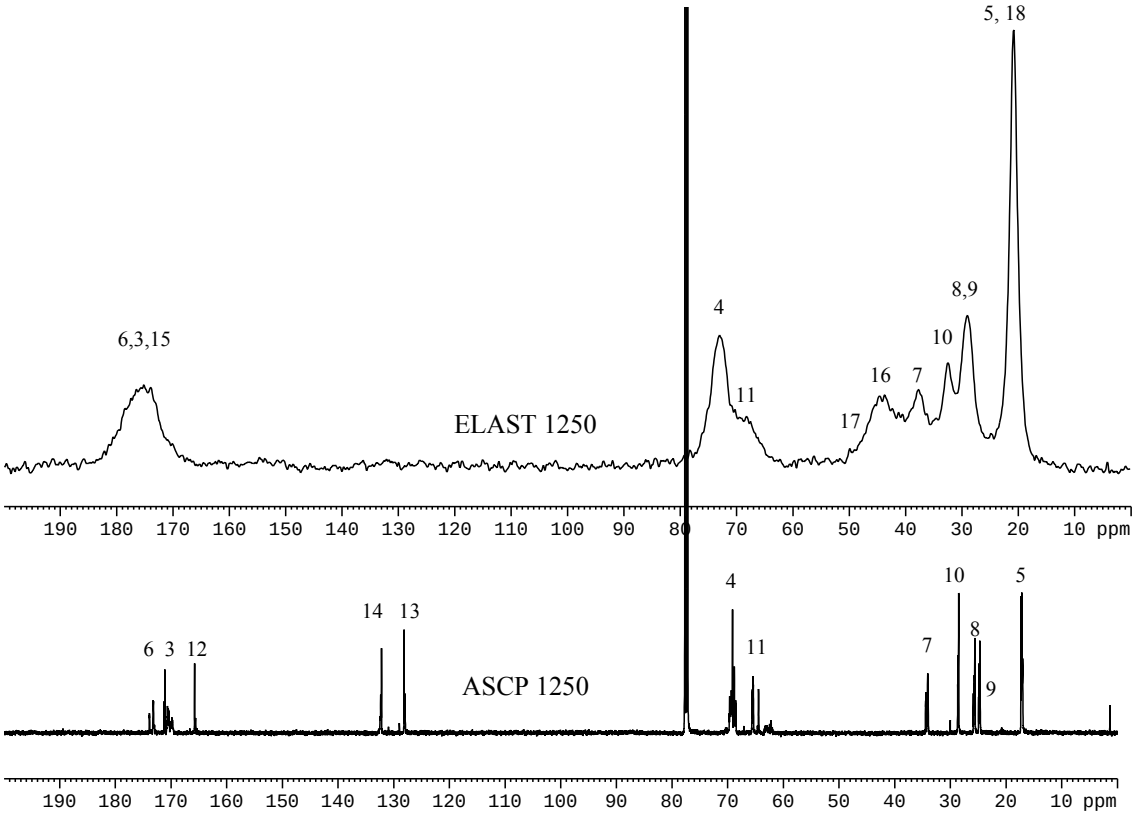

Figure 2- 1. A) The structure of the random star (SCP), the acrylated star copolymer (ASCP), and the crosslinked elastomer (ELAST). B) ^{13}C NMR spectrum of a representative acrylated star copolymer (ASCP 1250), and CP-MAS 13C solid state NMR spectrum of ELAST 1250. R_2 in the acrylate portion of ELAST 1250 is either a methyl group generated from the photoinitiator, 2,2-dimethoxy-2-phenylacetophenone (Irgacure 651)[109] or a hydrogen.

The prepolymers and elastomers were further investigated using ATR-FTIR. Figure 2-2A indicates the formation of 3 new bands upon acrylation (ASCP 1250) appearing at 810 cm^{-1}, 1407 cm^{-1}, and at 1628 cm^{-1}. These bands are assigned as follows: 813 cm^{-1} corresponds to the wagging vibration of the vinyl CH_2, 1407 cm^{-1} corresponds to the in-plane scissor vibration of the vinyl CH_2, and the 1635 cm^{-1} band is assigned to C=C stretching. Upon photocuring and the formation of ELAST 1250, these bands were greatly diminished in intensity (Figure 2-2B). The spectrum of ELAST 1250 was recorded at a depth of 1mm, where discs of ELAST 1250 with 2.5 mm diameter and 4

mm height were prepared in a Teflon mold. These samples were cured by exposing them to UV light at an angle perpendicular to the surface. Consequently, a 1mm section was removed and the new surface analyzed using ATR-FTIR. Other bands are assigned as follows: the band at 1750 cm^{-1} is assigned to C=O stretching, the band at 1080 cm^{-1} to C-O-C stretching, the band at 1450 cm^{-1} C-H stretching in methyl groups of DLLA, and the band at 1043 cm^{-1} to C-CH3 stretching vibrations [110, 111].

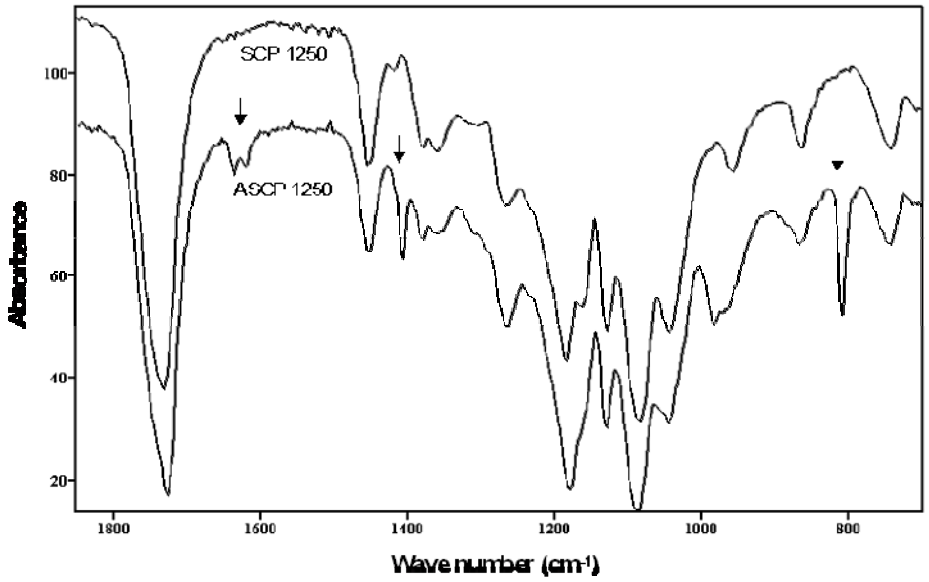

Figure 2-2A

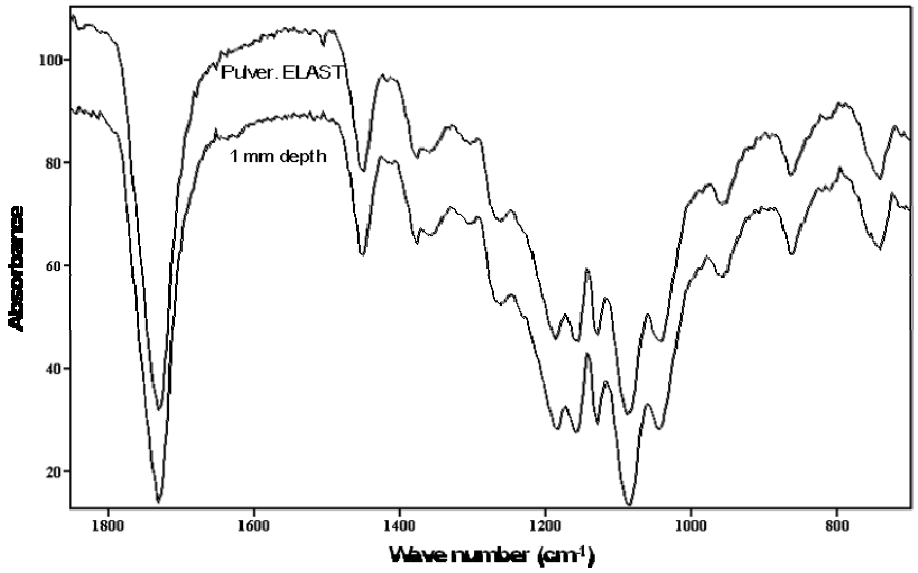

Figure 2-2B

Figure 2- 2. A) ATR-FTIR spectra of star copolymer (SCP 1250, top spectrum) and acrylated star copolymer (ASCP 1250, bottom spectrum), and photo-cured elastomer (ELAST 1250, bottom spectrum). Arrows indicate to the newly formed peaks as a result of acrylation process. (2B) ATR-FTIR spectrum for pulverized elastomer (ELAST 1250, top spectrum) and spectrum recorded at a depth of 1 mm (ELAST 1250, bottom spectrum)

A representative stress-strain diagram of the elastomers is presented in Figure 2-3. The mechanical, and thermal properties, of the elastomers are presented in Table 2-1. ELAST 1250 is much stiffer than ELAST 7800 with a modulus approximately 50 times greater, and it had a yield point, whereas ELAST 7800 is approximately 3 times more extendable. Correspondingly, ELAST 1250 had a glass transition temperature almost 20ºC higher than that of ELAST 7800, and the glass transition temperatures of both elastomers were below body temperature.

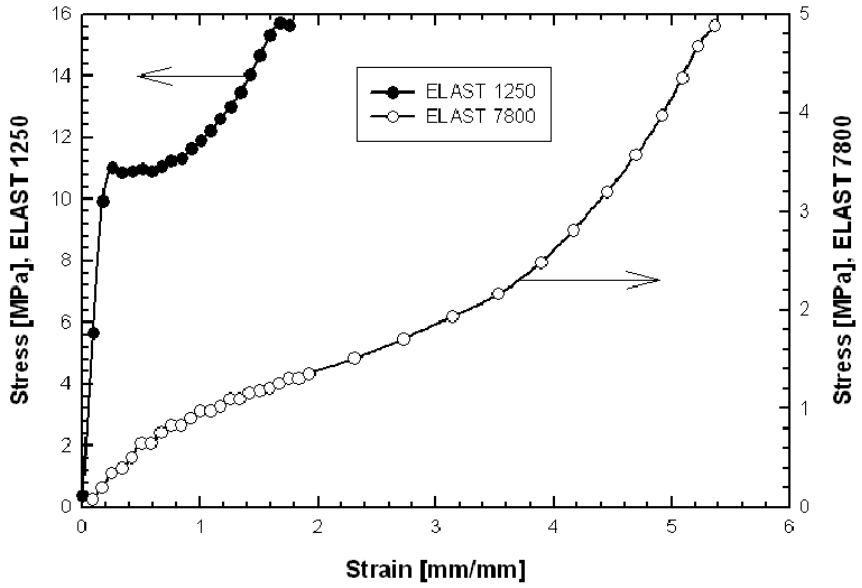

Figure 2- 3. A representative stress-strain diagram of the elastomers. The data represent the average of triplicate samples; the error bars were removed for clarity.

Table 2- 1. Mechanical and thermal properties of the elastomers. Data represent the average of triplicate samples given with the standard deviation about the average value.

Elastomer	E (MPa)	σ_b (MPa)	ε_b (mm/mm)	T_g (°C)
1250	57.3 ± 2.8	18.8 ± 2.8	1.9 ± 0.3	18 ± 1
7800	1.2 ± 0.1	5.4 ± 2.1	5.4 ± 0.5	-1 ± 1

2.3.2. Degradation Results

The changes in mechanical properties of the elastomers during the *in vivo* degradation period are given in Figure 2-4. ELAST 7800 cylinders exhibited little change in the modulus up to 4 weeks of implantation (Figure 2-4A); the modulus then decreased in a linear fashion up to week 14. By week 14, ELAST 7800 cylinders were very weak and their mechanical properties could not be measured. In contrast, the modulus of ELAST 1250 cylinders decreased continually with time, beyond the first week.

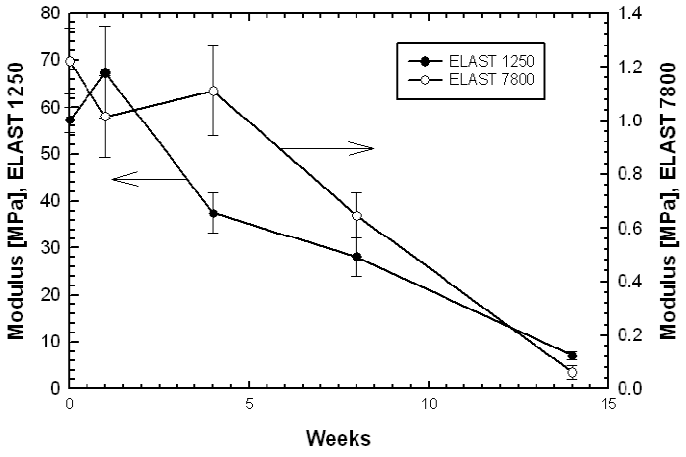

Figure 2-4A

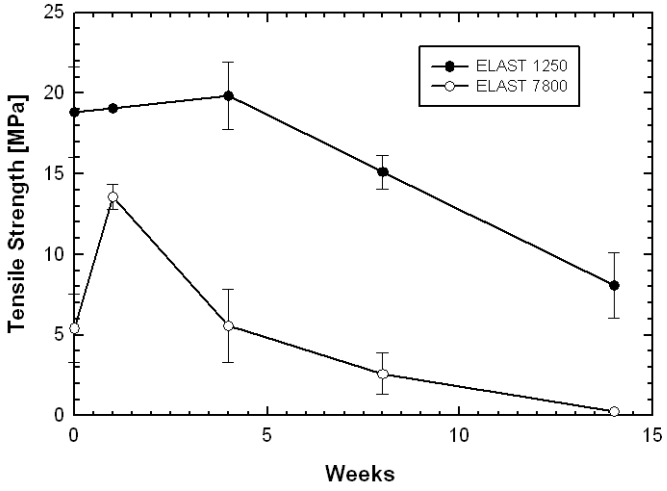

Figure 2-4B

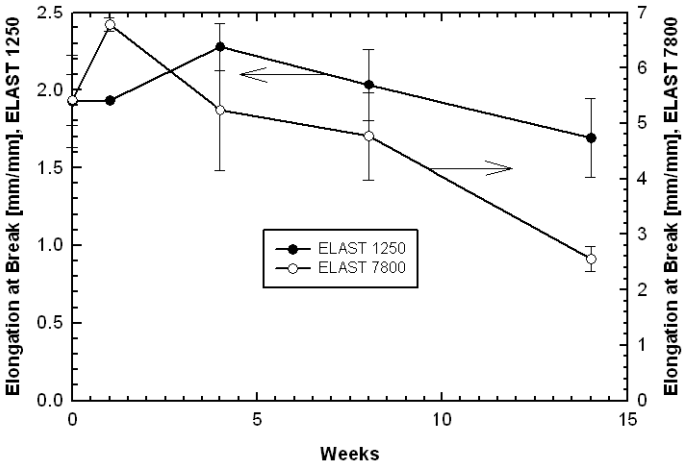

Figure 2-4C

Figure 2- 4. Effect of *in vivo* degradation on mechanical properties of ELAST 1250 and ELAST 7800, implanted subcutaneously in rats: A) modulus (E) B) ultimate tensile stress (σ_b) C) strain at break (ε_b). The data represent the average of triplicate samples and error bars the standard deviation about the average value. At week 1, ELAST 1250 was characterized using a single sample.

Changes in tensile strength of the elastomers during the *in vivo* degradation are shown in Figure 2-4B. The tensile strength of ELAST 7800 cylinders increased 2.5 times at week 1 to 13.6 ± 0.8 MPa from the initial value of 5.4 ± 2.1 MPa. At week 4 the tensile strength decreased to values similar to that of week 1, after which it decreased linearly until week 14. After week 14 the material was very weak and mechanical properties could not be measured. Similarly, ELAST 1250 experienced a linear decrease in tensile

strength from week 4 to week 14. After week 14 the material lost its integrity due to deep cracks formed in the material. The tensile strength of ELAST 1250 at week 1 was determined from a single sample, because of slippage of the other samples within the grips of the tensile tester.

In contrast to the observed decrease in modulus and tensile strength with degradation time, ELAST 1250 did not experience significant alteration in its strain at break; at week 14, the strain at break had only decreased to 88 % of the initial value of 1.9 ± 0.03 % (Figure 2-4C). The ELAST 7800 samples experienced a sharper decrease, retaining only 47 % of their initial value of 5.4 ± 0.5 %.

The increase in mechanical properties after a short period of exposure to water is attributed to the antiplasticization effect of water molecules penetrating the inter-chain spaces of elastomeric networks and establishing hydrogen-bonded bridges [112]. Similar observations have been reported in other studies. For example, Storey *et al*., who examined the *in vitro* degradation of thermally crosslinked methacrylate end-capped poly(trimethylene carbonate-co-D,L-lactide) of varying trimethylene carbonate composition, reported an increase in tensile strength for almost all trimethylene carbonate compositions [113]. This phenomenon is also observable in the data of Pego *et al*. and Karajalainen *et al*., who examined the degradation of high molecular weight poly(trimethylene carbonate) and aliphatic polyesters [51, 114].

In vivo, mass loss of ELAST 7800 was noticeable after week 4 (Figure 2-5). By

week 14 the samples had lost 14.5 ± 2.4 % of their dry mass, after which accelerated mass loss occurred; the dry mass of the remaining pasty material at week 20 was approximately 15 %. By week 26, there was no ELAST 7800 present at the implantation sites. The mass loss of the ELAST 7800 cylinders paralleled their water uptake (Figure 2-6) and sol content (Figure 2-7). Accelerated mass loss started after a significant increase in swelling and water uptake at week 14 (Figure 2-5). By contrast, mass loss of the highly crosslinked networks of ELAST 1250 began much later, starting after week 14, and the rate of mass loss was slower (Figure 2-5). The sol content of ELAST 1250, in contrast to that observed for ELAST 7800, remained below 10% throughout the degradation period (Figure 2-7). The onset of mass loss in the ELAST 1250 cylinders was accompanied by a slight increase in the sol content, increasing from 1.9 ± 1.9 % at week 14 to 8 ± 3.9 % at week 20, returning to essentially 0% by week 26 and then rising to 4.7 ± 0.0 % by week 30.

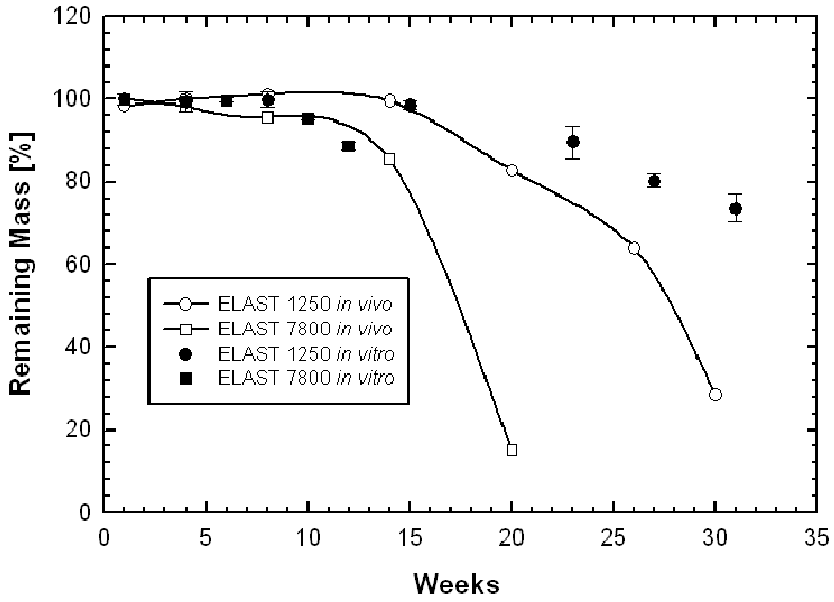

Figure 2- 5. Remaining mass of ELAST 1250 and ELAST 7800 during *in vivo* and *in vitro* degradation. Points represent the average of triplicate samples and error bars on each side of points

are the standard deviation from the average value. The data represent the average of triplicate samples and error bars the standard deviation about the average value.

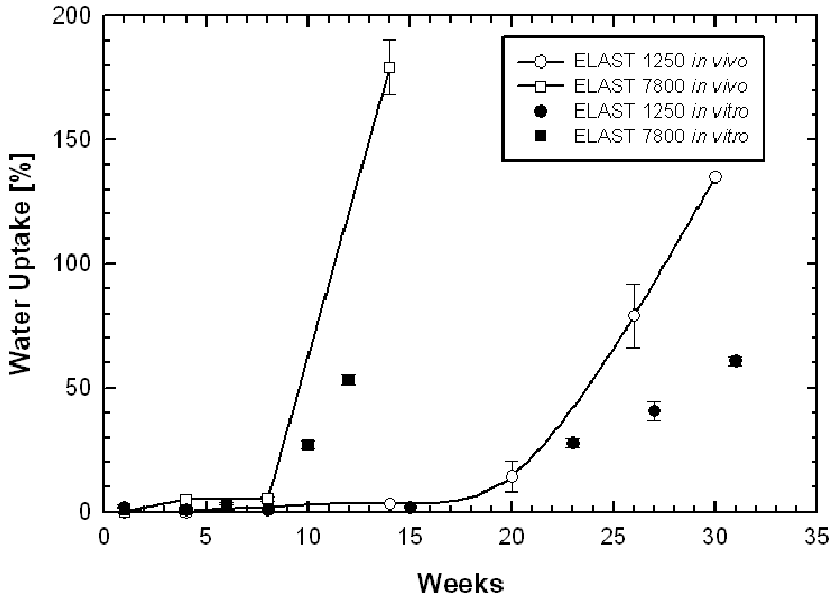

Figure 2- 6. Change in water uptake of ELAST 1250 and ELAST 7800 during *in vivo* and *in vitro* degradation. The data represent the average of triplicate samples and error bars the standard deviation about the average value.

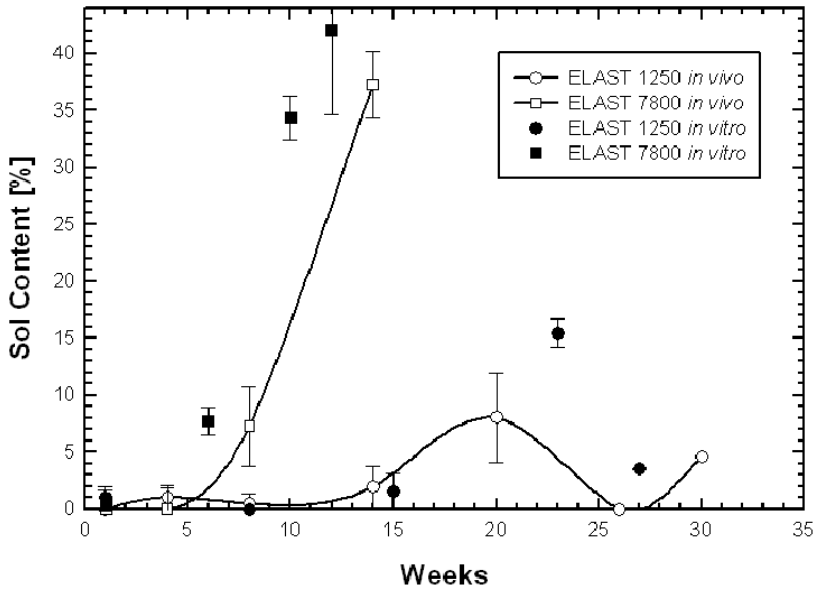

Figure 2- 7. Change in sol content of ELAST 1250 and ELAST 7800 during *in vivo* and *in vitro* degradation. The data represent the average of triplicate samples and error bars the standard deviation about the average value.

In the *in vitro* degradation studies of ELAST 1250, the onset of mass loss started at week 15, after which a linear mass loss was observed up to week 31. At 31 weeks the elastomer samples had lost 26.4 ± 3.3 % of their mass (Figure 2-5). The water uptake and sol content of the *in vitro* degraded ELAST 1250 samples are illustrated in Figures 2-6 and 2-7, respectively. Water uptake started to increase after week 15 and reached 60.8 ± 1.8 % at week 31, whereas the sol content remained below 17 % during the investigation period, and exhibited the same pattern as observed in the *in vivo* degraded samples.

In the *in vitro* degradation studies of ELAST 7800, and ELAST 1250, the water uptake, and mass loss closely followed the pattern observed in the *in vivo* degradation studies (Figures 2-5, 2-6, and 2-7). The rate of degradation, however, was faster for the *in vivo* degrading elastomers. *In vivo* degraded ELAST 1250, for example, lost 71.7 ± 2.0 % of its mass at week 30 compared to 26.4 ± 3.3 % for the *in vitro* degraded ELAST 1250 at week 31.

To help explain these results, SEM images were taken of the surface and of freeze-fractured cross-sectional areas of degrading cylinders at various times. SEM images of both elastomeric networks showed dense homogenous surfaces and bulk structures with very few pore defects (Figure 2-8A, w0). By week 1, shallow cracks had developed on the outer surface of ELAST 7800 cylinders, whereas the cross-section remained dense and intact (Figure 2-8A, w1). By week 4, deeper cracks had developed on the outer surface of ELAST 7800 cylinders (Figure 2-8A, w4). By week 8, the cracks had intensified on the outer surface of ELAST 7800 cylinders, dark regions had

developed, and crater-like circular spots with a diameter of 10 to 25 μm were observable (Figure 2-8A, w8). The dark regions on the surface of the elastomer are likely due to oxidative or enzymatic activity on the surface of the elastomer, as suggested by the absence of dark regions in cylinders degraded *in vitro* (Figure 2-8B). Both components of the elastomer, poly(DLLA) and poly(CL), are prone to oxidation [115], and poly(CL) is prone to enzymatic degradation [116].

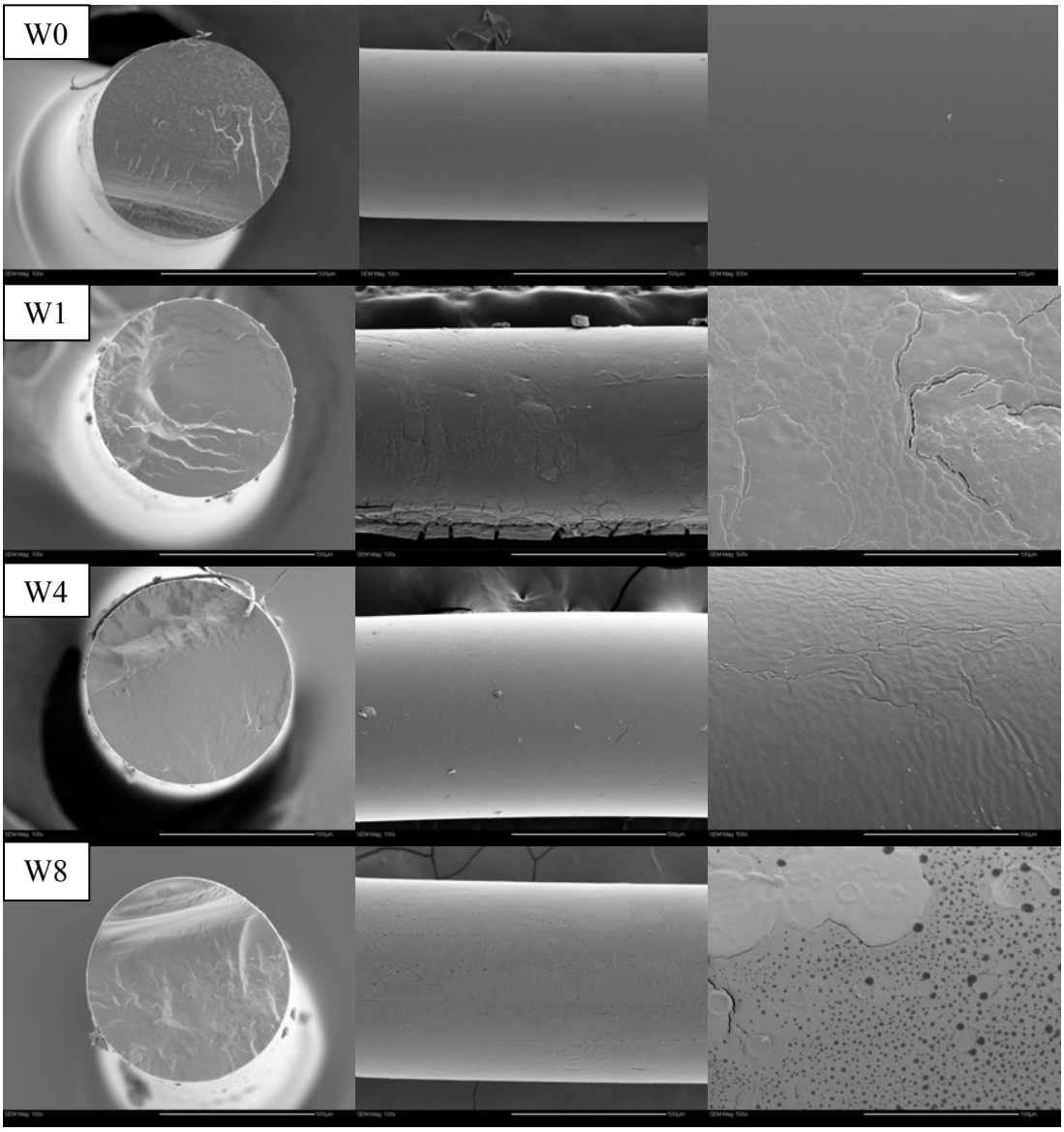

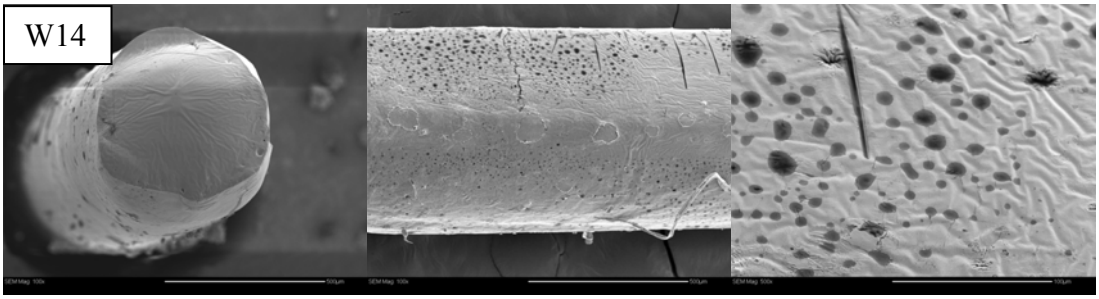

Figure 2-8A

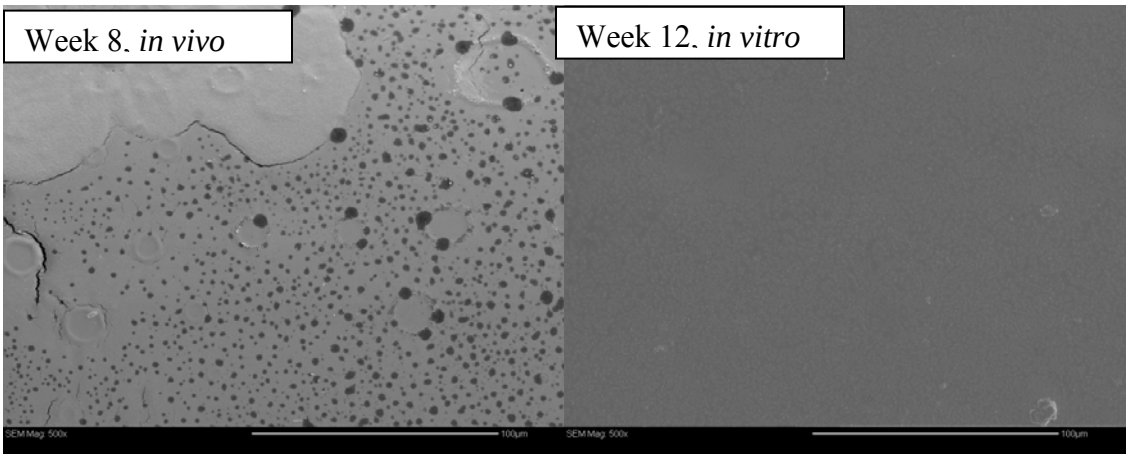

Figure 2-8B

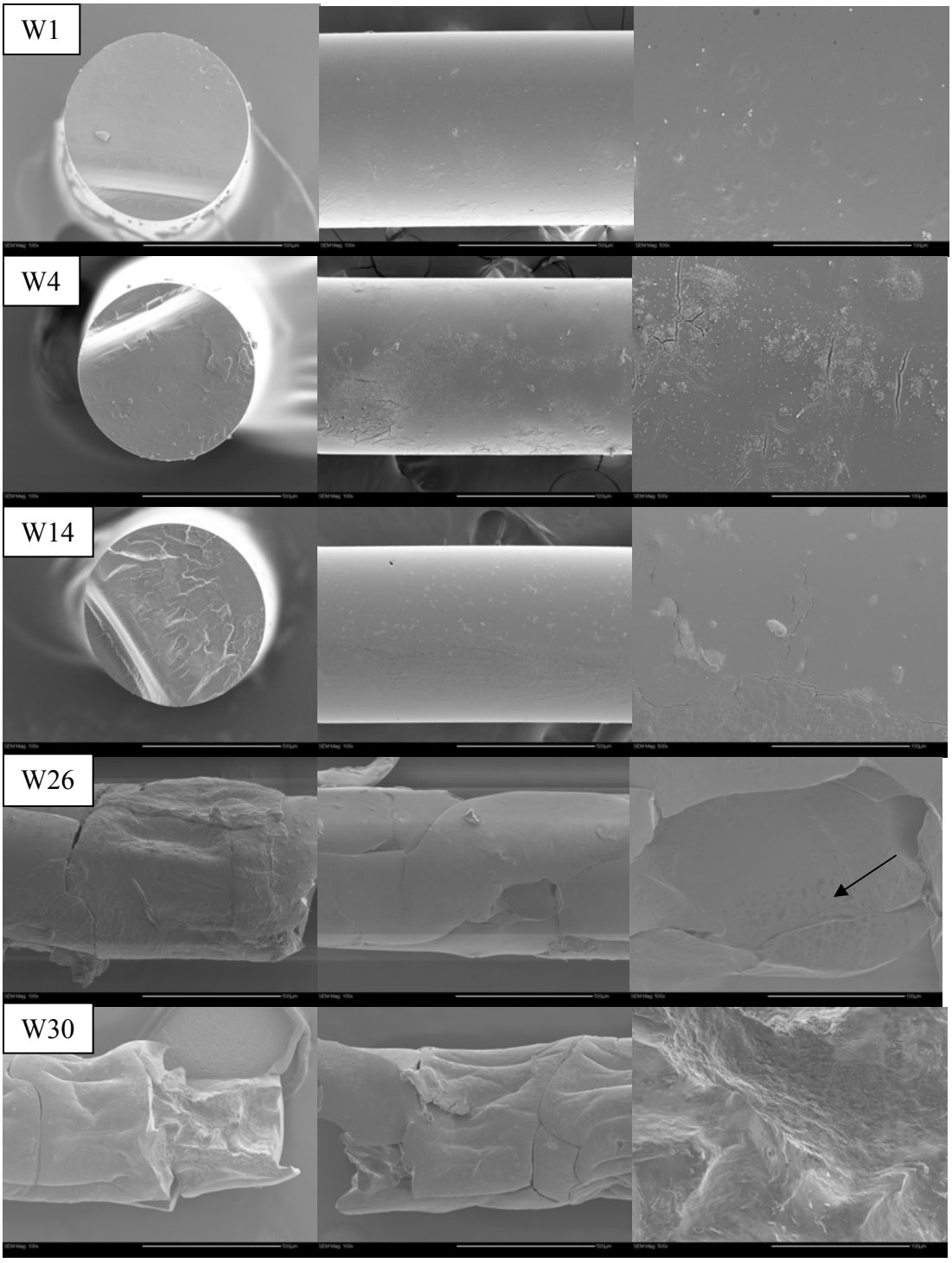

Figure 2-8C

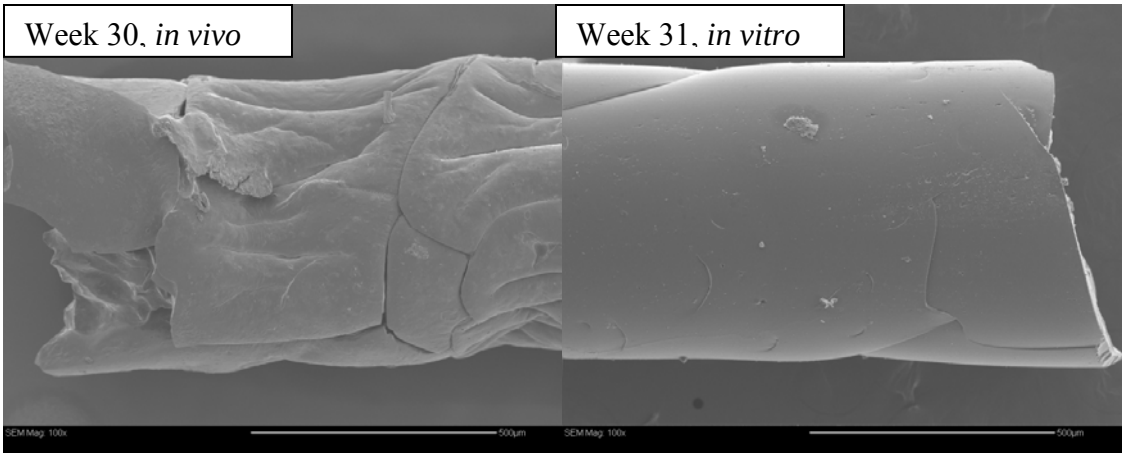

Figure 2-8D

Figure 2- 8. Scanning electron micrographs of in vivo and in vitro degraded elastomers: A) ELAST 7800 cylinders at different stages of *in vivo* degradation. B) Comparison of *in vivo* and *in vitro* degrading cylinders of ELAST 7800. (scale bar = 100 µm) C) ELAST 1250 cylinders at different stages of *in vivo* degradation. In A and C the scale bar is equal to 500 µm in the left side and middle images and is equal to 100 µm in the right side images. The arrow points to dark spots seen at week 26 for ELAST 1250 D) Comparison of *in vivo* and *in vitro* degrading cylinders of ELAST 1250. (scale bar = 500 µm)

SEM images of cross-sections of ELAST 1250 samples showed a dense material at different stages of the *in vivo* degradation (Figure 2-8C). Development of cracks also occurred in the highly cross-linked ELAST 1250 samples, but at much later stages of implantation compared to ELAST 7800 samples; cracks developed by week 14 in ELAST 1250 samples compared to week 4 in ELAST 7800 samples. The dark spots seen at week 8 in ELAST 7800 cylinders were seen at week 26 in ELAST 1250 samples, and were less numerous (Figure 2-8C). Furthermore, the surface of *in vivo* degraded ELAST 1250 was eroded more extensively than the surface of *in vitro* degraded ELAST 1250 (Figure 2-8D).

The hydrolytic degradation of ELAST 7800 cylinders occurred in a fashion consistent with the expected outcomes of bulk degradation, known to be composed of two phases as described in the Introduction. The first phase of the degradation of ELAST

7800 cylinders extended up to week 10, with significant loss of mechanical properties and only slight, or no, loss of mass. The second phase of bulk degradation began after week 10, wherein the hydrolysis reaction became autocatalyzed by the acidic degradation products. In this process, internal acidic degradation products require longer time to diffuse out of the sample, thus autocatalyzing the degradation process and generating an osmotically active region that draws in water. By week 14, the SEM images indicate that the ELAST 7800 cylinders had begun to deform, corresponding to an increase in sol content and water uptake. Consequently, the elastomer failed and turned into a pasty material by week 20. The homogenous core of ELAST 7800 at week 14 and the absence of pores and cavities normally seen in materials degrading by bulk hydrolysis [117] suggests the occurrence of relatively homogenous hydrolysis in ELAST 7800 rods. The soluble portion in DMSO of the pasty degraded material of ELAST 7800 at week 20 yielded a composition of 44.6% DLLA and 55.4% ε-caprolactone (CL), by means of ^{1}HNMR analysis. This result is in agreement with results reported by Pitt *et al*., who radio-labeled DLLA in copolymers of poly(DLLA-co-CL) with ^{14}C to determine any preferential erosion of lactide monomer over ε-caprolactone. They found only a slightly greater preferential lactide loss in spite of the rate constant of chain scission of poly(DLLA) being 2.8 times greater than that of poly(CL) [43].

In ELAST 1250, the hydrolytic degradation, however, proceeded in a different fashion. The first phase of degradation was similar to ELAST 7800, where significant loss of mechanical properties occurred without any loss in mass. The onset of mass loss and increase in water uptake, however, did not accompany an increase in sol content. The

decrease in mass without an increase in sol content indicates the formation of water-soluble degradation products. In their studies of the hydrolytic degradation of highly cross-linked poly(CL) networks, prepared from a prepolymer of molecular weight of 2110 Da, Storey *et al*., observed a similar pattern of degradation, wherein the mass loss was accompanied by an increase in the water uptake, but there was no increase in the sol content [54]. This result is attributed to crazing of the stiff, degrading ELAST 1250 due to the absorption of water [118]. As a result of crazing occurring concomitantly with hydrolysis, small cracks develop leading to fracturing. The cracks propagate faster in the stiffer ELAST 1250 than in the more ductile ELAST 7800. Crack propagation may also be exacerbated by the presence of residual stresses in the elastomer that may result from a non-uniform crosslinking reaction throughout the bulk of the elastomer.

SEM images of later stages of degradation of ELAST 1250 indicated clearly, the formation of deep cracks in both *in vitro* and *in vivo* degraded elastomers (Figure 2-8D). The cracks, however, were more intense in the *in vivo* degraded elastomers. This finding is likely due to the presence of mechanical stresses *in vivo*, caused by the movements of the animals, which are absent in the *in vitro* degrading elastomers. This movement results in faster crack propagation *in vivo*. This mechanism of enhanced *in vivo* compared to *in vitro* degradation due in part to dynamic loading leading to crack generation has been demonstrated previously in poly(lactide) implanted subcutaneously in rats in a similar manner as in this study [119]. There are also more recent *in vitro* studies that show that dynamic loading of poly(lactide-co-glycolide) porous scaffolds and foams leads to faster degradation [120, 121]. In our case, this cracking results in portions of the elastomer

breaking from the surface, leading to the slight increase in sol content at week 20 *in vivo*.

2.3.3. Tissue Response

In order to investigate the effect of cross-link density on tissue response, tissues surrounding both highly cross-linked, ELAST 1250 and low cross-linked, ELAST 7800 were studied histologically. Staining with Masson's trichrome was performed to determine the host reaction as reflected in capsule formation and composition. Masson's trichrome stains collagen blue, nuclei black, and cytoplasm and muscle fibers red. Histological results indicate a minor host reaction, consisting of a thin dynamic fibrous capsule (Figure 2-10). Cells present in the capsule were mainly fibroblasts with a few multinucleated giant cells at the interface of the implanted elastomers. The capsule thickness and cell type and number present were a function of the hydrolytic degradation activity of the elastomer. The minor degradation of ELAST 1250 up to week 30 was reflected in a stable capsule with less cellular concentration consisting mainly of fibroblasts. On the other hand, the high degradation activity of ELAST 7800 at week 14 was reflected in a thicker capsule and higher cellular activity.

At week 1, there was a minor inflammatory response at the site of implantation for both ELAST 1250 and ELAST 7800. Multi-nucleated giant cells, lymphocytes and neutrophils were plentiful adjacent to the implant-tissue interface. The cellular content gradually diminished until week 14. In the case of ELAST 7800 cylinder implants, drastic changes took place between weeks 14 and 20. At 20 weeks, there appeared to be a heightened inflammatory response in the implanted site, coinciding with the increase in

mass loss of the elastomer and the likely release of acidic degradation products. There was no visible sign of intact ELAST 7800 cylinders at the implantation site at week 20. The implantation site (together with the capsular area) developed into a fibrotic structure at this time point. Histologically, this structure exhibited features typical of the regular dense connective tissue such as ligament or tendon. Externally, this event coincided with the development of minor skin irritation so that rats responded to these internal changes by scratching, resulting in occasional skin lesions or sores. This response was relatively short-lived and subsided within one week. In the case of ELAST 1250, a well-organized capsule persisted throughout the study period with very little inflammatory response adjacent to the implant-tissue interface. No lesions developed for the duration of the study period with these cylinders.

With both ELAST 7800 and 1250 cylinders, vascularization at the implant site initially developed in the area adjacent to the implant. The degree of vascularization decreased over time such that by week 14 there was very little evidence of vascularization near the implantation site. This decrease in vascularization is indicative of stabilization of the host response and fibrous encapsulation of the implant. The capsule thickness surrounding ELAST 1250 implants at week 1 was approximately 20 μm in contrast to that surrounding the ELAST 7800 implants, which had a thickness of 70 μm. The capsule thickness of the ELAST 7800 implants increased to 90 μm by week 14, whereas the capsule surrounding ELAST 1250 cylinders maintained stable at a thickness of 70 μm from week 4 through to week 30.

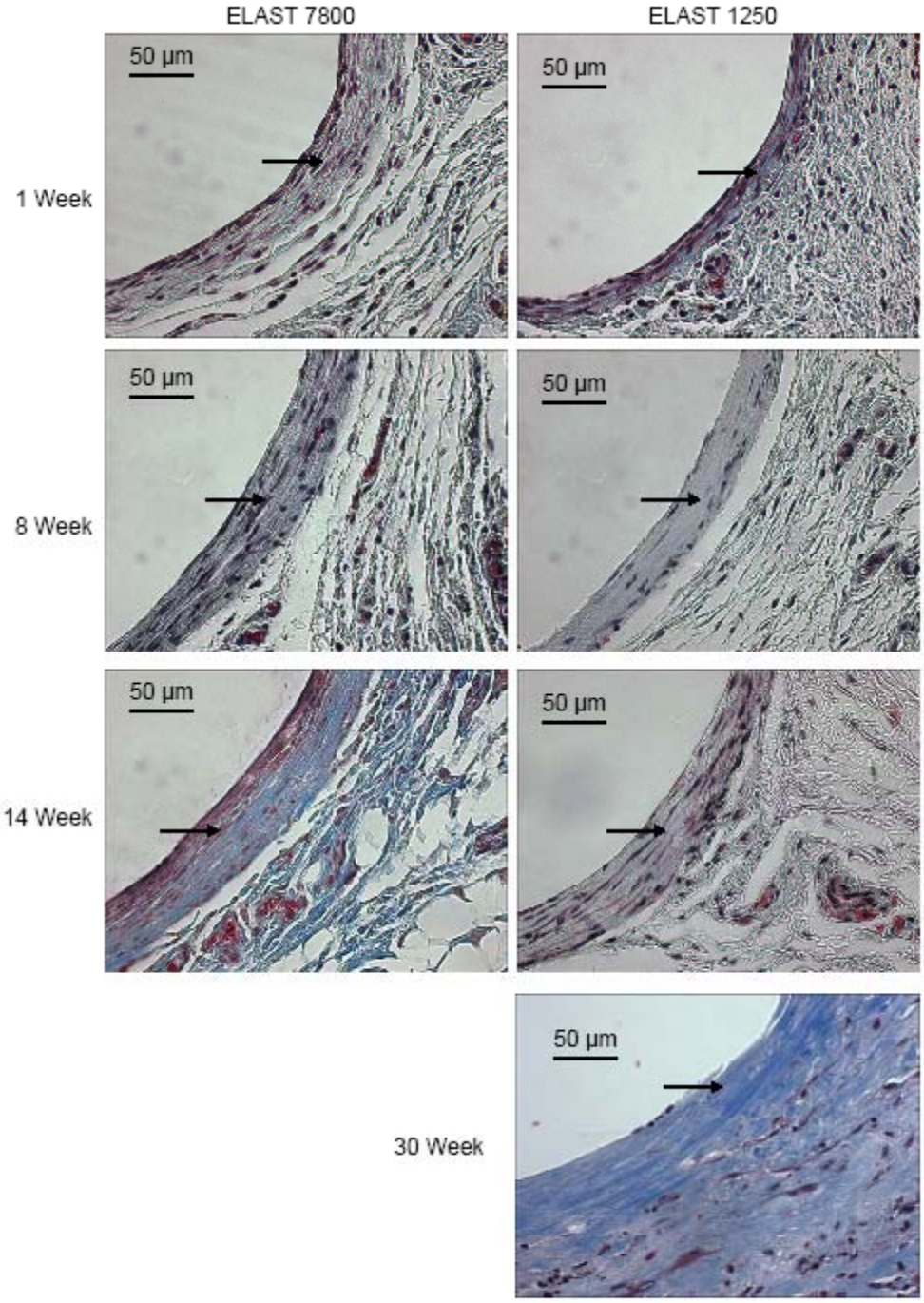

Figure 2- 9. Histological sections of the tissue surrounding the implant stained with Masson's trichrome at different stages of *in vivo* degradation. The left panel represents tissues surrounding ELAST 7800 and the right panel represents tissues surrounding ELAST 1250. The arrow indicates the capsule located at the implant-tissue interface.

2.4. CONCLUSIONS

Both high crosslink density ELAST 1250 and low crosslink density elastomers underwent primarily bulk hydrolysis along with a minor amount of surface erosion due to the physiological environment. The pattern and the rate of degradation, however, were different and a function of the crosslink density. In ELAST 7800, the onset of mass loss was accompanied by an increase in both water uptake and sol content, whereas, in the case of ELAST 1250, only the water uptake increased. This phenomenon was assigned to crazing leading to crack formation within the ELAST 1250. SEM analyses of the later stages of degradation indicated a distinct difference between the surfaces of *in vivo* and *in vitro* degraded elastomers. In the case of ELAST 7800, dark spots and pits observed in the *in vivo* degraded ELAST 7800, were absent in the *in vitro* degraded elastomers and in the case of ELAST 1250 there were far more numerous deep cracks and small particles and extensive surface erosion in the *in vivo* degraded elastomers. As a result, the rate of *in vivo* degradation was faster than the rate of *in vitro* degradation for both elastomers. The elastomers were very well tolerated in the rats; after 30 weeks, ELAST 7800 samples were totally degraded and ELAST 1250 samples lost 80 % of their mass. Tissue staining with Masson's trichrome indicated a minor host reaction, minimal vascularity, and insignificant inflammation. Furthermore, the surrounding fibrous capsule was thin and dynamic. Tissue response to implants in the case of ELAST 1250 was milder than that of ELAST 7800 samples.

3. CHAPTER THREE

The Role of Oxidation and Enzymatic Hydrolysis on the *In Vivo* Degradation of Trimethylene Carbonate based Photo-cross-linked Elastomers

Mamuscript published in Biomaterials. 2009, 30, p: 295 – 306.

Authors: Chapanian R[1], Tse MY[2], Pang SC[2], and Amsden BG[1*]

[1]Department of Chemical Engineering and [2]Department of Anatomy and Cell Biology
Queen's University, Kingston, Ontario, Canada, K7L 3N6

* To whom correspondence should be addressed

ABSTRACT

The *in vivo* degradation of trimethylene carbonate (TMC) containing elastomers was investigated, and the mechanism of degradation explored through *in vitro* degradation under enzymatic and oxidative conditions. The elastomers were prepared via UV initiated cross-linking of prepolymers of TMC and equimolar amounts of TMC and ε-caprolactone (CL). The degradation process was followed by investigating the changes in the mechanical properties, mass loss, water uptake, sol content, differential scanning calorimetry, and surface chemistry through attenuated total reflectance infrared (ATR-FTIR) spectroscopy. During i*n vivo* degradation, TMC and TMCCL elastomers exhibited surface erosion. The tissue response was of greater intensity in the case of the TMC elastomer. Both elastomers exhibited degradation in cholesterol esterase containing solutions *in vitro*, but no parallels were found between the rate of *in vivo* degradation and the rate of *in vitro* degradation. Only the TMCCL elastomer degraded in lipase. Degradation in a stable superoxide anion *in vitro* medium was consistent with the observed *in vivo* degradation results, indicating a role of oxidation through the secretion of this reactive oxygen species by adherent phagocytic cells in the degradation of these elastomers.

Keywords: *in vivo* degradation, enzymatic degradation, oxidative degradation, tissue response

3.1. INTRODUCTION

Synthetic biodegradable elastomers based on trimethylene carbonate (TMC) are potentially useful materials in many biomedical applications, such as tissue engineering scaffolds and drug delivery [19]. Importantly, TMC based polymers degrade by surface erosion without producing acidic products [122], and thus could possibly be used to prepare more effective acid sensitive protein delivery systems. We are interested in the use of photo-cross-linked biodegradable elastomers prepared from ω,ω′,ω′′-triacrylate star-poly(TMC) and star-poly(TMC-co-ε-caprolactone) for this purpose. The *in vivo* mechanism of degradation of, and tissue reaction to, such implants are of great importance, as they provide an idea about the environment in which the therapeutic proteins are retained and eventually released.

Upon implantation, a series of events occurs that results in monocytes moving from the blood to the implanted material surface. The monocytes adhere to the surface in a manner determined by the type, concentration, and conformation of proteins adsorbed to the material surface. Within 48 hours, monocytes are the predominant cell type at the biomaterial surface, and ultimately differentiate into monocyte-derived macrophages over a period of several weeks. On the surface, the macrophages spread and, as a result of frustrated phagocytosis, release reactive oxygen species as well as hydrolytic enzymes, and may fuse to form foreign body giant cells (FBGCs) [123]. FBGCs have an increased capacity for enzyme and reactive species secretion, and are longer lived than macrophages. The extent of monocyte adhesion and ultimately FBGC formation, as well as secretion capacity, have been shown to be determined by the chemistry of the material

surface [124-127]. Thus, there are multiple possible degradation mechanisms for implanted polycarbonates, including acid-base catalyzed hydrolysis, as well as enzymatically catalyzed hydrolysis and oxidation from reactive oxygen species as a result of the response of phagocytic cells.

The data to date indicate that acid or base catalyzed hydrolysis of the carbonate bonds plays a negligible role in *in vivo* degradation. Mizutani and Matsuda investigated the hydrolytic degradation of photo-cured poly(TMC) and copolymers of poly(TMC-co-ε-caprolactone) terminated with coumarin with different ratios of caprolactone (CL) at pH values ranging from 7.4 to 10.2. They found that, irrespective of copolymer composition, hydrolysis occurred on the surface, and the rate of hydrolysis increased as pH and CL content increased [128]. However, when the elastomers were prepared from *star*-poly(trimethylene carbonate) triacrylate, negligible hydrolysis occurred [129]. This difference in degradation is likely due to the photo-reversibility of the [2+2] cycloaddition linkage formed upon crosslinking with coumarin. Zhang *et al*. found that in *in vitro* environments with pH values ranging from 1 to 13, both high and low molecular weight uncrosslinked, linear poly(TMC) degraded extremely slowly. This result has been confirmed by others for low molecular weight poly(TMC) degrading in phosphate buffered saline [130]. Similar results have been reported for poly(ethylene carbonate) immersed in aqueous media with pH ranging from 1 to 12 by Stoll *et al*. [38].

Zhang *et al*., on the basis of the negligible *in vitro* degradation, also examined enzymatic degradation and showed that in the presence of lipase the polymer degraded

appreciably and in a manner consistent with surface erosion [19]. Moreover, poly(TMC) of greater than about 100 kDa degraded faster *in vivo* and *in vitro* in the presence of lipase than poly(TMC) of lower molecular weight [19]. They attributed this latter result to greater enzyme activity on the surface of the more hydrophobic, higher molecular weight, polymers.

In contrast to these results, Stoll *et al*. reported that poly(ethylene carbonate) was unaffected by the presence of hydrolytic enzymes in aqueous media [38]. They showed that, *in vitro*, poly(ethylene carbonate) did not degrade in the presence of hydroxyl radicals, but did degrade in a surface erosion manner in the presence of superoxide anion. Acemoglu *et al*., examined the *in vivo* degradation of both poly(ethylene carbonate) and poly(TMC) and found that poly(ethylene carbonate) degraded much faster [38, 44]. On the basis of the results of Stoll *et al*., it was proposed that the *in vivo* degradation of poly(ethylene carbonate) and poly(TMC) implants proceeds by oxidation via superoxide anion radicals and that the slower oxidation of poly(TMC) was due to the more stable six-membered ring of trimethylene carbonate that is proposed to form as a result of degradation [38, 44]. Others have also reported oxidative degradation of carbonate containing polymers in the presence of superoxide anion. For example, Lee *et al*. treated commercially available Maxon sutures made of a block copolymer of 32.5 wt% of TMC and 67.5 wt% of glycolide with different concentration of KO_2/18-crown-6 ether /THF and found significant mass losses over a 24 h time period [115]. They concluded that the degradation observed had occurred mainly in the glycolide blocks since the carbonate group in the poly(TMC) is less reactive toward nucleophilic attack. Recently, Christenson

et al. reported that, although the tested polymers were susceptible to both *in vitro* enzymatic and oxidative degradation, poly(carbonate urethane) degradation *in vivo* also was consistent with an oxidation mechanism [45].

Thus, it is currently unclear as to whether poly(TMC) undergoes degradation *in vivo* primarily through either oxidation or enzyme action. There has been only one study supporting enzymatic degradation, which was performed using *Thermomyces lanuginosus* lipase. Moreover, other esterases, in particular cholesterol esterase, have also been implicated in the degradation of polycarbonate based urethanes. It was reasoned, therefore, that cholesterol esterase may be effective in the degradation of poly(TMC) and its copolymers. Furthermore, more studies support the possibility that poly(TMC), like other polycarbonates, is degraded primarily through oxidative attack. We therefore hypothesized that oxidation also plays a role in the degradation of poly(TMC) elastomers.

TMC is also often co-polymerized with monomers such as ε-caprolactone and D,L-lactide to adjust mechanical properties and degradation rates. The literature indicates the susceptibility of poly(CL) segment of different copolymers to both oxidation and enzymatic hydrolysis [115, 116, 131]. For example, Gan *et al*. exposed blends of poly(D,L-lactide) and poly(ε-caprolactone) to *Pseudomonas* lipase and found that only CL regions were prone to enzymatic degradation [116]. Similar results have been reported by Li *et al*., who found that the 80 % weight loss in poly(CL) over 3 days of exposure to *Pseudomonas* lipase was reduced to 10 % in a blend of poly(CL) and L-lactide and to 0 % in poly (L-lactide) [131]. Moreover, Darwis *et al*. found that

crosslinking poly(CL) via radiation reduced the rate at which lipase AK degraded the samples, and that the rate of reduction increased as the crosslinking density increased.[132] The role of oxidation in the degradation of poly(CL) was demonstrated by Lee and Chu, who showed that poly(CL) was susceptible to superoxide ion-induced degradation [13]. Thus, it was reasoned further that oxidation would play a role in the degradation of elastomers prepared from prepolymers of poly(TMCCL).

Thus, the objective of this paper was to gain a better understanding of the *in vivo* degradation mechanism of photo-cured TMC and TMCCL elastomers, to determine the rate of change of their mechanical properties during degradation, and to determine the role of oxidation in the overall degradation process. To do this, *in vivo* degradation and *in vitro* enzymatic and oxidative degradation studies were conducted using elastomers made of TMC and equimolar amounts of TMC and CL. For literature comparison purposes, both *Thermomyces lanuginosus* lipase and porcine pancreas cholesterol esterase were used as model enzymes. The degradation process was followed by investigating the changes in the mechanical properties, mass loss, water uptake, sol content, and glass transition temperature. Changes in the surface features of the elastomers were followed by SEM and ATR-FTIR analyses, and the biological response was examined histologically by light microscopy.

3.2. MATERIALS AND METHODS

1,3-trimethylene carbonate (1,3-dioxan-2-one) was obtained from Boehringer Ingelheim, Germany and used as received. ε-Caprolactone (99 %) was obtained from

Lancaster Canada, dried over calcium hydride, and distilled under high vacuum. Toluene and dichloromethane were dried over calcium hydride and distilled under argon. Other chemicals were used without further purification. Chemicals used in polymer synthesis include stannous 2-ethylhexanoate (96%) obtained from Aldrich, Canada and glycerol obtained from BDH, USA. Chemicals used in the acrylation process include acryloyl chloride (96%), triethylamine (99.5%), and 4-dimethylaminopyridine (99%) obtained from Aldrich, Canada. 2,2-dimethoxy-2-phenylacetophenone used as a photoinitiator was obtained from Aldrich, Canada. Solvents used for purification of the synthesized polymers include ethyl acetate (99.9%) and methanol (99.8%), obtained from Fisher, Canada. Lipase from *Thermomyces lanuginosus* with a concentration of 10^5 units/g and cholesterol esterase from porcine pancreas with a concentration of 23,600 units/g were purchased from Aldrich, Canada. Materials used for oxidation studies included potassium superoxide, 18-crown-6 ether, iron (II) chloride (98%), cobalt chloride, hydrogen peroxide, and dried THF, all obtained from Sigma, Canada.

3.2.1. Star-Copolymer Polymerization

7800 g/mol star-copolymers of TMC and equimolar compositions of ε-caprolactone and TMC were prepared as described elsewhere [133]. Briefly, theoretical amounts of glycerol and monomers were placed in a dried glass ampoule. The ampoule was placed in an oil bath at 90 ºC, to melt the monomers. The ampoule was then purged with argon and the required amount of stannous 2-ethylhexanoate calculated on the basis of 3×10^{-3} mol of catalyst per mole of glycerol was added. The ampoule was vacuum-sealed and placed in an oven for 3 days at 130ºC. The termini of the star polymers formed

were acrylated using acryloyl chloride. 4-dimethylaminopyridine (DMAP) was used as a catalyst and triethylamine (TEA) was used to scavenge hydrochloric acid formed during the acrylation reaction. Polymers made of TMCCL were purified according to the following procedure: 50 mL of methanol were added to 10 g of the polymer, the mixture was mixed vigorously for 2 hrs using a magnetic stirrer, after which the mixture was kept at -20°C for 5 hrs. The methanol was decanted and the process repeated 3 times. Purification of the TMC polymer was identical with the exception of the addition 1 mL DCM per 10 g of polymer prior to the addition of methanol. The purity of the synthesized prepolymers and their degree of acrylation were determined using a 500 MHz Bruker Avance NMR.

3.2.2. Preparation of Elastomer Rods

Prepolymer of a given molecular weight was dissolved in ethyl acetate at a ratio of 1:1 (w:w) and 2,2-dimethoxy-2-phenylacetophenone was added (1.5 wt%) as a photo-initiator. The mixture was poured into Pyrex glass capillary tubes, which had previously been flame sealed at one end, and closed with a rubber septum at the open end. Five tubes were placed horizontally on a Petri dish and exposed for 10 minutes to long-wave UV radiation at an intensity of 10 mW/cm^2 using a Black-Ray 100 YP UV lamp. The septa were removed, the tubes were placed in a fume hood overnight and then in a vacuum desiccator. Following sol extraction using dichloromethane, the weights and dimensions of the rods were measured. Rods made of TMC had an average diameter of 0.86 ± 0.02 mm, an average length of 14.1 ± 0.9 mm, and an average weight of 10.8 ± 0.7 mg, while rods made of TMCCL had an average diameter of 0.83 ± 0.02 mm, an average

length of 15.4 ± 1 mm, and an average weight of 9.7 ± 0.9 mg. The ± represent standard deviations about the mean.

3.2.3. *In vivo* Degradation Studies

Elastomer rods were sterilized by immersion in 70 % ethanol for 1 hour and then left overnight to air dry in a laminar flow hood. Adult male Wistar rats (Charles River Laboratories, P.Q. Canada) weighing 250 g were anaesthetized with 2% isoflurane (Baxter Corporation) in oxygen by inhalation via an Engler ADS 1000 ventilator (Benson Medical Industries, Vancouver, Canada) at a total flow rate of 0.2 mL per min of O_2. At a level of surgical anesthesia (*i.e.* absence of tail and corneal reflexes), the rats were shaved at the nape of the neck. This site was chosen to minimize the possibility of the rats chewing on the implant site post-operatively. Implantation surgery was done under aseptic conditions. The shaved area was disinfected with Hibitane, and four 1 cm, longitudinal incisions were made to allow the implantation of four 1.5 cm elastomer rods. The skin at the incision site was blunt dissected from muscle tissue adjacent to the incision, and one rod was placed in each subcutaneous pocket thus formed. The incisions were closed by two simple interrupted square knots with 3-0 degradable Vicryl sutures. At 1, 4, 8, 16, 28 and 44 weeks following implantation, rats were anaesthetized with an intra-peritoneal injection of Somnotol (60 mg/kg) and, at a level of surgical anesthesia, the rats were shaved and the polymer implants excised with the surrounding skin. The fibrous tissue capsules surrounding the implants were opened and the rods were gently removed. In addition, one rod from each animal at each study point was excised with the surrounding tissue and fixed in 4% para-formaldehyde in phosphate-buffered saline,

embedded in paraffin, sectioned and stained with Masson's trichrome for histological examination.

Experimental protocols pertaining to the use of rats in this study were approved by the Animal Care Committee of Queen's University in accordance with the guidelines of the Canadian Council on Animal Care.

3.2.4. *In vitro* Enzymatic Degradation

Enzymatic degradation was conducted in duplicate using a 0.5 mL solution for each elastomeric rod. Each rod was located in a separate Eppendorf tube that was agitated on an Eppendorf Thermomixer at rotational speed of 550 rpm and temperature of 37˚C. The degradation solutions were replaced in a sterile laminar flow hood to prevent bacterial infection. Lipase solution was used as received (10^5 units/g) and replaced weekly. At time points of 1, 4, 6, and 8 weeks, two rods each of the TMC and TMCCL elastomers were washed with 70% ethanol and dried *in vacuo* at 40˚C. Cholesterol esterase (CE) was used at a concentration of 1 unit/ml, prepared by dissolving the powdered enzyme, 23,600 units/g, in a pH 7, 1X phosphate buffer. The prepared solution was stored at –70˚C until required. The CE degradation solution was replaced every 3 days to maintain high enzymatic activity [134].

3.2.5. *In Vitro* Oxidation Studies

Oxidation of the elastomers was investigated in both organic and aqueous media. The oxidation studies in organic media were conducted according to the method

established by Lee *et al*., which consisted of a mixture of KO_2 (0.01 M) and 18-crown-6 ether (0.002 M) in dried THF [115]. These conditions generate superoxide anion. The oxidation mixture was prepared under N_2 and the reaction was terminated by acidifying the mixture with 6M HCl [115]. The oxidation studies in aqueous media were conducted using two different radical generating systems. The first was Fenton's reagent with a Fe^{2+}/H_2O_2 molar ratio of 0.11 and 1% (v/v) of hydrogen peroxide in the final solution [135], and the second was an oxidative solution of $H_2O_2/CoCl_2$, where radicals were formed using a solution of 20% H_2O_2/0.1 M of cobalt chloride. This reaction produces hydroxyl radicals and hydroxyl anions. The mixture was replaced every 3 days to maintain high radical activity [45]. To determine the extent of any hydrolytic degradation, an *in vitro* degradation study was performed in pH 7.4 phosphate buffered saline. At time points of 1, 4, 12, 18, 24, and 30 weeks, 5 rods were removed from buffer and the mechanical properties, water uptake, sol content, and glass transition temperature measured.

3.2.6. Physical Measurements of Explanted Cylinders

Immediately after excision, the samples were weighed to determine the wet weight (w_w). To determine dry weight (w_d), samples were dried in a vacuum oven at 45˚C for 3 days. The water uptake was calculated using the following equation,

$$\text{water uptake}\,[\%] = \frac{w_w - w_d}{w_d} \times 100 \qquad (3\text{-}1)$$

Mass loss was calculated using the following equation,

$$\text{mass loss}[\%] = \frac{w_0 - w_d}{w_0} \times 100 \qquad (3\text{-}2)$$

in which w_0 is the initial weight of the sample before implantation. In order to determine sol content, dried samples were immersed in 3 mL dichloromethane per rod. The dichloromethane was replaced three times at 2 hr intervals, after which the samples were dried at 45˚C under vacuum for 3 days. The sol content was calculated using the following equation,

$$\text{sol content}\ [\%] = \frac{w_d - w_e}{w_d} \times 100 \qquad (3\text{-}3)$$

in which w_e is the weight of the sample after sol extraction. Water uptake, mass loss, and sol content were determined from triplicate samples unless otherwise mentioned.

From the 8 recovered rods at each point of the *in vivo* degradation study, 4 rods were used for tensile measurements, one rod for SEM studies, one rod along with those used in the tensile measurements were used to determine the sol content and thermal properties, and two rods were recovered along with the surrounding tissue for histology. As the intent was to obtain polymer properties that were representative of those present *in vivo*, the explanted rods were not treated following removal. The mechanical properties of the freshly excised elastomers were measured in uniaxial tension using an Instron uniaxial tensile tester model 4443. The crosshead speed was set at 500 mm/min according to ASTM D412. All specimens were tested at room temperature. Data analysis was

carried out using a Merlin 4.11 Series IX software package. SEM images were obtained using a JSM-840 scanning electron microscope using a 10 kV electric field and a tungsten filament. The samples were gold coated under vacuum using a VI-A pulse-sputter coating system from Anatech Ltd. The thermal properties of the elastomers were measured using a Q100 differential scanning calorimeter (TA Instruments Inc.). Samples with a weight of 8-12 mg were subjected to heating-cooling-heating cycles after cooling them to –80ºC. The rate of heating and cooling was 5ºC/min. The glass transition temperature was determined using the TA Universal Analysis software. Attenuated total reflectance Fourier transform infra-red (ATR-FTIR) analyses were performed using a Nicolet Avatar 320 FTIR with a golden gate, a single pass diamond attenuated total reflectance attachment was employed, operating with 32 scans and at a resolution of 4 cm^{-1}. Data was analyzed using GRAMS/32 AI(32) (6) software. Prior to analyses, samples were treated with 6 M urea in 12 mM Triton X-100, to remove adsorbed enzymes and proteins from the surface.

3.3. RESULTS

3.3.1. Prepolymer characterization

The chemical structures of the synthesized prepolymers are presented in Figure 3-1 and the physical properties of the prepolymers are listed in Table 3-1. Analysis via ^{1}H-NMR revealed that the TMCCL-78 prepolymer contained 49.4 mole % CL and 50.6 mole % TMC, and it was terminated with 54.6 mole % TMC and 45.5 mole % CL. Thus, under the polymerization conditions used, CL had a slightly higher reactivity than TMC. The number average molecular weight was 7300 g/ mol for the TMC prepolymer and 8200

g/mol for the TMCCL prepolymer, as measured by GPC. The degree of acrylation was high in each case, as determined from the reduction of the intensity of end group protons of H_{11} of CL at $\delta = 1.4$ ppm and H_6 of TMC at $\delta = 2.3$ ppm. The glass transition temperature of the prepolymers was far below physiologic and did not change after acrylation.

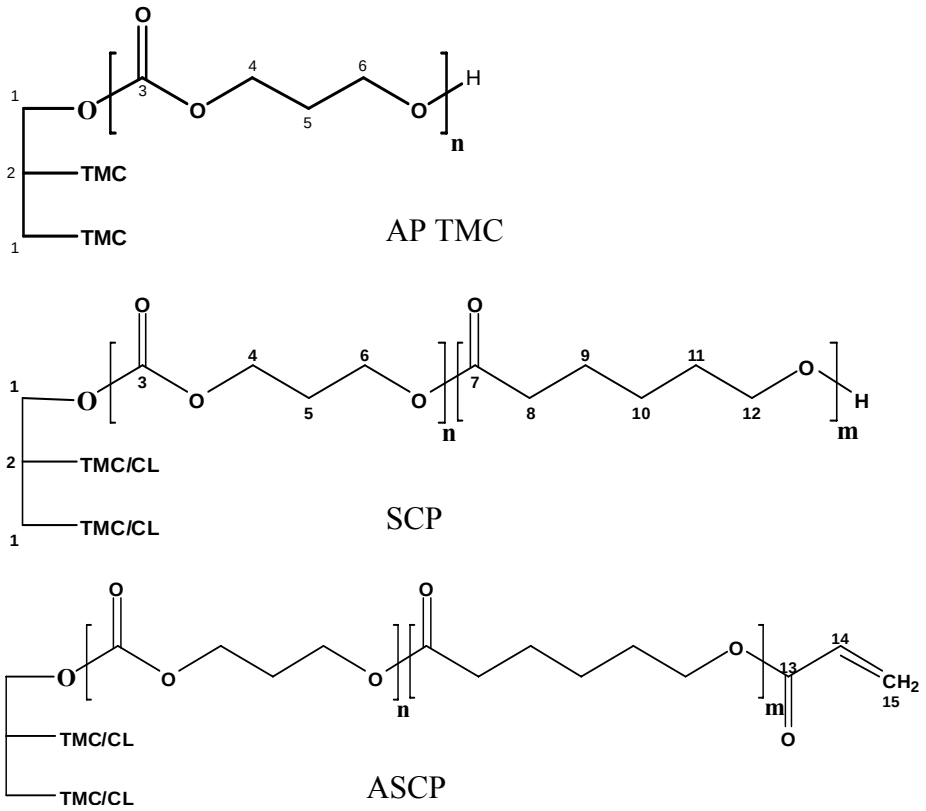

Figure 3- 1. The chemical structure of star-poly(TMC) (SP TMC), and star co-polymer TMCCL (SCP TMCCL), before and after acrylation (ASCP TMCCL refers to acrylated star copolymer of TMC and CL).

Table 3- 1. Physical properties of the synthesized prepolymers

Prepolymer	Mn (Da)	PI	Tg (^oC)[1]	Tg (^oC)[2]	DA [%]
TMC-78	7.3	1.6	-20.5	-20.5	85.5
TMCCL-78	8.2	1.7	-48.6	-48.4	90

[1] properties before acrylation
[2] properties after acrylation
DA: degree of acrylation, M_n determined by GPC

The thermal and initial mechanical properties of the elastomers are listed in Table 3-2. Representative stress-strain curves are shown in Figure 3-2. Both elastomers were rubbery and amorphous at ambient temperatures, as expected from the low values of glass transition temperatures. Furthermore, both elastomers were highly extensible. The TMC-78 elastomer extended almost 2 times more than TMCCL-78 elastomer and required 4 times greater stress to break. Moreover, the TMC elastomer had a more noticeable yield point than the TMCCL elastomer.

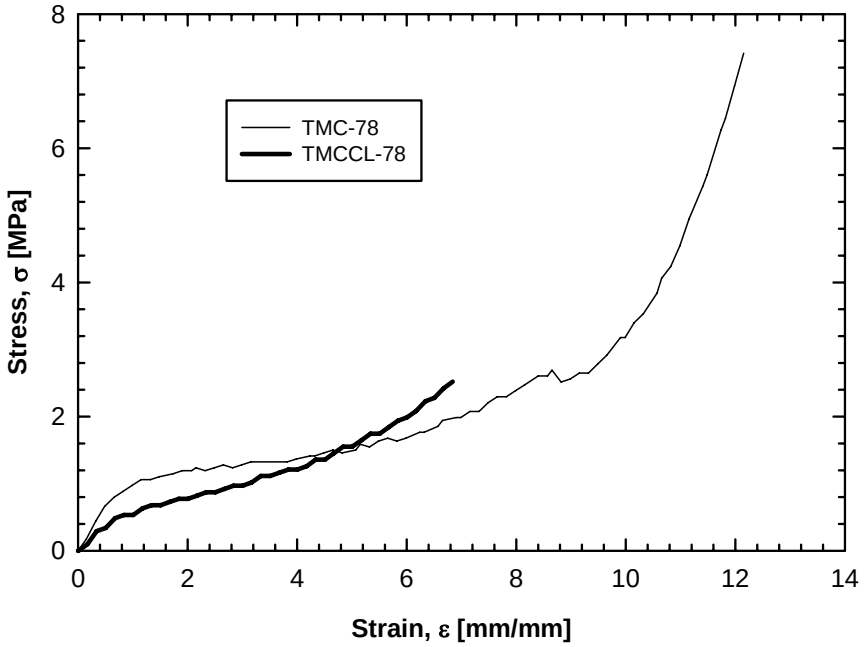

Figure 3- 2. Representative stress-strain curves of TMC-78 and TMCCL-78 elastomers.

Table 3- 2. Mechanical and thermal properties of synthesized elastomers.

Elastomer	E (MPa)	σ_b (MPa)	ε_b (mm/mm)	T_g (°C)	Sol Content [%]
TMC -78	1.44 ± 0.15	7.23 ± 0.16	11.80 ± 0.51	-12.1	15.60 ± 0.30
TMCCL-78	0.83 ± 0.14	1.73 ± 0.58	5.24 ± 1.52	-42.1	8.90 ± 1.10

E: Young's modulus, σ_b: stress at break, ε_b: elongation at break, T_g: glass transition temperature

3.3.2. *In vivo* degradation

The TMC-78 elastomer exhibited a mass loss profile consistent with a surface erosion mechanism, that is, a nearly linear mass loss with time (Figure 3-3). After an initially slower and nearly linear mass loss with time, the rate of mass loss increased markedly after week 28 for the TMCCL-78 elastomer. The overall *in vivo* degradation rate of the TMC-78 elastomer was 1.6 times faster than the TMCCL-78 elastomer; at week 44, TMC-78 elastomers had lost 33 ± 7.2 % of their initial mass, whereas TMCCL-78 elastomers had lost 20.6 ± 4.8 % of their initial mass.

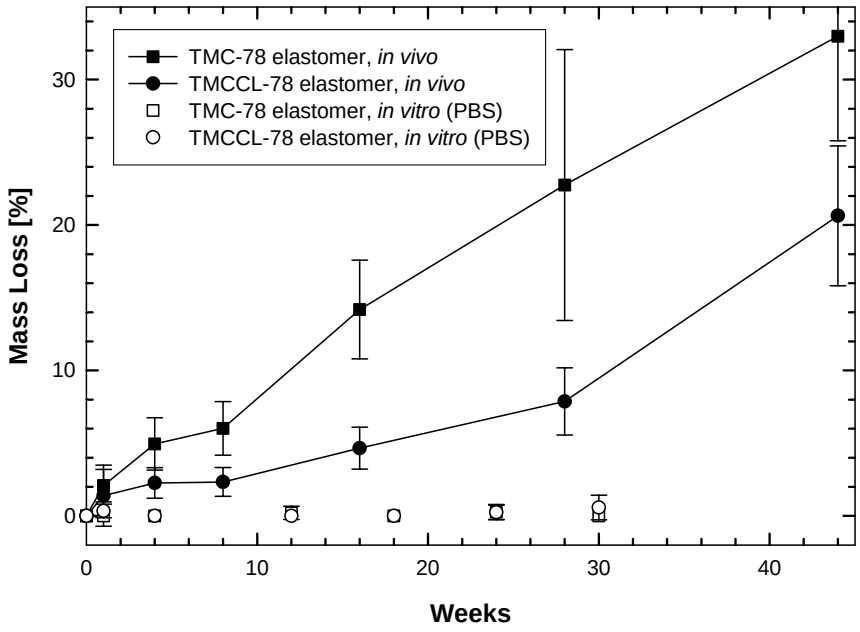

Figure 3- 3. Mass loss of TMC-78 and TMCCL-78 elastomers during the *in vivo* and *in vitro* degradation in PBS buffer.

The changes in the mechanical properties of elastomer rods during *in vivo* degradation are illustrated in Figure 3-4. The average Young's modulus (E) of the TMC-78 elastomers remained essentially constant up to week 16 (Figure 3-4A). After week 16,

it decreased significantly, and by week 44, the TMC-78 elastomer samples had retained only 55% of their initial modulus. In contrast, the average modulus of the *in vivo* degrading TMCCL-78 elastomer decreased slowly but continuously; by week 44, the samples had 58.8 % of their initial modulus (Figure 3-4A). The stress at break, σ_b, of the *in vivo* degrading TMC-78 elastomers decreased at week 1 from their initial average value of 7.2 ± MPa to 3.9 ± MPa and remained essentially constant around this value until week 16 (Figure 3-4B). After week 16, σ_b decreased continuously and by week 44 the TMC-78 elastomer had 24.3% of its initial stress at break value. The stress at break of the TMCCL-78 elastomers remained constant up to week 16 of the *in vivo* degradation, after which it experienced a nearly linear decrease, and by week 44 the TMCCL-78 elastomers had 40.8% of their initial value. The strain at break values remained nearly constant during the degradation process for both elastomers (Figure 3-4C). At week 44, the TMC-78 elastomers had 72.2 % of their initial value, while the TMCCL-78 elastomers had 83.6 % of their initial value.

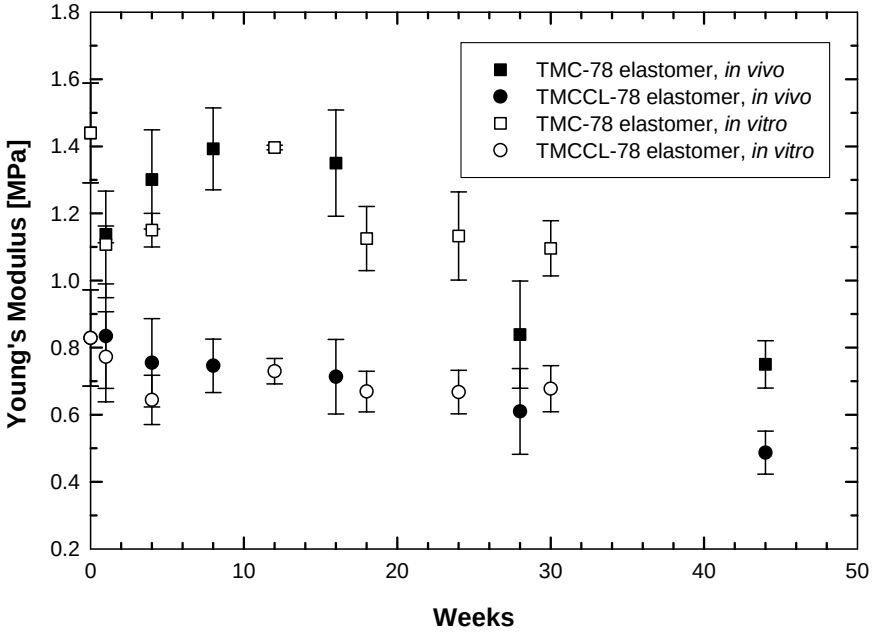

Figure 3-4A

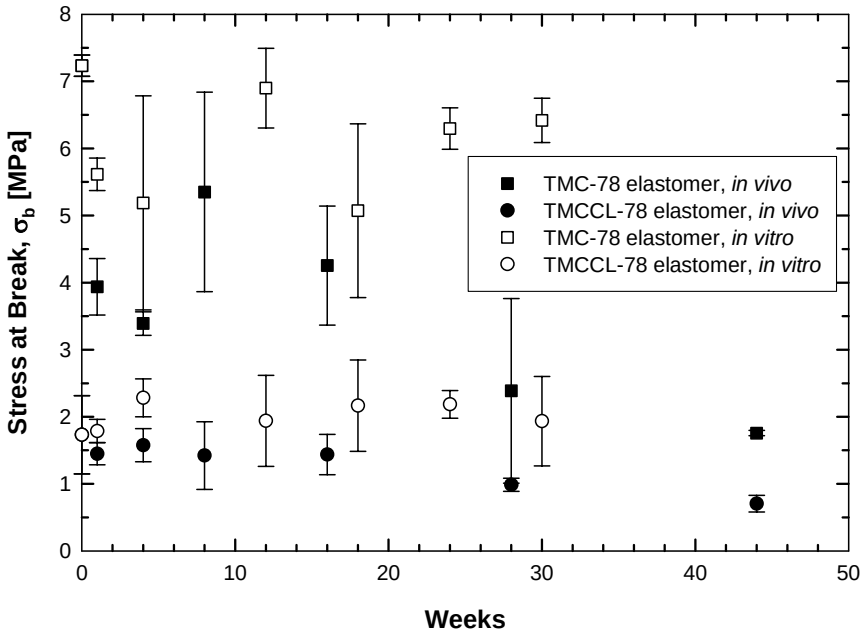

Figure 3-4B

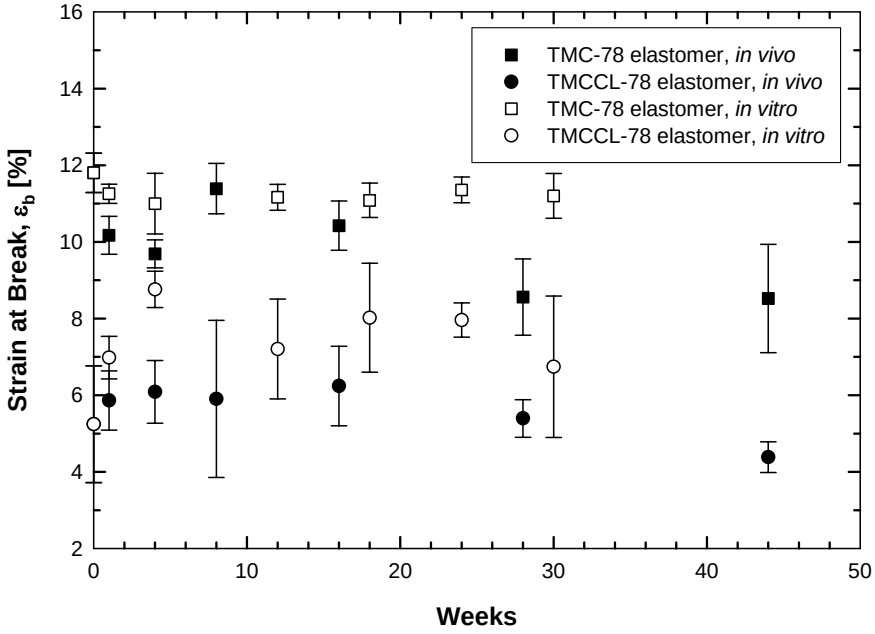

Figure 3-4C

Figure 3- 4. The changes in the mechanical properties of TMC-78 and TMCCL-78 elastomers during in vivo and in vitro degradation in PBS buffer. A) modulus (E) B) ultimate tensile stress (σ_b) C) elongation at break (ε_b).

The sol content, water absorption, and glass transition temperature of the elastomer samples were also measured during *in vivo* degradation, and these values are

provided in Table 3-3. The sol content of the networks increased only slightly during degradation, reaching a value of approximately 8% by week 44, and was similar for both the TMC-78 and TMCCL-78 elastomers. Similarly, both elastomers absorbed water to approximately the same extent, reaching values of approximately 6% in each case. The glass transition temperatures for both elastomers remained unchanged during the 44 weeks of the *in vivo* degradation (Table 3-3).

Table 3- 3. Sol content and water uptake of TMC-78 and TMCCL-78 elastomers after *in vivo* degradation and *in vitro* degradation in PBS buffer at 37 °C.

in vivo

	sol content [%]		water uptake [%]		T_g (°C)	
week	TMC-78	TMCCL-78	TMC-78	TMCCL-78	TMC-78	TMCCL-78
1	0.3 ± 0.5	1.5 ± 3.2	2.3 ± 0.7	2.3 ± 0.7	-12.5	-42
4	0.9 ± 0.9	0.3 ± 0.5	3.4 ± 0.6	2.5 ± 0.6	-12.1	-42.3
8	2.2 ± 1.1	2.7 ± 1.5	2.1 ± 1.1	3.9 ± 2.9	-12.1	-42
16	3.5 ± 0.9	2.4 ± 1.6	1.9 ± 1.5	3.4 ± 1.3	-12.7	-41.8
28	4.6 ± 4.5	6.3 ± 1.5	2.9 ± 1.2	3.2 ± 1.4	-15.3	-42.6
44	8.3 ± 1.1	7.8 ± 1.4	5.7 ± 4.7	6.1 ± 4.9	-13	-43.1

in vitro

	sol content [%]		water uptake [%]		T_g (°C)	
week	TMC-78	TMCCL-78	TMC-78	TMCCL-78	TMC-78	TMCCL-78
1	2.4 ± 1.7	2.0 ± 0.5	1.6 ± 0.6	1.5 ± 0.7	-12.3	-42.3
4	0.7 ± 0.6	0.6 ± 1.0	2.5 ± 1.0	2.1 ± 1.2	-11.9	-41.8
12	0.7 ± 0.6	0.0 ± 0.0	3.0 ± 0.9	2.7 ± 1.1	-11.7	-42
18	0.4 ± 0.6	0.6 ± 0.5	3.1 ± 0.9	2.4 ± 1.2	-11.9	-42.1
24	2.0 ± 0.8	1.9 ± 1.0	2.0 ± 0.9	1.2 ± 0.5	-12	-42.1
30	1.4 ± 0.5	1.0 ± 0.0	2.3 ± 0.6	3.0 ± 1.1	-12.7	-42.3

SEM images of both elastomeric networks showed smooth, homogenous surfaces at week 0 (Figure 3-5). At week 1, numerous pits were observed on the surface of TMC-78 elastomers, whereas the surface of TMCCL-78 elastomers was less pitted. At week 16, several pores were observed on the surface of TMC-78 elastomers, while the pores in

TMCCL-78 elastomers were less numerous and smaller in size and depth. The intensity of erosion varied from sample to sample and even on the same sample where some areas were severely eroded, while other areas exhibited less erosion. At week 28, TMC-78 elastomers started to lose their cylindrical shape, whereas the TMCCL-78 elastomers maintained their cylindrical shape, but the pores on their surface had become larger and more numerous. At week 44, the surface of TMC-78 elastomers appeared as they had at week 28, while on the TMCCL-78 elastomers, the pores had become more numerous on the surface.

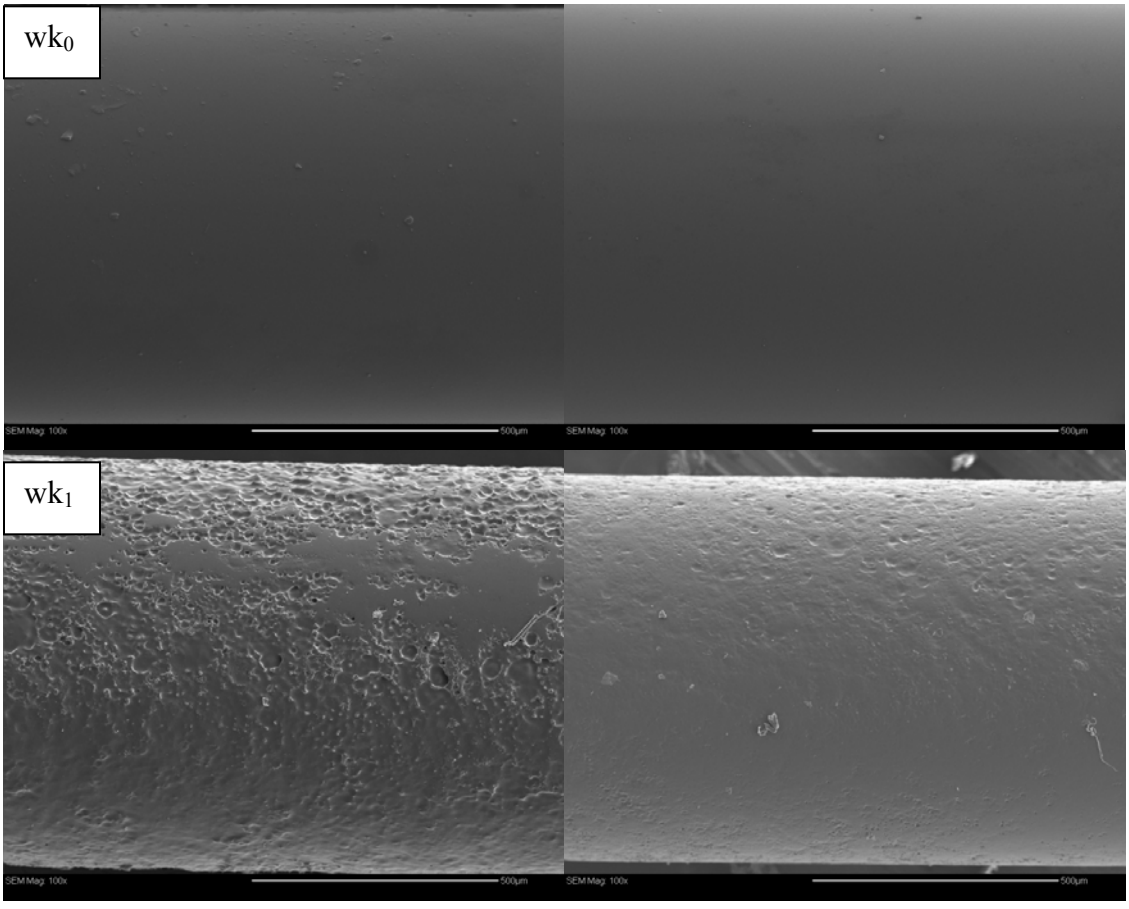

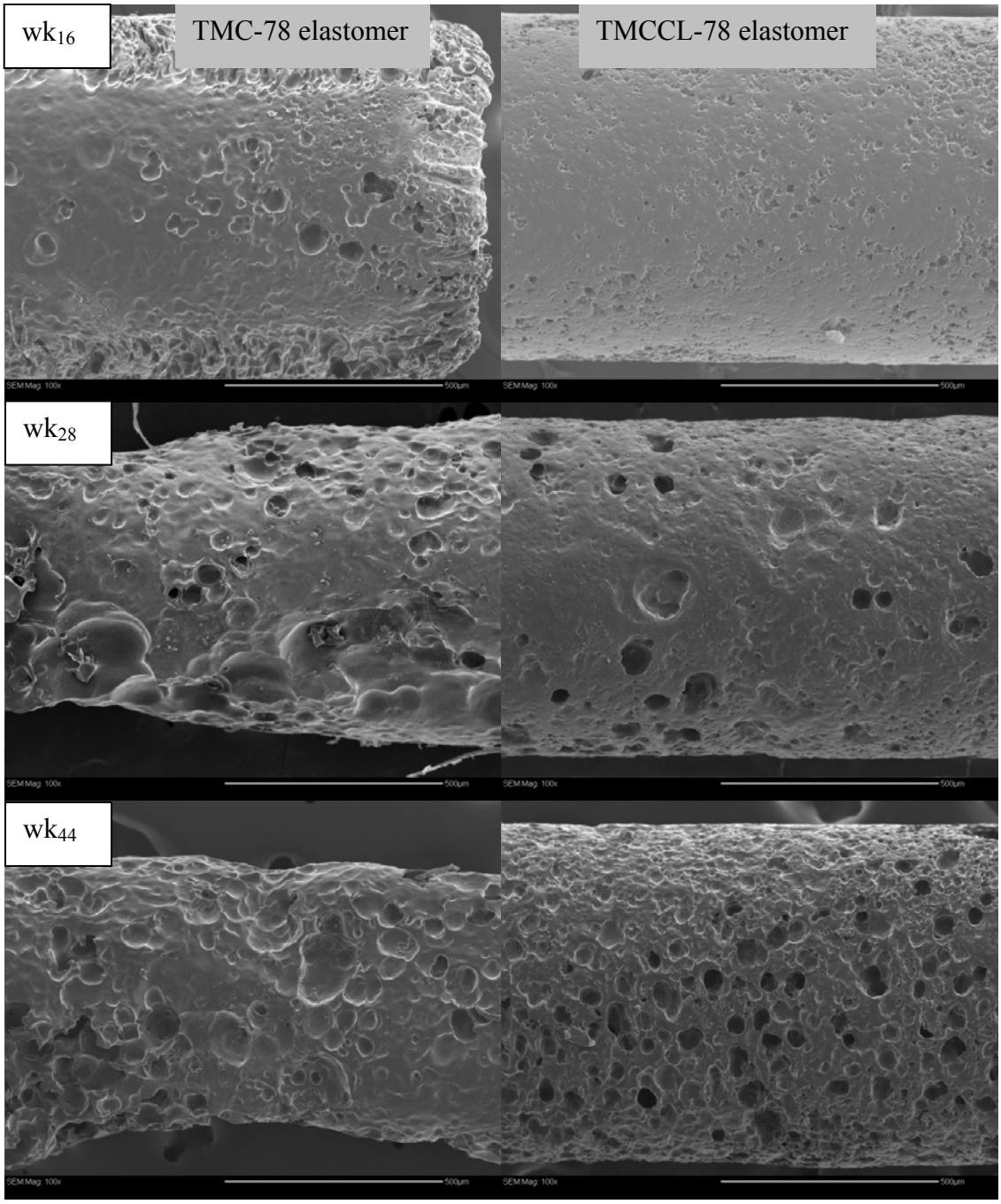

Figure 3- 5. SEM images of in vivo degraded elastomers. The left panel represents TMC-78 elastomers and the right panel represents TMCCL-78 elastomers. (bar = 500 µm)

To investigate the biological response to the implanted elastomers, the tissue surrounding the elastomers was evaluated histologically after staining with Masson's trichrome stain. At week 1, there was a typical inflammatory response at the site of

implantation for both TMC-78 and TMCCL-78 elastomers. Multi-nucleated giant cells, lymphocytes and neutrophils were plentiful adjacent to the implantation site. At the implant-tissue interface, there was a thin capsule containing macrophage-like or fibroblast-like cells encircling the implants. Neovascularization was evident surrounding the implantation site. The thickness of the capsule increased slightly at week 4 for both elastomers and remained almost unaltered thereafter during the 44 weeks of investigation. Collagen deposition as indicated by blue staining appeared first at the periphery of the capsule. 16 weeks following implantation, the full thickness of the capsule was occupied by collagen matrix with only a few fibroblast-like cells present (Figure 3-6A).

By week 4, the tissue reaction to the TMC-78 elastomer was different from that of the TMCCL-78 elastomer. In the case of the TMC-78 elastomer, 3 to 4 layers of macrophage-like cells surrounded the implant, the capsule contained numerous cells and blood-born cells were observable adjacent to the implant. In the case of the TMCCL-78 elastomer, only 1-2 layers of macrophage-like cells surrounded the implant, the capsule contained fewer cells, while blood-born cells were also observable in the areas surrounding the implant. At week 16, groups of cellular nodules were present surrounding both TMC-78 and TMCCL-78 tissue-elastomer interface. At a higher magnification, these cellular nodules resembled multinucleated foreign body giant cells (Figure 3-6B).

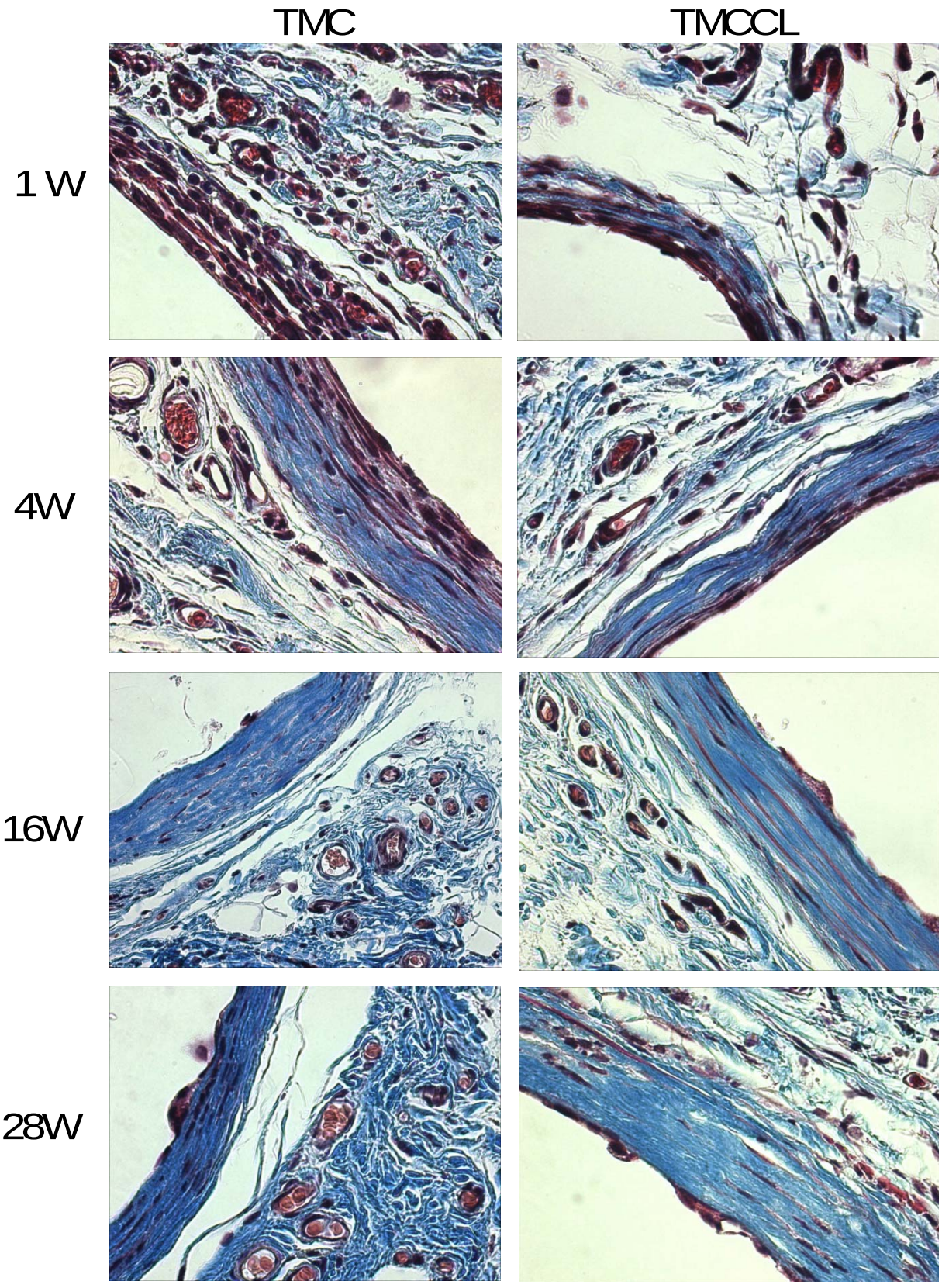
TMC
TMCCL
1 W
4W
16W
28W

TMC, 16W, 40X

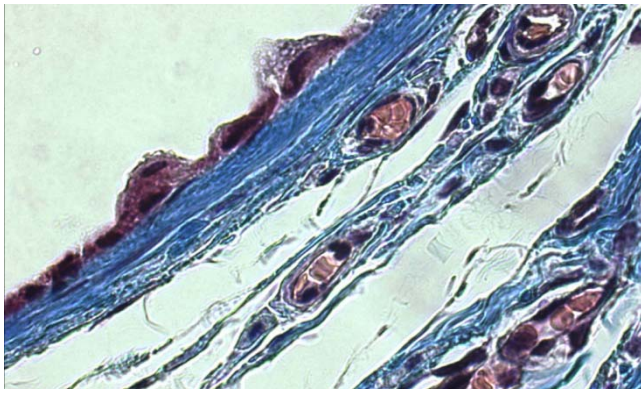

TMC, 44W, 40X

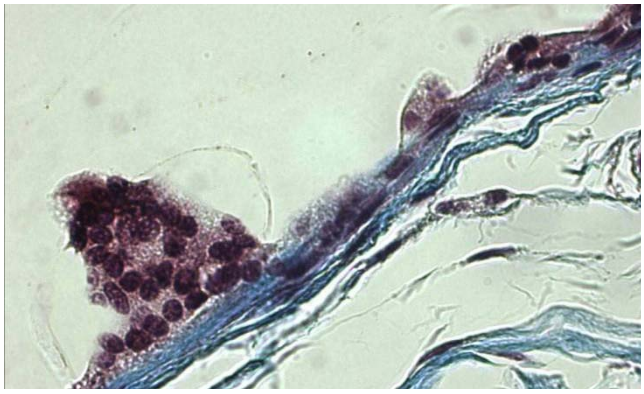

TMCCL, 44W, 40X

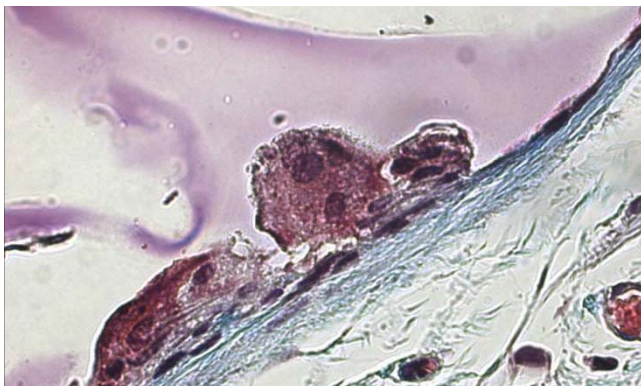

Figure 3- 6. Histological sections of the tissue surrounding the implant, stained with Masson's trichrome at different stages of in vivo degradation. The left panel represents tissues surrounding TMC-78 elastomer and the right panel represents tissues surrounding TMCCL-78 elastomer.

3.3.3. *In vitro* degradation in PBS buffer

In contrast to the *in vivo* observations, the TMC-78 and TMCCL-78 elastomers did not lose mass in PBS buffer over the 30 weeks of investigation (Figure 3-3). The

changes of Young's modulus of *in vitro* degraded samples generally closely followed those of the *in vivo* degraded elastomers (Figure 3-4A). However, the values of both stress and strain at break of both *in vitro* degraded TMC-78 and TMCCL-78 elastomers, remained unchanged after week 18, whereas for the *in vivo* degraded elastomers, these parameters decreased significantly for both elastomers (Figures 3-4B and C). The *in vitro* sol content and water uptake of TMC-78 and TMCCL-78 elastomers remained unchanged over the 30 weeks of investigation in PBS buffer (Table 3-3) and were lower at the later stages of degradation than those of the *in vivo* degraded samples.

The glass transition temperature of the hydrated TMC-78 elastomer was –18 ˚C, which was 6 ˚C lower than the dry TMC-78 elastomer, indicating significant plasticization of this elastomer upon water absorption. On the other hand, the glass transition temperature of the hydrated TMCCL-78 elastomer was –44.7˚C, which was only lower by 2.6˚C than when dry, and so this elastomer is not as plasticized by the absorption of water. Furthermore, both the hydrated TMC-78 and TMCCL-78 elastomers exhibited two endotherms. A sharp endotherm near 0 ˚C, corresponding to melting of free water in the elastomer, and another, broad, endotherm, near 82 ˚C for the TMC-78 elastomer and near 72 ˚C for the TMCCL-78 elastomer. The two endotherms disappeared during the second heating cycle of both hydrated elastomers. For both endotherms, the enthalpy increased and became wider with time. Both enthalpies were greater in the hydrated TMC-78 elastomer. For example, in the case of TMC-78, at week 1, the enthalpy was 1.3 J/g at 1 ºC and 13.8 J/g at 83 ºC; these values increased to 1.7 J/g and 15.9 J/g at week 20. In the case of TMCCL-78, at week 1, the enthalpy was 0.3 J/g at 1

ºC and 10.9 J/g at 72 ºC; these values increased to 0.4 J/g and 13.3 J/g at week 20.

3.3.4. Enzymatic Degradation

Lipase from *Thermomyces lanuginosus* and cholesterol esterase (CE) from porcine pancreas were used as model enzymes to investigate the susceptibility of TMC and TMCCL elastomers to enzymatic hydrolytic degradation. The TMCCL elastomers are more prone to enzymatic degradation than the TMC elastomers, and degraded at the same rate in the presence of both enzymes (Figure 3-7). Moreover, the TMCCL-78 elastomers displayed a linear mass loss with time. After 8 weeks, TMCCL-78 elastomers had lost 95 % of their initial mass in lipase and 92.5 % of their initial mass in CE. Conversely, and in contrast to the degradation of linear, uncrosslinked poly(TMC) reported by Zhang *et al*. [19], the TMC-78 elastomers were not degraded in the presence of lipase. These elastomers were, however, degraded by CE and had lost 19 % of their initial mass after 8 weeks (Figure 3-7). The rate of degradation of the TMC-78 in CE was lower than that recorded for TMCCL-78, in contrast to the *in vivo* degradation rates.

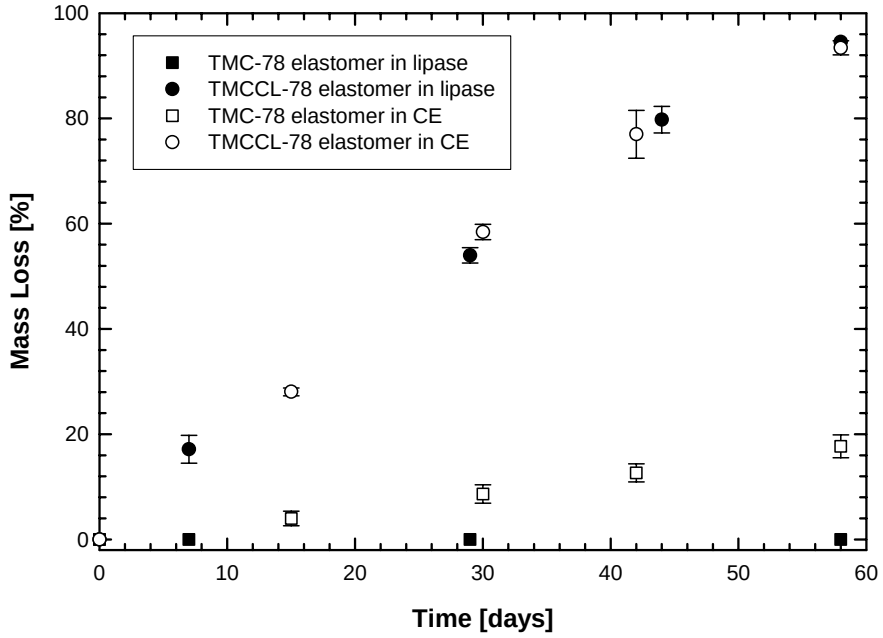

Figure 3- 7. Mass loss of TMC-78 and TMCCL-78 elastomers during *in vitro* enzymatic degradation in lipase and cholesterol esterase.

The surfaces of the enzymatically degraded elastomer rods were examined via SEM (Figure 3-8). TMCCL elastomers exposed to CE revealed a crater-shaped erosion pattern, whereas the surface of the TMC elastomers exposed to CE had dark regions seemingly randomly distributed across the surface. TMC and TMCCL elastomers exposed to lipase revealed erosion via outer layer shedding.

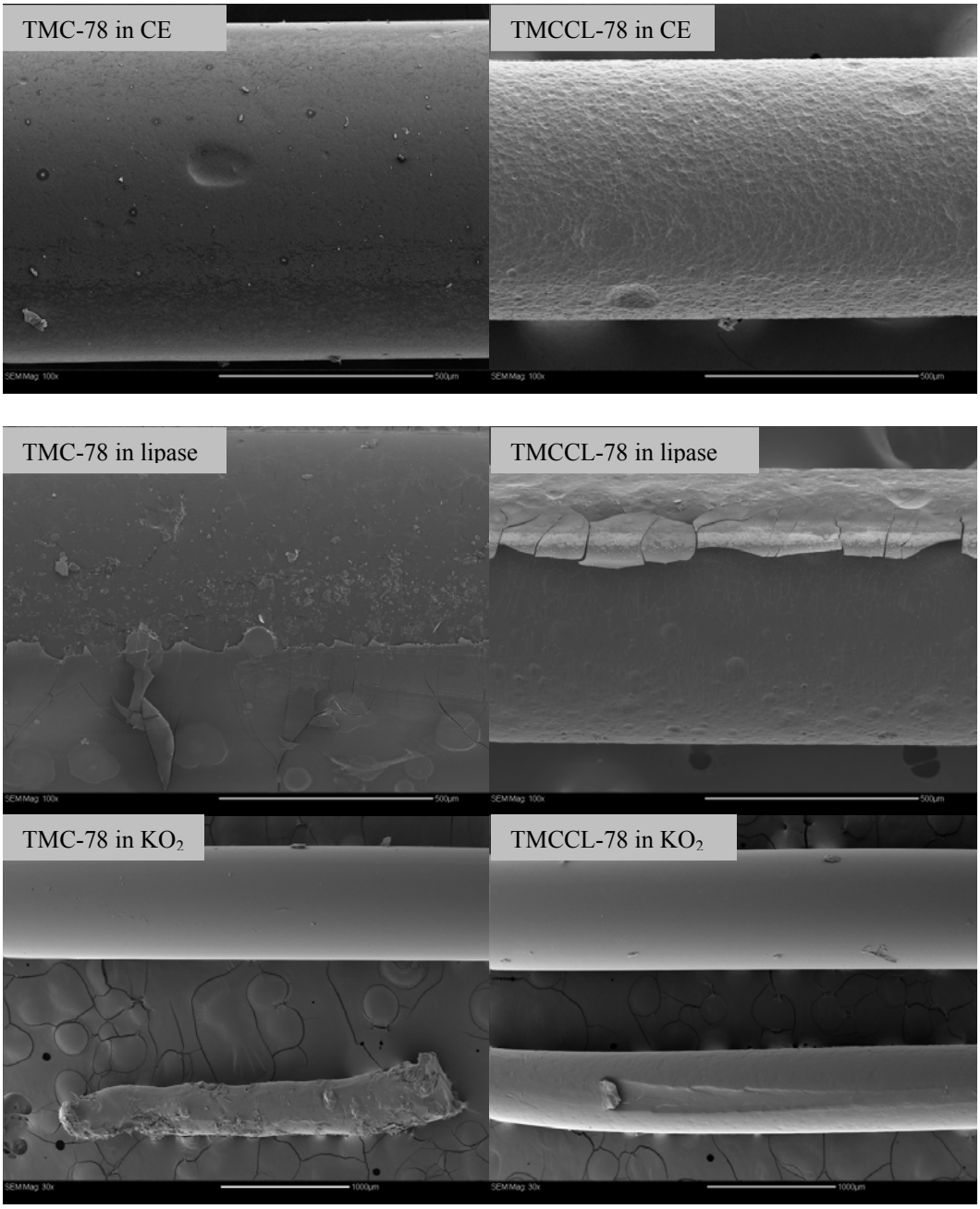

Figure 3- 8. SEM images of *in vitro* degraded elastomers in cholesterol esterase (top images) and lipase (middle images), after 4 weeks, and in 18-crown-6 ether/THF and in 18-crown-6 ether/KO_2/THF (bottom images), after 4 days. bar = 500 µm for top and middle images and bar = 1000 µm for bottom images.

3.3.5. Oxidative degradation

To investigate the susceptibility of TMC-78 and TMCCL-78 elastomers to oxidation, elastomer rods were subjected to solutions of $H_2O_2/CoCl_2$ and Fe^{2+}/H_2O_2 in

H_2O and to KO_2/18-crown-6 ether in THF. In $H_2O_2/CoCl_2$, neither TMC-78 nor TMCCL-78 elastomers lost mass over the 8 weeks studied. The radicals generated were not able to oxidize the surface of these elastomers, rather cobalt oxides precipitated on the surface, which turned brownish. In Fe^{2+}/H_2O_2 (Fenton's reagent), the TMC-78 elastomers did not degrade, whereas the TMCCL-78 elastomers turned into a pasty material after 6 months. Consequently, the T_g of the TMCCL-78 decreased to – 45.3 °C, from its initial value of – 42.1 °C. Furthermore, the elastomer was sufficiently degraded that it was soluble in organic solvents. ^{1}H NMR analysis indicated an unchanged molar ratio of TMC/CL in the degraded elastomer and the formation of new peaks at chemical shifts of 1.4, 1.7, 2.2, and 3.45 ppm. SEM images of TMC-78 and TMCCL-78 samples exposed to radicals generated by a mixture of 18-crown-6 ether/THF, in the absence and presence of KO_2, are given in Figure 3-8. In KO_2/18-crown-6 ether, both TMC-78 and TMCCL-78 elastomers lost mass. After 4 days, TMC-78 lost 85 % of its initial mass and TMCCL-78 lost 56 % of its initial mass.

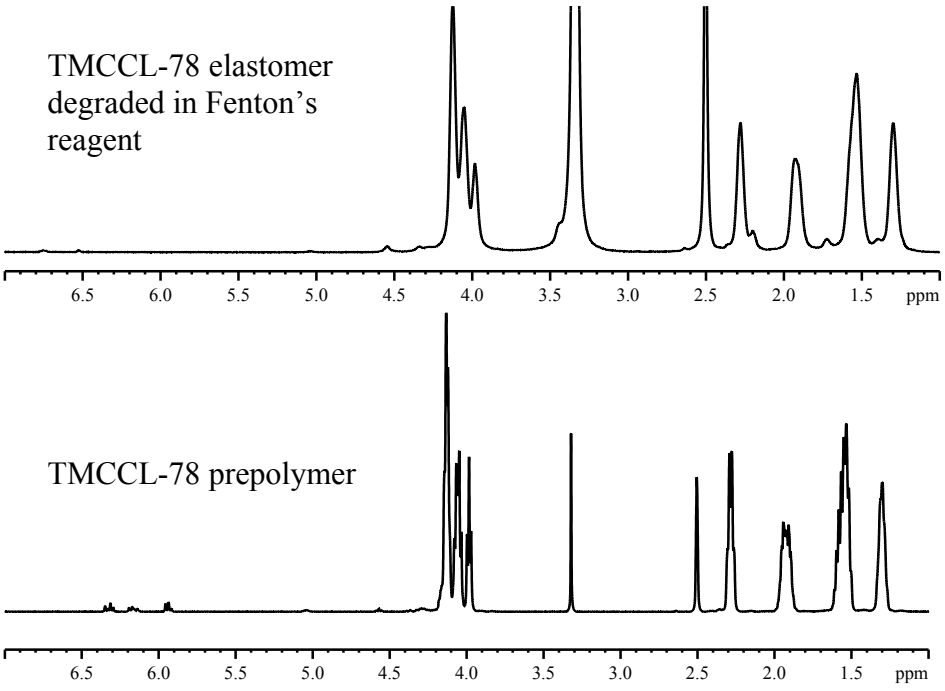

Figure 3- 9. ^{1} H NMR spectra of TMCCL-78 prepolymer and TMCCL-78 elastomer degraded in Fenton's reagent.

3.3.6. ATR-FTIR Analysis

The surface chemistry of the elastomers was examined using ATR-FTIR spectroscopy. New peaks appeared at 1537 cm^{-1}, 1656 cm^{-1}, and 3285 cm^{-1} in the *in vivo* degraded TMC-78 and TMCCL-78 elastomers, and these are attributed to adsorbed proteins (Figures 3-10A and 3-10B). Similar peaks appeared in samples exposed to lipase (TMCCL, lipase, wk4 in Figure 3-10A), but not to those exposed to CE. Those peaks disappeared in TMCCL-78 elastomers degraded by lipase, after treating the elastomer surface with urea/Triton X-100 (Figure 3-10A). A similar treatment was unable to remove the proteins attached to the *in vivo* degraded elastomers, however.

TMC-78 and TMCCL-78 elastomers exposed to KO_2/18-crown-6 ether /THF exhibited new peaks at 1620 cm^{-1}, 831 cm^{-1}, and 697 cm^{-1} for TMC (Figure 3-10B), and at 1666 cm^{-1}, 1620 cm^{-1}, and 697 cm^{-1} for TMCCL (Figure 3-10C). The peak at 1666 cm^{-1} is attributed to carboxylate ions while the peak at 1620 cm^{-1} is attributed to a carbonylate salt [136]. In addition, the carbonyl stretching band at 1735 cm^{-1} became weaker after oxidation, especially in TMC elastomers. The new peaks disappeared when KO_2/18-crown-6 ether /THF solution in which the elastomer was residing was acidified (Figure 3-10B and 3-10C).

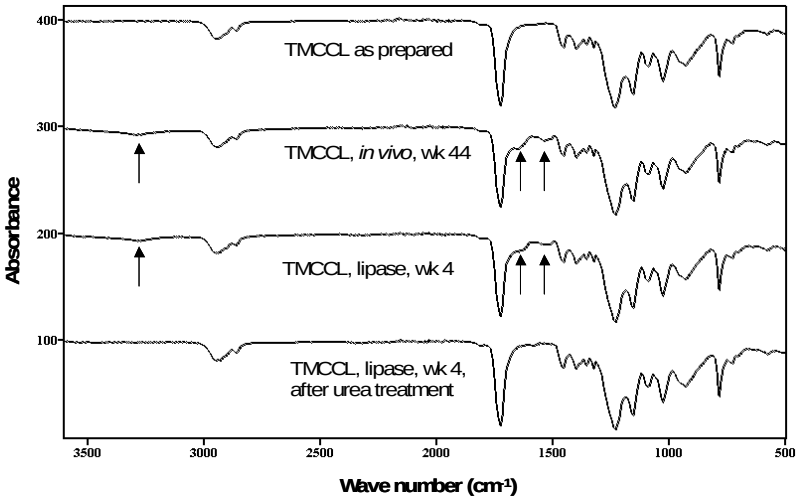

Figure 3-10A

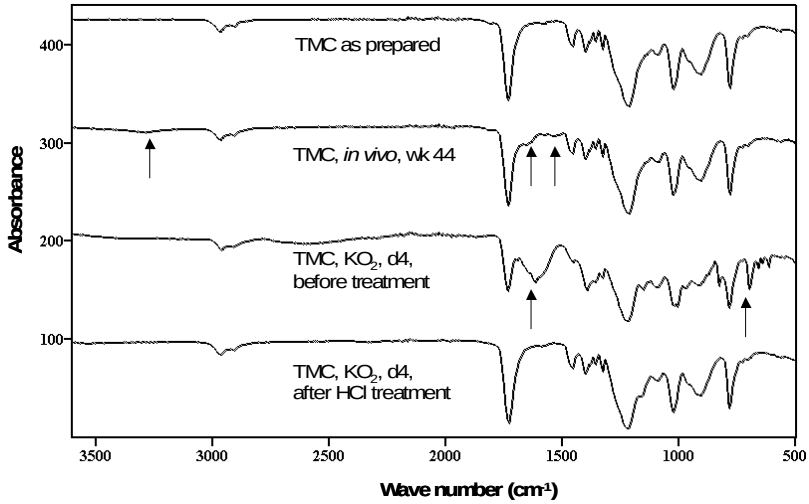

Figure 3-10B

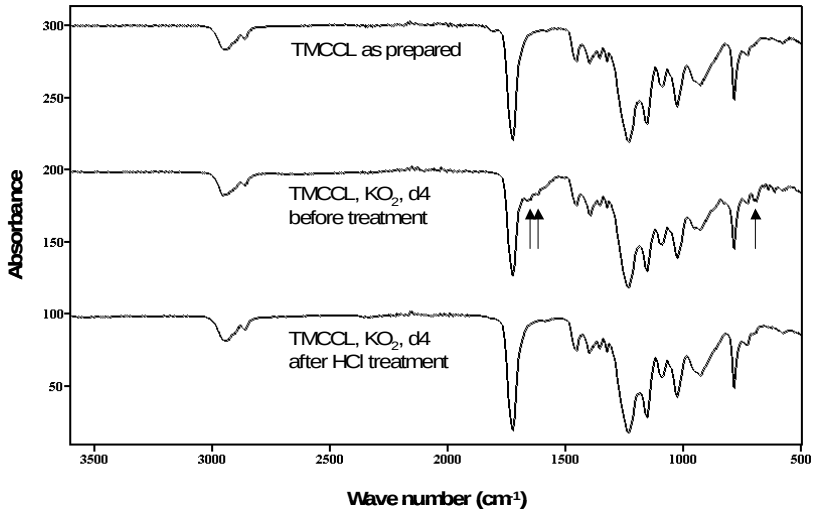

Figure 3-10C

Figure 3- 10. ATR-FTIR spectra of A) TMCCL-78 elastomer degraded *in vivo* and in lipase, and the effect urea/Triton X-100 treatment on the removal of lipase from the surface of elastomer. B) TMC-78 elastomer degraded *in vivo* and in 18-crown-6 ether/THF, and the effect of HCl treatment on the removal of carbonylate ion peaks. C) TMCCL-78 elastomer degraded 18-crown-6 ether/THF, and the effect of HCl treatment on the removal of carbonylate and carboxylate ion peaks.

3.4. DISCUSSION

All the results, *i.e*. linear mass loss with time, presence of extensive surface pitting, low and unchanged sol content, unchanged T_g, and maintenance of mechanical properties, are consistent with a surface erosion mechanism for both elastomers *in vivo*. This degradation is mediated by adherent phagocytic cells, with a negligible contribution of acid-base catalyzed hydrolysis. This mechanism of degradation has been reported previously for both linear, uncrosslinked poly(ethylene carbonate) [137, 138] and poly(trimethylene carbonate) [122]. Our results show that this degradation mechanism is also responsible for crosslinked poly(trimethylene carbonate) and poly(trimethylene carbonate-co-ε-caprolactone) of high trimethylene carbonate composition.

In contrast to the *in vitro* degraded elastomers in PBS buffer, the *in vivo* degraded elastomers lost a significant amount of strength, both at the initial stages upon implantation and after 16 weeks. This loss is likely due to the generation of surface cracks and pits during degradation. These cracks and pits act as stress risers during extension, initiating crack propagation throughout the elastomer and leading to premature failure.

The DSC analysis of the degrading TMC-78 and TMCCL-78 elastomers indicated that both elastomers are prone to crystallization in their hydrated state, as indicated by the presence of a broad endotherm near 82 ˚C for the TMC-78 elastomer and near 72 ˚C for the TMCCL-78 elastomer. The TMC-78 elastomer exhibited a larger endotherm than did the TMCCL-78 elastomer. Furthermore, the area endotherms of both TMC-78 and

TMCCL-78 elastomers increased with time. The endotherms centered at 0°C are due to free water molecules within the bulk of the elastomer. The larger free water content in the TMC-78 elastomer indicates a higher affinity to water or the presence of more pores in the structure of TMC-78 elastomer, which could be due to lower cross-link density in TMC-78 elastomer compared to TMCCL-78 elastomer as a result of lower degree of acrylation (Table 4-1). The endotherms present at higher temperature are attributed to crystallization of the polymer chains in the presence of absorbed water. Crystallization of hydrated, linear poly(trimethylene carbonate) has been reported in the literature as well [139]. The impact of this crystallization would likely be to retard the degradation rate as time progresses, although its influence did not appear noticeable up to 44 weeks *in vivo*.

The TMC-78 elastomer is more susceptible to degradation *in vivo* than is the TMCCL-78 elastomer, a result that agrees with the degradation of linear, uncrosslinked poly(trimethylene carbonate) versus poly(trimethylene carbonate-co-ε-caprolactone) previously reported [122]. Comparing the rate of the *in vivo* degradation mass loss to the *in vitro* enzymatic degradation mass loss, no parallels were found between the rate of degradation *in vivo* and the *in vitro* degraded elastomers in both lipase and CE. In contrast to the *in vivo* degradation rate, TMCCL-78 elastomers degraded faster than TMC-78 elastomers in both lipase and CE. This result cannot be attributed to differences in surface hydrophobicity resulting in different enzyme conformations on the surface, as has been used to explain the faster degradation of poly(trimethylene carbonate) of high versus lower molecular weight in the presence of lipase [19]. Measurement of the water contact angle on both elastomers showed that they were equivalent; the water contact

angle was 82.5 ± 1.6 º on TMC-78 and 82.6 ± 3.5 º on TMCCL-78. The difference between *in vivo* degradation rates versus *in vitro* enzymatic degradation rates could possibly be due to the following two reasons: 1) a milder phagocytic response in the case of the TMCCL-78 elastomer due to differences in protein adsorption to the surfaces and consequently lower local enzyme concentrations or the production of different enzymes, or 2) the contribution of reactive oxidative species.

In vitro oxidation studies revealed different degradation behavior in different oxidation media. Interestingly, TMC-78 elastomers degraded faster than TMCCL-78 elastomers in KO_2/18-crown-6 ether/THF. In aqueous oxidative media expected to better represent the *in vivo* condition, however, only TMCCL-78 elastomers exhibited degradation. The nature of the degradation of TMCCL-78 elastomers in aqueous Fenton's reagent was also different from their degradation in organic KO_2 solution. In Fenton's reagent, the elastomer underwent a bulk degradation yielding a pasty material. In organic KO_2 solution, the elastomer underwent surface degradation leaving the bulk of the elastomer apparently unchanged, as observed *in vivo*, and at rates that were in qualitative agreement with the degradation rates of the TMC-78 versus TMCCL-78 elastomers *in vivo*. As the organic KO_2 reaction generates superoxide anion whereas the Fenton's reagent produces hydroxyl anion, these results imply that the TMC-78 based elastomers are degraded by the action of superoxide anion released *in vivo*. Nevertheless, degradation by secreted hydrolytic enzymes may be occurring concurrently.

Morphological analyses revealed a milder cellular response to TMCCL-78

elastomer compared to TMC-78 and a clear role of the foreign body giant cells in phagocytosis of the implants through micro-pore formation. Foreign body giant cells are known to generate both reactive oxygen species as well as secrete enzymes such as CE as a response to inflammation [140-142]. Therefore, in order to determine the relative role of each degradation mechanism (enzyme versus oxidation), the surface chemistry of the *in vivo* degraded TMCCL-78 elastomer was studied and compared to the surface chemistry of TMCCL-78 elastomer degraded by lipase and CE, and by oxidation with KO_2.

Peaks were observed at 1537 cm^{-1}, 1656 cm^{-1}, and 3285 cm^{-1} in the *in vivo* degraded samples, which are attributed to protein adsorption on the surface of the elastomer, since similar peaks appeared on the surface of TMCCL-78 elastomers exposed to lipase, and were subsequently removed after treatment with urea/Triton X-100 (Figure 3-9A). Peaks formed upon *in vitro* oxidation disappeared upon acidification of the oxidizing solution, yielding a surface chemistry similar to the samples degraded *in vivo*, after the peaks attributed to protein adsorption are discounted. The microenvironment at the FBGC/biomaterial interface can be highly acidic [138], thus it is expected that acids rather than salts are present in the *in vivo* degraded elastomers. Thus, the ATR-FTIR analyses revealed that the surface chemistry of samples that had undergone *in vivo* degradation was identical to the surface chemistry of samples that had undergone both oxidation with KO_2 (after HCl treatment) and hydrolysis by lipase (after Urea/Triton X100 treatment) and CE. This is reasonable since both mechanistic pathways result in the same chemical groups being present. Therefore, ATR-FTIR cannot be used to discern

which *in vivo* degradative mechanism is dominant.

Considering the fact that both *in vitro* oxidation by KO_2 and *in vitro* enzymatic degradation by both lipase and CE yields surfaces similar to the surface of the *in vivo* degraded elastomers, it is likely that both oxidation and enzymatic hydrolysis play a possible role in the *in vivo* degradation process. However, considering similarities between the rates of the *in vivo* degradation and the *in vitro* oxidation in the presence of superoxide anion, it appears that oxidation has a dominant role in the *in vivo* degradation process.

In accordance with our detection of carbonylate salt (1620 cm^{-1}) [136] on the surface of TMC-78 elastomers (Figure 3-9B) and both carbonylate salt and carboxylate ions (1665 cm^{-1}) on the surface of TMCCL-78 elastomers (Figure 3-9C) in our ATR-FTIR analysis of the *in vitro* degraded samples, we propose that oxidative degradation proceeds through the formation of ionic end groups via a nucleophilic attack of superoxide ions, followed by a chain unzipping reaction [138] (Scheme 1).

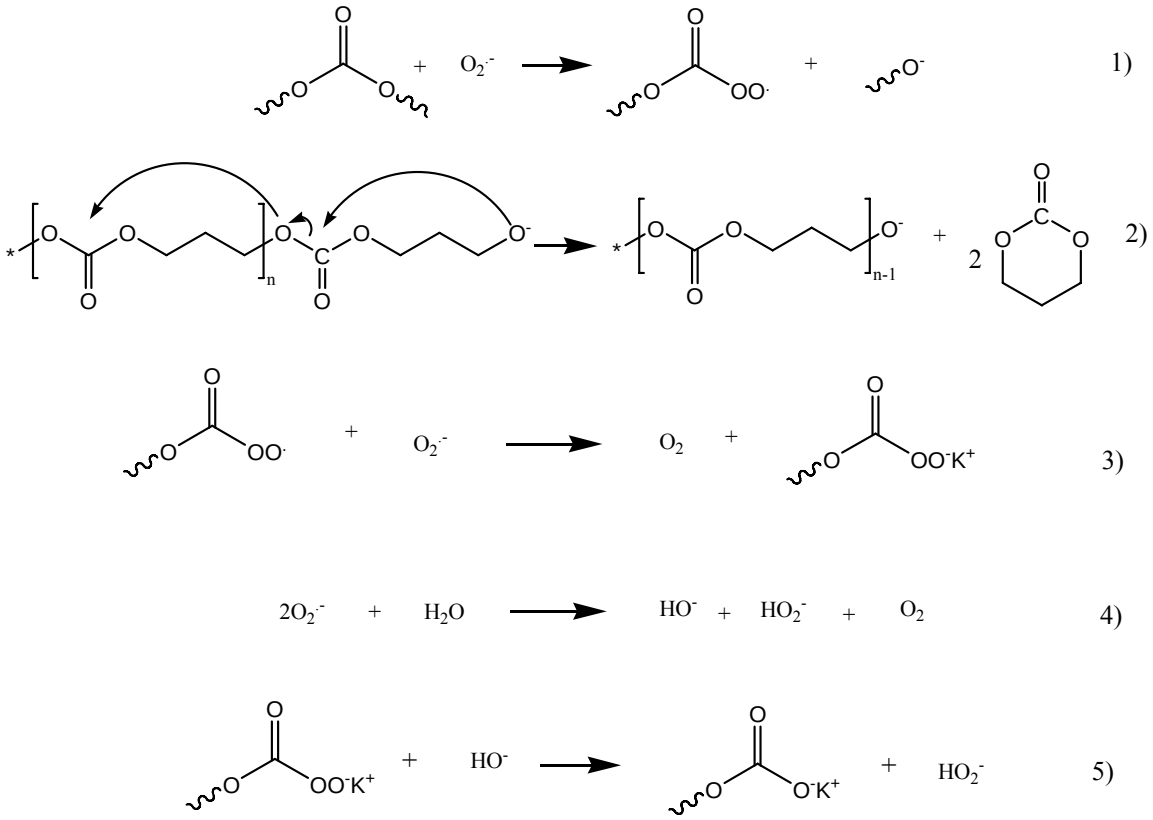

Scheme 1. Proposed oxidative degradation mechanism.

Initiation of ionic species through a nucleophilic attack is suggested in the literature for esters and polyesters and polycarbonates [115, 143], also chain unzipping reactions are suggested for linear poly(ethylene carbonate) and poly(TMC), starting from the end hydroxyl group [44]. Since we have a cross-linked network with very few hydroxyl groups, the reaction has most probably started by a random nucleophilc attack along the backbone of a network chain, followed by a chain unzipping reaction. *In vivo*, where H_2O is abundant, the formation of 1,3-propanediol and the release of CO_2 is possible as well [138].

The rate of the *in vitro* oxidation of TMCCL-78 elastomers was slower than that of TMC-78 elastomers in KO_2. This is attributed to a slower chain unzipping reaction in the random TMCCL copolymer elastomer compared to the TMC-78 homopolymer elastomer, an explanation that still needs to be verified. Another explanation for the slower TMCCL-78 elastomer oxidation is the possibility of the co-occurrence of transesterification reactions in the ester groups of CL [115], along with the chain unzipping reaction, which could occur at a different rate.

3.5. CONCLUSIONS

Both TMC-78 and TMCCL-78 photo-cross-linked elastomers underwent surface erosion when implanted subcutaneously in a rat model. The materials initiated a foreign body response resulting in the generation of foreign body giant cells that adhered to the elastomer surface. These adherent cells mediated the degradation of the elastomers. The roles of both enzymes secreted by the cells and reactive oxygen species in the degradation of the elastomers was examined *in vitro* and compared to the *in vivo* results. Our analysis indicates that oxidation has a dominant role in the *in vivo* degradation process.

4. CHAPTER FOUR

Osmotically Driven Protein Release from Photo-Cross-Linked Elastomers of Poly(trimethylene carbonate) and Poly(trimethylene carbonate-co-D,L-lactide)

Manuscript submitted for publication in European Journal of Pharmaceutics and Biopharmaceutics. May, 2009

Authors: R. Chapanian [1] and B.G. Amsden [1*]

[1]Department of Chemical Engineering
Queen's University, Kingston, Ontario, Canada, K7L 3N6

* To whom correspondence should be addressed

ABSTRACT

The potential of osmotic pressure driven release of proteins from poly(trimethylene carbonate) and poly(trimethylene carbonate-co-D,L-lactide) (poly(TMC-DLLA)) elastomers with varying amounts of DLLA was investigated using bovine serum albumin (BSA) as a model protein. The BSA was lyophilized with either trehalose or trehalose and NaCl as osmotigens to produce particles with sufficient osmotic activity. Elastomers composed solely of TMC were not suitable for osmotically driven release when trehalose was the main osmotigen in the solid particles. Copolymerizing TMC with small amounts of DLLA decreased the tear resistance and consequently increased the rate and the total amount of BSA released. Elongation at break played a significant role in determining the osmotic release behavior; elastomers with comparable Young's modulus and tensile strength, but smaller elongation at break, provided faster release rates. Elastomer degradation played a minor role in the osmotic release, as the mechanical properties underwent very little change during the investigated period of release. The poly(TMC-co-DLLA)(80:20) elastomer was able to provide near zero order release of BSA for up to 12 days, and the total amount of BSA released was 74 ± 4 % after 34 days, when small amounts of NaCl was added to trehalose. Studies using FITC-BSA indicated no significant reduction in the microenvironmental pH after 17 days of release. TMC elastomers copolymerized with small amounts of DLLA could possibly be considered a potential candidate in the localized delivery of acid sensitive proteins.

Keywords: elastomer, BSA, osmotic release, mechanical properties

4.1. Introduction:

The parenteral route remains the major route of protein administration [8]. Unfortunately, the pharmacokinetic half-life of many therapeutics proteins is short [90]. Thus, effective protein administration typically requires multiple injections, which are painful and costly. Moreover, the resulting systemic exposure may produce undesired side effects. Conventional non-parenteral routes of administration suffer from problems related to slow protein transport through the epithelium and to degrading enzymatic activity at the site of administration [144]. Thus, there is an increasing understanding in the pharmaceutical community of the importance of localized sustained delivery of proteins.

Protein therapeutics have been demonstrated to be released in a sustained and linear fashion from monolithic devices, when they are accompanied with osmotically active agents such as sugars and electrolytes [10, 87, 88, 91, 99]. Upon immersion in an aqueous media, water vapor diffuses through the polymer matrix to encounter a polymer-surrounded drug particle, referred to as a capsule. Water vapor dissolves the solid drug at the polymer-solid interface, generating a water activity gradient that draws water into the capsule. When the generated osmotic pressure is greater than the tear resistance of the elastomer, polymer bonds are broken and cracks are formed that connect the contents of the capsule to a pore network that extends to the surface of the device. As a result of the pressure difference, the contents of the capsule are pushed into the surrounding environment [8]. This process occurs in a layer-by-layer fashion moving into the interior, and can result in a constant release rate. Factors that control osmotically driven release

rates include polymer physical properties, drug properties, and device geometry. Important polymer properties include hydraulic permeability, modulus, tensile strength and elongation at break. The principal drug properties include osmotic activity, water solubility, particle size, particle size distribution, volumetric loading, and homogeneity of dispersion throughout the polymer [8, 20, 89, 91, 93, 94].

Recently, Gu *et al*. demonstrated the possibility of releasing proteins of different properties such as VEGF, IL-2, and IFN-γ from degradable elastomers synthesized from photo-cross-linked prepolymers of ω,ω,ω,-triacrylate, via the osmotic release mechanism. In this case, the proteins were lyophilized with trehalose and bovine serum albumin (BSA) [10, 35]. The device was able to provide a constant release for 5 to 20 days, depending on the device geometry, solid particle composition, and elastomer cross-link density [35, 64, 99]. Unfortunately, these elastomers degrade by hydrolysis to yield acidic degradation products that have been implicated in the denaturation of acid labile proteins such as VEGF, *in vitro*, after 7-10 days [10, 35].

Since polymers made of trimethylene carbonate (TMC) degrade without producing acidic degradation products [19, 38, 55], we hypothesized the possibility of releasing proteins via the osmotic release mechanism from TMC based elastomers with the objective of eliminating protein denaturing problems associated with the pH drop in the device. In this study, BSA was used as a model protein. It was lyophilized with trehalose and a mixture of trehalose and sodium chloride (NaCl) as osmotigens and incorporated into TMC-based elastomers. To obtain elastomers with different mechanical

properties, TMC was copolymerized with different amounts of DLLA, and the effect of mechanical properties on the release of BSA was investigated. The *in vitro* degradation of TMC-based elastomers, copolymerized with small amounts of DLLA, was followed by investigating the changes in mechanical properties, sol content, water uptake, mass loss, and attenuated total reflectance Fourier transform infra-red (ATR-FTIR) spectra. Fluorescein isothiocyanate labeled BSA (FITC-BSA) was used to track the *in vitro* release of protein particles from the elastomer and to assess the pH drop in the elastomer during release.

4.2. MATERIALS AND METHODS

D,L-Lactide (99+%) was obtained from Purac, the Netherlands, and purified by recrystallization from dried toluene. 1,3-trimethylene carbonate (1,3-dioxan-2-one) was obtained from Boehringer Ingelheim, Germany and used as received. Toluene and dichloromethane were dried over calcium hydride and distilled under argon. Other chemicals were used without further purification. Chemicals used in polymer synthesis include stannous 2-ethylhexanoate (96%) obtained from Aldrich, Canada and glycerol obtained from BDH, USA. Chemicals used in the acrylation process include acryloyl chloride (96%), triethylamine (99.5%), and 4-dimethylaminopyridine (99%), all obtained from Aldrich, Canada. 2,2-dimethoxy-2-phenylacetophenone used as photoinitiator was obtained from Aldrich, Canada. Solvents used for purification of the synthesized polymers include ethyl acetate (99.9%), and methanol (99.8%), and were obtained from Fisher, Canada. For the release studies, trehalose, bovine serum albumin (BSA), and NaCl were all obtained from Sigma, Canada. Chemicals used in calorimetric assays include Coomassie brilliant blue G obtained from Fluka, Canada, and phosphoric acid

(85%) and sulfuric acid (95-98%) obtained from Fisher, Canada.

4.2.1. Preparation of solid particles:

BSA was reconstituted with trehalose or a mixture of trehalose and NaCl in 5 mM succinate buffer with a final concentration of 400 mg in 10 ml of buffer. Reconstituted solutions were frozen in liquid nitrogen, and lyophilized on a Modulyo D freeze-dryer (Thermosavant, USA) at 100 μbar for 2 days. The lyophilized powder was ground using a mortar and pestle and sieved through a Tyler 60 sieve to yield particles less than 250 μm in diameter. Solid particles were composed of either 10 w/v% BSA, 90 w/v% trehalose, or 10 w/v% BSA, 25 w/v% NaCl, 65 w/v% trehalose.

4.2.2. Prepolymer Preparation

ω,ω,ω-triacrylate *star*-poly(TMC) and *star*-poly(TMC-co-D,L-lactide) of theoretical molecular weights of 7800 Da and with D,L-lactide content of 5, 20, and 50% by mole were prepared by ring-opening polymerization initiated with glycerol and catalyzed with stannous(II) ethylhexanoate at 130 ºC for 72 hrs, as described previously [102]. For acrylation, the warmed star-copolymer was poured into a dried round-bottomed flask, the flask sealed with a rubber septum, and then purged with dry argon. The following procedures were conducted in a glove box. Dried dichloromethane (DCM) was added to the flask at a ratio of polymer to solvent of 2:1 (w:v) to dissolve the polymer. Triethylamine was added at a molar ratio of 1 mole per mole of star-copolymer (SCP) hydroxyl group, while the 4-dimethylaminopyridine catalyst was added at a molar ratio of 2×10^{-3} mole per mole of SCP terminal hydroxyl group. Finally, acryloyl chloride

was diluted in dried DCM at a ratio of 1:1 (v:v) and added slowly in a drop-wise fashion at a ratio of 1.2 moles per mole of SCP hydroxyl group. For ^{1}H NMR analyses, the SCP and ASCP were dissolved in DMSO-d_6, and the spectra were acquired using a 500 MHz Bruker-Avance spectrometer.

4.2.3. Elastomeric Rod Preparation:

To prepare elastomeric rods, prepolymer of a given composition was dissolved in ethyl acetate at a ratio of 1:1 (w:w) and 1.5 w/w(polymer) % of 2,2-dimethoxy-2-phenylacetophenone was added as a photo-initiator. A previous optimization study indicated that this initiator concentration was sufficient to produce elastomers with low sol contents [105]. The mixture was poured into glass tubes sealed at one end, then closed with a rubber septum at the other end. The tube was connected to the shaft of a motor, rotated at 200 rpm, and exposed to long-wave UV light (320-480 nm) at an intensity of 40 mW/cm^2 for 2 min, using an EXFO E3000 light source. The purpose of rotating the samples, while being exposed to UV light, was to provide a homogenous exposure to UV radiation. The rubber septum was removed and the glass was cut from the sealed side to facilitate the evaporation of ethyl acetate. Samples were left in the fumehood overnight, and then exposed to vacuum for 48 hours. The elastomer rods were gently removed from the glass tubes, and the sol extracted using DCM. The density of the elastomers was measured using the volume displacement technique according to ASTM D792-08, where absolute ethanol was used as the displacing liquid.

4.2.4 *In Vitro* Degradation:

The *in vitro* degradation of the elastomers was performed in pH 7.4 phosphate buffered saline. The pH of the buffer was maintained by replacing the buffer once every week. The degradation process was followed by measuring mechanical properties, water uptake, sol content, mass loss, and surface chemistry. At time points of 1, 4, 12, 18, 24, 30 and 40 weeks, five rods were removed from the buffer, washed with distilled water, blotted dry, and their wet weight (w_w) measured. Four rods in their wet state were used to determine the mechanical properties, measured using an Instron uniaxial tensile tester model 4443. The crosshead speed was set at 500 mm/min according to ASTM D412. All specimens were tested at room temperature. Data analysis was carried out using a Merlin 4.11 Series IX software package. To determine dry weight (w_d), samples used for mechanical testing were dried in a vacuum oven at 45˚C for 3 days. The water uptake was calculated using the following equation,

$$\text{water uptake [\%]} = \frac{w_w - w_d}{w_d} \times 100 \qquad (4\text{-}1)$$

Mass loss was calculated using the following equation,

$$\text{mass loss[\%]} = \frac{w_0 - w_d}{w_0} \times 100 \qquad (4\text{-}2)$$

in which w_0 is the initial weight of the sample. In order to determine sol content, dried samples were immersed in 3 mL dichloromethane per rod. The dichloromethane was

replaced three times at 2 hr intervals, after which the samples were dried at 45˚C under vacuum for 3 days. The sol content was calculated using the following equation,

$$\text{sol content } [\%] = \frac{w_d - w_e}{w_d} \times 100 \qquad (4\text{-}3)$$

in which w_e is the weight of the sample after sol extraction. Water uptake, mass loss, and sol content were determined from triplicate samples unless otherwise mentioned. The fifth rod was used to investigate the chemical structural alteration during degradation via ATR-FTIR analyses, performed using a Nicolet Avatar 320 FTIR with a golden gate. A single pass diamond attenuated total reflectance attachment was employed, operating with 32 scans and at a resolution of 4 cm^{-1}. Data was analyzed using GRAMS/32 AI(32) (6) software.

4.2.5. Device preparation:

Sieved particles were added to 1:1 (w:w) prepolymer solution of ethyl acetate containing 1.5 w/w(polymer) % of 2,2-dimethoxy-2-phenylacetophenone as photo-initiator, and the mixture was homogenized by gently mixing with a syringe needle. The mixture was filled into a glass tube and crosslinked with rotation as described above. The elastomer rods were gently removed from the glass tubes, the solvent evaporated, and their dimensions and weight were recorded. Each rod was then placed in an Eppendorf tube with 1 ml sterile pH 7.4 phosphate buffered saline (PBS) containing 0.2 w/v% sodium azide. The PBS buffer was replaced frequently to approximate infinite sink

conditions, and at each time point, rods were blotted dry and weighed to determine the water uptake. The water uptake was determined using equation 1, where w_d was determined by subtracting the mass of particle released from the initial mass of the device. The amount of BSA in the release media was measured using a Bradford micro-assay [145]. Briefly, 150 μL of release media was added in duplicate in the wells of a 96 well plate. 150 μL of Bradford solution was then added using a multichannel pipette, the plate was located on a plate mixer for 1 min, then left for 10 min on the bench, and the color change was recorded at 595 nm using a μQuant Universal Microplate Spectophotometer model H1034 from Bio-Tek Instruments Inc. Quantification of released trehalose was performed using phenol-sulfuric acid calorimetric assay as follows [146]. 20 μL of 80% phenol in distilled water was added to 0.4 mL of released media, gently mixed, and 1 mL of concentrated sulfuric acid was added, the stream of acid being directed against the liquid surface. After 10 min the liquid was vortexed and left for 20 min at 30 °C, after which 300 μL was located in duplicate in a 96 well plate and the reading was taken at 480 nm.

4.3. RESULTS AND DISCUSSION

4.3.1. Prepolymer composition

The DLLA content in the star-copolymers, as determined from ^{1}H NMR, was very close to the feed ratio (Table 4-1), indicating a nearly complete consumption of the DLLA during the polymerization. At low DLLA composition, most of the TMC monomer reacted as well, with less than 2 % unreacted in poly(TMC), poly(TMC-co-DLLA)(95:5), and poly(TMC-co-DLLA)(80:20). However, with 50 mol% DLLA in the

feed, 13% of the TMC remained unreacted (Table 4-1). The higher amount of unreacted TMC monomer in poly(TMC-co-DLLA)(50:50) was due to the high viscosity of this prepolymer compared to other prepolymers. DLLA units are consumed first as they have higher reactivity than TMC [113]. Therefore, the remaining high content of unreacted TMC was due to the higher percentage of TMC monomer remaining in the reaction media once the viscosity was increased as a result of polymer chain growth.

^{1}H NMR analysis of poly(TMC-co-DLLA)(95:5) showed two methine signals, one at 4.98 ppm for non-terminal lactyl units and one at 5.09 for terminal lactyl units (Figure 4-1B). Using peaks corresponding to the end groups (H_7 of hydroxyl group of DLLA and H_{3*} of methylene group of TMC) it was determined that in the copolymers, the chains were predominantly terminated with lactyl units. In poly(TMC-co-DLLA)(95:5), for example, the amount of terminal lactyl was 34.3 % compared to 72.1 % in the case of poly(TMC-co-DLLA)(80:20) (Table 4-1). The accumulation of lactyl units at the end was due to transesterification, since the primary hydroxyl groups derived from TMC units are more reactive in transesterification, and consequently they become depleted [113]. A low amount of DLLA in the structure of the copolymer produced shorter DLLA blocks (Figure 4-1C). The average lactyl sequence length was determined from the integral of representative methine groups of lactyl units in the 4.9 - 5.3 ppm region [147]. In poly(TMC-co-DLLA)(50:50) the average lactyl sequence length $\overline{L}_{LA}$ was 2.8 compared to 1.49 in poly(TMC-co-DLLA)(80:20). Where the lower case (d) indicates to a lactyl unit surrounded with two other lactyl units (D). Determination of $\overline{L}_{LA}$ was performed with some approximation because of the incomplete separation of the

corresponding peaks. $\overline{L}_{LA}$ was calculated using the following equation [147, 148]:

$$\overline{L}_{LA} = \frac{1}{P_{L\to T}} = \frac{1}{P_{T\to L}} = \frac{DdD + (DdT + TdD) + (TTd + dTT) + TdT}{DdT + TTd + TdT} \quad (4\text{-}4)$$

Where $P_{L\to T}$ is the probability of a lactyl unit being beside a carbonyl unit from left to right direction.

The degree of acrylation was calculated from the ^{1}H NMR spectra by end-group analysis using the acrylate group peaks at δ = 5.98-6.07 ppm (H_8, H_9 and H_{10}). The degree of acrylation increased with increasing DLLA content in the prepolymer, ranging from 78% for poly(TMC) to 89.5% for poly(TMC-co-DLLA)(50:50) (Table 4-1). A significant decrease in hydroxyl peaks of terminal lactyl units at δ = 5.42 ppm (H_7) and terminal methylene groups of carbonyl units at 1.75 ppm (H_{4*}) and 3.47 ppm (H_{3*}) and terminal methyl groups of lactyl units at 1.26 ppm (H_{6*}) were observed after acrylation (Figure 4-1B). Using end group analysis of acrylate groups, the number average molecular weight (M_n) of poly(TMC-co-DLLA)(95:5) was found to be 9580 Da, M_n of poly(TMC-co-DLLA)(80:20) 9300 Da, and M_n of poly(TMC-co-DLLA)(50:50) 8300 Da (Table 4-1). These molecular weights are reasonably close to the theoretical molecular weight of 7800 Da, expected based on monomer and initiator feed ratios.

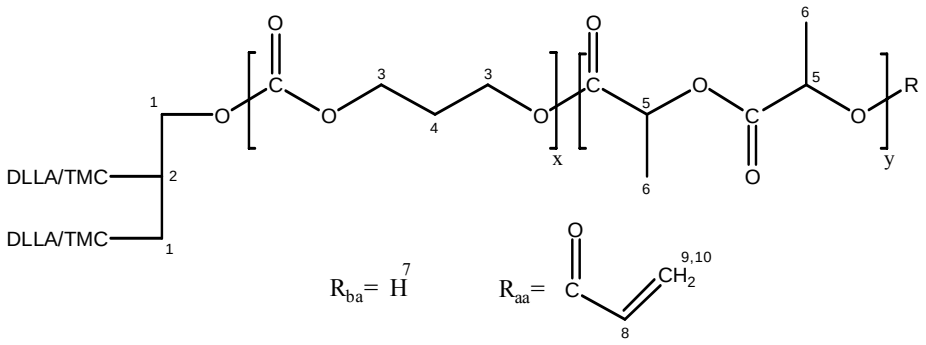

Figure 4-1A

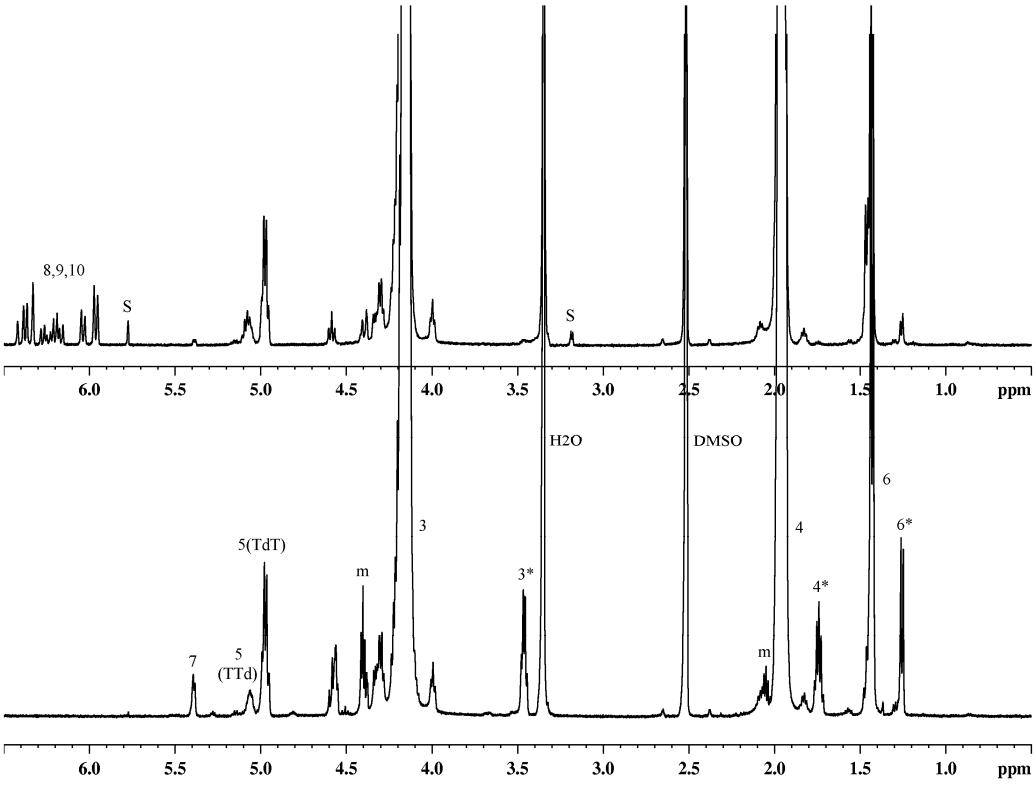

Figure 4-1B

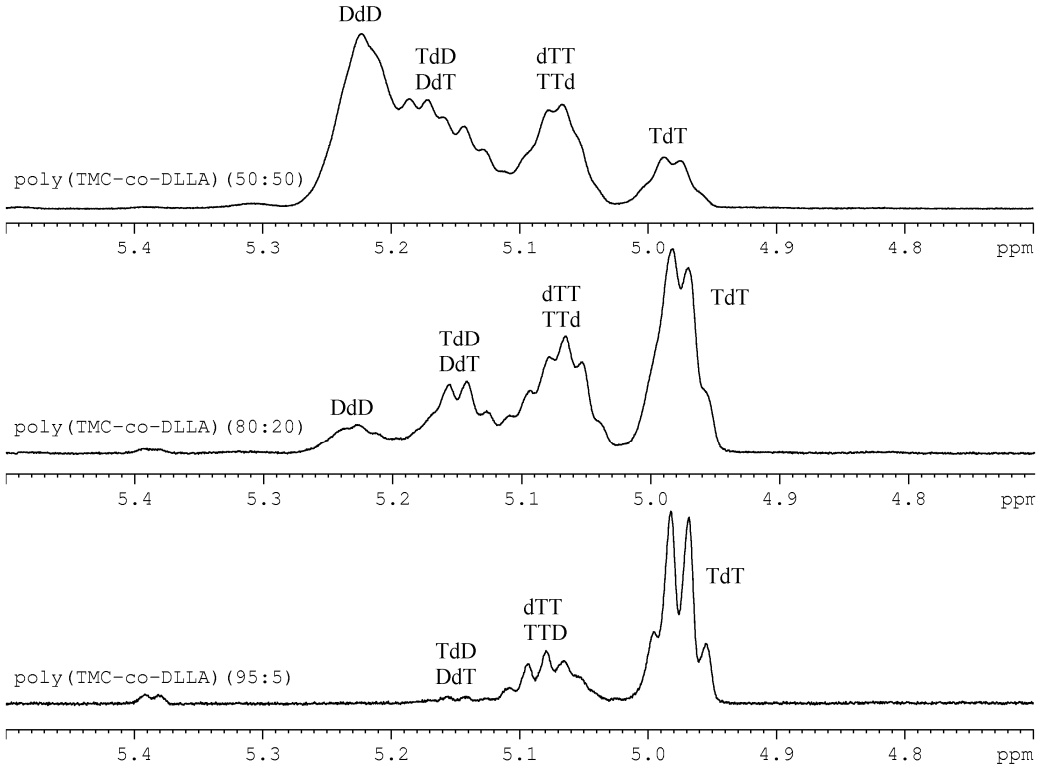

Figure 4-1C

Figure 4- 1. A) The chemical structure of poly(TMC-co-DLLA); the subscript ba refers to before acrylation while aa refers to after acrylation. B) ^{1}H-NMR of poly(TMC-co-DLLA)(95:5), before acrylation (bottom) and after acrylation (top); m = monomer, s = solvent. C) ^{1}H-NMR of methine group of lactyl units in poly(TMC-co-DLLA) with different molar composition of DLLA; DdD = lactyl unit surrounded by two lactyl units, DdT = lactyl unit surrounded by one lactyl and one carbonyl unit, TTd = carbonyl unit surrounded by one carbonyl and one lactyl units, TdT = lactyl unit surrounded by two carbonyl units.

Table 4- 1. Chemical and physical properties of synthesized prepolymers, determined from ^{1}H-NMR analyses.

prepolymer	DLLA content [%] mole	terminal DLLA [%] mole	unreacted TMC [%] mole	DA [%]	M_n [KDa]
TMC	-	-	<2%	78	9.97
TMCDLLA(95:5)	4.6	34.3	<1%	82.3	9.58
TMCDLLA(80:20)	19.9	72.1	<1%	84.6	9.3
TMCDLLA(50:50)	53.7	73.1	13%	89.5	8.3

DA: degree of acrylation, M_n was determined from ^{1}H NMR using end group analysis of acrylate groups

4.3.2. Elastomer Properties

Copolymerizing TMC with DLLA of up to 20 mol% did not change the stiffness of the elastomer (Figure 4-2). Poly(TMC), poly(TMC-co-DLLA)(95:5), and poly(TMC-co-DLLA)(80:20) elastomers had roughly equal Young's moduli of 1.8 ± 0.1 MPa, and the stress at break (σ_b) values of those elastomers were also not significantly different (Table 4-2). The σ_b value of the poly(TMC-co-DLLA)(95:5) elastomer was 2.6 ± 0.1 MPa, and that of poly(TMC-co-DLLA)(80:20) elastomer was 2.5 ± 0.1 MPa. The greatest σ_b value recorded for poly(TMC) elastomer was 2.6 MPa, and this was due to the slippage of elastomer samples from the grips of the tensile tester. Further addition of DLLA produced a stiffer elastomer; poly(TMC-co-DLLA)(50:50) had a Young's modulus of 3.3 ± 0.2 MPa, which was 1.8 times greater than the modulus of poly(TMC) and poly(TMC-co-DLLA) with DLLA contents of 5% and 20%. On the other hand, poly(TMC-co-DLLA)(50:50) had 1.3 times the σ_b as the other copolymers. Poly(TMC-co-DLLA)(50:50) had a σ_b of 3.2 ± 0.4 MPa, compared to 2.5 ± 0.1 MPa for poly(TMC-co-DLLA)(80:20) and 2.6 ± 0.1 MPa to poly(TMC-co-DLLA)(95:5). Addition of DLLA to the elastomers had a marked effect on the strain at break (ε_b). Adding only 5 mole% DLLA reduced the ε_b 1.4 times, while further addition of DLLA decreased ε_b 1.8 times in poly(TMC-co-DLLA)(80:20) and 2.7 times for poly(TMC-co-DLLA)(50:50).

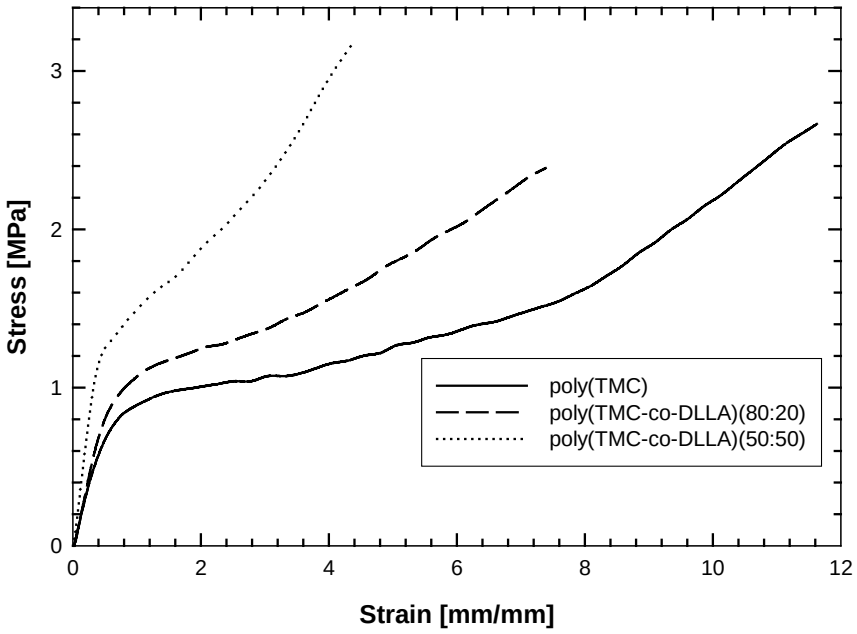

Figure 4- 2. Representative stress-strain curves of poly(TMC) and poly(TMC-co-DLLA) elastomers.

The elastomers were amorphous and rubbery at 37 °C (Table 4-2). The glass transition temperature increased with the increase in DLLA content, being –14.1 °C for the TMC elastomer, and increasing to 5.5 °C in poly(TMC-co-DLLA)(50:50) (Table 4-2). The increased degree of acrylation with increasing DLLA content in the elastomer resulted in elastomers with lower sol content (Table 4-2).

Table 4- 2. Physical and mechanical properties of synthesized elastomers.

Elastomer	sol content [%]	T_g [°C]	d [g.cm^{-3}]	E (MPa)	σ_b (MPa)	ε_b (mm/mm)
TMC	28.1 ± 0.5	-14.1	1.357	1.8 ± 0.1	> 2.6	> 12.9
TMCDLLA(95:5)	21.1 ± 0.5	-11.8	1.333	1.8 ± 0.1	2.6 ± 0.1	9.4 ± 0.4
TMCDLLA(80:20)	20.3 ± 0.4	-4.1	1.281	1.8 ± 0.1	2.5 ± 0.1	7.3 ± 0.4
TMCDLLA(50:50)	12.7 ± 0.6	5.5	1.270	3.3 ± 0.2	3.2 ± 0.4	4.7 ± 0.4

E, Young's modulus; σ_b, stress at break; ε_b, elongation at break. The values of glass transition temperature (T_g) are for sol-removed elastomers, and the values of network

density are for sol non-removed elastomers.

4.3.3. BSA Release

The volumetric loading in our experiments was kept below the percolation threshold to minimize the contribution of diffusion, and to obtain an effective osmotic release mechanism [89, 90]. To form solid particles with an appreciable osmotic activity, BSA was lyophilized with trehalose, which is known to be an effective lyoprotectant and a compatible osmolyte that accumulates in organisms under stress conditions [149]. A saturated solution of trehalose can provide an osmotic pressure of 92 atm at 37 °C [130].

Although trehalose was capable of generating effective BSA release from ε-caprolactone-D,L-lactide based elastomers [35, 99] trehalose was unable to generate significant BSA release from the TMC elastomer (Figure 4-3A). Moreover, these rods continued to draw in water and to swell for up to 40 days in PBS buffer (Figure 4-3B). Thus, it appears that elastomers composed solely of TMC are not suitable for osmotically driven release when trehalose is the main osmotically active component.

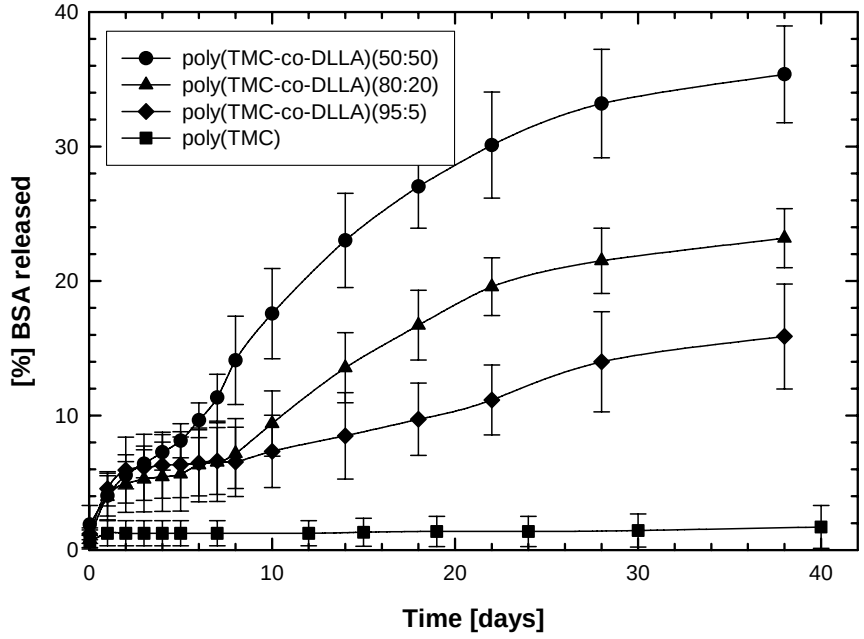

Figure 4-3A

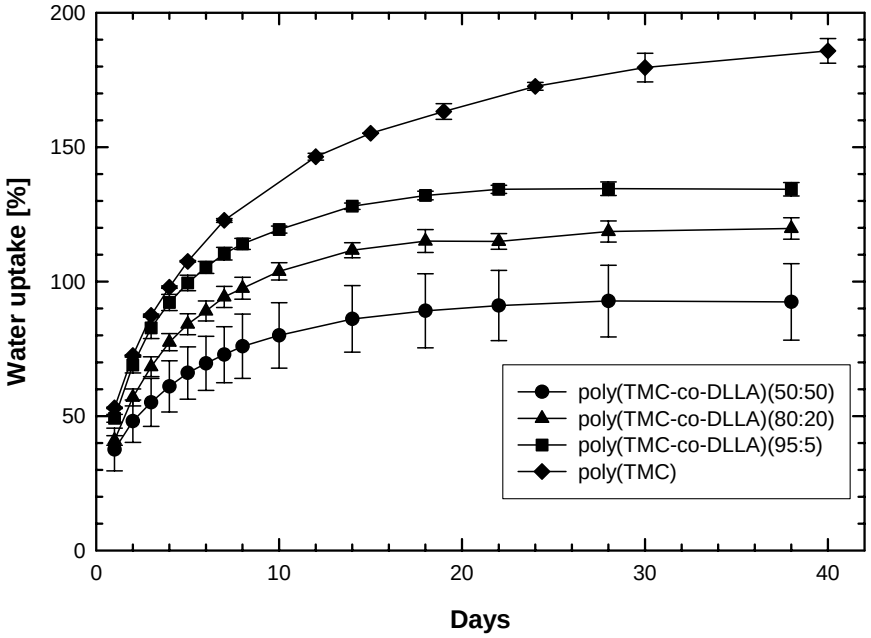

Figure 4-3B

Figure 4- 3. (A) BSA release from poly(TMC) and poly(TMC-co-DLLA) elastomeric rods, loaded with 25% by mass solid particles made of (10% (w/v) BSA and 90% (w/v) trehalose). (B) Percentage water uptake in poly(TMC) and poly(TMC-co-DLLA) elastomeric rods loaded with with 25% by mass solid particles. The data represent the average of triplicate samples and error bars the standard deviation about the average value.

Osmotic release is not only driven by the osmotic pressure of the solution generated within the capsule, but also by the mechanical properties of the elastomer [20, 93], which have been shown above to be influenced by the amount of DLLA incorporated into the polymer. For these elastomers, the release occurred in two phases. The first phase appeared to be primarily diffusionally controlled, releasing a total mass fraction of consistently approximately 6 ± 2%. This was followed by a second, faster release phase, due to the osmotic release mechanism. The release rate was faster, and larger amounts of BSA were released, when greater amounts of DLLA were incorporated in the elastomer; at day 38 elastomer made of poly(TMC-co-DLLA)(50:50) released 35.4 ± 3.6%, poly(TMC-co-DLLA)(80:20) released 23.2 ± 2.2 %, and poly(TMC-co-DLLA)(95:5) released 15.9 ± 3.9 % of encapsulated BSA. The second release period is attributed to the time required for sufficient amounts of water to be imbibed to generate enough pressure to induce cracking to generate micropores within the elastomer and thus initiate release through the osmotic mechanism. This time period decreased as the DLLA content of the elastomer increased. Thus, the strain at break of the elastomer plays a dominant role in determining the osmotic release behavior of particles with similar osmotic and physical properties.

These results are explained mathematically as follows. Water imbibition into a capsule is described by the following equation [93, 95]

$$\frac{dV}{dt} = \frac{k_w A(\Pi - p)}{h} \qquad (4\text{-}5)$$

where V is the amount of water imbibed, h is the capsule wall thickness, k_w is the hydraulic permeability of the polymer, A is the capsule surface area, Π is the osmotic

pressure of solid particle solution in the capsule, and p is the resisting pressure of the polymer expressed as [93],

$$p = \frac{E}{6}(5 - \frac{4}{\lambda} - \frac{1}{\lambda^4}) \qquad (4\text{-}6)$$

where E is the modulus and λ is the ratio of the swollen capsule radius to the original radius. Thus the smaller the elongation at break, the smaller λ, and the polymer has less tear resistance. Elastomers with greater resisting pressure require higher osmotic pressure in the capsule to rupture, because the crack formation occurs only when Π is larger than p. Thus, elastomers with greater expandability draw larger amounts of water before being ruptured (Figure 4-3B). This explanation is supported by the water uptake rates of the different elastomers (Figure 4-3B). Elastomers composed of solely TMC, which had the highest strain at break and lowest release rate, continually drew in water and swelled for up to 40 days in PBS buffer. Elastomers containing DLLA, on the other hand, reached an equilibrium water uptake around day 20, regardless of DLLA content.

4.3.4. Influence of Polymer Degradation

To determine the effect of the change in mechanical properties of the elastomer during the osmotic release, the hydrolytic degradation of poly(TMC-co-DLLA)(95:5) and poly(TMC-co-DLLA)(80:20) elastomers was investigated *in vitro*. Elastomers with low compositions of DLLA were chosen, since they produce fewer acidic degradation products and thus are potentially better candidates for localized delivery of acid sensitive proteins. The changes in mechanical properties during the *in vitro* degradation are given in Figure 4-4.

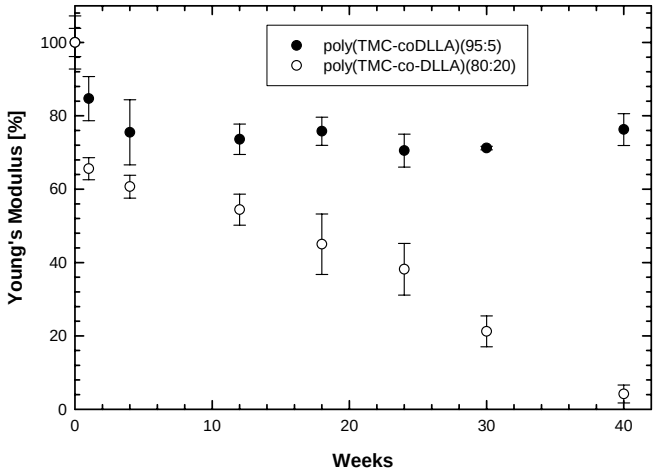

Figure 4-4A

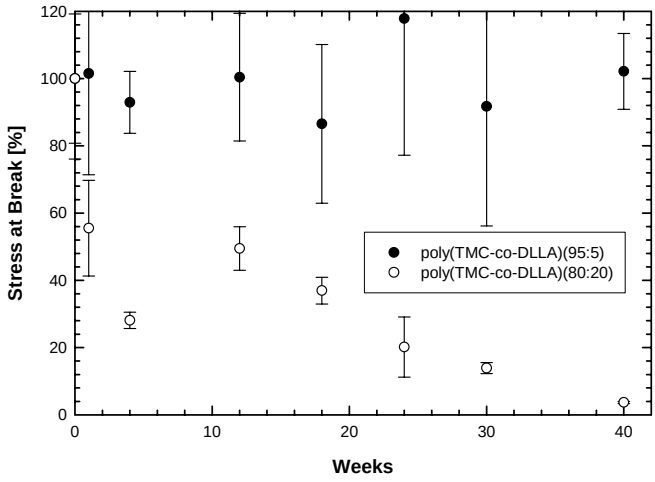

Figure 4-4B

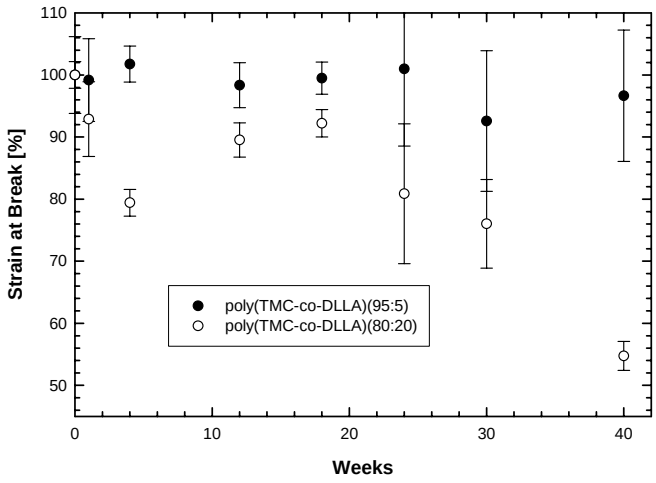

Figure 4-4C

Figure 4- 4. Effect of *in vitro* degradation on mechanical properties of poly(TMC-co-DLLA)(80:20) elastomer A) modulus (E) B) ultimate tensile stress (ε_b) C) strain at break (σ_b). The data represent the average of triplicate samples and error bars the standard deviation about the average value.

After a slight decrease in the modulus at week 1, poly(TMC-co-DLLA)(95:5) elastomer exhibited no change in modulus during the degradation process. This decrease was due to the plasticization effect of water molecules. In the case of poly(TMC-co-DLLA)(80:20) elastomer, the modulus experienced a 34.4% decrease in its initial value at week 1, and then it decreased gradually up to week 12. After week 12, the modulus decreased at a faster rate, becoming almost immeasurable by week 40 (Figure 4-4A). Changes in tensile stress at break of the elastomers are shown in Figure 4-4B. Similarly to the observed change in modulus, the poly(TMC-co-DLLA)(95:5) elastomer did not experience a significant change in its stress at break values during the 40 weeks of degradation. Poly(TMC-co-DLLA)(80:20) elastomer, on the other hand, experienced a linear drop in its stress at break values with time starting from week 12 (Figure 4-4B). In contrast to the observed decrease in modulus and tensile strength with degradation time, the poly(TMC-co-DLLA)(80:20) elastomer did not experience significant alteration in its strain at break until after week 24; by week 40, the strain at break had decreased to 55 % of its initial value (Figure 4-4C). The poly(TMC-co-DLLA)(95:5) elastomers did not experience any drop in their strain at break values during the degradation period (Figure 4-4C).

Poly(TMC-co-DLLA)(95:5) elastomer lost only 2 % of its mass during the 40 weeks of investigation, and this mass loss was accompanied with a 1.3 ± 0.5 % increase in sol content. In the case of the poly(TMC-co-DLLA)(80:20) elastomer, mass loss started at week 12, and by week 40 the elastomers lost 13.5 ± 1.2 % of their initial mass (Figure 4-5). These elastomers increasingly began to absorb water after week 12,

reaching a wet mass increase of 36 ± 0.5 % by week 40. This increase in water uptake was accompanied with an increase in the sol content, which reached 62 ± 8 % at week 40. It can be concluded from these results that there is little influence of changes in mechanical properties of the elastomers due to degradation on the BSA release behavior, as they do not change appreciably over the release time frame.

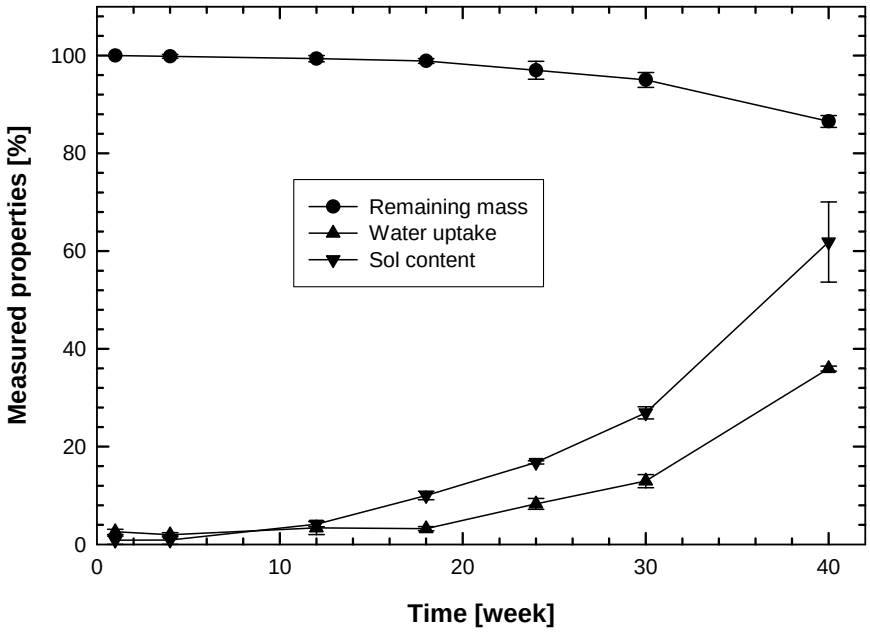

Figure 4- 5. Change in water uptake, sol content, and mass loss of poly(TMC-co-DLLA)(80:20) elastomer during in vitro degradation in PBS buffer. The data represent the average of triplicate samples and error bars the standard deviation about the average value.

To confirm that the drop in mechanical properties at week 1 was due to plasticization effects and not to hydrolysis, and to investigate the structure of degraded elastomer, the surface of degraded poly(TMC-co-DLLA)(80:20) was investigated using ATR-FTIR (Figure 4-6). The band at 1750 cm^{-1} was assigned to C=O stretching, the band at 2970 cm^{-1} and 2908 cm^{-1} were due to symmetric and asymmetric CH stretch in methine groups of TMC and methyl and methine groups of DLLA. After immersing in

buffer the band at 2908 cm^{-1} shifted to 2916 cm^{-1} and it became stronger, and a new band was formed at 2850 cm^{-1}. These bands were present only on the outer surface and not in the cross-section. The newly formed band at 2850 cm^{-1} and the shifted band at 2916 cm^{-1} returned to their initial intensity and location with time (Figure 4-6B). A possible explanation is that hydrophilic regions of the elastomer become preferentially oriented at the surface due to hydration initially [111]. When the amount of water increases in the elastomer (Figure 4-5), polymeric chains, at the surface region, reorient themselves. As a result, the intensity of bands at 2850 cm^{-1} and 2916 cm^{-1} decrease and finally disappear (Figure 4-6B). Similar phenomenon occurred in hydrated poly(TMC) elastomer, known to degrade very slowly by hydrolysis (Figure 4-6C) [55]. Thus the formation of bands at at 2850 cm^{-1} and 2916 cm^{-1} and the decrease in their intensity is due to surface orientation and not due to degradation. At week 30 of the *in vitro* degradation, a band appeared at 1600 cm^{-1}, due to the formation of carboxylate ion in the degraded elastomer (Figure 4-6A). The intensity of the band at 1600 cm^{-1} became stronger at week 40 as the degradation progressed. ATR-FTIR results do not show any significant degradation at week 1, thus changes in mechanical properties at week one is due to a non-degradation result.

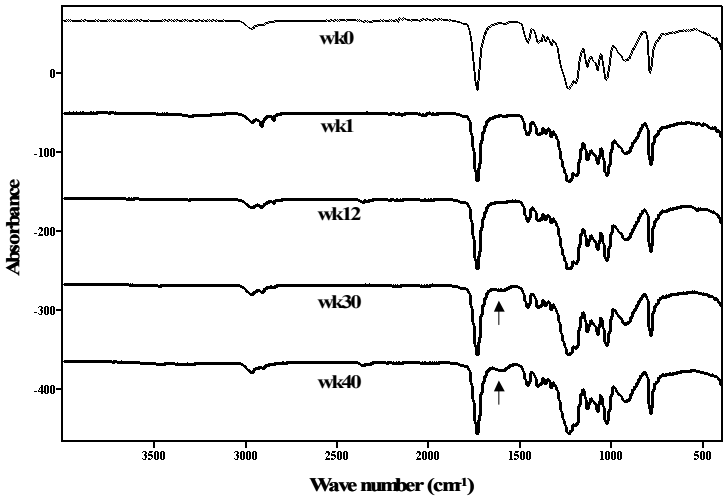

Figure 4-6A

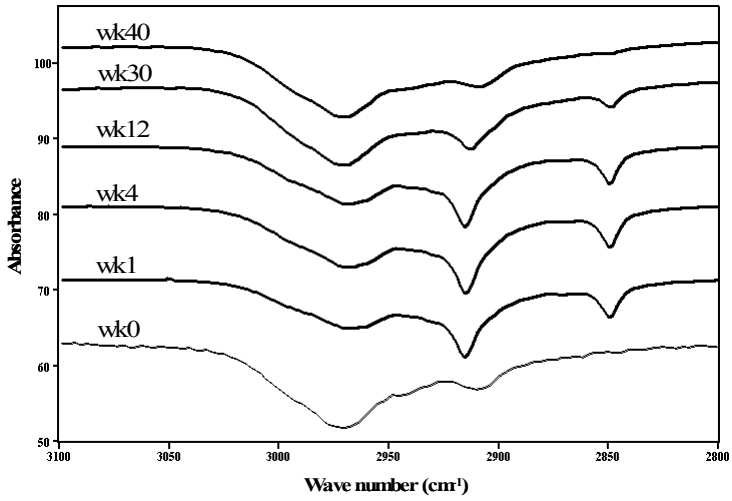

Figure 4-6B

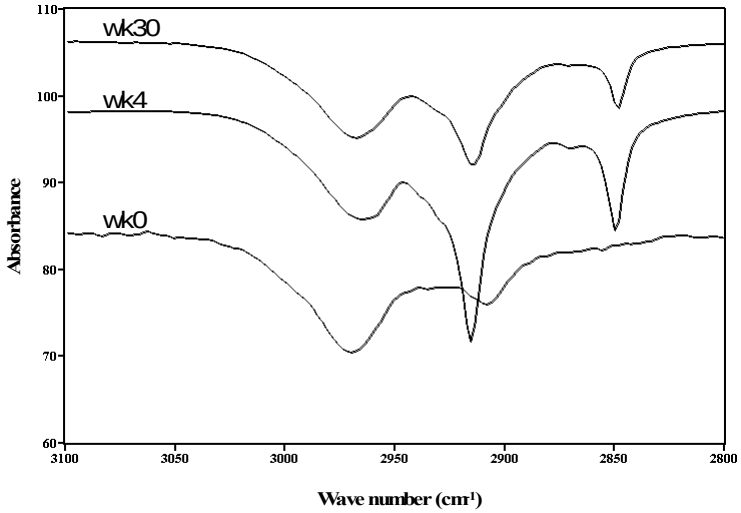

Figure 4-6C

Figure 4- 6. ATR-FTIR analyses of *in vitro* degraded poly(TMC-co-DLLA)(80:20) elastomer. A) Changes in the entire region. B) Changes in CH stretch region of *in vitro* degraded poly(TMC-co-DLLA)(80:20) elastomer. C) Changes in CH stretch region of *in vitro* degraded degraded poly(TMC) elastomer. Arrows indicate to carboxylate ion peaks.

4.3.5. Microenvironmental pH

The rate of DLLA hydrolysis is slow, and so it was reasoned that there would be little change in the microenvironmental pH within the interior of the elastomer during degradation. To test this hypothesis, and to investigate why the total release of the

particles was low, FITC-BSA was lyophilized with trehalose under the same conditions as BSA and these particles were loaded into poly(TMC-co-DLLA)(80:20). The FITC-BSA loaded elastomer was imaged at depths of up to 160 μm, prior to (Figure 4-7A), and after, 17 days of release (Figure 4-7B), via laser scanning confocal microscopy (Figure 4-7). The results show that the FITC-BSA particles maintained their fluorescence after 17 days of release. As FITC no longer fluoresces below pH 5, it can be concluded that the internal pH did not drop significantly. From the images it is apparent that particle release occurs from surface regions of the rods and progresses into the centre with time, in accordance with the osmotic release mechanism. However, by 17 days, when release had almost ceased, only those particles in the outer region of the rod were released. This is likely due to an insufficient water activity gradient being formed between the water in the outer region of the rod containing unreleased trehalose and BSA in the microcracks formed, and the water contacting encapsulated particles in the inner regions of the rod.

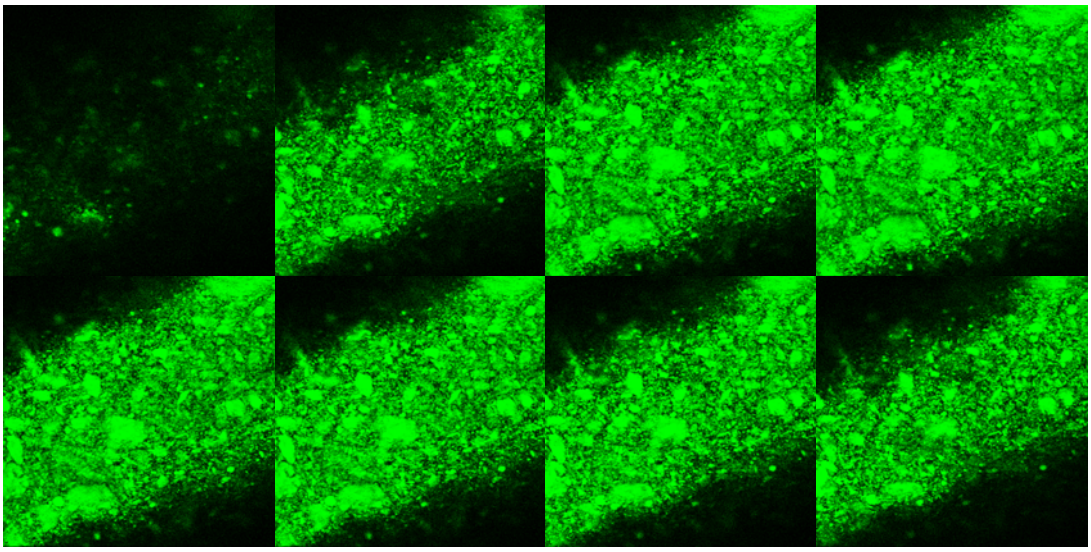

Figure 4-7A

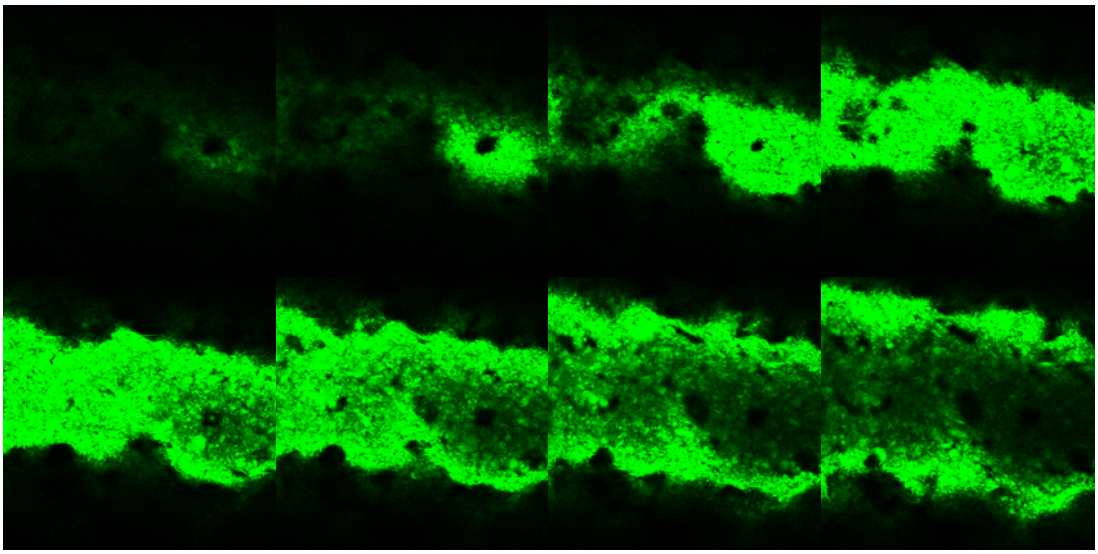

Figure 4-7B

Figure 4- 7. A) Images of FTIC-BSA in as prepared sample at 20 μm depth intervals. B) Images of FTIC-BSA, lyophilized with trehlaose, and loaded with a 25% by mass in poly(TMC-co-DLLA)(80:20) elastomer after 17 days of release in PBS buffer. Images were taken in the radial direction towards the centre of the rod at 20 μm intervals.

4.3.6. Influence of particle loading:

To examine the effect of the initial volumetric loading of particles on the release rate and total amount of BSA release, rods of poly(TMC-co-DLLA)(80:20) with 3 volumetric loadings of 8.3 v/v%, 12.6 v/v% and 21.5 v/v% (corresponding to 10 w/w%, 15 w/w% and 25 w/w%) were prepared and the rate of BSA release measured. The volumetric loading did not have a significant impact on the total amount of BSA release (Figure 4-8A). The rate of release was slightly greater initially in the case of lower volumetric loadings. The water uptake, however, was 3 times greater when the loading was 25% compared to 10% loading (Figure 4-8B). Elevated amounts of water in the device could potentially denature unreleased protein therapeutics. Therefore, since the volumetric loading does not have significant impact on the rate and total amount of BSA release, provided the loading is below the critical loading, it is advisable to use lower

volumetric loadings.

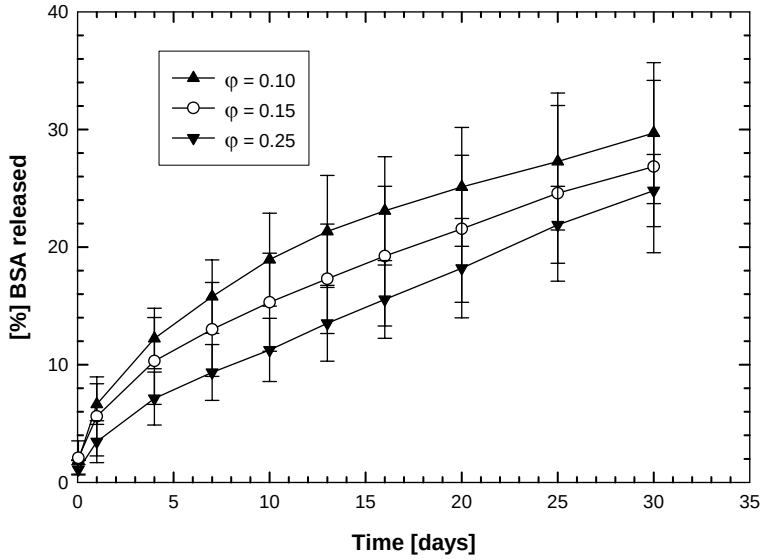

Figure 4-8A

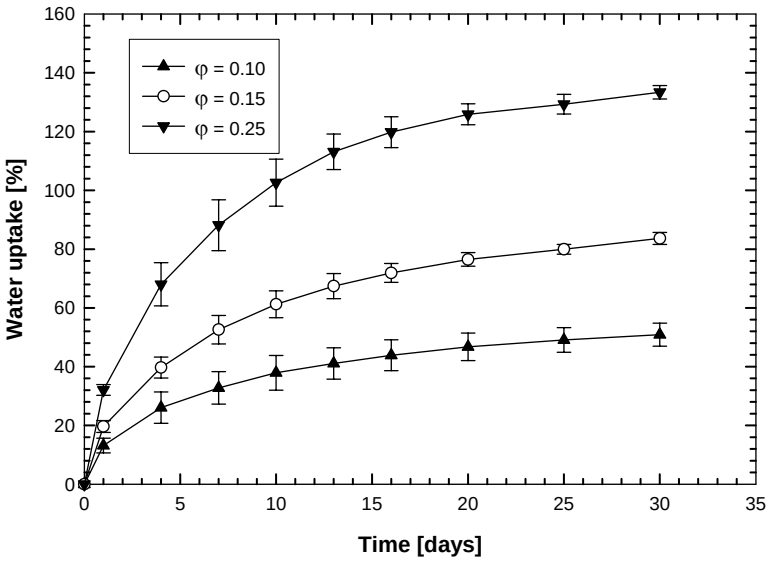

Figure 4-8B

Figure 4- 8. A) Effect of particle loading on the release of BSA from poly(TMC-co-DLLA)(80:20) elastomer. B) Percentage water uptake in poly(TMC-co-DLLA)(80:20) elastomer at different particle loadings. φ represents the percentage of the mass loading.

4.3.7. Influence of increasing osmotic activity of solid particles

In an effort to increase the osmotic activity of the encapsulated solid excipient, BSA was lyophilized with a mixture of trehalose and NaCl. As noted above, a saturated

solution of trehalose has an osmotic pressure of 92 atm, while a saturated solution of NaCl can provide an osmotic pressure of 345 atm at 37 °C [91]. The effect of increasing the osmotic pressure within the swelling particle capsule was dependent on the nature of the elastomer. Increasing the osmotic pressure of solid excipient had a minor effect on providing an effective release from TMC elastomer (Figure 4-9A). For these rods, the cumulative release of BSA was 17.1 ± 7.7 % at day 10, the rate of release increased after day 10 reaching 52.6 ± 10.9 % at day 34, and the increase in the rate of release was accompanied with a decrease in water uptake (Figure 4-9B). By contrast, increasing the osmotic pressure of encapsulated solid particles increased both the release rate and total amount of BSA release from poly(TMC-co-DLLA)(80:20). The release was approximately zero order for a period of 12 days, and was sustained for a period of 34 days. The total amount of BSA released was 73.5 ± 3.8 % after 34 days (Figure 4-9A). Moreover, both BSA and trehalose were released at similar rates, as has been found previously [64, 87]. The water uptake profile in this system exhibited a maximum at day 7, after which it decreased (Figure 4-9B). This result confirms that effective osmotic release occurs at low values of water uptake.

The following equation [93] for osmotic pressure driven release from cylindrical rubbery non-degradable polymer matrices was fitted to experimental data to evaluate the time required for a capsule layer to burst (t_b).

$$\frac{m_t}{m_T} = \frac{1}{1+\frac{R}{x}}\left[(2+\frac{x}{R})(\frac{t}{t_b}) - \frac{x}{R}(\frac{t}{t_b})^2\right] \qquad (4\text{-}7)$$

where m_t/m_T is the mass fraction of drug released, x is the thickness of the particle layer

[93], t is the time, and R is the diameter of the cylindrical device. Particle layers were assumed to have the structure of a concentric cannuli. The thickness of the particle layer was calculated from $x = \bar{h} + 2r_0$, in which $\bar{h}$ could be evaluated using the following equation:

$$\bar{h} = \frac{L - nd}{n + 1} \qquad (4\text{-}8)$$

where, L is the length of a cube matrix, which has an equivalent volume to a cylindrical device, and n is the number of solid particles in any one dimensional direction within the cube, and it could be calculated from the following equation

$$n = \frac{L}{d}\phi^{\frac{1}{3}} \qquad (4\text{-}9)$$

where, ϕ is the volumetric loading and d is the diameter of solid particles. The average diameter of the device was 1.54 ± 0.01 mm, the average length was 12.56 ± 0.18 mm, and the average radius of solid particles was 78.7 ± 21.2 μm. The area of solid particles, which had a non-circular shape, was measured using Motic images plus 2 software and the radius of a circle with an equivalent area was calculated. The density of solid particles was taken as 1.587 g.cm^{-3}, based on the density of its components. The density of the elastomer was 1.281 g.cm^{-3} (Table 4-2), and the volumetric loading was 7.7%. Based on these numbers the average thickness of the particle layer was calculated to be 345.7 μm. By fitting the model to experimental data using a least squares approach, t_b was found to be 11.2 ± 2.4 days (R^2 = 0.989). The time to burst is proportional to the square of the particle size according to the following equation [93]:

$$t_b = \frac{r_0^2}{k_w}\int_1^{\lambda_c} \frac{\left[\left[\lambda^3 + (\frac{\bar{h}}{r_0}+1)^3 - 1\right]^{1/3} - \lambda\right]}{(\pi - p)} d\lambda \qquad (4\text{-}10)$$

Where r_0 is the radius of the particle and λ_c is the ultimate radial extension of the swollen capsule. Large time to burst indicates to relatively large particles within the device. The model provides very good fit to the experimental data, especially for the initial 12 days (Figure 4-8A). The model does not provide an adequate representation of the release at later stages. This is most probably due to longer times required for the drug to be forced out and diffuse out of the device when the polymer cracking activity extends deep towards the centre of the cylinder. Trehalose was released at a rate identical to the rate of BSA release.

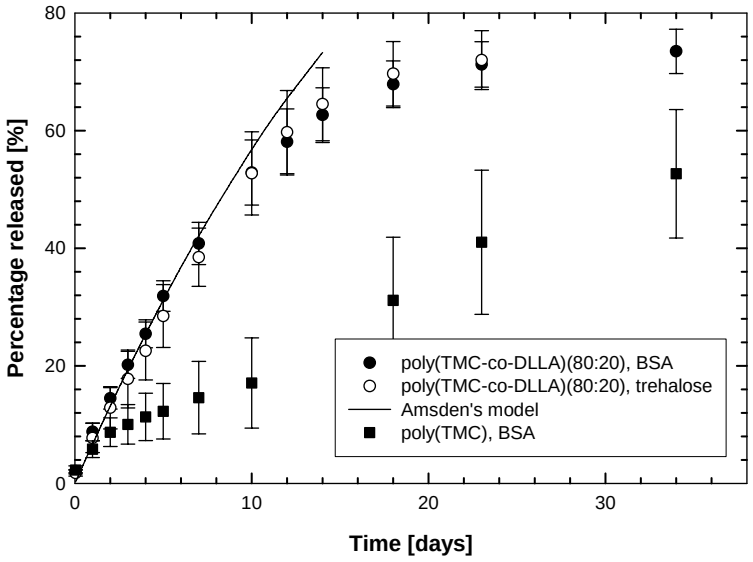

Figure 4-9A

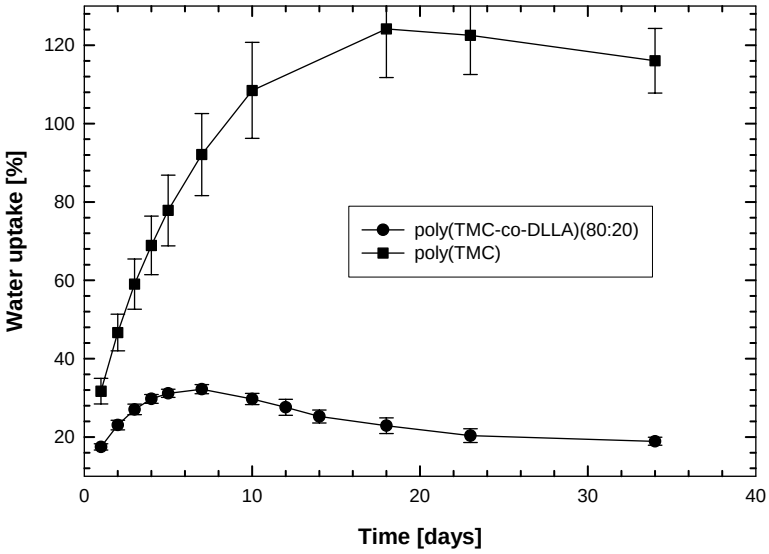

Figure 4-9B

Figure 4- 9. (A) BSA and trehalose release from poly(TMC) and poly(TMC-co-DLLA)(80:20) elastomeric rods, loaded with 10% by mass of solid particles made of (10% BSA (w/v), 25% NaCl (w/v) and 65% (w/v) trehalose). B) Percentage water uptake in poly(TMC) and poly(TMC-co-DLLA) elastomeric rods loaded with 10% by mass solid particles. The data represent the average of triplicate samples and error bars the standard deviation about the average value.

4.4. CONCLUSION:

Poly(TMC-co-DLLA) elastomers with low DLLA content have a higher potential of success than poly(DLLA-co-CL)(50:50) elastomer, investigated previously[10, 35], in localized delivery of acid labile proteins. This is due to two reasons: the first is that lower content of DLLA generates less acid degradation products, and acid autocatalysed degradation stage will proceed at a slower rate compared to poly(DLLA-co-CL)(50:50) elastomer. The second reason is that unlike the ester groups of ε-CL [110], the carbonate groups of the TMC chains undergo very little hydrolysis even at pH values as low as 2 [19]. The *in vitro* degradation study indicated that degradation played a minor role in the osmotic release, since mechanical properties undergo very little change during the investigated period of release. Elongation at break plays a dominant role in determining

osmotic release behavior when the device is elastic and embedded particles have sufficient osmotic activity to rupture the elastomer. To improve osmotic release properties, TMC was copolymerized with DLLA. The incorporation of small amounts of DLLA decreased the tear resistance of the elastomer, and improved the osmotic release of the incorporated protein. The poly(TMC-co-DLLA)(80:20) elastomer was able to provide a near zero order release of BSA for up to 12 days, and the total amount of BSA released was 74 ± 4 % after 34 days. The degradation results indicate that TMC elastomers copolymerized with small amounts of DLLA degrade slowly with no significant reduction in the microenvironmental pH. Therefore, they could possibly be considered as potential candidates in the localized delivery of acid sensitive proteins.

5. CHAPTER FIVE

Combined Delivery of Bioactive $VEGF_{165}$ and HGF from Poly(trimethylene carbonate) Based Photo-Cross-Linked Elastomers

Manuscript submitted for publication in Journal of Controlled Release. July, 2009

Authors: R. Chapanian [1] and B.G. Amsden [1,2*]

[1]Department of Chemical Engineering
[2]Human Mobility Research Centre

Queen's University, Kingston, Ontario, Canada, K7L 3N6

* To whom correspondence should be addressed

ABSTRACT

The ability of trimethylene carbonate (TMC) based elastomers to release bioactive vascular endothelial growth factor ($VEGF_{165}$) and hepatocyte growth factor (HGF) separately and in a combined fashion using an osmotic release mechanism was investigated. A TMC based elastomer was chosen since TMC degrades without producing potentially harmful acidic degradation products, and its mechanical properties can be tailored by copolymerizing with D,L-lactide (DLLA) and ε-caprolactone (ε-CL), and by controlling the cross-link density. The bioactivity of released $VEGF_{165}$ and HGF were assessed using the proliferation of human aortic endothelial (HAEC) and CCL 208 monkey epithelial cell lines. $VEGF_{165}$ and HGF were lyophilized separately or together with trehalose, rat serum albumin (RSA) and NaCl. No significant elastomer degradation occurred during the initial 8 weeks, during which the bulk of embedded growth factors were released. The presence of small amounts of NaCl in the release media did not affect the viability of HAEC and CCL 208 cells. The TMC based elastomer was able to provide a sustained release of highly bioactive $VEGF_{165}$ and HGF for more than 10 days. When released in combination from the same device, $VEGF_{165}$ and HGF were released at similar rates. This study demonstrates the potential of TMC based elastomers combined with an osmotic mechanism to release bioactive acid sensitive growth factors alone and in combination.

Keywords: $VEGF_{165}$, HGF, growth factor delivery, osmotic release

5.1. INTRODUCTION:

Therapeutic angiogenesis using growth factors is a promising treatment for chronic myocardial and limb ischemia [4]. Angiogenesis is initiated by the activation, migration and proliferation of endothelial cells from pre-existing blood vessels to form new capillaries and vessels. Numerous cell types, proteolytic enzymes, cytokines and growth factors participate in the process [150]. It is proposed that a polymer-based system providing sustained delivery of relevant growth factors could provide a maximum efficacy/dose relationship by overcoming the obstacles pertinent to systemic and bolus injections of these growth factors. These obstacles include maintenance of growth factor *in vivo* stability and potential adverse side effects associated with high concentrations and systemic exposure of the growth factors [5].

In order to produce a clinically viable, polymer based sustained delivery device, a simultaneous solution of growth factor denaturing problems is required. These problems are related to the growth factor stability during the device synthesis and during the delivery process. Irreversible inactivation during the device synthesis may occur when a growth factor is exposed to physical, mechanical and chemical stresses, which are specific to the preparation technique [5, 16]. Potential sources of irreversible growth factor inactivation during delivery include adsorption to hydrophobic and charged surfaces, low micro-environmental pH, and elevated levels of moisture [16]. Other requirements for a successful polymer based growth factor delivery system include a reduced initial burst, efficient pharmacokinetics, and a near complete release of the embedded growth factor. For example, the initial burst of VEGF, a highly specific

mitogen that promotes the formation of blood vessels, could lead to the formation of abnormal short-lived blood vessels full of glomeruloid bodies [17, 18]. Growth factor/matrix interaction [12, 15] and a drop in microenvironmental pH decreases the bioactivity of released growth factors [9-11], and the non-complete release (trapped proteins) could cause immunogenicity [8].

To overcome the low pH problem, which is considered to be a significant obstacle in the commercialization of PLGA microspheres as a delivery vehicle for therapeutic proteins [69], Zhu *et al.* used basic salts such as $Mg(OH)_2$ and $MgCO_3$ [16]. Others blended PEG with PLGA [74]. Incorporating 3 % of $Mg(OH)_2$ within the solid excipient increased the total fraction of BSA from 20 % to 80 %. BSA maintained its structural integrity and did not aggregate for over one month [16]. Others have reported that adding PEG also improved the stability of BSA and ovalbumin in PLGA/PEG microspheres [79, 80]. These strategies, however, provide a limited assistance to overcome the low pH problem, since adding basic salts or PEG only postpones the drop in microenvironmental pH. For example, the pH was found to be less than six in as short a time as four days in half of the pores, when PLGA was loaded with 3% $MgCO_3$. Blending PEG with PLGA, on the other hand, maintained the pH at between 5 and 5.8 during four weeks of incubation in PBS [74]. However, the use of PEG results in a significant burst effect of approximately 60% of loaded VEGF [32], which reduces the efficiency of the device, and it could lead the formation of abnormal and short lived blood vessels [17, 18].

Since angiogenesis is a complex process, the combined release of different growth

factors with distinct kinetics and cellular influence was found to achieve a more effective angiogenesis [30]. Hao *et al*. found that the sequential growth factor delivery of $VEGF_{165}$ and platelet derived growth factor beta polypeptide (PDGF-BB) induced the formation of mature, stable vessels because PDGF-BB recruited smooth muscle cells that stabilized sprouted endothelial cells [30]. Xin *et al*., on the other hand, reported that combined delivery of $VEGF_{165}$ and HGF achieved a more effective therapeutic angiogenesis than that achieved with either growth factors administered alone [151]. Moreover, the combination therapy had an amplified, synergistic effect [151].

The osmotic release from photo-cross-linked elastomers is a promising technique for the delivery of growth factors [8]. This technique can provide many of the requirements for a successful polymer based growth factor delivery system [5]. It provides a linear and sustained release of bioactive growth factors for a period of longer than two weeks with a low initial burst [35]. The osmotic pressure release mechanism is governed by the osmotic activity of embedded particles and by mechanical properties of the matrix. In osmotic pressure drug release, water vapor diffuses through the polymer matrix until it encounters a polymer-surrounded drug particle. At the particle/polymer interface, the water phase dissolves a portion of the particle, forming an activity gradient between the capsule and the surrounding medium. The activity gradient draws water into the capsule generating an osmotic pressure equal to the osmotic pressure of a saturated solution [8]. The generated pressure in the capsule is resisted by the viscoelastic nature of the polymer [8]. The outcome of this resistance is one of the following: 1) when the polymer is unable to resist the pressure generated in the capsule, polymer bonds are

broken, and cracks are formed, which connect the contents of the capsule to the pore network, pushing the dissolved contents toward the surface as a result of the pressure gradient, or 2) when the generated pressure in the capsule is unable to initiate bond breakage in the polymer, a thermodynamic equilibrium is established and the encapsulated drug is not released until the polymer degrades [8, 20]. The osmotic release mechanism dominates when the total volumetric loading of the active agent in the polymer matrix is below the percolation threshold for particle loading [89, 90].

Recently we illustrated that by a careful choice of the elastomer composition, the microenvironmental pH drop can be reduced significantly in the pores and channels of the elastomer. Copolymerizing TMC with other monomers such as DLLA decreased the polymer tear resistance and consequently increased the rate and the total amount of BSA released. The micro-environmental pH in the device did not drop significantly after 17 days, when TMC was copolymerized with small amounts of DLLA [poly(TMC-co-DLLA)(80:20)]. The objectives of this study are to investigate the ability of TMC based elastomers to release bioactive growth factors in a sustained fashion utilizing the osmotic pressure mechanism, and to investigate the ability of the system to provide combined growth factor release with similar kinetics. To achieve our objectives, two model growth factors: $VEGF_{165}$ and HGF were chosen, which were lyophilized together or separately with trehalose, rat serum albumin (RSA) and NaCl. Trehalose and NaCl provided the osmotic pressure driving the release. The released growth factors were quantified using the ELISA technique and their bioactivity was assessed using cell line assays.

5.2. MATERIALS AND METHODS

D,L-Lactide (99+%) was obtained from Purac, the Netherlands, and purified by recrystallization from dried toluene. 1,3-trimethylene carbonate (1,3-dioxan-2-one) was obtained from Boehringer Ingelheim, Germany and used as received. ε-Caprolactone was obtained from Lancaster, Canada, dried over calcium hydride, distilled under high vacuum and stored over activated 4 μm molecular sieves. Toluene and dichloromethane were dried over calcium hydride and distilled under argon. Other chemicals were used without further purification. Chemicals used in polymer synthesis include stannous 2-ethylhexanoate (96%) obtained from Aldrich, Canada and glycerol obtained from BDH, USA. Chemicals used in the acrylation process include acryloyl chloride (96%), triethylamine (99.5%), and 4-dimethylaminopyridine (99%), all obtained from Aldrich, Canada. 2,2-dimethoxy-2-phenylacetophenone used as photoinitiator was obtained from Aldrich, Canada. Solvents used for purification of the synthesized polymers include ethyl acetate (99.9%) andmethanol (99.8%) were obtained from Fisher, Canada. For the release studies, recombinant human $VEGF_{165}$, HGF, epidermal growth factor (EGF) and a $VEGF_{165}$ ELISA kit were purchased from Peprotech Inc., Canada. An HGF ELISA kit was purchased form R&D Systems (USA). Trehalose and NaCl were obtained from Sigma, Canada, and rat serum albumin (RSA) from Innovative Research (USA). Chemicals used in calorimetric assays include Coomassie brilliant blue G obtained from Fluka, Canada, and phosphoric acid (85%) and sulfuric acid (95-98%) obtained from Fisher, Canada. For VEGF release studies, human aortic endothelial cells (HAEC) were purchased from Cambrex Inc., USA. EGM-2 media was purchased from Lonza, NJ, USA. CCL 208 cell line was purchased from ATCC The Global Bioresource Center

(USA). Ham's F-12K medium was purchased from Invitrogen (Canada). A WST-1 cell proliferation assay kit was purchased from Roche Ltd, Canada.

5.2.1. Preparation of solid particles:

$VEGF_{165}$ and HGF together or separately were reconstituted with RSA, trehalose and NaCl in 5 mM succinate buffer at pH 7.4 to a final concentration of 0.1 g in 1.27 ml of buffer. Reconstituted solutions were frozen in liquid nitrogen, and lyophilized on a Modulyo D freeze-dryer (Thermosavant, USA) at 100 μbar for 2 days. The lyophilized powder was ground using a mortar and pestle and sieved through a Tyler 60 sieve to yield particles less than 250 μm in diameter. Solid particles were composed of 9.8 % RSA, 88.5 % trehalose, 0.1% VEGF, and 1.72% di sodium succinate. When particle contained NaCl 5 % of trehalose was replaced with NaCl.

5.2.2. Prepolymer Preparation

4000 and 7800 Da acrylated *star*-poly(TMC-co- ε-CL-co- D,L-lactide) prepolymers with a theoretical composition of 50 mole % TMC, 25 mole % ε-CL and 25 mole % D,L-lactide were prepared as described previously [55]. The polymerization was performed in the presence of stannous(II) ethylhexanoate at 130 °C for 72 hrs. For acrylation of the star-copolymer chain ends, the heated star-copolymer was poured into a dried round-bottomed flask, the flask sealed with a rubber septum, and purged with dry argon. The following procedures were conducted in a glove box. Dried dichloromethane (DCM) was added to the flask at a ratio of polymer to solvent of 2:1 (w:v) to dissolve the polymer. Triethylamine was added at a molar ratio of 1 mole per mole of star-copolymer

(SCP) hydroxyl group, while the 4-dimethylaminopyridine catalyst was added at a molar ratio of 2×10^{-3} mole per mole of SCP terminal hydroxyl group. Finally, acryloyl chloride was diluted in dried DCM at a ratio of 1:1 (v:v) and added slowly in a drop-wise fashion at a ratio of 1.2 moles per mole of SCP hydroxyl group. The synthesized prepolymers were characterized using ^{1}H NMR using a 500 MHz Bruker-Avance spectrometer and DMSO-*d6* as a solvent.

5.2.3. Elastomeric Rod Preparation:

To prepare elastomeric rods, prepolymer of a given composition was dissolved in ethyl acetate at a ratio of 1:1 (w:w) and 1.5 w/w(polymer) % of 2,2-dimethoxy-2-phenylacetophenone was added as a photo-initiator [105]. The mixture was poured into glass tubes sealed at one end, and capped with a rubber septum at the other end. The tube was connected to the shaft of a motor rotated at 200 rpm, and exposed to long-wave UV light (320-480 nm) at an intensity of 40 mW/cm^2 for 2 min, using an EXFO E3000 light source. The purpose of rotating the samples, while being exposed to UV light, was to provide a homogenous exposure to UV light. The rubber septum was removed and the glass was cut from the sealed side to facilitate the evaporation of ethyl acetate. Samples were left in the fume hood overnight, and then exposed to vacuum to remove solvent. The elastomer rods were gently removed from the glass tubes, and their sol fraction extracted using DCM.

5.2.4. *In Vitro* Degradation Study:

The *in vitro* degradation of particle-free elastomer rods was performed in pH 7.4

phosphate buffered saline. The pH of the buffer was maintained by replacing the buffer once a week. The degradation process was followed by measuring mechanical properties, water uptake, sol content, and mass loss. At time points of 1, 4, 8, 18, and 28 weeks, four rods were removed from the buffer, washed with distilled water, blotted dry, and their wet weight (w_w) measured. The water uptake was calculated using the following equation,

$$\text{water uptake}[\%] = \frac{w_w - w_d}{w_d} \times 100 \qquad (5\text{-}1)$$

Mass loss was calculated using the following equation,

$$\text{mass loss}[\%] = \frac{w_0 - w_d}{w_0} \times 100 \qquad (5\text{-}2)$$

in which w_0 is the initial weight of the sample before implantation. To determine dry weight (w_d), wet samples were dried in a vacuum oven at 45˚C for 3 days. Dried rods were used to determine the mechanical properties, recorded using an Instron uniaxial tensile tester model 4443. The crosshead speed was set at 500 mm/min according to ASTM D412. All specimens were tested at room temperature. Data analysis was carried out using a Merlin 4.11 Series IX software package. In order to determine sol content, samples used to determine mechanical properties were immersed in 3 mL dichloromethane per rod. The dichloromethane was replaced three times at 2 hr intervals, after which the samples were dried at 45˚C under vacuum for 3 days. The sol content was

calculated using the following equation,

$$\text{sol content } [\%] = \frac{w_d - w_e}{w_d} \times 100 \qquad (5\text{-}3)$$

in which w_e is the weight of the sample after sol extraction. Water uptake, mass loss, and sol content were determined from triplicate samples unless otherwise mentioned. The density of the elastomers was measured using the volume displacement technique according to ASTM D792-08, where absolute ethanol was used as the displacing liquid.

5.2.5. Device preparation:

Sieved particles were added to 1:1 (w:w) prepolymer solution of ethyl acetate containing 1.5 w/w(polymer) % of 2,2-dimethoxy-2-phenylacetophenone as photo-initiator, and the mixture was homogenized by gently vortexing. The mixture was filled into a glass tube and cross-linked with rotation as described above. For VEGF release studies, glass tubes were sterilized with 70% ethanol, the rubber septum was removed and the glass was cut in a laminar flow hood. To evaporate ethyl acetate and obtain sterile rods, glass rods were cut from two sides containing photocrosslinked elastomer, and they were lyophilized and sealed under vacuum, after which rods were released from glass molds in a laminar flow hood.

For growth factor studies, the release was performed in EGM-2 or F12-K basal media. Each rod was placed into a sterile O-ring tube with 1 ml of EGM-2 basal media, and the tubes were located on a flat shaker set at a temperature of 37 °C and a rotation of 300 rpm. The release media was replaced frequently to provide approximate infinite sink

conditions. At each time point, rods were removed and placed into a new tube containing fresh media using sterile tweezers, while the release media was frozen in liquid nitrogen and stored at –80 °C. For experiments wherein growth factors were not loaded into the elastomer, the release was performed in sterile PBS buffer, and at each time point, rods were blotted dry and weighed to determine the water uptake. The water uptake was determined using equation 1, where W_d was determined by subtracting the amount of powder released, from the initial dry mass of the device. $VEGF_{165}$ and HGF were quantified using their corresponding ELISA kits and RSA was quantified using a Bradford micro-assay at 595 nm [145].

5.2.6. Human aortic endothelial cell (HAEC) culture

HAEC cells were cultured in EGM-2 media supplemented with 2% fetal bovine serum (FBS), 0.04% hydrocortisone, 0.4% human fibroblast growth factor-B, 0.1% VEGF, 0.1% R3-insulin growth factor-1, 0.1% ascorbic acid, 0.1% recombinant human epidermal growth factor, 0.1% GA-1000 (gentamicin, amphotericin B), and 0.1% heparin. The cells were incubated under standard conditions until they reached greater than 80% confluence.

5.2.7. CCL 208 monkey epithelial cell culture

CCL 208 cells were cultured in Ham's F12-K medium with 2 mM L-glutamine adjusted to contain 1.5 g/L sodium bicarbonate and supplemented with 60 ng/ml epidermal growth factor and 10% fetal bovine serum. The cells were incubated under standard conditions until they reached greater than 80% confluence.

5.2.8. Bioactivity assay

The bioactivity of the released VEGF was assessed through its ability to stimulate the proliferation of HAEC cells. Proliferation of HAECs was determined using the WST-1 assay. Standard VEGF solutions were prepared in EGM-2 basal media using lyophilized VEGF under identical conditions as used to prepare solid excipients. 100 μL of standard VEGF solutions along with daily collected VEGF samples were added to 96 well micro-plates, after which 100 μL of HAEC cells with a concentration of 75 000 cells/mL, suspended in EGM-2 basal media supplemented with 0.08% hydrocortisone, 0.2% GA-1000, 0.2% ascorbic acid, 0.2% heparin, and 0.5% FBS were added as well to each well. Cells were incubated for 1 day at 37°C, 5% CO_2, and a relative humidity of 95 %, after which 20 μL of WST-1 reagent was added to each well and the color development was assessed at 450/690 nm after 4 hrs of incubation. Cells between passages of 3 and 5 were used to evaluate the bioactivity of released VEGF. The bioactivity is reported as a percent of the activity expressed by the cells incubated with the release medium divided by the activity that would be expressed by cells exposed to an equivalent concentration of freshly reconstituted VEGF, as determined from the standards. Pictures of cells incubated at different concentrations of standard VEGF and with VEGF release media at different stages of the release were recorded using a phase contrast Fisher brand microscope.

The bioactivity of the released HGF was assessed through its ability to stimulate the proliferation of CCL-208 epithelial cells . Cell proliferation was determined using the

WST-1 assay. Standard HGF solutions were prepared in Ham's F-12K basal media using lyophilized HGF under identical conditions as used to prepare solid excipients. 100 μL of standard HGF solutions along with daily collected HGF samples were added to 96 well micro-plates, after which 100 μL of CCL-208 cells with a concentration of 75 000 cells/mL, suspended in Ham's F-12K basal media supplemented with 5% FBS were added as well to each well. Cells were incubated for 2 day at 37°C, 5% CO_2, and a relative humidity of 95 %, after which 20 μL of WST-1 reagent was added to each well and the color development was assessed at 450/690 nm after 4 hrs of incubation. The percentage bioactivity was evaluated as done for VEGF with HAEC cells.

5.3. RESULTS and DISCUSSION:

In order to decrease the tear resistance of the TMC elastomer to generate effective release rates, D,L-lactide can be incorporated into the prepolymer [97]. However, D,L-lactide degrades relatively quickly to generate acidic degradation products. To reduce the rate of accumulation of acidic degradation products within the device, ε-caprolactone was copolymerized to produce a terpolymer prepolymer.

5.3.1. Terpolymer Characterization:

In the following discussion, the synthesized terpolymers are referred to as TMCCLDLLA-40 for the 4000 Da prepolymer and TMCCLDLLA-78 for the 7800 Da prepolymer. Both TMCCLDLLA-40 and TMCCLDLLA-78 had molar ratios close to the intended theoretical values as determined from ^{1}H NMR (Table 1). For example, TMCCLDLLA-40 consisted of 51 % TMC, 25 % ε-CL, and 24 % DLLA. As has been

noted previously for both poly(D,L-lactide-co-ε-CL) and poly(TMC-co-D,L-lactide) prepolymers [97, 105], the terpolymers were terminated predominantly by lactyl groups. For example, for TMCCLDLLA-40, 59.8 % the termini were DLLA, 11 % TMC, and 29.2 % CL as determined from terminal hydroxyl groups of H_{11} of lactyl and caproyl units and the terminal methylene group of carbonyl units H_{3*} at 3.45 ppm (Figure 5-1B). The accumulation of lactyl and caproyl units at the chain ends was due to a transesterification reaction. The primary hydroxyl groups derived from carbonyl units of TMC are more likely to undergo transesterification, consequently they become depleted [113]. The yield of polymerization was above 99%. A small amount of unreacted TMC monomer was present, as detected at 4.39 ppm, which was removed during the purification process.

The degree of acrylation was calculated from the ^{1}H NMR spectra by end-group analysis using acrylate group peaks at δ = 5.92-6.07 ppm (H_{12}, H_{13} and H_{14}). For each prepolymer it was found to be around 85 %. A significant decrease in hydroxyl peaks of terminal lactyl units at δ = 5.35 ppm (H_{11}), in hydroxyl peaks of terminal caproyl units at δ = 5.48 ppm (H_{11}) and in the terminal methylene group of carbonyl units at 3.45 ppm were observed after acrylation (Figure 5-1B).

The number average molecular weight (M_n) was also calculated using end group analysis. of the M_n of TMCCLDLLA-40 was 4600 Da while the M_n of TMCCLDLLA-78 was 9400 (Table 5-1). These molecular weights are reasonably close to the theoretical molecular weights of 4000 and 7800 Da, expected based on monomer and initiator feed

ratios.

The lactyl units were more randomized along the backbone than caproyl or carbonyl units. In the ^{1}H NMR spectra, lactyl units yielded four signals centered around 5.05 ppm, compared to two signals for caproyl units around 2.35 ppm, and one signal for carbonyl units at 1.95 ppm (Figure 5-1B). As the chain structure determines the degradation characteristics [147], a highly randomized DLLA is desirable to reduce the rate of hydrolytic degradation. The average length of lactyl sequence length in the TMCCLDLLA-40 prepolymer was approximately 1.6, while the average caproyl sequence length was 3.1, calculated based on equations reported in the literature [147]. The respective DDD and CCC block lengths were roughly the same in the TMCCLDLLA-78 prepolymer; the average DDD length was 1.6 while the average CCC length was 3.2.

Table 5- 1. Chemical and physical properties of synthesized prepolymers, determined from ^{1}H-NMR analyses.

prepolymer	DLLA content / *DLLA content	CL content /* CL content	TMC content /* TMC content	DA [%]	M_n [kDa]
TMCCLDLLA-40	24.8/61.4	25.2/26.8	49.9/11.8	86	4.6
TMCCLDLLA-78	24.3/58.4	25.3/33.5	50.4/8.1	83	9.4

* indicates to the terminal content of the monomer, DA: degree of acrylation, M_n was determined from ^{1}H NMR using end group analysis of acrylate groups

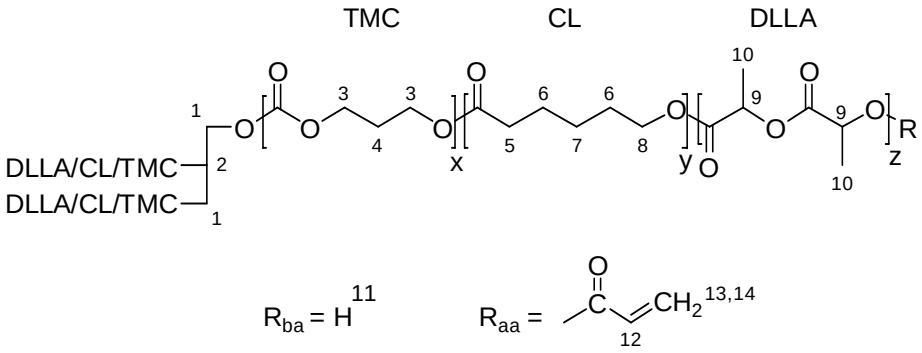

Figure 5-1A

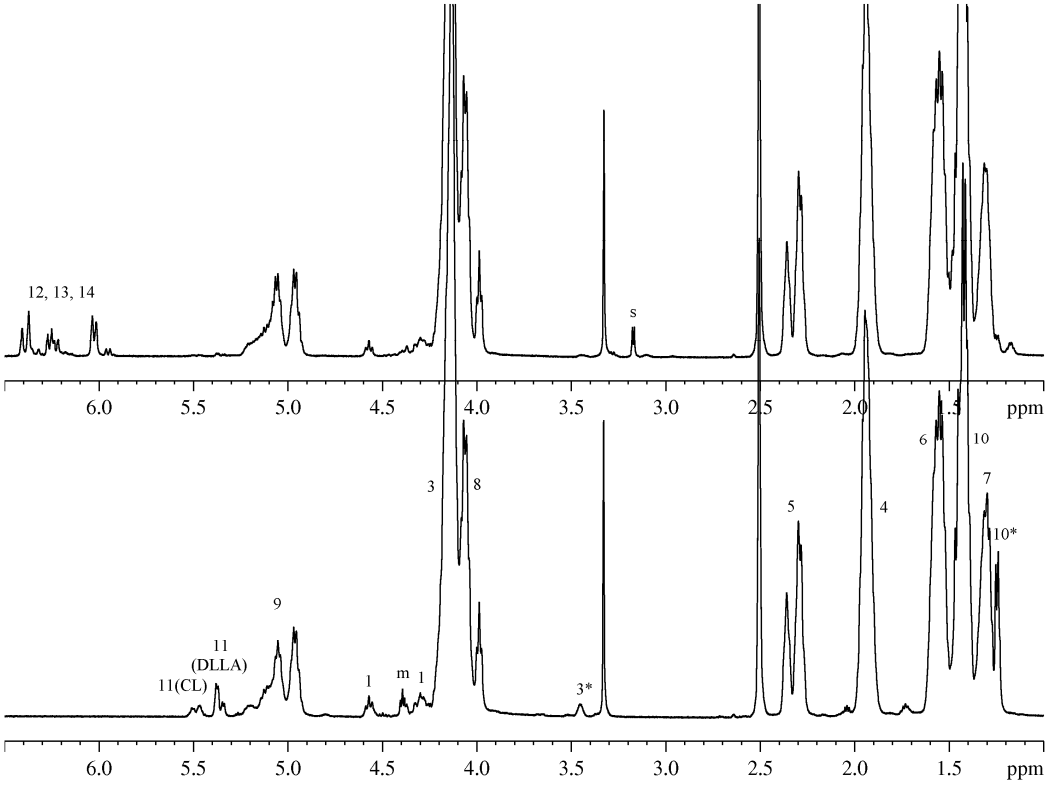

Figure 5-1B

Figure 5- 1. A) The chemical structure of TMCCLDLLA terpolymer prepolymer; the subscript ba refers to before acrylation while aa refers to after acrylation, x, y, and z indicate to the molar ratio of TMC, ε-CL, and DLLA in the prepolymer. B) ^{1}H-NMR of TMCCLDLLA-40 terpolymer prepolymer, before acrylation (bottom) and after acrylation (top); m = monomer, s = solvent.

The TMCCLDLLA-40 elastomer had a 1.1 times greater Young's modulus (E) than the TMCCLDLLA-78 elastomer. The Young's modulus of the TMCCLDLLA-40 elastomer was 0.83 ± 0.01 MPa compared to 0.9 ± 0.0 MPa for the TMCCLDLLA-78 elastomer. Increasing the cross-link density did not impact the tensile strength (σ_b) significantly; the TMCCLDLLA-40 elastomer had a σ_b of 2.76 ± 0.41 MPa compared to 2.82 ± 0.23 for the TMCCLDLLA-78 elastomer. Elongation at break (ε_b), on the other hand, was the most affected by the increase in the cross-link density; ε_b decreased 1.8 times from 7.54 ± 0.47 mm/mm TMCCLDLLA-78 elastomer to 4.28 ± 0.31 mm/mm in TMCCLDLLA-40 elastomer (Table 5-2).

Table 5- 2. Physical and mechanical properties of synthesized elastomers.

Elastomer	sol content [%]	T_g [^oC]	d [$g.cm^{-3}$]	E (MPa)	σ_b (MPa)	ε_b (mm/mm)
TMCCLDLLA-40	11.8 ± 0.6	-12.9	1.30	0.90 ± 0.00	2.76 ± 0.41	4.28 ± 0.31
TMCCLDLLA-78	14.4 ± 0.8	-13.8	1.34	0.83 ± 0.01	2.82 ± 0.23	7.54 ± 0.47

E, Young's modulus; σ_b, stress at break; ε_b, elongation at break. The values of glass transition temperature (T_g) are for sol-removed elastomers, and the values of network density are for sol non-removed elastomers.

5.3.2. RSA Release

To determine formulation factors that control the rate and extent of protein release from the elastomers, the release of RSA was studied first. Formulation parameters considered were the prepolymer molecular weight (which determines the crosslink density and thus the mechanical properties of the elastomer), the total volume fraction of particles initially loaded, and the incorporation of NaCl in the lyophilized powder.

5.3.3. Effect of Elastomer Mechanical Properties

In the absence of incorporated NaCl in the particles, RSA release from elastomers

prepared using the TMCCLDLLA-78 prepolymer loaded with 25% particles occurred in a nearly zero order manner. The release occurred slowly at 0.58 %/day, with only a total mass fraction of RSA released of 20 ± 6 % after 37 days (Figure 5-2A). For therapeutic growth factor delivery, this release rate would be too slow. The TMCCLDLLA-40 elastomer provided a zero order release for up to 5 days at a rate of 5.2%/day, releasing a total mass fraction of 26.8 ± 4.7 %; after 5 days the release was sustained, reaching a total mass fraction release of 45 ± 3.4 %. The initial linear rate of release from the TMCCLDLLA-40 elastomer was 8 times faster than the release rate from the TMCCLDLLA-78 elastomer at the same particle loading.

Increasing the elastomer crosslink density by reducing the prepolymer molecular weight generated faster release rates and an increase in the total mass fraction of RSA released. These results are explained as follows. During osmotically driven release, water is imbibed into a capsule at a rate of [93, 95]

$$\frac{dV}{dt} = \frac{k_w A(\Pi - p)}{h} \qquad (5\text{-}4)$$

where V is the amount of water imbibed, h is the capsule wall thickness, k_w is the hydraulic permeability of the polymer, A is the capsule surface area, Π is the osmotic pressure of solid particle solution in the capsule, and p is the resisting pressure of the polymer. Elastomers with greater resisting pressure thus require higher osmotic pressure in the capsule to rupture the surrounding membrane. When an elastomer is deformed, part of the internal energy is stored elastically in the chains and is released upon crack growth as a driving force for fracture. The remainder of the energy is dissipated through molecular motions into heat, and it is unavailable to break the chains. In elastomers with

high crosslink density, chain motion is restricted, and the network is unable to dissipate much energy. Consequently, this results in a brittle fracture in the network at low values of elongation [152]. Thus, crack formation and propagation occurred in a more efficient manner in TMCCLDLLA-40 elastomer rods, providing a faster osmotic release rate and greater percentage of release.

This explanation is supported by the water uptake rates in elastomers with different cross-link density (Figure 5-2B). TMCCLDLLA-78 elastomer rods with a loading level similar to that of TMCCLDLLA-40 elastomer rods drew in significantly more water (Figure 5-2B). The positive impact of the increased cross-link density on the release rate and total amount of RSA released is in agreement with previously reported data [35]. The impact of the cross-link density, however, was far more significant in this study.

5.3.4. Effect of loading and NaCl on release and water uptake:

Data in the literature indicate that the osmotic release rate is proportional to the particle size and to the volumetric loading, provided the loading is below the percolation threshold [88]. The matrix swelling, on the other hand, is inversely proportional to the particle loading [88]. Thus it is expected that higher particle loading would provide faster rates of release because of the resulting thinner polymer wall that surrounds a given entrapped particle [89].

In our experiments with TMCCLDLLA-40 elastomer rods, increasing the loading

from 10 % to 25 % provided a faster initial release rate. The total released amount, however, was not affected significantly (Figure 5-2A). The linear release period with the 10 % loading was longer, lasted 7 days, and occurred at a rate of 3.24%/day, compared to a linear release period of 5 days that occurred at a rate of 5.2%/day in the case of the 25 % loading (Figure 5-2A). The water uptake was proportional to the loading with 2.7 times difference between the 10 % and the 25 % loadings. Equilibrium water uptake was around 80 % in devices loaded with 25 % particles, and it was 30 % in the case of the 10 % particle loading (Figure 5-2B). Thus, there was no advantage obtained by increasing the particle loading within the elastomer rods.

To increase the osmotic pressure of encapsulated particles, 5 % of NaCl was added. Although NaCl has high osmotic activity, its usage in high concentrations is not desirable for *in vivo* applications, since depending on its concentration it may irritate the surrounding tissue [93]. Adding 5 % of NaCl in the solid particles increased the release rate and total amount released. The release was of zero order for 5 days, and it occurred at a rate of 9 %/day, releasing 45 ± 5 % of embedded RSA. After that, the release proceeded in a monotonically decreasing fashion. The total amount of RSA released was 77 ± 4 % after 50 days in PBS buffer (Figure 5-2A). The rate of water uptake was faster when particles contained 5 w/v% of NaCl, and it decreased after reaching a maximum (Figure 5-2B). Faster water uptake rates translated to faster rates of crack formation and propagation, thus providing faster rates of release (Figure 5-2A).

The preliminary exploration of formulation parameters indicated that prolonged

and nearly complete release of entrapped RSA could be effectively achieved from TMCCLDLLA-40 elastomers loaded at 10 w/w% particles and with the particles containing 5 w/w% NaCl. This formulation was therefore further investigated for $VEGF_{165}$, HGF, and combined $VEGF_{165}$ and HGF release and bioactivity studies.

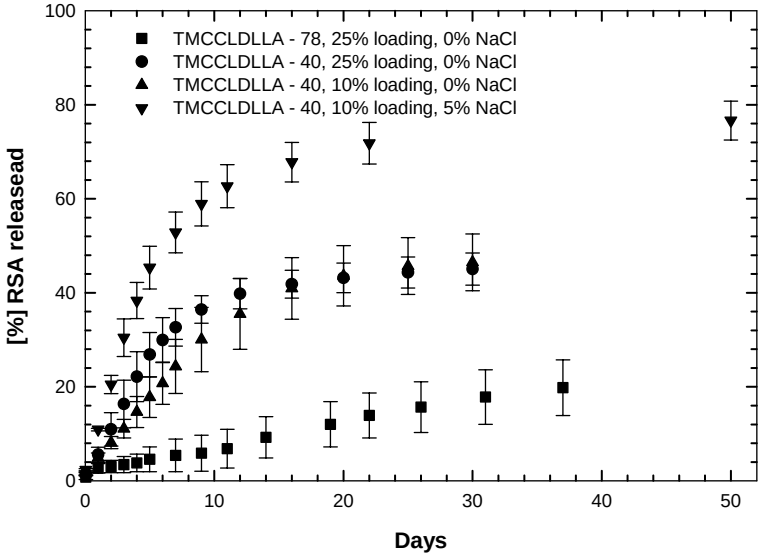

Figure 5-2A

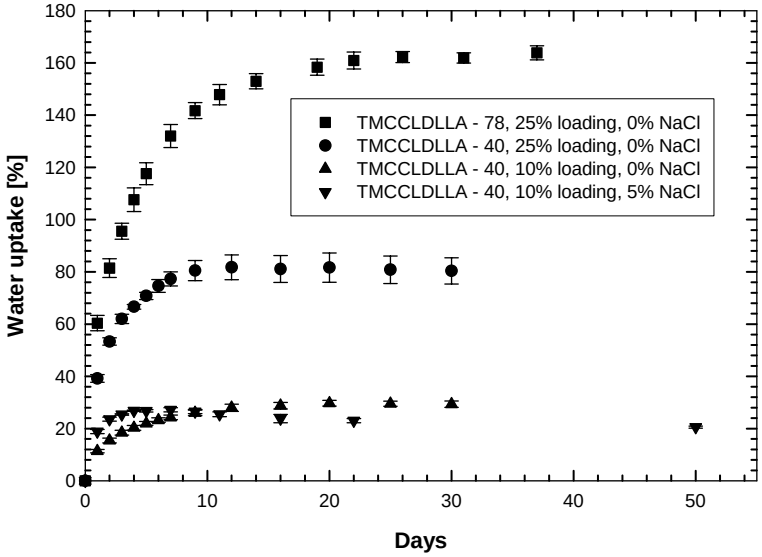

Figure 5-2B

Figure 5- 2. A) The effect of loading, cross-link density, and NaCl on the release of RSA from TMCCLDLLA elastomers. B) Effect of loading, cross-link density, and NaCl on the percentage of

water uptake in TMCCLDLLA elastomers. The data represent the average of triplicate samples and error bars the standard deviation about the average value.

5.3.5. Influence of Polymer Degradation

The mechanical properties of the elastomer are important in controlling the release rate via the osmotic mechanism. To determine the effect of changes in mechanical properties of the elastomer during the *in vitro* degradation on the osmotic release, the *in vitro* degradation of TMCCLDLLA-40 elastomer was investigated in PBS buffer. The changes in mechanical properties during the *in vitro* degradation period are given in Figure 5-3.

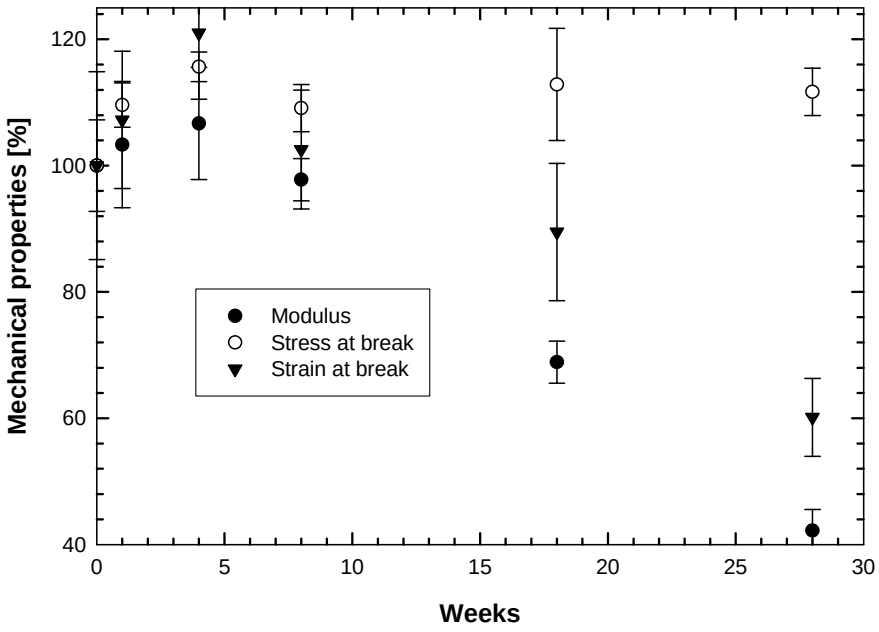

Figure 5- 3. The effect of *in vitro* degradation in PBS buffer on mechanical properties of TMCCLDLLA-40elastomer. Samples were tested after being dried. The data represent the average of triplicate samples and error bars the standard deviation about the average value.

After a slight initial increase in the modulus (E) at week 1 and week 4, E started to decrease in a linear fashion. At week 28, E lost 57.8 % of its initial value, dropping

from 0.9 ± 0.0 MPa to 0.38 ± 0.03 MPa. The stress at break (σ_b) changed in a similar fashion to E during the degradation; after an initial increase, an almost linear decrease was observed. At week 28 σ_b lost 57.8 % of its initial value, dropping from 2.76 ± 0.41 MPa at week 0 to 1.66 ± 0.17 MPa at week 28. In contrast to the observed decrease in E and σ_b with degradation, the strain at break (ε_b) did not change significantly during the *in vitro* degradation period. The osmotic release is governed by the modulus and by tear properties of the elastomer [20, 93], and since no significant alteration in those values were detected during the release period, it was concluded the that alteration in mechanical properties did not affect the release.

Changes in water uptake, sol content, and mass loss during the *in vitro* degradation were detected long after the near complete release of embedded particles. The degradation of the network occurred in a manner consistent with the bulk degradation mechanism. The sol content of the network increased as a result of hydrolysis. The sol portion also increased the osmotic activity in the interior of the elastomer, drawing in more water. An increase in the sol content and water uptake was detected at week 18 of the degradation (Figure 5-4). At week 28 sol content increased to 22.0 ± 1.0 %, water uptake increased to 24.0 ± 1.7 %, and the elastomer lost 9.2 ± 0.4 % of its initial mass (Figure 5-4). The *in vitro* degradation study, where no significant change in mechanical properties as well in the sol content and water uptake were detected, indicates the occurrence of no significant degradation during the initial 8 weeks, and since the bulk of the release occurs during the initial 2-4 weeks (Figure 5-2A) it was expected that hydrolysis would not cause any damage to the embedded acid sensitive

growth factors.

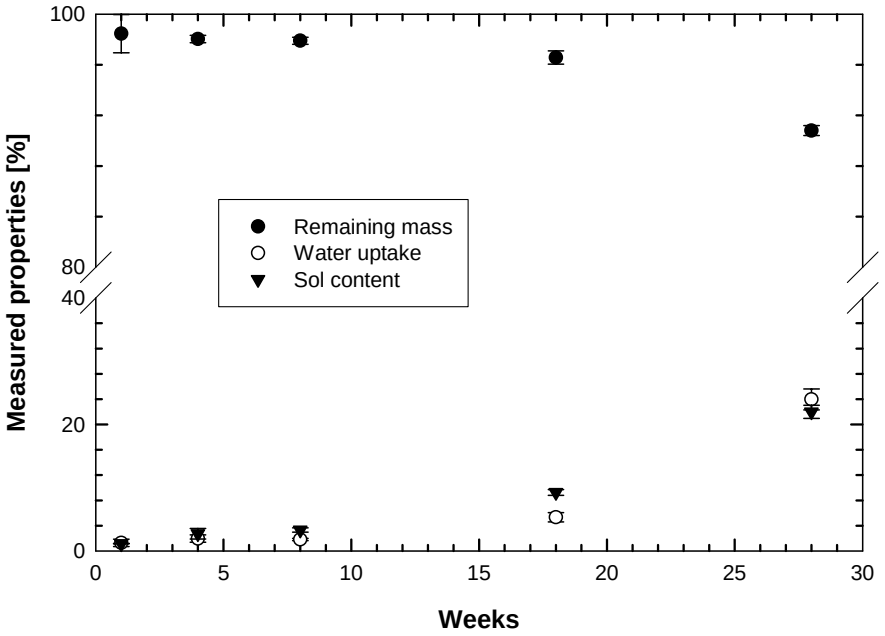

Figure 5- 4. Changes in water uptake, sol content, and mass loss of TMCCLDLLA-40 elastomer during the *in vitro* degradation in PBS buffer. The data represent the average of triplicate samples and error bars the standard deviation about the average value.

5.3.6. VEGF and HGF Release and Bioactivity:

In this study, rat serum albumin (RSA) was used along with trehalose as a lyoprotectant for VEGF. Albumin is widely used as a blocking agent, and it was expected that it would reduce or eliminate the adsorption of growth factors to hydrophobic surfaces during the release. It has been shown that VEGF and BSA are unaffected during the photo-cross-linking process due to the rapid reaction of the acrylate functional groups with the free radicals generated, provided the molar ratios of acrylate to photoinitiator (DMPA) was greater than or equal to 0.1 [65, 66]. In our experiments the molar ratio of acrylate/DMPA was 12. Thus, it was expected that lyophilized VEGF/RSA and HGF/RSA would maintain their bioactivity during the photo-polymerization reaction.

For VEGF, HGF, and combined VEGF and HGF quantification and bioactivity analyses, 3 rods were selected randomly from 40 rods, prepared for *in vivo* efficacy studies. Therefore some variation in the rate of release is expected as a result of variation in the loading.

VEGF was released at essentially the same rate as the RSA, as expected from previous results [35]. A sustained release of VEGF over 14 days was achieved. 220 ng/ml/day of VEGF was released for the initial 3 days, around 60 ng/ml/day for the following 4 days, and around 6 ng/ml/day for the following 7 days. In total, 65 ± 13 % of the embedded VEGF was released (Figure 5-5A). HGF was released at an almost similar rate as $VEGF_{165}$ (Figure 5-5B). These release results are similar to those reported in Gu *et al.* 2007. However, in Gu *et al.* the elastomer was composed of 50 mole % DLLA and 50 mole % CL and the VEGF bioactivity decreased during the release period, as a result of a decrease in microenvironmental pH to less than 5 brought on by the hydrolysis of the lactide component of the elastomer. This reasoning was a result of a previous study in which FITC-BSA molecules with trehalose were entrapped within elastomers composed of 80:20 mole % TMC and DLLA, and fluorescence of the pH sensitive FITC was monitored with time [97]. The reduction in the molar ratio of DLLA and the inclusion of TMC into the elastomer provided a near-neutral microenvironmental pH [97] and thus, it was expected that the bioactivity of the released VEGF would be maintained.

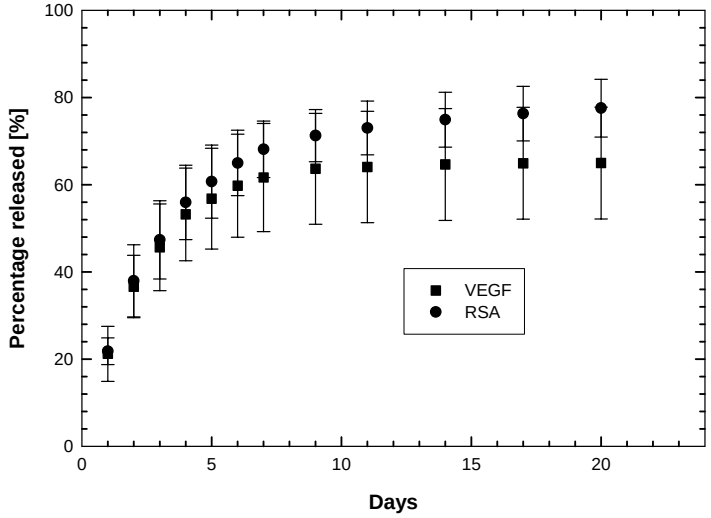

Figure 5-5A

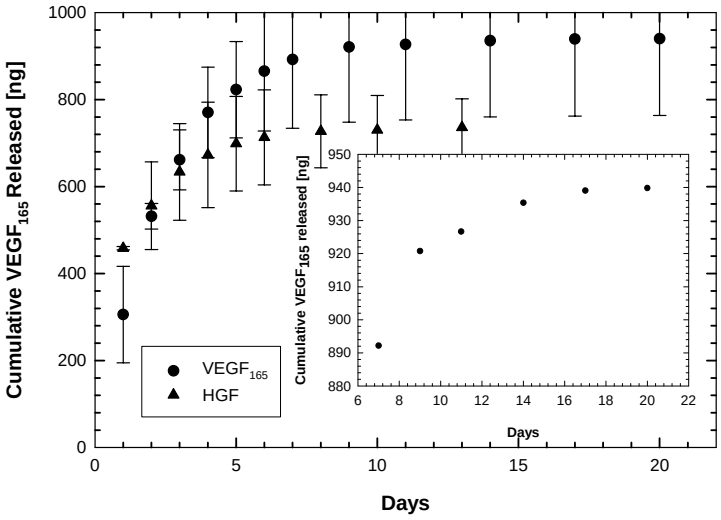

Figure 5-5B

Figure 5- 5. A) The percentage release of RSA and $VEGF_{165}$ from TMCCLDLLA-40 elastomer. RSA was quantified using the Bradford assay and $VEGF_{165}$ was quantified using the VEGF165 ELISA. B) The cumulative mass of $VEGF_{165}$ and HGF released separately from TMCCLDLLA-40 elastomer rods. The data represent the average of triplicate samples and error bars the standard deviation about the average.

The bioactivity of VEGF within the release media was assessed using an *in vitro* assay based on the proliferation of HAECs grown in the presence of the release media. This assay is a modified version of an assay published in the literature [153]. The percent bioactivity of the $VEGF_{165}$ was calculated with respect to the proliferation of HAECs

grown in the presence of as-received VEGF. The bioactivity of released HGF, on the other hand was assessed using an *in vitro* assay based on the proliferation of CCL 208 epithelial cells grown in the presence of the release media. An epithelial cell line was chosen because of a reported role of HGF in the growth, movement and differentiation of epithelial and endothelial cells in different tissues and organs [26, 27].

Both released $VEGF_{165}$ and HGF were highly bioactive, retaining around 80% bioactivity over the time period of significant release (Figure 5-6). Images of HAEC cells grown with release media indicated that the released VEGF was highly bioactive over the entire period of release. The HAEC were able to proliferate and create microtubule like connections (Figure 5-7). In the absence of VEGF, HAEC were viable after 24 hrs, but they were unable to proliferate and create microtubule-like connections (Figure 5-7A). In the case of HGF, no significant visual differences could be seen between CCL 208 cells grown in the release media and the control. Furthermore, the release of NaCl from the particles in the elastomer into the release media did not adversely affect HAEC and CCL 208 cells viability, indicating that the inclusion of a low fraction of NaCl in the formation may be tolerated *in vivo*.

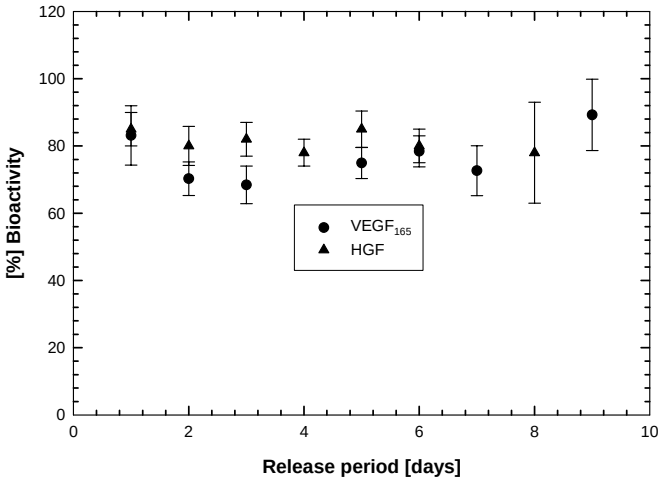

Figure 5-6A

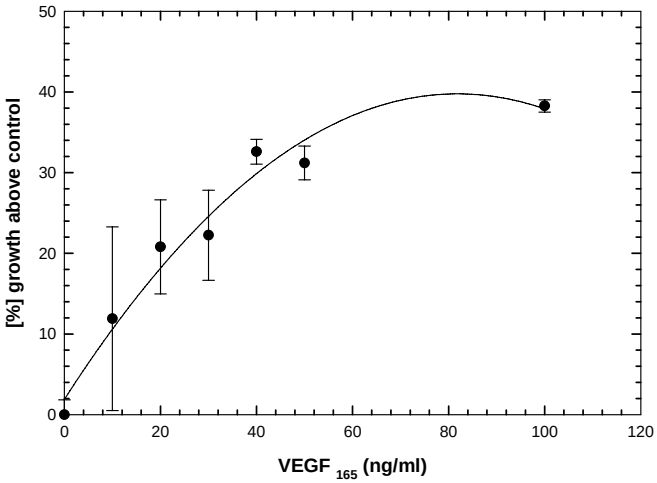

Figure 5-6B

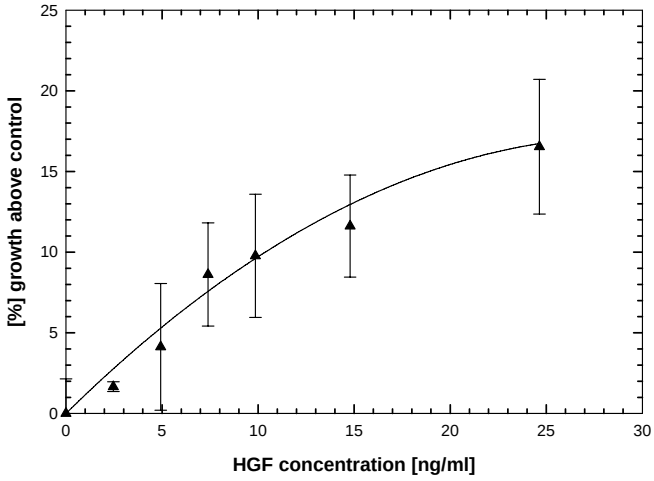

Figure 5-6C

Figure 5- 6. A) The bioactivity of released $VEGF_{165}$ and HGF quantified as the ratio of $VEGF_{165}$ or HGF from the standard growth curve to the amount quantified from the ELISA. Cells were seeded at a concentration of 7500 cell/well in 96-well plate for 24 hrs for HAEC cells and for 48 hrs for CCL 208 cells in the presence of different concentrations of standard $VEGF_{165}$ or HGF and with release media collected at different time points. B) The standard growth curve of HAECs seeded at a concentration of 7500 cell/well in 96-well plate for 24 hrs. C) The standard growth curve of CCL 208 cells seeded at a concentration of 7500 cell/well in 96-well plate for 48 hrs. The proliferation was recorded after 4 hrs of addition of the WST-1 reagent. The data represent the average of triplicate samples and error bars the standard deviation about the average value.

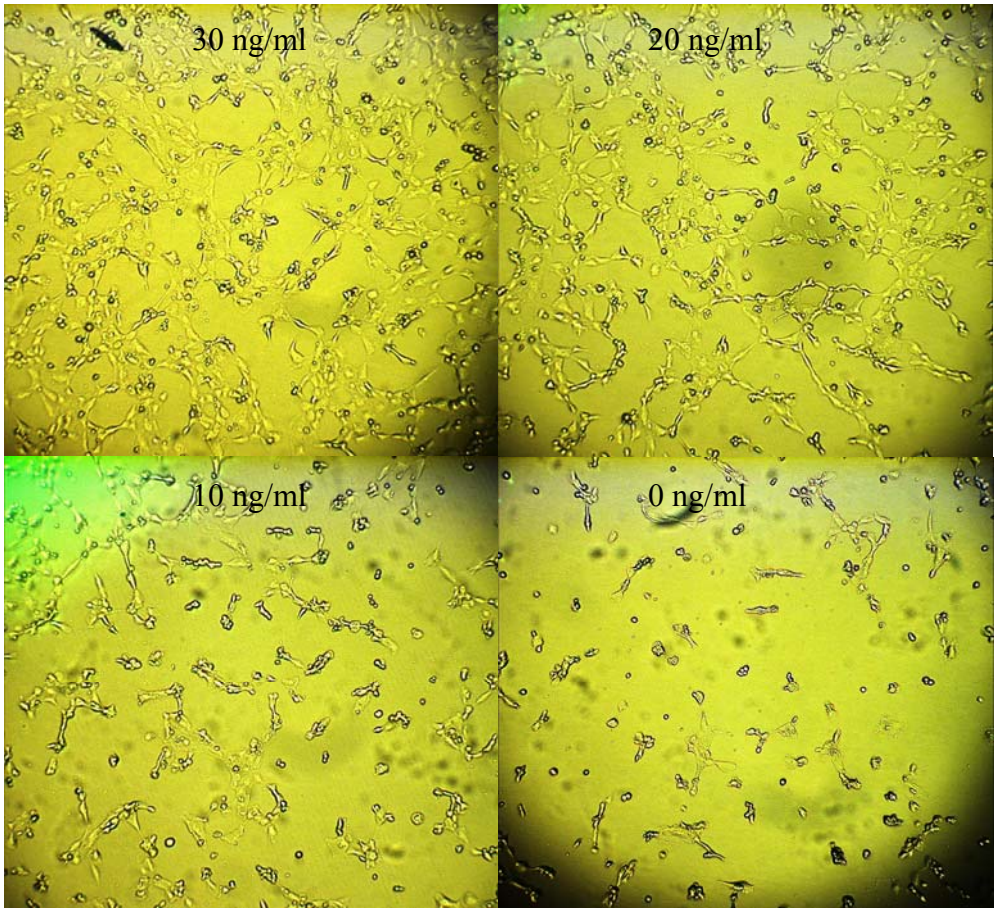

Figure 5-7A

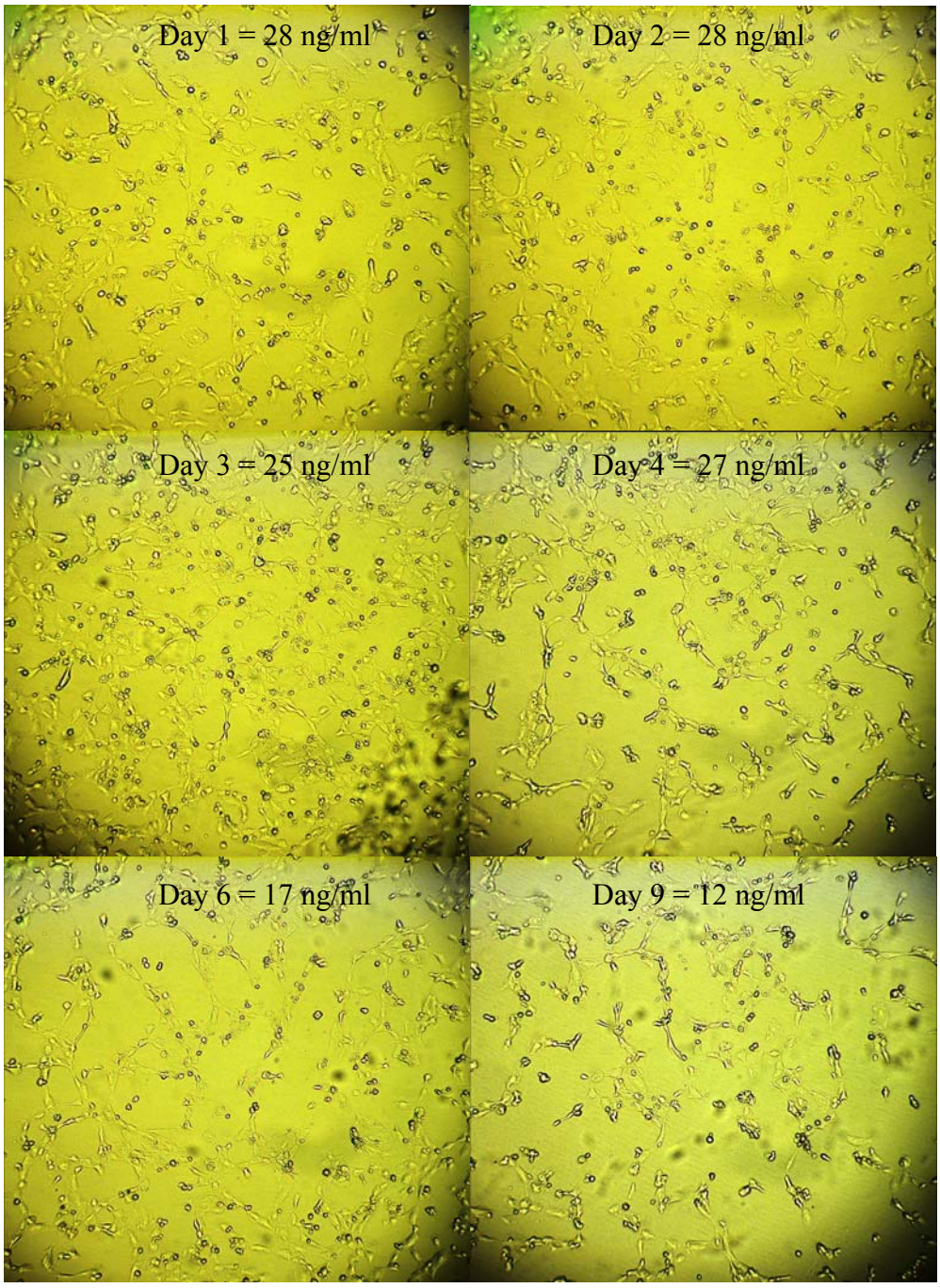
Day 1 = 28 ng/ml
Day 2 = 28 ng/ml
Day 3 = 25 ng/ml
Day 4 = 27 ng/ml
Day 6 = 17 ng/ml
Day 9 = 12 ng/ml

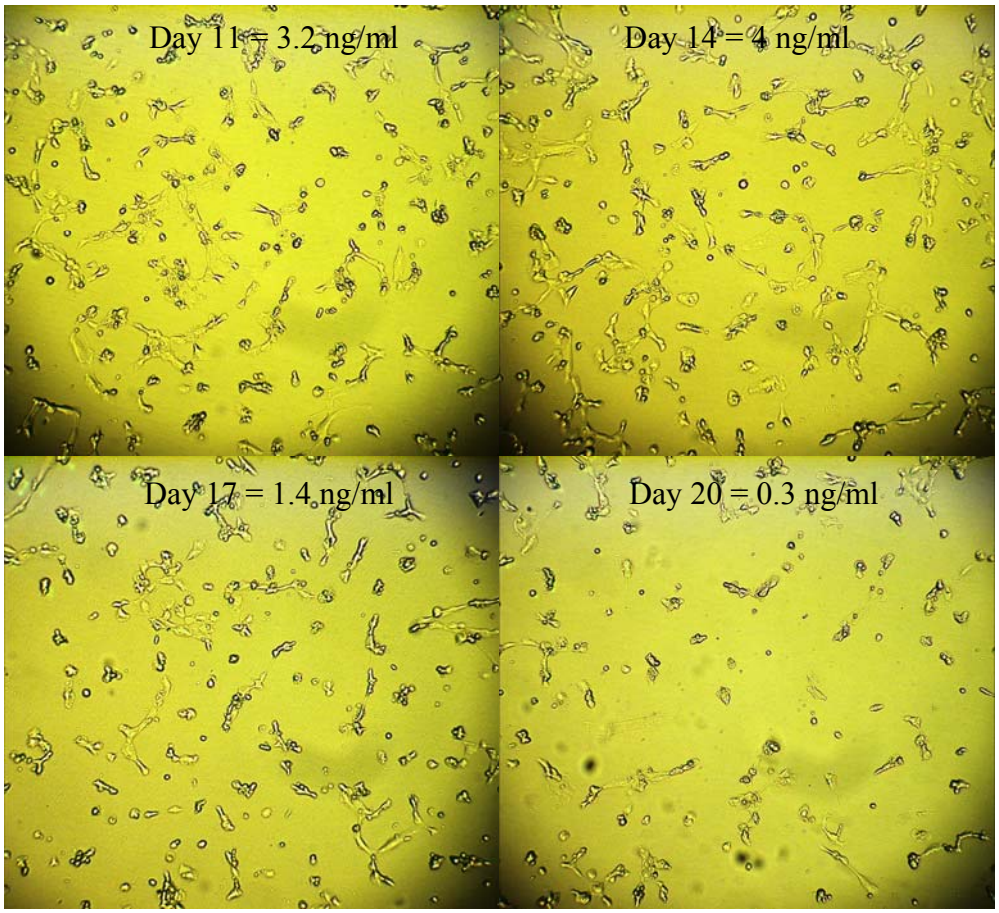

Figure 5-7B

Figure 5- 7. A) Images of HAEC cells seeded at a concentration of 7500 cells/well in a 96-well plate and cultured for 24 hrs in the presence of different concentrations of standard VEGF165. B) Images of HAECs seeded at a concentration of 7500 cells/well in 96-well plate and cultured for 24 hrs in the presence of $VEGF_{165}$ release media, collected at different time points. Numbers indicate to the average $VEGF_{165}$ concentration determined by ELISA.

5.3.7. Combined release of $VEGF_{165}$ and HGF:

$VEGF_{165}$ and HGF were incorporated at similar amounts in the solid particles, and they were released at similar rates from a TMC based elastomer (Figure 5-8). Particles loading in this case was 13.5 %, as a result, the release occurred at a faster rate than the previous release experiments. The release of $VEGF_{165}$ and HGF at similar rates is expected and it is in agreement with previous data on the osmotic release, where growth factors with distinct physical properties were released at a similar rate [35]. Since incorporation of similar amounts of $VEGF_{165}$ and HGF provided similar release rates, the system could possibly provide distinct rates of release as well by simply changing the initial amount of the desired growth factor in the solid particles.

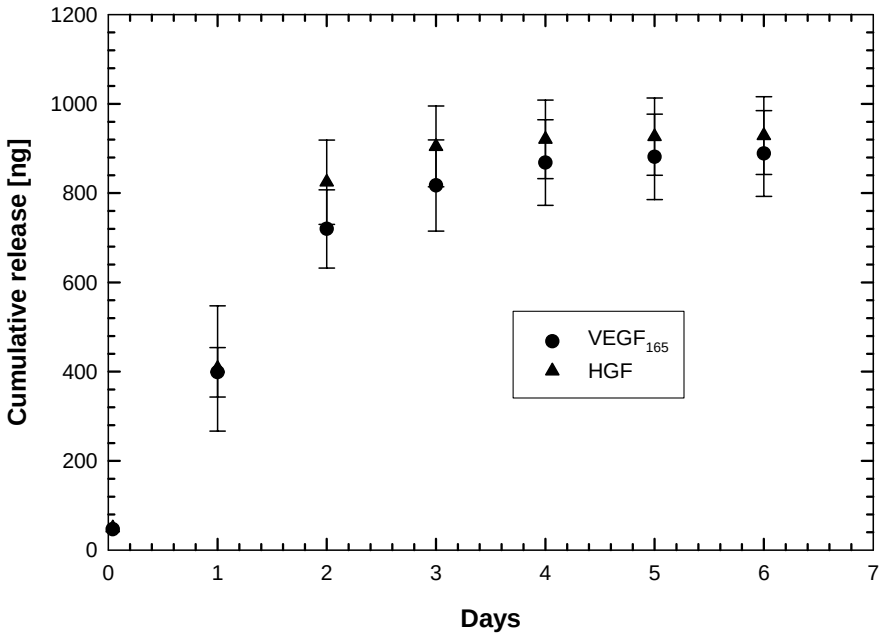

Figure 5- 8. The cumulative release of combined VEGF*165* and HGF from TMCCLDLLA-40 elastomer, lyophilized with RSA, trehalose and NaCl. RSA was quantified using the Bradford assay. VEGF*165* and HGF were quantified using their corresponding ELISA kits. The loading of solid particles was 13.5 %. The data represent the average of triplicate samples and error bars the standard deviation about the average value.

Beside the ability of the osmotic release in providing similar rates of release of different growth factors, it may provide sequential release as well. This could be achieved easily by using a two layer cylindrical device. The inner layer of the cylinder could be loaded with a growth factor such as PDGF-BB, that would stabilize sprouted endothelial cells [30], as a result of the biological action of $VEGF_{165}$, released initially from the outer layer of the cylinder.

5.4. Conclusions:

Elastomers made of TMCCLDLLA-40 were able to provide a sustained release of highly bioactive $VEGF_{165}$ and HGF for more than 10 days. No significant degradation occurred in the network during the initial 8 weeks, during which the bulk of embedded growth factor was released. Increasing the cross-link density of synthesized elastomer increased the release rate and total amount of embedded particles. The bioactivity of released $VEGF_{165}$ and HGF were assessed using proliferation assays with HAEC and CCL 208 cell lines, respectively. Released $VEGF_{165}$ and HGF were highly bioactive over the release period. The presence of small amounts of NaCl significantly improved the efficiency of the osmotic release. The presence of NaCl in the release media did not adversely affect HAEC and CCL 208 cells viability, indicating that the inclusion of a low fraction of NaCl in the formulation may be tolerated *in vivo*. Further, the ability of the system to release combined growth factors at similar rates, and a method for releasing growth factor at distinct sequences was suggested. The results represent an improvement over previously published data on the delivery of bioactive VEGF from photo-cross-linked degradable elastomer.

6. CHAPTER SIX

In Vivo Angiogenic effects of $VEGF_{165}$ and HGF Released Alone And In Combination From Biodegradable Elastomers

Authors: Chapanian R[1], Tse MY[2], Pang SC[2], and Amsden BG[1*]

[1]Department of Chemical Engineering and [2]Department of Anatomy and Cell Biology
Queen's University, Kingston, Ontario, Canada, K7L 3N6

* To whom correspondence should be addressed

ABSTRACT

Therapeutic angiogenesis through the localized release of angiogeneic growth factors from implanted polymers is a promising approach to treat ischemia. In this study, we examine the potential of VEGF and HGF released alone or in combination via an osmotic mechanism from biodegradable, photocrosslinked elastomers in inducing angiogenesis. Using ^{125}I-VEGF$_{165}$ as a probe, the *in vivo* and *in vitro* release kinetics were shown to be identical. The growth factors released from elastomer rods implanted subcutaneously in rats induced angiogenesis. The induction of blood vessel formation was dose dependent for both growth factors investigated. Rods with a high dose of VEGF$_{165}$ that released around 1000 ng of VEGF$_{165}$ over 14 days induced the formation of new capillaries and blood vessels, whereas, rods that released around 100 ng of VEGF$_{165}$ over 14 days were unable to induce blood vessel formation. Rods with a high dose of HGF that released around 1000 ng of HGF over 14 days induced the formation of blood vessels; however, its effectiveness in inducing new blood vessel formation was less than the effectiveness of rods that provided a similar dose of VEGF$_{165}$. Combined release of VEGF$_{165}$ and HGF induced the most effective angiogenesis. Newly formed capillaries and blood vessels were normal looking and they were connected to the surrounding vasculature. Angiogenesis was concentrated in the capsule area and did not span the tissue. The newly formed blood vessels were not stable, but regressed when the release of growth factors were decreased. This study demonstrates the possibilty of utilizing photo-cross-linked elastomers to release growth factors locally to treat ischemia.

6.1. Introduction:

Therapeutic angiogenesis using growth factors is immerging as a promising treatment for chronic myocardial and limb ischemia [4, 9, 154]. Angiogenesis is initiated by the activation, migration and proliferation of endothelial cells that sprout from pre-existing blood vessels to form new capillaries and blood vessels. Numerous cell types, proteolytic enzymes, cytokines and growth factors participate in the process [150, 155, 156]. Vascular endothelial growth factor (VEGF) and hepatocyte growth factor (HGF) are widely investigated angiogenic growth factors [12, 23, 24, 26, 150, 151, 157, 158].

The dose and duration of release of angeogenic growth factors are important for a successful therapy [12, 17]. A potential approach for effective therapeutic angiogenesis is localized release from a polymer implant. A successful polymer-based sustained delivery system could provide a maximum efficacy/dose relationship by overcoming obstacles pertinent to systemic and bolus injections such as *in vivo* stability and adverse side effects, [5] such as renal and hematopoietic end-organ damage in the case of $VEGF_{165}$ [7]. To commercialize a polymer-based sustained release delivery system for growth factors, a simultaneous solution of protein denaturing problems is required [5]. These problems are related to protein stability during the device synthesis and during the delivery process. Irreversible protein inactivation during the device synthesis occurs when a protein is exposed to physical, mechanical and chemical stresses, which are specific to each preparation technique [5, 16]. Potential sources of irreversible protein inactivation during delivery include adsorption to hydrophobic surfaces, interaction with charged surfaces, highly acidic micro-environmental pH, and elevated levels of moisture

[12, 16]. Other issues that require a special attention are the initial burst release and the non-complete release of embedded growth factors [8, 92].

Most of the polymer-based sustained delivery devices that have been investigated can provide sustained release for a period of 2 to 3 weeks. However, the minimum time required to induce successful therapeutic angiogenesis with a given growth factor remains to be elucidated [17]. Doses of VEGF as low as 15 ng/day are unable to induce blood vessel formation while doses as high as 1500 ng/day induce large, abnormal and short lived blood vessels [12, 15, 17, 18]. Similar results have been reported for HGF; Ozeki *et al*. found that the delivery of 1 μg of HGF from a gelatin hydrogel over 14 days was unable to induce blood vessel formation, whereas the delivery of 5 μg of HGF from the same device over 14 days induced blood vessel formation [12].

Xin *et al.* on the other hand found that the combination delivery of $VEGF_{165}$ and HGF achieved a more effective therapeutic angiogenesis than the therapy where either of the growth factors was administered [151]. The combination therapy had an amplified synergistic effect, and it was greater than having an additive impact [151].

The osmotic release from photo-cross-linked, biodegradable elastomers is a promising approach for the delivery of growth factors [8]. This approach can provide many of the requirements for a successful polymer based growth factor delivery system [5]. It provides a linear and sustained release of bioactive growth factors for a period of longer than two weeks with a low initial burst [35]. Recently we illustrated that by a

careful choice of the elastomer composition, an acidic microenvironmental pH, linked to the degradation of many therapeutic proteins incorporated in degradable polyester depots [10, 69], can be reduced significantly in the pores and channels of the elastomer. Photo-cross-linked elastomers made of a terpolymer prepolymer of poly(TMC-co-ε-CL-co-DLLA) with a molar composition of (50:25:25) and M_n of 4000 Da was able to release bioactive $VEGF_{165}$ for over 2 weeks *in vitro* [Chapter 5].

The objectives of this study were to compare the kinetics of the *in vivo* and *in vitro* osmotic release of angiogenic growth factors from a TMC based photo-cross-linked elastomer, to investigate the ability of the released growth factors to induce blood vessel formation *in vivo,* and to investigate combination angiogenic therapy by the co-delivery of $VEGF_{165}$ and HGF from a single device. The *in vivo* release kinetics were investigated by using ^{125}I-$VEGF_{165}$ as a probe, and the angiogenic ability of the released growth factors was evaluated subcutaneously in rats by gross examination of the tissue surrounding the implant and by histology.

6.2. MATERIALS AND METHODS

D,L-Lactide (99+%) was obtained from Purac, the Netherlands, and purified by recrystallization from dried toluene. 1,3-trimethylene carbonate (1,3-dioxan-2-one) was obtained from Boehringer Ingelheim, Germany and used as received. ε-Caprolactone was obtained from Lancaster, Canada, dried over calcium hydride, distilled under high vacuum and stored over activated 4 μm molecular sieves. Toluene and dichloromethane were dried over calcium hydride and distilled under argon. Other chemicals were used

without further purification. Chemicals used in polymer synthesis include stannous 2-ethylhexanoate (96%) obtained from Aldrich, Canada and glycerol obtained from BDH, USA. Chemicals used in the acrylation process include acryloyl chloride (96%), triethylamine (99.5%), and 4-dimethylaminopyridine (99%), all obtained from Aldrich, Canada. 2,2-dimethoxy-2-phenylacetophenone used as photoinitiator was obtained from Aldrich, Canada. Solvents used for purification of the synthesized polymers include ethyl acetate (99.9%) and methanol (99.8%) were obtained from Fisher, Canada. For the release studies, recombinant human $VEGF_{165}$ was purchased from Peprotech Inc., Canada. Trehalose and NaCl were obtained from Sigma, Canada, and rat serum albumin (RSA) from Innovative Research (USA). ^{125}I-$VEGF_{165}$ was purchased from PerkinElmer Life and Analytical Sciences (USA). An HGF ELISA kit was purchased from R&D Systems (USA), and a $VEGF_{165}$ ELISA kit was purchased from Peprotech (Canada).

6.2.1. Prepolymer Preparation

Termini-acrylated *star*-poly(TMC-co- ε-CL-co- D,L-lactide) with a theoretical composition of 50 mole% of TMC, 25 mole% of ε-CL and 25 mole % of D,L-lactide and a number average molecular weight of 4000 Da was prepared as described previously [55]. Polymerization was performed in the presence of stannous(II) ethylhexanoate at 130 °C for 72 hrs. For acrylation, the star-copolymer was heated to 60 ºC then poured into a dried round-bottomed flask, the flask sealed with a rubber septum, and purged with dry argon. The following procedures were conducted in a glove box. Dried dichloromethane (DCM) was added to the flask at a ratio of polymer to solvent of 2:1 (w:v) to dissolve the polymer. The 4-dimethylaminopyridine catalyst was added at a molar ratio of 2×10^{-3}

mole per mole of SCP terminal hydroxyl group. Triethylamine was added at a molar ratio of 1 mole per mole of star-copolymer (SCP) hydroxyl group. Finally, acryloyl chloride was diluted in dried DCM at a ratio of 1:1 (v:v) and added slowly in a drop-wise fashion at a ratio of 1.2 moles per mole of SCP hydroxyl group. The synthesized prepolymer was characterized using ^{1}H NMR obtained by a 500 MHz Bruker-Avance spectrometer with DMSO-*d6* as a solvent [Chapter 5].

6.2.2. Preparation of Growth Factor Containing Elastomer Rods

For release kinetic studies, 5 μCi of ^{125}I-VEGF$_{165}$ with a specific activity of 136.5 μCi/μg was dissolved in a solution made of 200 μg of VEGF, 360 mg of trehalose and 39.8 mg of RSA in 20 ml of 5 mM succinate buffer. The mixture was frozen in liquid nitrogen, lyophilized for 48 hrs, and sealed under vacuum. The lyophilized product was ground and sieved to yield solid particles with diameters of less than 250 μm. Dissolved prepolymer (1g polymer: 0.7 ml ethyl acetate) containing 1.5 %wt of DMAP as a photoinitiator was added to the pre-weighed solid particles to obtain 20 % loading by mass. An optimization study indicated that such an initiator concentration is sufficient to produce elastomers with low sol contents [105]. The mixture was vortexed, poured into a cylindrical glass tubes sealed at one end, and capped with a rubber septum at the other end, the tube was connected to the shaft of a motor rotated at 200 rpm, and exposed to long-wave UV light (320-480 nm) at an intensity of 40 mW/cm^2 for a duration of 2 min, using an EXFO E3000 light source. The purpose of rotating the samples, while being exposed to UV light, was to provide a homogenous exposure to UV light, and to prevent particle settling. The glass tubes were sterilized with 70% ethanol, the rubber septum was

removed and the glass was cut from the sealed side in a laminar fume hood. The glass rods were lyophilized and sealed under vacuum, after which the rods were released from the glass molds in a laminar flow hood. The final rods had a weight of 21.1 ± 1.5 mg, a length of around 1.3 cm, and a diameter of around 1.40 mm.

6.2.3. *In vivo* and *in vitro* release kinetics of $VEGF_{165}$:

After removing from glass molds, the radioactivity of the rods was measured using a gamma counter. Four elastomeric rods were implanted subcutaneously in adult male Wistar rats (Charles River Laboratories, P.Q. Canada) weighing 250 g. The implantation procedures were described previously [102]. At 1, 4, 7, 11 and 15 days following the implantation, rats were anaesthetized with an intra peritoneal injection of Somnotol (60 mg/kg) and, at a level of surgical anaesthesia, the rats were shaved and the cylinders excised with the surrounding skin. The fibrous tissue capsules surrounding the implants were cut from the side and the cylinders were pulled out gently with tweezers. The remaining radioactivity was measured and the amount of $VEGF_{165}$ released was calculated. For the *in vitro* release studies, two rods were chosen arbitrarily. The rods were located in eppendorf tubes that contained 1 ml of PBS buffer, and the tubes were located on a shaker set at 500 rpm and 37 °C. The buffer was replaced daily to provide an infinite sink, and at each time point rods were bolted dry and the remaining radioactivity was measured to evaluate the amount of $VEGF_{165}$ released.

6.2.4. *In vivo* angiogenesis studies:

For the *in vivo* angiogenesis studies, particle loading in the elastomers was 10 %

by mass, and in addition to trehalose and RSA, solid particles contained around 5% of NaCl. The *in vivo* angiogenesis studies comprised five groups: 1) The control rods that comprised blank elastomers and elastomers that released trehalose, RSA, and NaCl without growth factors, 2) rods with high dose of $VEGF_{165}$ that released around 1000 ng $VEGF_{165}$ over 14 days, and 3) rods with low dose of $VEGF_{165}$ that released around 100 ng $VEGF_{165}$ over 14 days, 4) rods with high dose of HGF that released around 1000 ng HGF over 14 days, and 5) rods that combined high dose of $VEGF_{165}$ and high dose of HGF and released around 1000 ng $VEGF_{165}$ and 1000 ng HGF simultaneously over 14 days. The implantation study was performed as described above. At 1, 2 and 4 weeks post implantation, the skin tissue that contained the implants was removed and imaged for gross evaluation of blood vessel formation. For histological analyses, rods and surrounding tissue were cut and fixed in 4% paraformaldehyde in phosphate-buffered saline, processed for paraffin embedding, and stained with Masson's trichrome. The *in vitro* release of $VEGF_{165}$ and HGF were evaluated using the corresponding ELISA kits.

6.3. Results and Discussion:

6.3.1. *In vivo* and *in vitro* release kinetics:

The device provided sustained release of ^{125}I-$VEGF_{165}$ in PBS buffer over 43 days (Figure 6-1). The release rate was faster initially. From day 1 to day 7 the release occurred in a linear fashion releasing 31.2 ± 1.1 % of embedded ^{125}I-$VEGF_{165}$. After that, the release proceeded in a sustained, but monotonically decreasing fashion. By day 43, 48.0 ± 1.5 % of embedded ^{125}I-$VEGF_{165}$ had been released. The *in vivo* release kinetics and the *in vitro* release kinetics were identical (Figure 6-1). At day 15, the implanted rods

had released 37.6 ± 3.1 % of their ^{125}I-VEGF$_{165}$ content compared to 38 ± 1.1 % for the *in vitro* releasing rods.

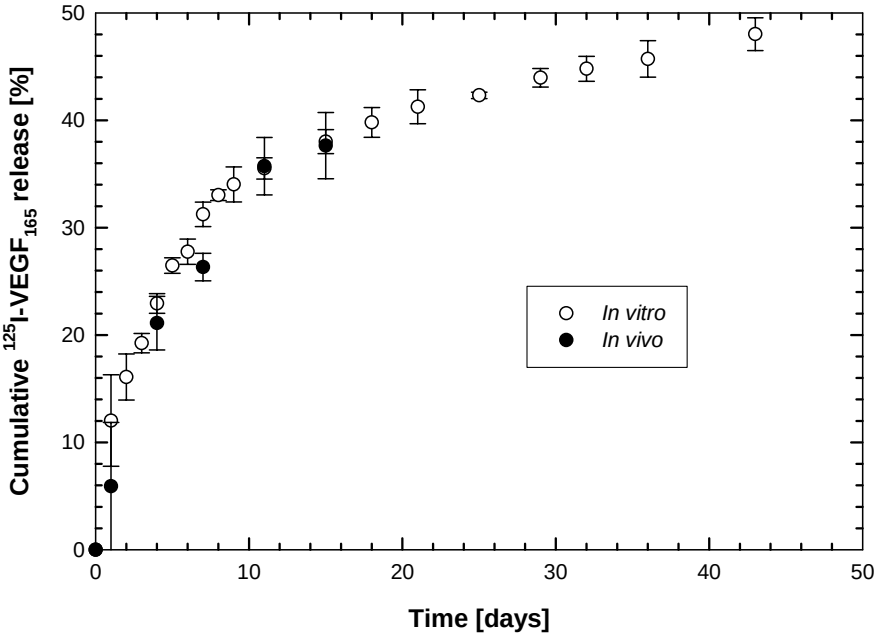

Figure 6- 1. In vivo and in vitro release kinetics of ^{125}I-VEGF$_{165}$ from TMCCLDLLA-4k elastomer. The data represent the average of triplicate samples for the in vivo and duplicate for in vitro, and error bars the standard deviation about the average value.

Unlike delivery techniques that are based on diffusion and matrix degradation [6], the osmotic delivery technique was able to provide a direct *in vivo-in vitro* release correlation. This result is due to the nature of the osmotic release, where water vapor diffuses through the polymer matrix until it encounters a polymer-surrounded drug particle. At the particle/polymer interface, the water phase dissolves a portion of the particle, forming an activity gradient between the capsule and the surrounding medium. The activity gradient draws water into the capsule generating an osmotic pressure that cracks the elastomer, pushing the content toward the surface [8, 20].

6.3.2. *In vivo* angiogenesis:

Gross examination of the skin tissue surrounding the implanted rods indicated that elastomers that released a combination of trehalose, RSA, and NaCl were able to induce angiogenesis (Figure 6-2A).

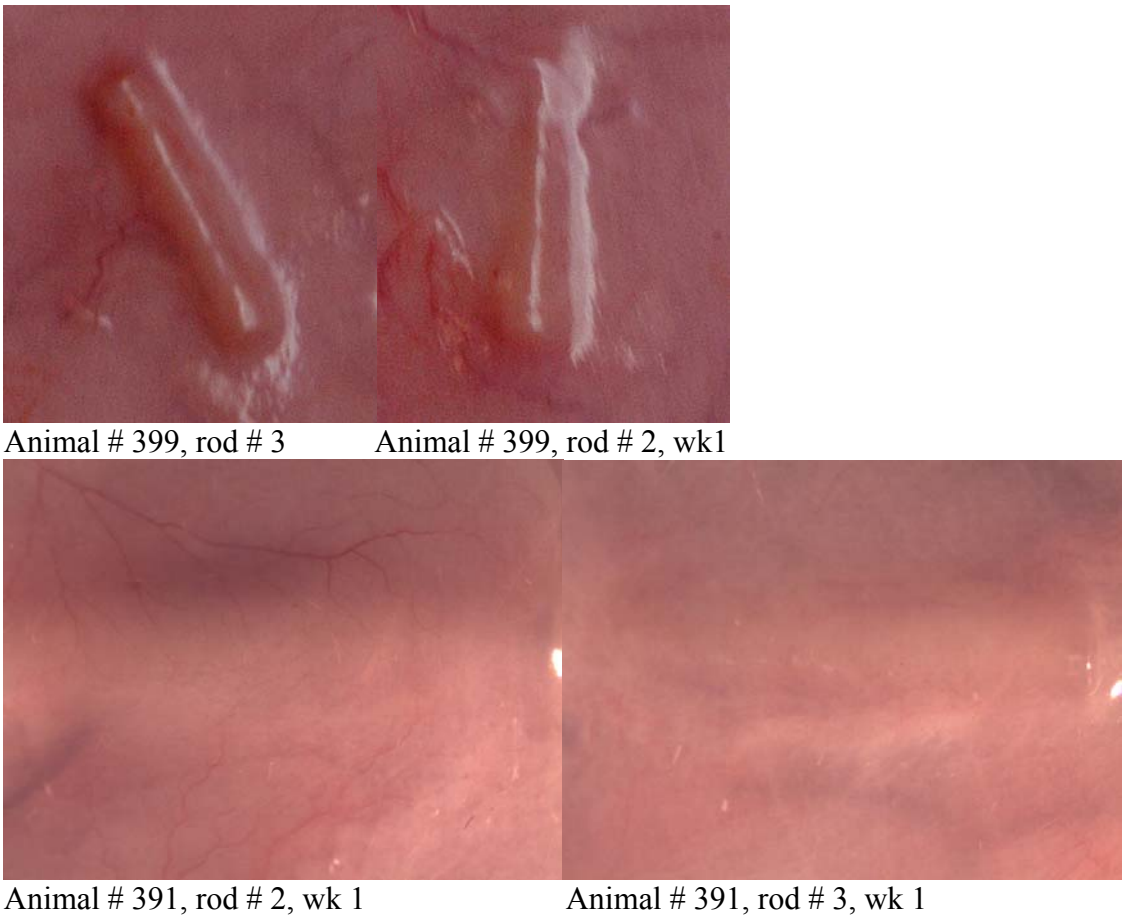

Animal # 399, rod # 3 Animal # 399, rod # 2, wk1

Animal # 391, rod # 2, wk 1 Animal # 391, rod # 3, wk 1

Figure 6- 2. Images of the skin tissue of rats surround the control rods at week 1. control rods released RSA, trehalose and NaCl. Rods in this study had a diameter of 1.40 mm.

Small amounts of NaCl being released from the implants did not cause inflammation to the tissue. A small amount of NaCl was added to increase the osmotic pressure of embedded particles in order to provide an efficient osmotic release [Chapter 5]. Previously, we found that the presence of small amounts of NaCl in the release media did not adversely affect the viability of human aortic endothelial cells (HAEC) [Chapter

5]. High concentrations of NaCl, however, should be avoided since NaCl has high tonicity, and therefore it would likely cause irritation to the tissue when it is released at high concentrations [8]. A limited number of blood vessels observed in the vicinity of the control implants are due to the preexisting blood vessels or they were fomed as a result of an inflammatory response to the elastomer material and not as a response to the released excipints.

The ability of $VEGF_{165}$ to induce blood vessel formation was dose dependent. Rods with a low dose of $VEGF_{165}$ that released around 100 ng of $VEGF_{165}$ over 14 days were unable to induce the formation of new blood vessels (Figure 6-3).

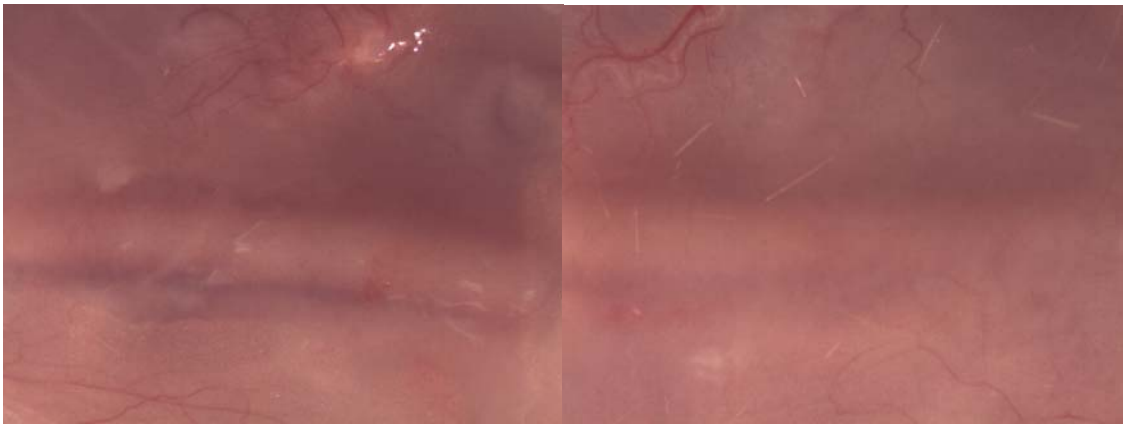

Animal # 397, rod # 1, wk 1 Animal # 397, rod # 2, wk 1

Animal # 401, rod # 2, wk 2 Animal 401, rod # 3, wk 2

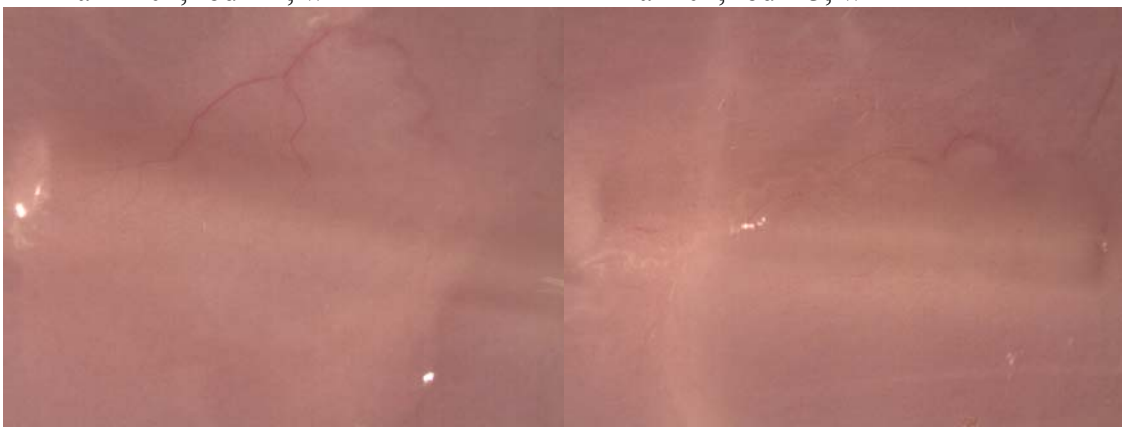

Animal # 410, rod # 1, wk 4 Animal # 410, rod # 2, wk 4

Figure 6- 3. Figure (3) Images of the skin tissue of rats exposed to a sustained low dose of $VEGF_{165}$ released from implanted elastomer rods at different time points. A) week 1, B) week2 and C) week 4. Rods in this study had a diameter of 1.40 mm.

Rods with a high dose of $VEGF_{165}$ that released around 1000 ng of $VEGF_{165}$ over 14 days induced the formation of new capillaries and blood vessels (Figure 6-2).

Capillaries and blood vessels were normal looking and they were connected to the surrounding vasculature (Figure 6-2). No glomeruloid bodies or abnormal looking blood vessels were seen. The newly formed blood vessels were concentrated around the implant and did not span the surrounding tissue. This was most probably due to the limited diffusion of the released $VEGF_{165}$ into the surrounding tissue. As a result, endothelial cells sprouted from preexisting blood vessels toward the capsule, moving along the concentration gradient.

These results are in agreement with the results published by Davies *et al*. who investigated the angiogenic effect of VEGF, delivered into a porous scaffold of polyurethane using an osmotic pump. They found that the dose and duration of released VEGF played a critical role in producing stable blood vessels [17]. Delivery of 15 ng/day of VEGF *in vivo* was insufficient in inducing angiogenesis after 10 days. Delivery of 150 ng/day of VEGF for 42 days produced normal looking blood vessels, which were stable for 80 days after termination of the release. Blood vessels produced by a dose of 1500 ng/day, on the other hand, were larger initially, and they regressed after 20 days [17]. In our experiments, the newly formed blood vessels were not stable and they regressed when the amount of released $VEGF_{165}$ decreased with time. Gross examination of the explanted tissue surrounding implants indicated the existence of a smaller number of blood vessels at week 2. At week 4 no blood vessels were seen around the implant (Figure 6-4).

Animal # 384, rod # 1 Animal # 382, rod # 3 wk1

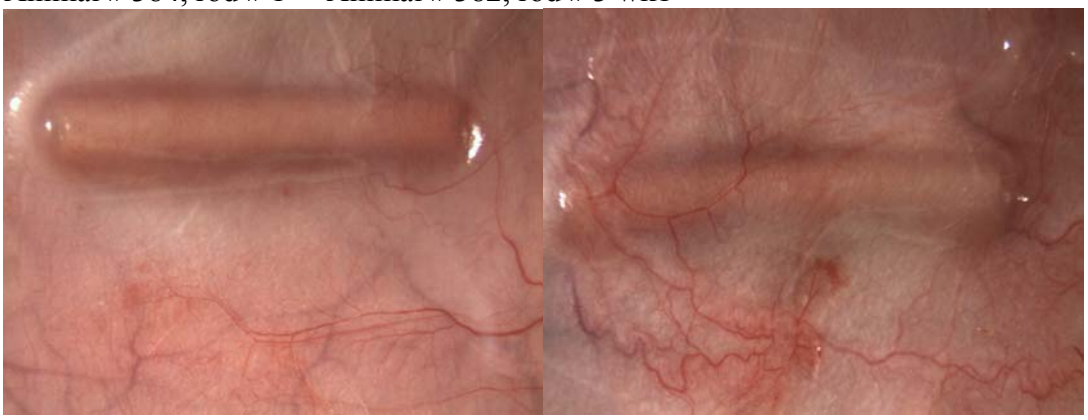

Animal # 376, rod # 2 wk 2 Animal # 376, rod # 3 wk 2

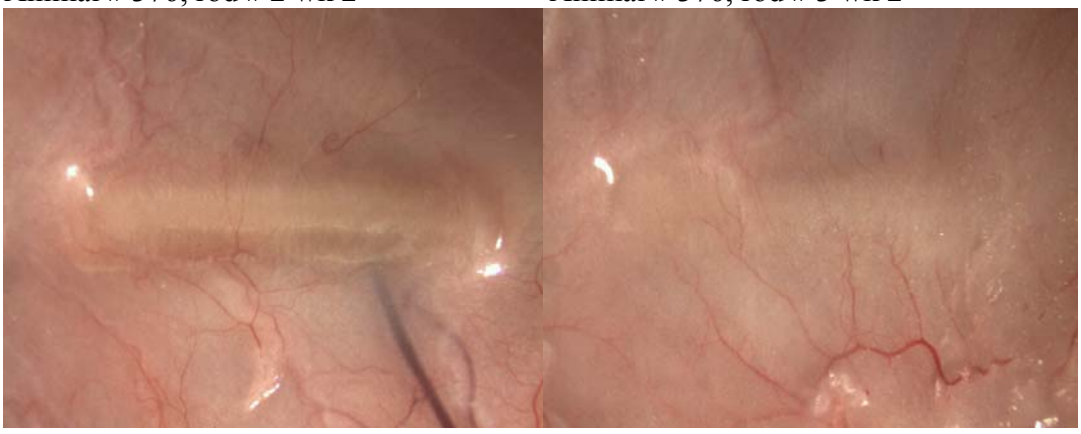

Animal # 372, rod # 3 wk 4 Animal # 372, rod # 1 wk 4

Figure 6- 4. Images of the skin tissue of rats exposed to a sustained high dose of $VEGF_{165}$ released from implanted elastomer rods at different time points. A) week 1, B) week2 and C) week 4. Rods in this study had a diameter of 1.40 mm.

Unlike rods with a high dose of $VEGF_{165}$, rods with a high dose of HGF were able to induce a limited amount of angiogenesis (Figure 6-5). However, when high doses of $VEGF_{165}$ and high doses of HGF were released in combination from the same rod (Figure

6-6), a greater number of blood vessels were formed at week one compared to rods that released a high dose of $VEGF_{165}$ alone (Figure 6-6).

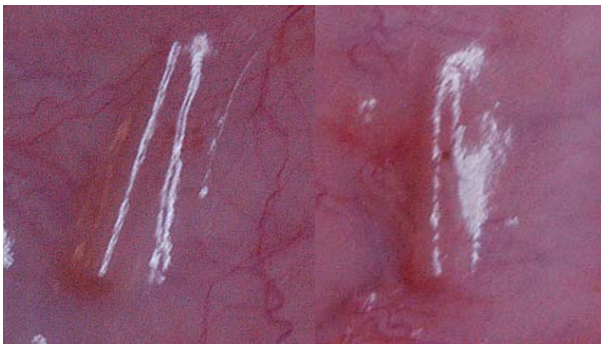

Animal # 387, rod # 2 Animal # 387, rod # 4, wk 1

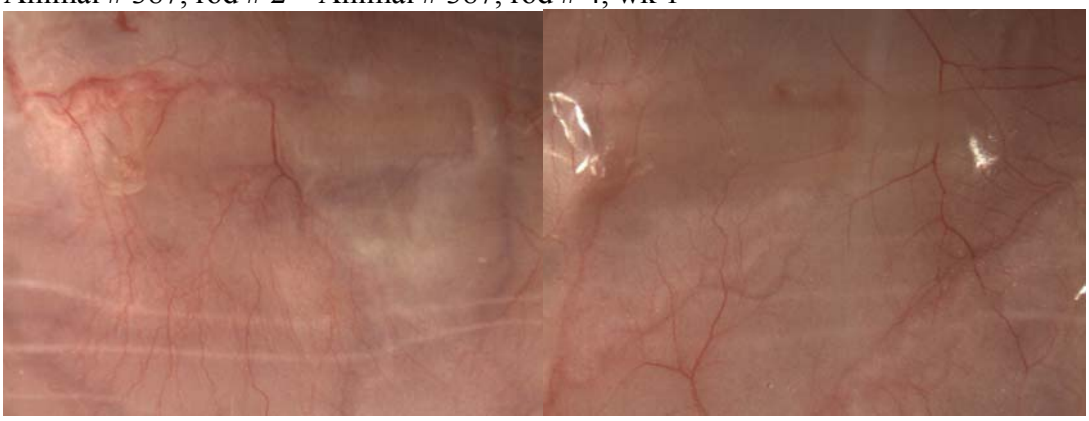

Animal # 379, rod # 3, wk 2 Animal # 379, rod # 2, wk 2

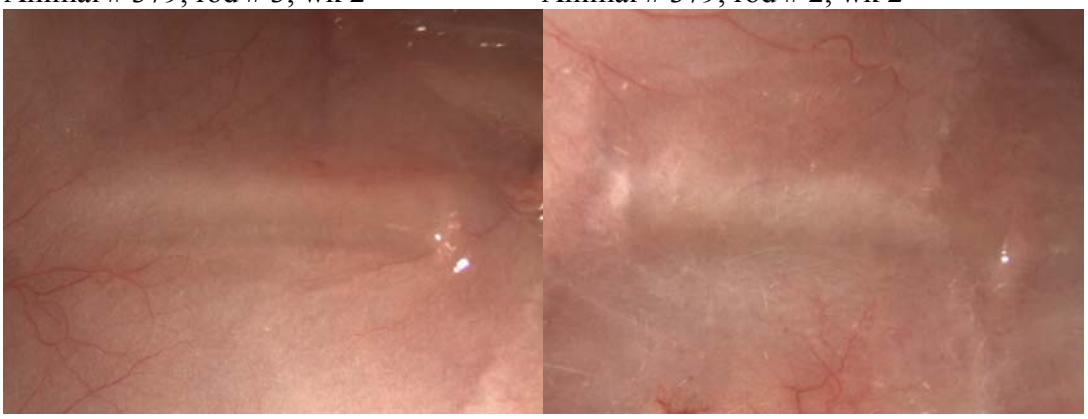

Animal # 373, rod # 1, wk 4 Animal # 373, rod # 4, wk 4

Figure 6- 5. Images of the skin tissue of rats exposed to a sustained high dose of HGF released from implanted elastomer rods at different time points. A) week 1, B) week2 and C) week 4. Rods in this study had a diameter of 1.40 mm.

The inability of rods with a high dose of HGF to induce limited amount of

angiogenesis could be due to the release of insufficient amounts of HGF required to induce the formation of blood vessels. Results published by Ozeki *et al*. indicate no formation of blood vessels when 1 μg of HGF was delivered over 14 days from a gelatin hydrogel. However, when 5 μg and 10 μg of HGF were delivered over the same period, significant angiogenesis occurred in the skin tissue of the mouse [12]. In a different study, the delivery of 200 ng of HGF to rat corneas using Hydron^{TM} pellets induced no significant increase in neovascular area over the control. The same amount of $VEGF_{165}$, however, increased the neovascular area more than 3 times over the control in 6 days [151].

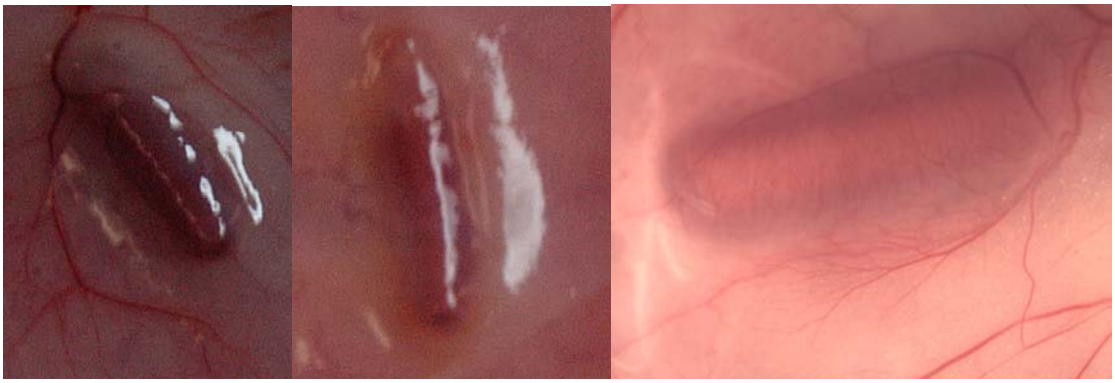

Animal # 388, rod # 2Animal # 396, rod # 2 Animal # 388, rod # 2, wk 1

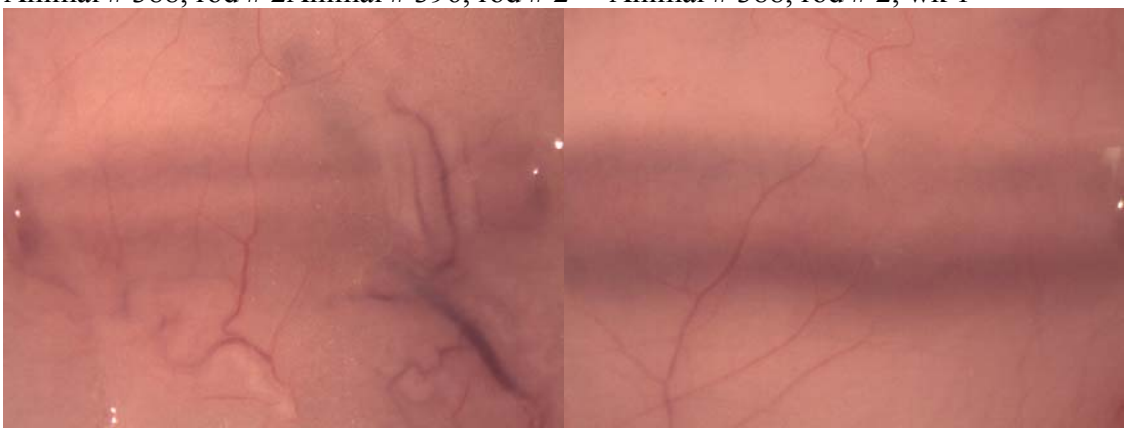

Animal # 406, rod # 1, wk 2 Animal # 406, rod # 2, wk 2

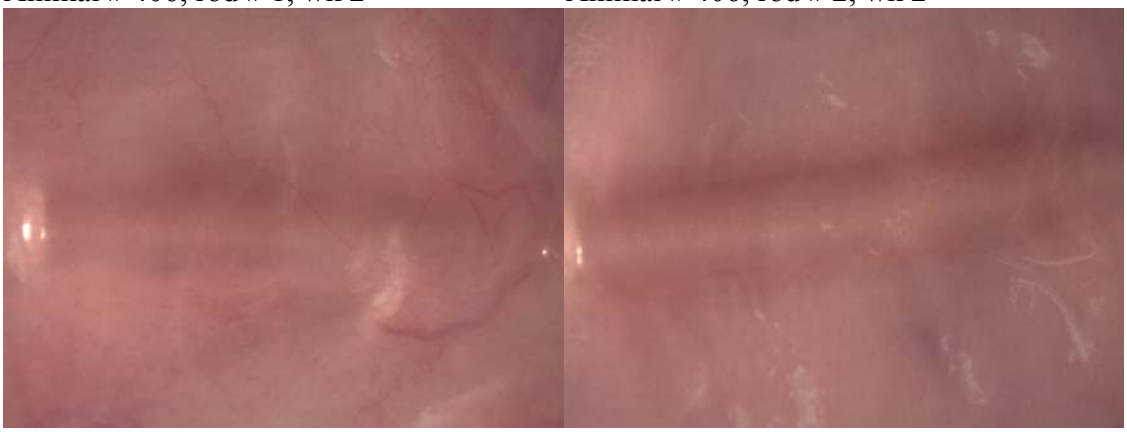

Animal # 409, rod # 2, wk 4 Animal # 409, rod # 3, wk 4

Figure 6- 6. Images of the skin tissue of rats exposed to a combination of sustained high dose of $VEGF_{165}$ and HGF released from implanted elastomer rods at different time points, A) week 1, B) week2 and C) week 4. Rods in this study had a diameter of 1.40 mm.

Xin *et al*. found that the combined release of $VEGF_{165}$ and HGF achieved more effective therapeutic angiogenesis. The combined treatment, wherein 33 ng/day of each growth factor was released over 6 days using Hydron^{TM} pellets had a synergistic effect.

[151]. Although the biological activity of HGF is mediated by producing VEGF secreted by cells upon activation by HGF [12, 151], the authors believe that the synergistic actions of HGF are likely independent of the further increase in VEGF production [151]. Although increased angiogenesis occurred when $VEGF_{165}$ and HGF were released in combination, the newly formed blood vessels were not stable, and they regressed when the release of growth factors decreased.

To obtain a better diffusion of growth factors, fibrosis around the implant should be minimized. This could be achieved by co-releasing of inflammation suppressant such as dexamithazone [72], and by using a hydrophilic coating [159]. Co-releasing of PDGF-BB can stabilize the newly formed blood vessels by recruiting smooth muscle cells.

6.3.3. Histology:

The neovascularization in the tissue surrounding the blank elastomers occurred only outside the capsule area as a result of the foreign body response. Rods that released a high dose of $VEGF_{165}$ contained many newly formed blood channels within the capsule. These channels were lined with endothelial cells, and they contained red blood cells (Figure 6-7). Blood cells were observed in the capsule both at day 7 and day 11. Further histological investigation is required to determine the effectiveness of high dose HGF rods in inducing angiogenesis.

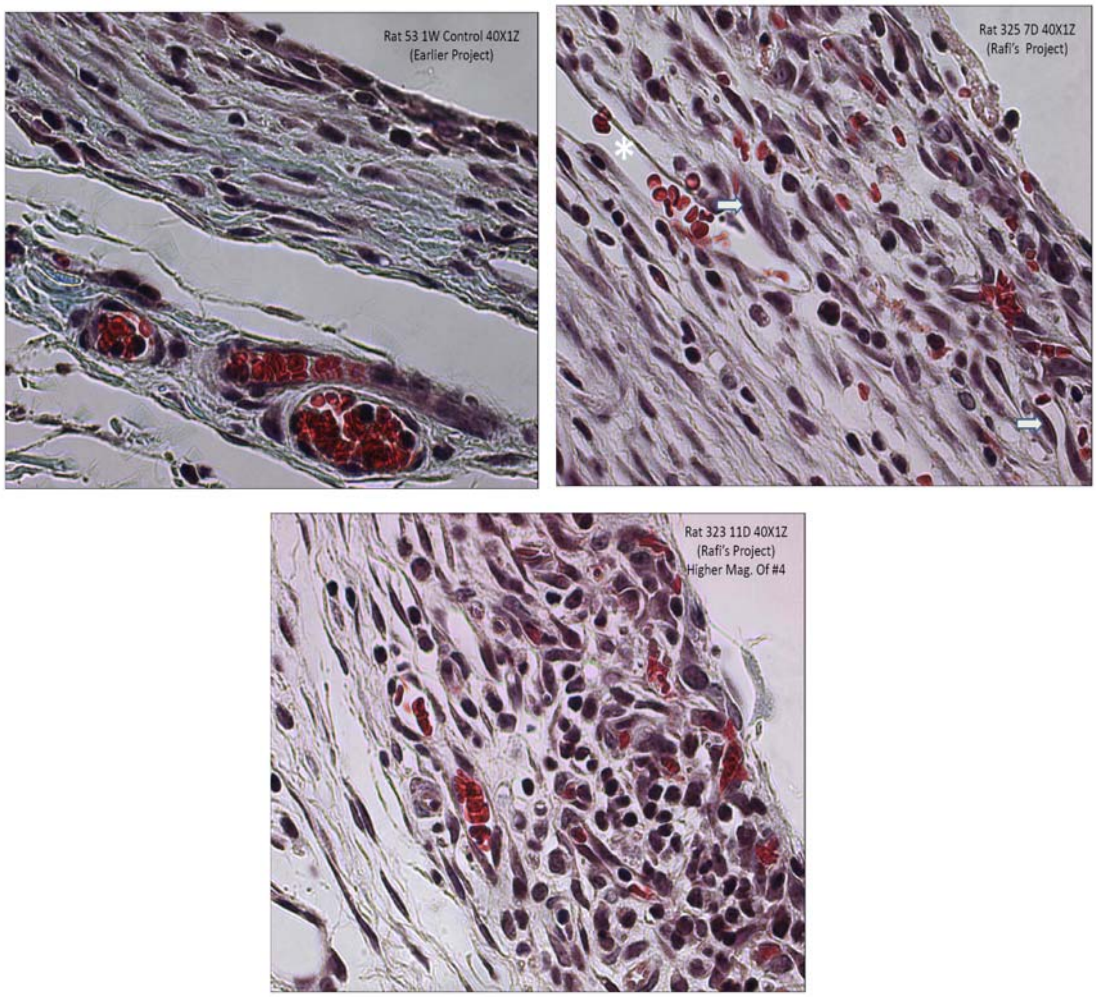

Figure 6- 7. Histological sections of the tissue surrounding the implant stained with Masson's trichrome. A) A blank rod at wk 1, B) rods that released a high dose of $VEGF_{165}$ at wk1, C) rods that released a high dose of $VEGF_{165}$ at day 11. Asterisks indicate red blood cells in the newly formed vessels, while the arrows indicate endothelial cells lining in the newly formed vessels.

6.4. Conclusions:

The osmotic release using a photo-cross-linked elastomer based on TMC provided similar *in vivo* and *in vitro* release rates determined using ^{125}I-$VEGF_{165}$ as a probe. Released $VEGF_{165}$ and HGF were able to induce blood vessel formation. Angiogenesis was a dose dependent in both $VEGF_{165}$ and HGF. Combined release of $VEGF_{165}$ and HGF induced more effective angiogenesis. Capillaries and blood vessels were normal looking and they were connected to the surrounding vasculature. The newly formed

blood vessels were concentrated around the implant and they did not span the surrounding tissue. Formed blood vessels were not stable, and they regressed when the $VEGF_{165}$ release decreased. This study demonstrates the potential of the use of osmotic pressure driven co-delivery of growth factors from biodegradable elastomers to induce angiogenesis.

7. CHAPTER SEVEN

7.1. CONTRIBUTION TO ARTICLES:

In all the five articles presented in this thesis, I wrote the first version of the manuscript. Dr. Amsden corrected all my writings and provided suggestions to improve the writing and organization of the manuscripts.

I prepared all the prepolymers and elastomers in this study and characterized them using NMR, DSC, ATR-FTIR, GPC, and uniaxial tensile strain. I formulated all growth factors and prepared the delivery devices including the delivery devices that contained ^{125}I-VEGF$_{165}$. I designed and conducted all the *in vitro* bioactivity assays and quantified the released proteins and growth factors in this thesis. Mr. Charles B. Cooney prepared the samples and acquired the SEM images. Mr. Jeff Mewburn acquired the confocal microscopy images. Dr. Francoise Sauriol ran the CP-MAS ^{13}C NMR experiment. All the analyses of SEM, confocal microscopy, and CP-MAS ^{13}C NMR were conducted by me. The animal studies and histology presented in Chapters 2, 3, and 6 were conducted by Drs. Pang and Tse, my role was to provide a minor assistance such as shaving the back of the animals, and staining some of the embedded and sectioned tissue samples with Masson's trichrome.

The following ideas in this thesis belong to me:

1. To conduct *in vitro* oxidative and *in vitro* enzymatic degradation studies and to compare the rate of degradation to the rate of *in vivo* degradation.
2. To propose an oxidative degradation mechanism.

3. To use ATR-FTIR to analyze the surface chemistry of degraded elastomers.
4. To investigate the impact of molecular composition of the elastomer on the osmotic release.
5. To use ATR-FTIR and CP-MAS ^{13}C NMR to characterize DLLACL elastomers.
6. To use NaCl to increase the release rate and the total amount of embedded proteins.
7. To use small amounts of DLLA in the final composition of the elastomer.
8. To prepare sterile excipients and delivery devices by sealing lyophilized sterile excipients and delivery devices under vacuum.
9. To improve the yield of acrylation process by conducting the experiment in a dry glove box.
10. To fit the experimental data to a model developed by Amsden to extract the time required for a capsule layer to rupture.
11. To lyophilize growth factors from a pH 7.4 succinate buffer.

8. CHAPTER EIGHT

8.1. GENERAL DISCUSSION

The aim of this thesis was to develop and characterize biodegradable elastomers for localized angiogenic growth factor delivery to treat ischemic tissue. Trimethylene carbonate (TMC), known to degrade without producing acid degradation products [19] was chosen as a base material for the delivery vehicle to eliminate acid degradation products implicated in denaturing $VEGF_{165}$ [6, 10]. The osmotic release mechanism was used because of its ability to provide a zero order release without an initial burst [8], and since the osmotic release is based on fracture formation and propagation [20], the delivery vehicle was made of crosslinked networks. In addition to being able to provide a zero order release without an initial burst, the osmotic release was able to provide *in vivo* release rates that were identical to the *in vitro* release rates [chapter 6]. Photo-cross-linked elastomers made solely of TMC were unable to provide efficient osmotic release of embedded BSA/trehalose because of their large tear properties. To overcome this problem, the mechanical properties of TMC elastomer were tailored by copolymerizing TMC with DLLA and ε-CL, and/or by controlling the cross-link density of the elastomer. Using small amounts of NaCl beside trehalose improved the release efficiency without having tonicity related problems [chapter 6].

Small amounts of DLLA were added to accelerate the degradation rate of TMCCL network that degraded slowly *in vivo* [55]. Small amounts of DLLA (25 mole %) were randomly distributed in the structure of the elastomer, and this did not yield a

significant drop in the microenvironmental pH during the release period [97]. As mentioned in the introduction, $VEGF_{165}$ and HGF were chosen as model growth factors in this study, because of previous difficulties associated with their sustained release in a bioactive form, and because of issues related to their ability to induce the formation of stable blood vessels when administered alone [6, 10, 12, 14, 21, 22]. $VEGF_{165}$ and HGF were formulated with trehalose, albumin and NaCl to protect growth factors during the lyophilization and release. Trehalose and NaCl provided osmotic pressure to rupture the elastomer and release the growth factors [160].

Initially, blank rods were implanted subcutaneously in rats to investigate the degradation mechanism, the rate of degradation, and tissue response. Then, an optimum formulation for the delivery device was developed. Finally, after investigating the *in vivo* release kinetics, the efficacy of the proposed device to induce angiogenesis was tested in rats by subcutaneous implantation.

8.1.1. *In vivo* degradation mechanism:

The aim of the initial step of this study was to investigate the *in vivo* degradation mechanism of blank photo-cross-linked elastomers in order to obtain insights into the degrading zone in which growth factors will be released to initiate a desired biological function. Another aim of the *in vivo* degradation study was to determine the time period during which the device would reside in the body. Techniques used to investigate the *in vivo* degradation mechanism included ATR-FTIR, SEM, uniaxial tensile strain, differential scanning calorimetry, mass loss, sol content, water uptake, and histology.

Two sets of *in vivo* degradation studies were performed. The first group was composed of elastomers made of poly(DLLA-co-ε-CL) that degrade by hydrolysis [102], used as a control, and the second group was composed of elastomers made of poly(TMC) and poly(TMC-co-ε-CL) that degrade by surface erosion [19, 129].

8.1.2. *In vivo* degradation of elastomers made of poly(DLLA-co-ε-CL):

Elastomers with two different cross-link densities made of prepolymers of poly(DLLA-co-ε-CL) with equimolar amounts of monomers were implanted in rats for a long term *in vivo* degradation study. The cross-link density was varied by using prepolymers of two molecular weights, 1250 and 7800 Da. Synthesized elastomers covered a wide range of mechanical properties; the ELAST 1250 was much stiffer than the ELAST 7800 with a modulus approximately 50 times greater, whereas the ELAST 7800 was approximately 3 times more extendable. After 30 weeks, the ELAST 7800 rods were totally degraded and the ELAST 1250 rods had lost 80 % of their mass. Both elastomers degraded *in vivo* primarily by bulk degradation. In the ELAST 7800 the onset of mass loss was accompanied by an increase in both water uptake and sol content, whereas in the ELAST 1250, only the water uptake increased. This interesting phenomenon, observed previously in the literature [54], was attributed to crack formation and propagation in the ELAST 1250, which was far stiffer than the ELAST 7800. The occurrence of a yield point after a very short elongation in ELAST 1250 had a great impact on the degradation pattern. The transition to a plastic deformation stage after a very short value of elongation facilitated the crack formation and propagation upon the swelling of the elastomer. Formed cracks provided an easy passage to the small

molecular weight degradation products to diffuse out of the elastomer, and as a result no increase in the sol content was observed in ELAST 1250 [96]. Crack formation and propagation contributed to a significant difference in the degradation pattern between the ELAST 1250 and ELAST 7800. The rate of *in vivo* degradation of both elastomers was faster than the rate of *in vitro* degradation in PBS buffer. The difference was attributed to the effect of the physiological conditions. The impact of the physiological conditions was far more significant on the degradation of the denser network, where extensive shedding and cracking occurred. Dark spots and pits observed in the *in vivo* degraded elastomers were absent in the *in vitro* degraded elastomers. These findings were in accordance with findings reported in the literature where cross-linked networks of hydrolytacilly degrading elastomers were found to degrade by enzymatic surface erosion *in vivo* in addition to the hydrolytic bulk degradation [103].

The tissue response was mild and dynamic. A heightened, short-lived inflammatory response occurred at the peak of degradation. The tissue response was milder with the higher cross-linked network. This study along with previous studies conducted in our group indicate that elastomers made of poly(DLLA-co-ε-CL) could be used for osmotic delivery of non-pH sensitive growth factors. However, the size of the device should be considered as a significant design parameter to minimize the negative tissue response during the peak of degradation. This study indicates as well that there is an optimum cross-link density that can provide the longest time period, where the mass loss linearly follows the drop in mechanical properties. This degradation behavior is desirable in tissue engineering applications to enhance the growth of newly formed

tissues [161]. Thus, due to deep cracks, the highly cross-linked network (ELAST 1250) lost its mechanical strength before losing any mass, whereas the low cross-linked network (ELAST 7800) lost 15 % of its mass, before degrading into a weak material [56]. This result is in agreement with results published by Storey *et al.*, who reported a 2% of weight loss with the loss of the mechanical strength of a crosslinked elastomer, prepared from a copolymer with a number of average molecular weight of 2100 Da, and a molar composition of 55.3 mol % of D,L-lactide and 55.3 mol % of ε-CL [54].

8.1.3. *In vivo* degradation of elastomers made of poly(TMC) and poly(TMC-co-ε-CL):

The degradation of elastomers made of 7800 Da poly(TMC) (TMC-78) and 7800 Da poly(TMC-co-ε-CL) (TMCCL-78) of equimolar amounts of monomers were studied. Both elastomers underwent very little hydrolytic degradation in PBS buffer over 30 weeks. *In vivo*, however, TMC-78 elastomers lost 33 ± 7.2 % of their initial mass over 44 weeks and TMCCL-78 elastomers lost 20.6 ± 4.8 % of their initial mass over the same time period. TMC-78 and TMCCL-78 elastomers degraded *in vivo* in a manner consistent with a surface erosion mechanism. A linear mass loss with time, presence of extensive surface pitting, low and unchanged sol content, unchanged T_g, and maintenance of mechanical properties, were observed for both elastomers *in vivo*. The *in vivo* degraded elastomers lost a significant amount of strength, after 16 weeks, and this loss was attributed to the generation of surface cracks and pits during degradation, which acted as stress risers during extension, initiating crack propagation throughout the elastomer and leading to premature failure. SEM and histology images indicated that both poly(TMC-78) and poly(TMCCL-78) elastomers were degraded by the action of foreign body giant

cells, attached to the surface. Foreign body giant cells are known to generate both reactive oxygen species as well as secrete enzymes such as cholesterol esterase to degrade an implanted biomaterial [140-142]. The determination of the exact mechanism of *in vivo* degradation is very important for growth factor delivery materials. For example, the presence of harmful oxidative species in the vicinity of released growth factors could result in a rapid cellular degradation of oxidized growth factors [162].

Therefore, in order to determine the relative role of each degradation mechanism (enzyme versus oxidation), the rate of degradation and the surface chemistry of the *in vivo* degraded elastomers were studied and compared to the rate of degradation and the surface chemistry of elastomers degraded *in vitro* by lipase and cholesterol esterase and by superoxide anion. The results indicated that oxidation plays a significant role in the *in vivo* degradation of TMC-78 and TMCCL-78 elastomers [55]. This result is in agreement with results published lately by Bat *et al*., who reported a significant role of oxidation in the macrophage culture mediated degradation of gamma irradiated poly(TMC) films [163]. Those findings disprove the erroneous concept published by Zhang *et al.* that TMC elastomers degrade *in vivo* by enzymatic action [19], and that the reason behind the very slow degradation of low molecular weight TMC polymers *in vivo* is the higher hydrophilicity of the elastomer that allows the enzymes to obtain a less active configuration on the surface [19].

Dadsetan *et al*. based on their observation of three new bands at 3225 cm^{-1}, 1654 cm^{-1} and 1541 cm^{-1} on the surface of the *in vivo* degraded poly(ethylene carbonate)

polymers, concluded the formation of a carbonate ion and hydroxyl group during the *in vivo* degradation [138]. In our *in vivo* degradation studies and *in vitro* enzymatic degradation in lipase, three bands, very similar to the ones reported by Dadestan *et al*., were appeared at 3285 cm^{-1}, 1656 cm^{-1} and 1537 cm^{-1}. We were able to remove those bands from the surface of lipase degraded TMCCL-78 elastomer, but not the lipase degraded TMC-78 elastomer, using urea/triton 100x treatment. Based on this finding and the observation that a carbonate ion yields only one band at 1640 cm^{-1} as reported in [136] and observed at 1620 cm^{-1} in [55], and not two bands as reported by Dadestan *et al*., indicate that the findings reported by this group require a revision.

A mechanism for the oxidative degradation of TMC-78 and TMCCL-78 elastomers that proceeds through the formation of ionic end groups via a nucleophilic attack of superoxide ions, followed by a chain unzipping reaction was proposed. The suggested mechanism was supported by the presence of carbonylate and carboxylate ion bands in ATR-FTIR spectra of the elastomer surfaces [55]. Faster oxidation rates of TMCCL-78 elastomer was attributed to a different chain unzipping reaction in TMCCL-78 and the possibility of a transesterification reaction, occurring due to the presence of an ester bond [55].

TMC-78 and TMCCL-78 elastomer degradation studies indicate that those elastomers are potentially suitable materials to eliminate the microenvironmental pH drop and its negative impact on the bioactivity of imbedded growth factors [6]. Cross-linked elastomers, however, degraded at rates slower than the degradation rate of high molecular

weight TMC and TMCCL linear polymers. After normalizing the surface area, the cross-linked TMC-78 elastomer, produced in this work, was found to degrade 7-8 times slower than the high molecular weight linear poly(TMC) that had a number average molecular weight of 316 kDa, produced by Pego *et al*. [122]. Cross-linked networks, however, are better candidates for the osmotic delivery intended in this thesis, since the osmotic release is governed by the fracture formation and propagation [20, 89], and thermoset networks have a much higher tendency to undergo fracture than high molecular weight thermoplastics [152].

8.1.4 Tissue Response:

To analyze the tissue response to implanted elastomers, elastomers along with the surrounding tissue were explanted, embedded in paraffin, sectioned, and stained with Masson's trichrome. Tissue response of implanted materials was mild, and elastomers were very well tolerated in rats over a long period of implantation, extending up to 44 weeks. A distinct fibrous capsule was formed during the first week for all implanted elastomers. The cellular content and the thickness of the capsule were different from material to material, and they were dynamic and a function of the mechanism and rate of degradation. In the case of elastomers prepared from low crosslink density, terminally acrylated poly(DLLA-co-ε-CL), the onset of mass loss was translated into an increased vascularization and capsule thickness. The tissue response was milder in the case of the high crosslink density poly(DLLA-co-ε-CL) elastomer that degraded at a slower rates than the low crosslink density elastomer [56]. In the case of poly(TMC) and poly(TMC-co-ε-CL) elastomers, foreign body giant cells were formed at the interface of the

elastomer, and generated pits on the surface of the elastomer. The tissue response was milder in the case of poly(TMC-co-ε-CL) than in poly(TMC) elastomer [55].

In all implanted elastomers a collagenous capsule was formed around the implant within the first week of the study. The capsule thickness in the case of DLLACL elastomers remained less than 100 μm during the degradation, and it was significantly thinner than the capsule thickness of 400-600 μm reported for PLA and PLGA polymers [47]. Foreign body giant cells observed in the case of TMC and TMCCL elastomers were observed as well in the literature in the case of the high molecular weight linear TMC polymer that had a number average molecular weight of 316 KDa [122]. Interestingly, foreign body giant cells did not form in the case of low molecular weight TMC polymers that had number average molecular weights of 620, 1600 and 2400 Da, investigated by Timbart *et al*. [164]. Thus, understanding why materials with similar chemistry, but different physical properties could prompt so much different foreign body response *in vivo*, would be an exciting field to investigate.

8.1.5. Osmotic release:

The potential of osmotic pressure driven release of therapeutic proteins from photo-cross-linked poly(TMC) based elastomers was investigated. $VEGF_{165}$ and HGF were formulated with trehalose, albumin and NaCl to protect the growth factors during fabrication and to provide osmotic activity during the release. To provide efficient crack formation and propagation, the mechanical properties of synthesized elastomers were tailored by copolymerizing TMC with DLLA and ε-CL and by controlling the cross-link

density.

8.1.6. Osmotic release from poly(TMC) elastomer:

Elastomers made of poly(TMC) were not suitable for osmotically driven release of therapeutic proteins when trehalose was intended to be the only osmotigen in the solid particles [97]. As mentioned, trehalose is a desired osmotigen since it has low values of isotonicity, and consequently it is expected to produce less tissue irritation [8]. The TMC elastomer has strong tear resistance; as a result, a greater osmotic pressure is required to induce efficient crack formation. To overcome this problem, the mechanical properties of TMC elastomers were tailored using two techniques: copolymerizing TMC with other monomers such as ε-CL and DLLA and/or increasing the crosslink density of the elastomer by using prepolymers of lower molecular weights.

8.1.7. Effect of copolymerization on osmotic release:

The mechanical properties of elastomers could be tailored easily by changing the cross-link density and molecular composition, so that they match the mechanical properties of a target tissue [39]. The same could be done to adjust the degradation kinetics [43, 56]. Since the osmotic release is governed by the mechanical properties of the elastomer [8, 20], the release kinetics could be tailored by altering the mechanical properties of the elastomer via the crosslink density and/or the molecular composition. Controlling the osmotic release kinetics, by means of adjusting the mechanical properties through the molecular composition has not been investigated in the literature.

TMC was copolymerized with different amounts of DLLA (5, 20, and 50 mole%) to investigate the impact of altering the mechanical properties via the molecular composition on the release kinetics. Copolymerizing TMC with DLLA decreased the elongation at break without having a significant impact on the Young's modulus, and consequently the tear resistance of the elastomer decreased, providing greater release efficiency.

Although TMCDLLA copolymers were able to provide greater release rates with trehalose as the sole osmotigen, the total amount of BSA released was less than 50%. To increase the osmotic pressure, and to provide greater release efficiency, 25% of NaCl was added to solid particles. As a result, poly(TMC-co-DLLA)(80:20) elastomer provided a near zero order release of albumin for up to 12 days, and the total amount of albumin released was 74 ± 4 % after 34 days. A model developed by Amsden for the osmotic release of electrolytes from non-degradable silicone elastomers was fitted to experimental data to extract the time required for a capsule layer to burst (t_b). The model provided a very good fit to experimental data. Two assumptions of the model were verified during the experimental work: 1) the material is depleted from the surface to the centre, and this was verified through our experiments with FITC-BSA [97], 2) the model assumes that the time during which the solution is forced from the ruptured capsule is negligible compared to the time required for a capsule or a particle layer to rupture. This assumption was found to be correct, and the calculated time of the burst corresponded to an average particle layer thickness, where solid particles were depleted [97].

8.1.8. Effect of cross-link density on osmotic release:

The effect of crosslink density on osmotic release was investigated using terpolymers of TMCCLDLLA of a molar ratio of (50:25:25). To vary the cross-link density, prepolymers of two different molecular weights of 4000 Da and 7800 Da were made. Increasing the cross-link density had a significant impact on improving the efficiency of the osmotic release. Increasing the cross-link density increased the modulus 1.1 times, and decreased the elongation at break 1.8 times. The tear resistance in this case decreased because of a decrease in the elongation at break. It was concluded that tear properties, rather than the modulus, had a greater impact on the osmotic release potential of the elastomer [97]. Increasing the osmotic release rate by increasing the cross-link density was reported previously by Gu *et al*.. The impact of the cross-link density on the release rate observed in this study, however, was far more significant. The release rate increased 8 times when the number average molecular weight of the terpolymer prepolymer of TMCDLLACL was decreased from 7800 Da to 4000 Da. Whereas, Gu *et al*. reported only a 1.2 times increase in the release rate when the number average molecular weight of their DLLACL elastomers was decreased from 7800 Da to 2700 Da [165].

8.1.9. Effect of loading and NaCl on release:

Increasing the loading did not have a significant impact on the release rate. On the other hand, the higher the loading, the greater the water uptake or the swelling of the device. Greater loading is not desirable since a high content of water in the device could denature therapeutic proteins. Adding small amounts of NaCl in the formulation of solid

particles increased the release rate and total amount of albumin released. High amounts of NaCl were avoided since they could cause inflammation when released *in vivo*. The proportional impact of the loading on the release rate was more significant in data reported in the literature, wherein the release of electrolytes from non-degradable elastomers were investigated [88, 91, 166]. The insignificant impact of the loading in our study is most probably due to the occurrence of an ineffective osmotic release in the elastomers, where the impact of loading on the release rate was investigated. The impact of NaCl on increasing the release rate was in agreement with the data published in the literature [88].

8.1.10. Microenvironmental pH:

Since VEGF undergoes an accelerated degradation at pHs of as low as 5 [21], it was necessary to investigate the pH drop in the device that contained DLLA, known to degrade by hydrolysis. For that purpose FITC-BSA was lyophilized with trehalose and embedded in poly(TMC-co-DLLA) (80:20) (TMCDLLA-78) elastomer, and the device was located in an infinite sink of PBS buffer, as in a regular release experiment. This composition was used since it was expected that small amounts of DLLA in the composition of the elastomer would accelerate the degradation of TMC and TMCCL elastomers [55]. FITC-BSA maintained strong fluorescing abilities after 17 days, and since the FITC molecule loses its fluorescing ability by a drop in pH and it does not fluoresce below pH 5 [10], it was concluded that the microenvironmental pH remained above 5 during the release. Incorporating low amounts of DLLA in the structure of the copolymer produced highly randomized lactyl units. In poly(TMC-co-

DLLA)(80:20),7.8K the average length of lactyl unit was1.49, and it increased to 2.8 in poly(TMC-co-DLLA)(50:50),7.8K prepolymer. A network with highly randomized lactyl units is expected to degrade slowly without a significant autocatalysis, since acid degradation products of lactyl units are fairly spread in the network. ATR-FTIR analyses of degraded poly(TMC-co-DLLA)(80:20),7.8K elastomer indicated very slow degradation and the formation of carboxylate ion bands after 30 weeks in PBS buffer.

This study indicates that replacing an acid producing ester such as DLLA with a non-acid producing carbonate such as TMC can minimize or eliminate the pH drop in the pores and cavities of the device. The pH in BSA/trehalose loaded TMCDLLA(80:20) elastomer remained above 5 after 17 days compared to BSA/trehalose loaded DLLACL(50:50) elastomer, where the pH dropped to below 5 in as short as 7 days [10]. This study indicates as well that TMC based elastomers are far more suitable than PLGA based polymeric systems, where the pH could drop to as low as 2 [76].

8.1.11. Advantages of TMCCLDLLA-40 terpolymer in growth factor delivery:

This elastomer was able to provide an efficient osmotic release using the osmotic pressure generated from trehalose with a minor contribution of NaCl. The TMCCLDLLA-40 elastomer with a molar composition of (50:25:25) had far smaller tear resistance than the TMC-78 and TMCDLLA-78 elastomer with a molar composition of (80:20). The TMCCLDLLA-40 elastomer provided a zero order release for 6 days followed by a sustained release for over 2 weeks. 80 % of the embedded albumin was released over 50 days. The DLLA monomer was randomly distributed in the structure of

the elastomer, and the hydrolytic degradation proceeded very slowly during the release period. The molar ratio of acrylate/DMPA was 12, much higher than 0.1, determined by Gu *et al.* to be the minimum required to protect VEGF/albumin molecules from free radicals, generated during the photo-polymerization process. A small amount of DLLA was added to the elastomer to accelerate the rate of degradation since we found that TMCCL elastomer degrades very slowly *in vivo* [55]. Although adding small amounts of DLLA accelerated the rate of *in vitro* degradation, its impact on the *in vivo* degradation rate and mechanism needs to be verified, since large amounts of DLLA beside TMC prohibits the formation of foreign body giant cells and decreases the rate of *in vivo* degradation [122]. If the presence of small amounts of DLLA hampers the *in vivo* degradation, it could be replaced by CL, since TMCCL(50:50)-40 elastomer was found to have comparable mechanical properties to that of TMCCLDLLA(50:25:25)-40 proposed in this study.

8.1.12. Bioactivity of released VEGF and HGF:

After solving the pH drop problem, it was necessary to investigate the *in vitro* bioactivity of the released $VEGF_{165}$ and HGF. The bioactivity of $VEGF_{165}$ was evaluated based on its ability to induce the proliferation of human aortic endothelial cells, and the bioactivity of HGF was evaluated based on its ability to induce the proliferation of CCL 208 monkey long epithelial cells. The released VEGF and HGF were highly bioactive, and they maintained a high level of bioactivity (~ 80%) throughout the release period. VEGF was released at a rate similar to the rate of embedded albumin. A sustained release of VEGF was provided for 20 days *in vitro*. 215 ng/ml/day of VEGF was released during

the initial 3 days, around 60 ng/ml/day during the following 4 days, and around 6ng/ml/day during the following 7 days. 60 ± 10 % of embedded VEGF was released. The release of HGF occurred at similar rates to that of $VEGF_{165}$. This study represents an improvement over a previous study, where the osmotic release was used to deliver acid sensitive VEGF from DLLACL(50:50)-78 elastomers [165]. Released VEGF was able to induce the proliferation of HAECs even after 2 weeks. Whereas VEGF released from DLLACL(50:50)-78 lost its bioactivity after 7-8 days. Beside the pH drop to less than 5 brought on by the hydrolysis of the lactide component of DLLACL(50:50)-78 elastomer, Gu *et al*. had lyophilized $VEGF_{165}$ from a pH 5 buffer [165], which in itself could locate the growth factor under degradation strain [21] in the device. In our study the lyophilization of $VEGF_{165}$ was done from a buffer that had a pH 7.4 to minimize the rate of growth factor degradation.

8.1.13. Comparing the rate of *in vitro* and *in vivo* release of VEGF:

In the next step, we aimed at investigating the rate of *in vivo* release of $VEGF_{165}$ and comparing it to the rate of *in vitro* release. This step was achieved by using ^{125}I-$VEGF_{165}$. The radioactivity of explanted rods was measured and compared to the radioactivity of rods located in an infinite sink of PBS buffer at identical time points. The rate of *in vivo* and *in vitro* release of $VEGF_{165}$ from osmotically functioning device was found to be identical. This significant finding indicates that despite differences in the *in vivo* and *in vitro* sink conditions, a device that functions on the osmotic release mechanism can provide identical *in vivo* and *in vitro* release rates. This finding gives the osmotic release mechanism superiority over other release techniques that are based on

diffusion and/or matrix degradation [6].

8.1.14. *In vivo* efficacy of released $VEGF_{165}$ and HGF:

The aim of the final step was to investigate the ability of released growth factors ($VEGF_{165}$ and HGF) to induce angiogenesis *in vivo*. Elastomers in this study were made of TMCCLDLLA-40, and solid particles were composed of 10 % RSA, 85 % trehalose, and 5 % NaCl, in addition to the growth factors. $VEGF_{165}$ and HGF were released separately or in combination from the same rod. Growth factors were released at two doses: rods with a high dose that released around 1000 ng of a growth factor in 14 days, and rods with a low dose that released 100 ng of a growth factor in 14 days. Rods that released a combination of high doses of growth factors released around 1000 ng of VEGF and 1000ng of HGF from the same rod. Angiogenesis was dose dependent in both VEGF and HGF. Low doses of release were unable to induce angiogenesis in both VEGF and HGF, and these results are in agreement with data published in the literature [12, 17]. Combined release of VEGF and HGF induced the most effective angiogenesis, and this was in agreement with the results of Xin *et al.* [151].

The release of a high dose of VEGF and a combined high dose of VEGF and HGF induced the formation of a localized edema around the implant. Tabata *et al*. reported the formation of an edema in their VEGF releasing collagen matrix, and they suggested that the edema was a sign of a bioactive VEGF that was released from the collagen matrix [15].

Histological investigations indicated the formation of a fibrotic capsule around the elastomeric device within the first week of the release. Newly formed blood vessels were concentrated in the capsule area and they did not span the tissue. VEGF was found to diffuse a longer distance when it was released from alginate based hydrogels [14]. This indicates that the dense capsule formed around the device had a limiting impact on the diffusion of growth factors.

The developed device provided sustained and bioactive growth factors for longer than two weeks with no initial burst. In addition no explantation is required since the device is biodegradable, and it will degrade within 1-2 years. The newly formed capillaries and blood vessels were normal looking and they were connected to the surrounding vasculature. The newly formed blood vessels, however, were not stable, and they regressed when the release of growth factors decreased.

The overall significance of these findings are that growth factors delivered using TMC based photo-cross-linked elastomers can induce angiogenesis, and that osmotic release mechanism can deliver bioactive growth factors at an *in vivo* release rate identical to the *in vitro* release rate.

8.2. Summary of accomplishments:

It was demonstrated through this thesis that:

1. Growth factors released from photo-cross-linked elastomers, using the osmotic release mechanism, are able to induce angiogenesis *in vivo.*

2. The *in vitro* released HGF and $VEGF_{165}$ were highly bioactive, and they maintained their bioactivity over 3 weeks, determined using cell based bioactivity assays.
3. Unlike diffusion and matrix degradation based release techniques [6], the osmotic release is able to provide *in vivo* release rates similar to *in vitro* release rates.
4. TMC based elastomers can provide effective osmotic release with trehalose as the main osmotigen.
5. Pressure-resisting properties of TMC can be tailored by copolymerizing it with monomers such as ε-CL and DLLA and by altering the crosslink density.
6. Synthesized photo-cross-linked elastomers were very well tolerated in rats over a long period, extending up to 44 weeks.
7. The rate of *in vivo* degradation of poly(DLLA-co-ε-CL) elastomers was faster than the rate of *in vitro* degradation, and the elastomers degraded *in vivo* primarily by hydrolysis. ELAST 7800 rods were totally degraded in rats.
8. Elastomers made of poly(TMC) and poly(TMC-co-ε-CL) degraded *in vivo* by foreign body giant cells attached to the surface, and oxidation played a significant role in the degradation of these elastomers. A mechanism for degradation by oxidation was suggested.
9. Tear properties are important factors in the osmotic release, and their importance was more significant than the modulus in this study.

8.3. Conclusions and recommendations:

The osmotic release from photo-cross-linked elastomers is a promising technique

for the delivery of growth factors. This technique can provide many of the requirements for a successful polymer based growth factor delivery system [5]. It provides a linear and sustained release of growth factors for a period of longer than two weeks with a low initial burst. In this thesis it was also illustrated that the osmotic release can provide similar *in vitro* and *in vivo* rates, and that the microenvironmental pH drop problem can be solved by a careful choice of the elastomer composition. The released growth factors were bioactive and they induced blood vessel formation.

For a further success in the osmotic delivery of growth factors from photo-cross-linked elastomers, it is strongly recommended:

1. To search for materials that degrade at faster rates.
2. To decrease fibrosis around the implant to provide better distribution of growth factors in the vicinity of the device. This could be accomplished by co-releasing inflammation suppressant drugs such as dexamithazone [72] or by controlling the hydrophilicity of the surface [159].
3. To obtain a complete release of embedded growth factors. This could be accomplished by using an inner cylindrical layer that contains stronger osmotigens [92, 98].
4. To measure the microenvironmental pH drop more accurately. This could be accomplished by using lyso-sensor yellow/blue and SNARF-1 dextran and to measure the pH distribution in the device [74].
5. To conduct more realistic *in vitro* bioactivity experiments. This could be accomplished by seeding macrophages on the surface of the device and evaluating the *in vitro* bioactivity of released growth factors to determine the effect of

released oxidative species and degradative enzymes.

6. To produce stable and long living blood vessels. This could be accomplished by dual delivery of VEGF and platelet derived growth factor (PDGF) known to recruit smooth muscle cells that stabilize the newly formed capillaries and blood vessels [13].
7. To establish a convenient and attractive technique for delivery. This could be accomplished by producing injectable photo-cross-linked microspheres. Since crack formation and propagation occurs more effectively in cross-linked networks, cured microspheres can provide more efficient osmotic release than non-cured microspheres.
8. To investigate the concentrations of NaCl that could cause inflammation, and to explore the possibility of replacing serum albumin with synthetic peptides.
9. To determine the impact of the presence of small amounts of DLLA on the *in vivo* degradation rate and mechanism of TMC based elastomers.

References

[1] D.V. Cokkinos, C. Pantos, G. Heusch, H. Taegtmeyer, Editors, Myocardial Ischemia: From Mechanisms to Therapeutic Potentials. [In: Basic Sci. Cardiol., 2006; 21], 2006.

[2] H.M. Piper, D. Garcia-Dorado, Prime causes of rapid cardiomyocyte death during reperfusion. Annals of Thoracic Surgery 68(5) (1999) 1913-1919.

[3] H. Helotera, K. Alitalo, The VeGf family, the inside story. Cell 130(4) (2007) 591-592.

[4] M. Simons, Angiogenesis: where do we stand now? Circulation 111(12) (2005) 1556-1566.

[5] F. Wu, T. Jin, Polymer-Based Sustained-Release Dosage Forms for Protein Drugs, Challenges, and Recent Advances. Aaps Pharmscitech 9(4) (2008) 1218-1229.

[6] T.K. Kim, D.J. Burgess, Pharmacokinetic characterization C-14-vascular endothelial growth factor controlled release microspheres using a rat model. Journal of Pharmacy and Pharmacology 54(7) (2002) 897-905.

[7] J.J. Lopez, M. Simons, Local extravascular growth factor delivery in myocardial ischemia. Drug Delivery 3(3) (1996) 143-147.

[8] B. Amsden, Review of osmotic pressure driven release of proteins from monolithic devices. Journal of Pharmacy and Pharmaceutical Sciences 10(2) (2007) 129-143.

[9] J. Esaki, A. Marui, Y. Tabata, M. Komeda, Controlled release systems of angiogenic growth factors for cardiovascular diseases. Expert Opin. Drug Delivery 4(6) (2007) 635-649.

[10] F. Gu, R. Neufeld, B. Amsden, Sustained release of bioactive therapeutic proteins from a biodegradable elastomeric device. Journal of Controlled Release 117(1) (2007) 80-89.

[11] Z.S. Haidar, R.C. Hamdy, M. Tabrizian, Protein release kinetics for core-shell hybrid nanoparticles based on the layer-by-layer assembly of alginate and chitosan on liposomes. Biomaterials 29(9) (2008) 1207-1215.

[12] M. Ozeki, T. Ishii, Y. Hirano, Y. Tabata, Controlled release of hepatocyte growth factor from gelatin hydrogels based on hydrogel degradation. Journal of Drug Targeting 9(6) (2001) 461-471.

[13] T.P. Richardson, M.C. Peters, A.B. Ennett, D.J. Mooney, Polymeric system for dual growth factor delivery. Nature Biotechnology 19(11) (2001) 1029-1034.

[14] E.A. Silva, D.J. Mooney, Spatiotemporal control of vascular endothelial growth factor delivery from injectable hydrogels enhances angiogenesis. Journal of Thrombosis and Haemostasis 5(3) (2007) 590-598.

[15] Y. Tabata, M. Miyao, M. Ozeki, Y. Ikada, Controlled release of vascular endothelial growth factor by use of collagen hydrogels. Journal of Biomaterials Science-Polymer Edition 11(9) (2000) 915-930.

[16] G.Z. Zhu, S.R. Mallery, S.P. Schwendeman, Stabilization of proteins encapsulated in injectable poly (lactide-co-glycolide). Nature Biotechnology 18(1) (2000) 52-57.

[17] N. Davies, S. Dobner, D. Bezuidenhout, C. Schmidt, M. Beck, A.H. Zisch, P. Zilla, The dosage dependence of VEGF stimulation on scaffold neovascularisation. Biomaterials 29(26) (2008) 3531-3538.
[18] G. von Degenfeld, A. Banfi, M.L. Springer, R.A. Wagner, J. Jacobi, C.R. Ozawa, M.J. Merchant, J.P. Cooke, H.M. Blau, Microenvironmental VEGF distribution is critical for stable and functional vessel growth in ischemia. Faseb Journal 20(14) (2006) 2657-+.
[19] Z. Zhang, R. Kuijer, S.K. Bulstra, D.W. Grijpma, J. Feijen, The in vivo and in vitro degradation behavior of poly(trimethylene carbonate). Biomaterials 27(9) (2006) 1741-1748.
[20] R. Schirrer, P. Thepin, G. Torres, Water-absorption, swelling, rupture and salt release in salt silicone-rubber compounds. Journal of Materials Science 27(13) (1992) 3424-3434.
[21] C. Goolcharran, J.L. Cleland, R. Keck, A.J.S. Jones, R.T. Borchardt, Comparison of the rates of deamidation, diketopiperazine formation, and oxidation in recombinant human vascular endothelial growth factor and model peptides. Aaps Pharmsci 2(1) (2000).
[22] A.H. Zisch, M.P. Lutolf, J.A. Hubbell, Biopolymeric delivery matrices for angiogenic growth factors. Cardiovascular Pathology 12(6) (2003) 295-310.
[23] B.A. Keyt, L.T. Berleau, H.V. Nguyen, H. Chen, H. Heinsohn, R. Vandlen, N. Ferrara, The carboxyl-terminal domain (111-165) of vascular endothelial growth factor is critical for its mitogenic potency. Journal of Biological Chemistry 271(13) (1996) 7788-7795.
[24] Y.A. Muller, H.W. Christinger, B.A. Keyt, A.M. deVos, The crystal structure of vascular endothelial growth factor (VEGF) refined to 1.93 angstrom resolution: multiple copy flexibility and receptor binding. Structure 5(10) (1997) 1325-1338.
[25] S.M. Jay, W.M. Saltzman, Controlled delivery of VEGF via modulation of alginate microparticle ionic crosslinking. Journal of Controlled Release 134(1) (2009) 26-34.
[26] L.E. Donate, E. Gherardi, N. Srinivasan, R. Sowdhamini, S. Aparicio, T.L. Blundell, Molecular evolution and domain-structure of plasminogen-related growth-factors (hgf/sf and hgf1/msp). Protein Science 3(12) (1994) 2378-2394.
[27] H.J. Zhou, M.J. Mazzulla, J.D. Kaufman, S.J. Stahl, P.T. Wingfield, J.S. Rubin, D.P. Bottaro, R.A. Byrd, The solution structure of the N-terminal domain of hepatocyte growth factor reveals a potential heparin-binding site. Structure 6(1) (1998) 109-116.
[28] H. Aoyama, D. Naka, Y. Yoshiyama, T. Ishii, J. Kondo, M. Mitsuka, T. Hayase, Isolation and conformational analysis of fragment peptide corresponding to the heparin-binding site of hepatocyte growth factor. Biochemistry 36(33) (1997) 10286-10291.
[29] R. Appasamy, M. Tanabe, N. Murase, R. Zarnegar, R. Venkataramanan, D.H. Vanthiel, G.K. Michalopoulos, Hepatocyte growth-factor, blood clearance, organ uptake, and biliary-excretion in normal and partially hepatectomized rats. Laboratory Investigation 68(3) (1993) 270-276.
[30] X.J. Hao, E.A. Silva, A. Mansson-Broberg, K.H. Grinnemo, A.J. Siddiqui, G. Dellgren, E. Wardell, L.A. Brodin, D.J. Mooney, C. Sylven, Angiogenic effects of sequential release of VEGF-A(165) and PDGF-BB with alginate hydrogels after myocardial infarction. Cardiovascular Research 75(1) (2007) 178-185.

[31] X.D. Cao, M.S. Shoichet, Delivering neuroactive molecules from biodegradable microspheres for application in central nervous system disorders. Biomaterials 20(4) (1999) 329-339.
[32] T.W. King, C.W. Patrick, Development and in vitro characterization of vascular endothelial growth factor (VEGF)-loaded poly(DL-lactic-co-glycolic acid)/poly(ethylene glycol) microspheres using a solid encapsulation/single emulsion/solvent extraction technique. Journal of Biomedical Materials Research 51(3) (2000) 383-390.
[33] S. Meyenburg, H. Lilie, S. Panzner, R. Rudolph, Fibrin encapsulated liposomes as protein delivery system - Studies on the in vitro release behavior. Journal of Controlled Release 69(1) (2000) 159-168.
[34] A.L. Weiner, Liposomes for protein delivery: selecting manufacture and development processes. ImmunoMethods 4(3) (1994) 201-209.
[35] F. Gu, R. Neufeld, B. Amsden, Osmotic-driven release kinetics of bioactive therapeutic proteins from a biodegradable elastomer are linear, constant, similar, and adjustable. Pharmaceutical Research 23(4) (2006) 782-789.
[36] A.E. Elcin, Y.M. Elcin, Localized angiogenesis induced by human vascular endothelial growth factor-activated PLGA sponge. Tissue Engineering 12(4) (2006) 959-968.
[37] M.K. Smith, M.C. Peters, T.P. Richardson, J.C. Garbern, D.J. Mooney, Locally enhanced angiogenesis promotes transplanted cell survival. Tissue Engineering 10(1-2) (2004) 63-71.
[38] G.H. Stoll, F. Nimmerfall, M. Acemoglu, D. Bodmer, S. Bantle, I. Muller, A. Mahl, M. Kolopp, K. Tullberg, Poly(ethylene carbonate)s, part II: degradation mechanisms and parenteral delivery of bioactive agents. Journal Of Controlled Release 76(3) (2001) 209-225.
[39] B. Amsden, Curable, biodegradable elastomers: emerging biomaterials for drug delivery and tissue engineering. Soft Matter 3(11) (2007) 1335-1348.
[40] S. Hurrell, R.E. Cameron, Polyglycolide: Degradation and drug release. Part II: Drug release. Journal of Materials Science-Materials in Medicine 12(9) (2001) 817-820.
[41] N.A. Weir, F.J. Buchanan, J.F. Orr, G.R. Dickson, Degradation of poly-L-lactide: Part 1: in vitro and in vivo physiological temperature degradation. Proceedings of the Institution of Mechanical Engineers Part H-Journal of Engineering in Medicine 218(H5) (2004) 307-319.
[42] J.W. Leenslag, A.J. Pennings, R.R.M. Bos, F.R. Rozema, G. Boering, Resorbable materials of poly(l-lactide) .7. invivo and invitro degradation. Biomaterials 8(4) (1987) 311-314.
[43] C.G. Pitt, M.M. Gratzl, G.L. Kimmel, J. Surles, A. Schindler, Aliphatic polyesters .2. the degradation of poly(dl-lactide), poly(epsilon-caprolactone), and their copolymers invivo. Biomaterials 2(4) (1981) 215-220.
[44] M. Acemoglu, Chemistry of polymer biodegradation and implications on parenteral drug delivery. International Journal of Pharmaceutics 277(1-2) (2004) 133-139.
[45] E.M. Christenson, S. Patel, J.M. Anderson, A. Hiltner, Enzymatic degradation of poly(ether urethane) and poly(carbonate urethane) by cholesterol esterase. Biomaterials 27(21) (2006) 3920-3926.

[46] Y.D. Wang, Y.M. Kim, R. Langer, In vivo degradation characteristics of poly(glycerol sebacate). journal of biomedical Materials Research Part A 66A(1) (2003) 192-197.
[47] J.P. Bruggeman, B.J. de Bruin, C.J. Bettinger, R. Langer, Biodegradable poly(polyol sebacate) polymers. Biomaterials 29(36) (2008) 4726-4735.
[48] L. Wang, C.S. Chaw, Y.Y. Yang, S.M. Moochhala, B. Zhao, S. Ng, J. Heller, Preparation, characterization, and in vitro evaluation of physostigmine-loaded poly(ortho ester) and poly(ortho ester)/poly(D,L-lactide-co-glycolide) blend microspheres fabricated by spray drying. Biomaterials 25(16) (2004) 3275-3282.
[49] K.W. Leong, B.C. Brott, R. Langer, Bioerodible polyanhydrides as drug-carrier matrices .1. characterization, degradation, and release characteristics. Journal of Biomedical Materials Research 19(8) (1985) 941-955.
[50] W.F.A. den Dunnen, M.F. Meek, D.W. Grijpma, P.F. Robinson, J.M. Schakenraad, In vivo and in vitro degradation of poly[(50)/(50) ((85)/(L)(15)/(D))LA/epsilon-CL], and the implications for the use in nerve reconstruction. Journal of Biomedical Materials Research 51(4) (2000) 575-585.
[51] T. Karjalainen, M. HiljanenVainio, M. Malin, J. Seppala, Biodegradable lactone copolymers .3. Mechanical properties of epsilon-caprolactone and lactide copolymers after hydrolysis in vitro. Journal of Applied Polymer Science 59(8) (1996) 1299-1304.
[52] M. Malin, M. HiljanenVainio, T. Karjalainen, J. Seppala, Biodegradable lactone copolymers .2. Hydrolytic study of epsilon-caprolactone and lactide copolymers. Journal of Applied Polymer Science 59(8) (1996) 1289-1298.
[53] A.M. Reed, D.K. Gilding, Biodegradable polymers for use in surgery - poly(glycolic)-poly(lactic acid) homo and co-polymers .2. invitro degradation. Polymer 22(4) (1981) 494-498.
[54] R.F. Storey, T.P. Hickey, Degradable polyurethane networks based on d,l-lactide, glycolide, epsilon-caprolactone, and trimethylene carbonate homopolyester and copolyester triols. Polymer 35(4) (1994) 830-838.
[55] R. Chapanian, M.Y. Tse, S.C. Pang, B.G. Amsden, The role of oxidation and enzymatic hydrolysis on the in vivo degradation of trimethylene carbonate based photocrosslinkable elastomers. Biomaterials 30(3) (2009) 295-306.
[56] R. Chapanian, M.Y. Tse, S.C. Pang, B.G. Amsden, Long Term In Vivo Degradation, and Tissue Response to, Photo-Cross-Linked Elastomers Prepared from Star Shaped Prepolymers of Poly(e-Caprolactone-co-D,L-Lactide) journal of biomedical Materials Research Part A (Published on line in March 2009).
[57] N. Kipshidze, V. Chekanov, P. Chawla, L.R. Shanker, J.B. Gosset, K. Kumar, D. Hammen, J. Gordon, M.H. Keelan, Angiogenesis in a patient with ischemic limb - Induced by intramuscular injection of vascular endothelial growth factor and fibrin platform. Texas Heart Institute Journal 27(2) (2000) 196-200.
[58] V.S. Chekanov, G.V. Tchekanov, M.A. Rieder, R. Eisenstein, D.M. Wankowski, D.H. Schmidt, V.V. Nikolaychik, P.I. Lelkes, Biologic clue increases capillary ingrowth after cardiomyoplasty in an ischemic cardiomyopathy model. Asaio Journal 42(5) (1996) M480-M487.
[59] H. Hall, T. Baechi, J.A. Hubbell, Molecular properties of fibrin-based matrices for promotion of angiogenesis in vitro. Microvascular Research 62(3) (2001) 315-326.

[60] S.E. Sakiyama-Elbert, J.A. Hubbell, Development of fibrin derivatives for controlled release of heparin-binding growth factors. Journal of Controlled Release 65(3) (2000) 389-402.
[61] A.H. Zisch, U. Schenk, J.C. Schense, S.E. Sakiyama-Elbert, J.A. Hubbell, Covalently conjugated VEGF-fibrin matrices for endothelialization. Journal of Controlled Release 72(1-3) (2001) 101-113.
[62] Y.M. Elcin, V. Dixit, T. Gitnick, Extensive in vivo angiogenesis following controlled release of human vascular endothelial cell growth factor: Implications for tissue engineering and wound healing. Artificial Organs 25(7) (2001) 558-565.
[63] Shiladitya, Nanometer liposomes containing two drugs in different part of the lipd layer for controlled delivery2007.
[64] F. Gu, H.M. Younes, A.O.S. El-Kadi, R.J. Neufeld, B.G. Amsden, Sustained interferon-gamma delivery from a photocrosslinked biodegradable elastomer. Journal of Controlled Release 102(3) (2005) 607-617.
[65] F. Gu, R. Neufeld, B. Amsden, Maintenance of vascular endothelial growth factor and potentially other therapeutic proteins bioactivity during a photo-initiated free radical cross-linking reaction forming biodegradable elastomers. European Journal of Pharmaceutics and Biopharmaceutics 66(1) (2007) 21-27.
[66] C.C. Lin, S.M. Sawicki, A.T. Metters, Free-radical-mediated protein inactivation and recovery during protein photoencapsulation. Biomacromolecules 9(1) (2008) 75-83.
[67] Y. Tang, J. Singh, Controlled delivery of aspirin: Effect of aspirin on polymer degradation and in vitro release from PLGA based phase sensitive systems. International Journal of Pharmaceutics 357(1-2) (2008) 119-125.
[68] S. Nishino, A. Kishida, H. Yoshizawa, Morphology control of polylactide microspheres enclosing irinotecan hydrochloride with polylactide based polymer surfactant for reduction of initial burst. International Journal of Pharmaceutics 330(1-2) (2007) 32-36.
[69] E.S. Lee, M.J. Kwon, H. Lee, J.J. Kim, Stabilization of protein encapsulated in poly(lactide-co-glycolide) microspheres by novel viscous S/W/O/W method. International Journal of Pharmaceutics 331(1) (2007) 27-37.
[70] J.L. Cleland, E.T. Duenas, A. Park, A. Daugherty, J. Kahn, J. Kowalski, A. Cuthbertson, Development of poly-(D,L-lactide-coglycolide) microsphere formulations containing recombinant human vascular endothelial growth factor to promote local angiogenesis. Journal of Controlled Release 72(1-3) (2001) 13-24.
[71] C. Shih, A bioactive agent delivering system comprised of microparticles within a biodegradable to improve release profiles2003.
[72] S.D. Patil, F. Papadmitrakopoulos, D.J. Burgess, Concurrent delivery of dexamethasone and VEGF for localized inflammation control and angiogenesis. Journal of Controlled Release 117(1) (2007) 68-79.
[73] F. Quaglia, L. Ostacolo, G. Nese, G. De Rosa, M.I. La Rotonda, R. Palumbo, G. Maglio, Microspheres made of poly (epsilon-caprolactone)-based amphiphilic copolymers: Potential in sustained delivery of proteins. Macromolecular Bioscience 5(10) (2005) 945-954.
[74] A.G. Ding, S.P. Schwendeman, Acidic Microclimate pH Distribution in PLGA Microspheres Monitored by Confocal Laser Scanning Microscopy. Pharmaceutical Research 25(9) (2008) 2041-2052.

[75] K. Fu, D.W. Pack, A.M. Klibanov, R. Langer, Visual evidence of acidic environment within degrading poly(lactic-co-glycolic acid) (PLGA) microspheres. Pharmaceutical Research 17(1) (2000) 100-106.
[76] B. Gallez, K. Mader, H.M. Swartz, Noninvasive measurement of the pH inside the gut by using pH-sensitive nitroxides. An in vivo EPR study. Magnetic Resonance in Medicine 36(5) (1996) 694-697.
[77] P.A. Burke, Determination of internal pH in PLGA microspheres using 31P NMR spectroscopy. Proc. Int. Symp. Controlled Release Bioact. Mater. 23rd (1996) 133-134.
[78] K.C. Wong-Moon, X. Sun, X.C. Nguyen, B.P. Quan, K. Shen, P.A. Burke, NMR spectroscopic evaluation of the internal environment of PLGA microspheres. Molecular Pharmaceutics 5(4) (2008) 654-664.
[79] W.L. Jiang, S.P. Schwendeman, Stabilization and controlled release of bovine serum albumin encapsulated in poly(D, L-lactide) and poly(ethylene glycol) microsphere blends. Pharmaceutical Research 18(6) (2001) 878-885.
[80] E.C. Lavelle, M.K. Yeh, A.G.A. Coombes, S.S. Davis, The stability and immunogenicity of a protein antigen encapsulated in biodegradable microparticles based on blends of lactide polymers and polyethylene glycol. Vaccine 17(6) (1999) 512-529.
[81] C. Aschkenasy, J. Kost, On-demand release by ultrasound from osmotically swollen hydrophobic matrices. Journal of Controlled Release 110(1) (2005) 58-66.
[82] J.L. Sharon, D.A. Puleo, Immobilization of glycoproteins, such as VEGF, on biodegradable substrates. Acta Biomaterialia 4(4) (2008) 1016-1023.
[83] J.M. Anderson, Biological responses to materials. Annual Review of Materials Research 31 (2001) 81-110.
[84] M.B. Gorbet, M.V. Sefton, Biomaterial-associated thrombosis: roles of coagulation factors, complement, platelets and leukocytes. Biomaterials 25(26) (2004) 5681-5703.
[85] K.L. Christman, R.J. Lee, Biomaterials for the treatment of myocardial infarction. Journal of the American College of Cardiology 48(5) (2006) 907-913.
[86] J.Y. Lim, H.J. Donahue, Cell sensing and response to micro- and nanostructured surfaces produced by chemical and topographic patterning. Tissue Engineering 13(8) (2007) 1879-1891.
[87] B. Amsden, Y.L. Cheng, A generic protein delivery system based on osmotically rupturable monoliths. Journal of Controlled Release 33(1) (1995) 99-105.
[88] V. Carelli, G. Dicolo, C. Guerrini, E. Nannipieri, Drug release from silicone elastomer through controlled polymer cracking - an extension to macromolecular drugs. International Journal of Pharmaceutics 50(3) (1989) 181-188.
[89] B.G. Amsden, Y.L. Cheng, Enhanced fraction releasable above percolation-threshold from monoliths containing osmotic excipients. Journal of Controlled Release 31(1) (1994) 21-32.
[90] R.A. Siegel, J. Kost, R. Langer, Mechanistic studies of macromolecular drug release from macroporous polymers .1. experiments and preliminary theory concerning completeness of drug release. Journal of Controlled Release 8(3) (1989) 223-236.
[91] R. Gale, S.K. Chandrasekaran, D. Swanson, J. Wright, Use of osmotically active therapeutic agents in monolithic systems. Journal of Membrane Science 7(3) (1980) 319-331.

[92] M. Kajihara, T. Sugie, T. Hojo, H. Maeda, A. Sano, K. Fujioka, S. Sugawara, Y. Urabe, Development of a new drug delivery system for protein drugs using silicone (II). Journal of Controlled Release 73(2-3) (2001) 279-291.
[93] B. Amsden, A model for osmotic pressure driven release from cylindrical rubbery polymer matrices. Journal of Controlled Release 93(3) (2003) 249-258.
[94] B.G. Amsden, Y.L. Cheng, M.F.A. Goosen, A mechanistic study of the release of osmotic agents from polymeric monoliths. Journal of Controlled Release 30(1) (1994) 45-56.
[95] F. Theeuwes, Elementary osmotic pump. Journal of Pharmaceutical Sciences 64(12) (1975) 1987-1991.
[96] A.N. Gent, P.B. Lindley, Internal rupture of bonded rubber cylinders in tension. Proceedings of the Royal Society of London Series a-Mathematical and Physical Sciences 249(1257) (1959) 195-&.
[97] R. Chapanian, B. Amsden, Osmotically driven protein release from photo-cross-linked elastomers of poly(trimethylene carbonate) and poly(trimethylene carbonate-co-D,L-lactide). European Journal of Pharmaceutics and Biopharmaceutics submitted (2009).
[98] M. Kajihara, T. Sugie, M. Mizuno, N. Tamura, A. Sano, K. Fujioka, Y. Kashiwazaki, T. Yamaoka, S. Sugawara, Y. Urabe, Development of new drug delivery system for protein drugs using silicone (I). Journal of Controlled Release 66(1) (2000) 49-61.
[99] F. Gu, B. Amsden, R. Neufeld, Sustained delivery of vascular endothelial growth factor with alginate beads. Journal of Controlled Release 96(3) (2004) 463-472.
[100] A.R. Webb, J. Yang, G.A. Ameer, Biodegradable polyester elastomers in tissue engineering. Expert Opinion on Biological Therapy 4(6) (2004) 801-812.
[101] F. Gu, R. Neufeld, B. Amsden, Sustained release of bioactive therapeutic proteins from a biodegradable elastomeric device. Journal of Controlled Release 117(1) (2007) 80-89.
[102] B.G. Amsden, M.Y. Tse, N.D. Turner, D.K. Knight, S.C. Pang, In vivo degradation behavior of photo-cross-linked star-poly(epsilon-caprolactone-co-D,L-lactide) elastomers. Biomacromolecules 7(1) (2006) 365-372.
[103] C.G. Pitt, R.W. Hendren, A. Schindler, S.C. Woodward, The enzymic surface erosion of aliphatic polyesters. Journal of Controlled Release 1(1) (1984) 3-14.
[104] Y.D. Wang, G.A. Ameer, B.J. Sheppard, R. Langer, A tough biodegradable elastomer. Nature Biotechnology 20(6) (2002) 602-606.
[105] B.G. Amsden, G. Misra, F. Gu, H.M. Younes, Synthesis and characterization of a photo-cross-linked biodegradable elastomer. Biomacromolecules 5(6) (2004) 2479-2486.
[106] S.M. Li, Hydrolytic degradation characteristics of aliphatic polyesters derived from lactic and glycolic acids. Journal of Biomedical Materials Research 48(3) (1999) 342-353.
[107] S.I. Jeong, B.S. Kim, Y.M. Lee, K.J. Ihn, S.H. Kim, Y.H. Kim, Morphology of elastic poly(L-lactide-co-epsilon-caprolactone) copolymers and in vitro and in vivo degradation behavior of their scaffolds. Biomacromolecules 5(4) (2004) 1303-1309.
[108] M. Bertmer, A. Buda, I. Blomenkamp-Hofges, S. Kelch, A. Lendlein, Biodegradable shape-memory polymer networks: characterization with solid-state NMR. Macromolecules 38(9) (2005) 3793-3799.

[109] S.J. Bryant, C.R. Nuttelman, K.S. Anseth, Cytocompatibility of UV and visible light photoinitiating systems on cultured NIH/3T3 fibroblasts in vitro. Journal of Biomaterials Science-Polymer Edition 11(5) (2000) 439-457.
[110] H. Kweon, M.K. Yoo, I.K. Park, T.H. Kim, H.C. Lee, H.S. Lee, J.S. Oh, T. Akaike, C.S. Cho, A novel degradable polycaprolactone networks for tissue engineering. Biomaterials 24(5) (2003) 801-808.
[111] N.T. Paragkumar, E. Dellacherie, J.L. Six, Surface characteristics of PLA and PLGA films. Applied Surface Science 253(5) (2006) 2758-2764.
[112] M.M. Breuer, Binding of small molecules to hair .1. hydration of hair and effect of water on mechanical properties of hair. Journal of the Society of Cosmetic Chemists 23(8) (1972) 447-&.
[113] R.F. Storey, S.C. Warren, C.J. Allison, A.D. Puckett, Methacrylate-endcapped poly(d,l-lactide-co-trimethylene carbonate) oligomers. Network formation by thermal free-radical curing. Polymer 38(26) (1997) 6295-6301.
[114] A.P. Pego, A.A. Poot, D.W. Grijpma, J. Feijen, In vitro degradation of trimethylene carbonate based (Co)polymers. Macromolecular Bioscience 2(9) (2002) 411-419.
[115] K.H. Lee, C.C. Chu, The role of superoxide ions in the degradation of synthetic absorbable sutures. Journal of Biomedical Materials Research 49(1) (2000) 25-35.
[116] Z.H. Gan, D.H. Yu, Z.Y. Zhong, Q.Z. Liang, X.B. Jing, Enzymatic degradation of poly(epsilon-caprolactone)/poly(DL-lactide) blends in phosphate buffer solution. Polymer 40(10) (1999) 2859-2862.
[117] I. Grizzi, H. Garreau, S. Li, M. Vert, Hydrolytic degradation of devices based on poly(dl-lactic acid) size-dependence. Biomaterials 16(4) (1995) 305-311.
[118] J.R. Fried, Polymer Science and Technology. Prentice Hall PTR, New Jersey, 1995.
[119] F.W. Cordewener, F.R. Rozema, R.R.M. Bos, G. Boering, Material properties and tissue reaction during degradation of poly(96l/4d-lactide) - a study in-vitro and in rats. Journal of Materials Science-Materials in Medicine 6(4) (1995) 211-217.
[120] Y.B. Fan, P. Li, L. Zeng, X.J. Huang, Effects of mechanical load on the degradation of poly(D,L-lactic acid) foam. Polymer Degradation and Stability 93(3) (2008) 677-683.
[121] Y. Yang, Y. Zhao, G. Tang, H. Li, X. Yuan, Y. Fan, In vitro degradation of porous poly(-lactide-co-glycolide)/beta -tricalcium phosphate (PLGA/beta -TCP) scaffolds under dynamic and static conditions. Polym. Degrad. Stab. 93(10) (2008) 1838-1845.
[122] A.P. Pego, M.J.A. Van Luyn, L.A. Brouwer, P.B. van Wachem, A.A. Poot, D.W. Grijpma, J. Feijen, In vivo behavior of poly(1,3-trimethylene carbonate) and copolymers of 1,3-trimethylene carbonate with D,L-lactide or epsilon-caprolactone: Degradation and tissue response. journal of biomedical Materials Research Part A 67A(3) (2003) 1044-1054.
[123] J.M. Anderson, Biological responses to materials. Annu Rev Mater Res 31 (2001) 81-110.
[124] T.O. Collier, J.M. Anderson, Protein and surface effects on monocyte and macrophage adhesion, maturation, and survival. Journal Of Biomedical Materials Research 60(3) (2002) 487-496.

[125] L.A. Matheson, J.P. Santerre, R.S. Labow, Changes in macrophage function and morphology due to biomedical polyurethane surfaces undergoing biodegradation. Journal Of Cellular Physiology 199(1) (2004) 8-19.
[126] J.E. McBane, J.P. Santerre, R.S. Labow, Role of protein kinase C in the monocyte-derived macrophage-mediated biodegradation of polycarbonate-based polyurethanes. Journal Of Biomedical Materials Research Part A 74A(1) (2005) 1-11.
[127] J.E. McBane, J.P. Santerre, R.S. Labow, The interaction between hydrolytic and oxidative pathways in macrophage-mediated polyurethane degradation. Journal Of Biomedical Materials Research Part A 82A(4) (2007) 984-994.
[128] M. Mizutani, T. Matsuda, Photocurable liquid biodegradable copolymers: in vitro hydrolytic degredation behaviors of photocured films kof coumarin-endcapped poly(epsilon-caprolactone-*co*-trimethylene carbonate). Biomacromolecules 3 (2002) 249-255.
[129] T. Matsuda, I.K. Kwon, S. Kidoaki, Photocurable biodegradable liquid copolymers: Synthesis of acrylate-end-capped trimethylene carbonate-based prepolymers, photocuring, and hydrolysis. Biomacromolecules 5(2) (2004) 295-305.
[130] S. Sharifpoor, B. Amsden, In vitro release of a water-soluble agent from low viscosity biodegradable, injectable oligomers. European Journal of Pharmaceutics and Biopharmaceutics 65(3) (2007) 336-345.
[131] S.M. Li, L.J. Liu, H. Garreau, M. Vert, Lipase-catalyzed biodegradation of poly(epsilon-caprolactone) blended with various polylactide-based polymers. Biomacromolecules 4(2) (2003) 372-377.
[132] D. Darwis, H. Mitomo, T. Enjoji, F. Yoshi, K. Makuuchi, Enzymatic degradation of radiation crosslinked poly(epsilon-caprolactone). Polymer Degradation and Stability 62(2) (1998) 259-265.
[133] B. Amsden, G. Misra, F. Gu, H. Younes, Synthesis and characterization of a photocrosslinked biodegradable elastomer. Biomacromolecules 5(6) (2004) 2479-2486.
[134] F. Jaffer, Y. Finer, J.P. Santerre, Interactions between resin monomers and commercial composite resins with human saliva derived esterases. Biomaterials 23(7) (2002) 1707-1719.
[135] Y. Yavuz, A.S. Koparal, U.B. Ogutveren, Phenol removal through chemical oxidation using Fenton reagent. Chemical Engineering & Technology 30(5) (2007) 583-586.
[136] X.R. Zhang, J.K. Pugh, P.N. Ross, Evidence for epoxide formation from the electrochemical reduction of ethylene carbonate. Electrochemical and Solid State Letters 4(6) (2001) A82-A84.
[137] Y. Cha, P. Reardon, S. Mah, L. Whitcomb, In vitro enzymic surface erosion of polyethylene carbonate in the presence of macrophages. Proc. Int. Symp. Controlled Release Bioact. Mater. 21ST (1994) 126-127.
[138] M. Dadsetan, E.M. Christenson, F. Unger, M. Ausborn, T. Kissel, A. Hiltner, J.M. Anderson, In vivo biocompatibility and biodegradation of poly(ethylene carbonate). Journal of Controlled Release 93(3) (2003) 259-270.
[139] A.C. Albertsson, M. Eklund, Influence of Molecular-Structure on the Degradation Mechanism of Degradable Polymers - in-Vitro Degradation of Poly(Trimethylene Carbonate), Poly(Trimethylene Carbonate-Co-Caprolactone), and Poly(Adipic Anhydride). Journal of Applied Polymer Science 57(1) (1995) 87-103.

[140] M.S. Cohen, B.E. Britigan, D.J. Hassett, G.M. Rosen, Phagocytes, O2 Reduction, and Hydroxyl Radical. Reviews of Infectious Diseases 10(6) (1988) 1088-1096.
[141] R.S. Labow, E. Meek, L.A. Matheson, J.P. Santerre, Human macrophage-mediated biodegradation of polyurethanes: assessment of candidate enzyme activities. Biomaterials 23(19) (2002) 3969-3975.
[142] L.A. Matheson, R.S. Labow, J.P. Santerre, Biodegradation of polycarbonate-based polyurethanes by the human monocyte-derived macrophage and U937 cell systems. Journal Of Biomedical Materials Research 61(4) (2002) 505-+.
[143] A.R. Forrester, V. Purushotham, Mechanism of hydrolysis of esters by superoxide. Journal of the Chemical Society-Chemical Communications(22) (1984) 1505-1506.
[144] Frokjaer, Biomaterilas for delivery and targeting of proteins and nucleic acids, CRC press, 2005.
[145] M.M. Bradford, Rapid and sensitive method for quantitation of microgram quantities of protein utilizing principle of protein-dye binding. Analytical Biochemistry 72(1-2) (1976) 248-254.
[146] M. Dubois, K.A. Gilles, J.K. Hamilton, P.A. Rebers, F. Smith, Colorimetric method for determination of sugars and related substances. Analytical Chemistry 28(3) (1956) 350-356.
[147] S.M. Li, J.L. Espartero, P. Foch, M. Vert, Structural characterization and hydrolytic degradation of a Zn metal initiated copolymer of L-lactide and epsilon-caprolactone. Journal of Biomaterials Science-Polymer Edition 8(3) (1996) 165-187.
[148] R. Yamadera, M. Murano, Determination of randomness in copolyesters by high resolution nuclear magnetic resonance. Journal of Polymer Science Part a-1-Polymer Chemistry 5(9PA1) (1967) 2259-&.
[149] J.K. Kaushik, R. Bhat, Why is trehalose an exceptional protein stabilizer? An analysis of the thermal stability of proteins in the presence of the compatible osmolyte trehalose. Journal of Biological Chemistry 278(29) (2003) 26458-26465.
[150] C. Fischbach, D.J. Mooney, Polymers for Regenerative Medicine, 2006, pp. 191-221.
[151] X. Xin, S. Yang, G. Ingle, C. Zlot, L. Rangell, J. Kowalski, R. Schwall, N. Ferrara, M.E. Gerritsen, Hepatocyte growth factor enhances vascular endothelial growth factor-induced angiogenesis in vitro and in vivo. Am. J. Pathol. 158(3) (2001) 1111-1120.
[152] K.A.a.Y. RJ, Fracture behaviour of polymers, Elsevier science publishing Co., New York, 1983.
[153] C.A. Kavanagh, T.A. Gorelova, I.I. Selezneva, Y.A. Rochev, K.A. Dawson, W.M. Gallagher, A.V. Gorelov, A.K. Keenan, Poly(N-isopropylacrylamide) copolymer films as vehicles for the sustained delivery of proteins to vascular endothelial cells. J. Biomed. Mater. Res., Part A 72A(1) (2005) 25-35.
[154] M. Nomi, H. Miyake, Y. Sugita, M. Fujisawa, S. Soker, Role of growth factors and endothelial cells in therapeutic angiogenesis and tissue engineering. Curr Stem Cell Res Ther 1(3) (2006) 333-343.
[155] R.J. Tomanek, G.C. Schatteman, Angiogenesis: new insights and therapeutic potential. Anat. Rec. 261(3) (2000) 126-135.

[156] E.J. Battegay, Angiogenesis: mechanistic insights, neovascular diseases, and therapeutic prospects. J. Mol. Med. (Berlin) 73(7) (1995) 333-346.
[157] E. Van Belle, B. Witzenbichler, D. Chen, M. Silver, L. Chang, R. Schwall, J.M. Isner, Potentiated angiogenic effect of scatter factor/hepatocyte growth factor via induction of vascular endothelial growth factor The case for paracrine amplification of angiogenesis. Circulation 97(4) (1998) 381-390.
[158] R. Morishita, S. Nakamura, S. Hayashi, Y. Taniyama, A. Moriguchi, T. Nagano, M. Taiji, H. Noguchi, S. Takeshita, K. Matsumoto, T. Nakamura, J. Higaki, T. Ogihara, Therapeutic angiogenesis induced by human recombinant hepatocyte growth factor in rabbit hind limb ischemia model as cytokine supplement therapy. Hypertension 33(6) (1999) 1379-1384.
[159] C.P. Quinn, C.P. Pathak, A. Heller, J.A. Hubbell, Photo-cross-linked copolymers of 2-hydroxyethyl methacrylate, poly(ethylene glycol) tetra-acrylate and ethylene dimethacrylate for improving biocompatibility of biosensors. Biomaterials 16(5) (1995) 389-396.
[160] R. Chapanian and B. Amsden, Combined Delivery of Bioactive VEGF165 and HGF from poly(trimethylene carbonate based photo-cross-linked elastomers. Journal of controlled release submitted (2009).
[161] L.E. Freed, G. Vunjaknovakovic, R.J. Biron, D.B. Eagles, D.C. Lesnoy, S.K. Barlow, R. Langer, Biodegradable polymer scaffolds for tissue engineering. Bio-Technology 12(7) (1994) 689-693.
[162] N. Sitte, K. Merker, T. Von Zglinicki, T. Grune, K.J.A. Davies, Protein oxidation and degradation during cellular senescence of human BJ fibroblasts: part I - effects of proliferative senescence. Faseb Journal 14(15) (2000) 2495-2502.
[163] E. Bat, T.G. van Kooten, J. Feijen, D.W. Grijpma, Macrophage-mediated erosion of gamma irradiated poly(trimethylene carbonate) films. Biomaterials 30(22) (2009) 3652-3661.
[164] L. Timbart, M.Y. Tse, S.C. Pang, O. Babasola, B.G. Amsden, Low Viscosity Poly(trimethylene carbonate) for Localized Drug Delivery: Rheological Properties and in vivo Degradation. Macromolecular Bioscience 9(8) (2009) 786-794.
[165] Gu, Design and establishment of a biodegradable device from a sustained and adjustable rate of release of bioactive protein drugs. 2006, PhD, Queen's University, Kingston, 2006.
[166] R. Sutinen, O. Bilbaorevoredo, A. Urtti, P. Paronen, Effect of sodium-chloride on the mechanical and osmotic properties of silicone matrices. International Journal of Pharmaceutics 57(2) (1989) 155-161.